RELIABILITY BASED LIVE LOADS FOR STRUCTURAL ASSESSMENT OF BRIDGES ON HEAVY-HAUL RAILWAY LINES

Thesis presented in fulfilment of the requirements for the degree of

Doctor of Philosophy

Faculty of Engineering and the Built Environment
Department of Civil Engineering

University of Cape Town

UNIVERSITY OF CAPE TOWN

Author: Kabani Matongo

Supervisor: Prof Pilate Moyo

Cape Town, June 2018

The copyright of this thesis vests in the author. No quotation from it or information derived from it is to be published without full acknowledgement of the source. The thesis is to be used for private study or non-commercial research purposes only.

Published by the University of Cape Town (UCT) in terms of the non-exclusive license granted to UCT by the author.

University of Cape Town

This page is intentionally left blank

DECLARATION

I know the meaning of plagiarism and declare that all of the work in the document, save for that which is properly acknowledged is my own. This dissertation has not been submitted before for any degree or examination at any other University.

Signed by candidate

Matongo Kabani

June 2018

ABSTRACT

The highest live loads on railway lines are on dedicated freight corridors operated as heavy-haul lines. These lines carry high axle loads above 25 tonnes and total tonnage above 20 million tonnes per annum over distances greater than 150km. The South African iron ore line currently operates long trains of length 4.1km with 30 tonne per axle wagons on a narrow gage (1065mm) line over a distance of 861km. The operation of heavy haul lines require close monitoring and structural performance evaluation of existing bridges. This study covered both analytical studies and field measurements of bridge dynamic response and static vertical loads required to compute moments shear for beam-type bridges. The field study of dynamic amplification factors was based on strain measurements on the Olifants bridge located on the heavy-haul iron line in South Africa. The Olifants bridge is a 23 span box girder consisting of 2 continuous span segments of 11 spans at either end and a drop span in the middle. The collected strain data consisted 1174 loaded and 1372 empty train crossing events from June 2016 to March 2017. The probabilistic study was based on weigh-in-motion data of heavy-haul freight collected from January 2016 to August 2016. The study was limited to single span, 2 span and 4 span bridges with equal spans and did not consider fatigue.

The dynamic response parameters of interest were frequency time evolution of bridge under heavy loads and dynamic amplification factors. An approximate formula derived using 2 dimensional beam model with moving masses is presented. The approximate formulae predicts the reduced frequency within 12% of the estimate from field vibration measurements of an 11 span continuous bridge with train to bridge linear mass ratio of 88%. The approximate formula

underestimates the frequency as the stiffening contribution from train suspension system is ignored in a moving mass approximation. Dynamic amplification factors from strain measurements of a continuous 11 span bridge where considerably higher with maximum of 12% compared to 5% from a moving force analytical model for train speed below 60km/h. The amplification from measurements were considerably higher due to the additional local amplification of strains in upper flange of the box girder. A comparison of amplification factors for loaded and empty trains shows that increase in gross weight increases amplification factors. Furthermore, dynamic amplification factors are not dependent on changes in speed during train crossing.

Different extrapolation techniques were used to obtain load effects from the same block maxima data. It was shown that the normal, GEV and Bayesian extrapolation methods give load effects within 1% of each other with the normal extrapolation being marginally on the lower end. This observation holds across beam types and span lengths from 5m to 50m. Although the GEV allows for all the three extreme type distributions, an analysis based on available weigh-in-motion data of axle weights show that the fitted distributions using Bayesian and Maximum Likelihood Estimate for all load effects for the span ranges are all Weibull type. On the other hand it is known that the domain of attraction for the normal distribution is Gumbel type. The study also found that extrapolated loads effects are less sensitive to increase in return period beyond 50 years. This aspect is significant as return period is a measure of safety target when determining design values for loads.

The study investigated the impact of traffic volume increase and wagon axle load dependencies. The load effects on heavy-haul were shown to be more sensitive to the weak dependence than to traffic growth over the remaining service life of 50 years. The increase in return levels of load effects is less than 1% for traffic volume growth of 4% over a period of 50 years in contrast to the much higher values between 6% and 9% reported on highway bridges for 3% traffic volume growth over 40 year period. Assessment loads that account for some wagon axle

dependence have lower return values of load effects than the assume that axle loads are independent which is consistent with theory.

DEDICATION

Dedicated to my wife Angie, my kids Nakwezi and Katanekwa, the wider Kabani family and all those who will take this research to the next level

ACKNOWLEDGEMENTS

I would like to extend my gratitude to Prof Pilate Moyo for the research supervision and mentorship, the CoMSIRU directors, the Carnegie Foundation, CoMSIRU and Transnet for the research financial support. I thank my collegues whom I shared my experience with and these include Patrick Bukenya, Philemon Arito, Faridah Chebet, Rakesh Gopinath and all my CoMSIRU collegues. Special thanks goes Yorm Amesu and Philbert Habimana who helped in bridge instrumentation and initial tests as well as Dr Fulvio Bussata whom I worked with on the bridge monitoring system.

I would also like to thank laboratory and technical staff particularly Nooredien Hassen and Tahil Mukadam for facilitating access to all the required equipment and Chris for the help on site. My special thanks goes to Charles Nicholas for the technical help in fabricating some custom made add-ons for sensors. I would like thank Herman Havenga and the team at Kairos for getting the monitoring system running. I extend my appreciation to staff at Transnet particularly Derrick and Basel in Vrendedal, Georg Hetasch and Brenda Scott in Pretoria for their great help in making all this work possible.

Table of Contents

List of Figures

List of symbols and glosarry

β, β_1	Reliability index, Reliability index with refence of one year
γ_{Dn} and γ_{LL}	Dead load and live load factors respectively
λ	Non dimensioanlised frequencies
μ, σ and ξ	Location, scale and shape factors respectively
$\phi(x)$	Mode shape functions
A,B,C and D	Mode shape constants
DA	Dynamic amplification
DAF	Dynamic amplification factor
Dn and LL	Dead load and live loads respectively
f_0, η_0	First flexural frequency (Hz)
F_Z	cumulative distribution function of Z
L	Bridge span length
L_Φ	Bridge characteristic span length
$q(t)$	Generalised coordinates
R_{dyn} and R_{stat}	Dynamic and static response respectively
RF	Load rating factor

S	Nondimensionalised speed parameter
AASHTO	American Association of State Highway and Transportation Officials
AREA	American Railway Engineering Association
ASD	Allowable Stress Design
ASR	Allowable Stress Rating
E	Youngs modulus
ERRI	European Rail Research Institute
I	Moment of inertia
LFD	Load Factor Design
LFR	Load Factor Rating
LRFD	Load and Resiatnce Factor Design
LRFR	Load and Resiatnce Factor Rating
UIC	International Union of Railways
W	Vertical displacement

Chapter 1

INTRODUCTION

1.1 Background and research motivation

Bridges are important transport nodes enabling connectivity over natural barriers such as rivers and seas. Modern bridges are designed to have a service life of between 75 to 120 years. During this time, several factors such as increases in traffic volume, changes in vehicle types resulting from changes in axle configurations or axle loads and material deterioration affect the structural performance of bridges. Bridges may also suffer from defects as a result of inadequate design requirements or inappropriate material specification and construction methods [Das, 2010]. Bailey *et al.* [2002](as cited in Cremona 2012) analysed a total of 138 bridge failures and found that 47% of the failures were loading related while design mistakes accounted for 21%.

Traffic loads are one of the principal loading cases on railway bridges. From the dawn of railway transport, railway locomotive axle loads have progressively increased from 2.2 tonnes in the year 1829 to over 25 tonnes after 1960 with the highest axles being on freight rail lines [Hayward, 2011]. Tobias *et al.* [1996] analysed a total of 508 freight trains in the United States of America and reported an average axle load of 31.9 tonnes with a maximum axle load of 49.4 tonnes for Coal hopper type freight trains. In South Africa, the heavy axle trains are on the Iron Ore freight line with maximum of 30 tonnes per axle having been

increased from previous 26 tonne per axle. The development of railway bridge design loads has progressed to reflect these changes by initially considering the static loads as uniform line loads to the current system that makes use of both point and line loads to provide load effects envelopes [Cooper, 1894, Hayward, 2011, 2013]. The load models have been adapted to also account for dynamic effects that arise from the moving loads, the surface roughness, wheel irregularities and the hunting motion of the wagons.

Although railway bridge live load models have been constantly updated to reflect both current traffic and future projected traffic, there is a need to regularly check bridge structural performance against network specific loads. In highway bridge applications, it has been shown that design loads as formulated by codes are generally more conservative to be used for assessment [O'Connor and Eichinger, 2007, Pelphrey *et al.*, 2008, Ghosn *et al.*, 2012]. The inherent conservatism in design loads arises from the need to provide load effects envelopes for a wide range of bridge types, traffic volumes and traffic composition. The cost implications of being conservative at design stage are less severe with research in Europe showing that a 40% increase in bridge design load only resulted in between 2% and 4% increase in construction costs [Calgaro and Tschumi, 2010]. The inherent conservatism in live loads given in design codes has not been demonstrated in railway bridge applications. Tobias *et al.* [1996] reported that the existing freight traffic in United States induced moments and shears that were equal to and in some cases exceeded the moments and shears obtained from the live loading code namely the Cooper E80 loading and the American Railway Engineering Association (AREA) alternative loading. Similarly, the live load model in Load Model 71 which is the basis of 'BS EN 1991-2:2003' may not be adequate to cover future needs imposed by increase in axle loads [Calgaro and Tschumi, 2010, ERRI-D192/RP2, 1994, EERI-D192/RP3, 1994].

In order to perform structural assessment of railway bridges, an appropriate analysis method which quantifies safety consistent with the limit states philosophy adopted in design must be adopted. This assessment framework is

already available in the form of structural reliability theory and is briefly discussed in section 1.2. Research into assessment loads for highway bridges has been done with the general consensus that such an assessment load must account for the site specific loads where such data is readily available and in addition account for the remaining life which is generally less than the design service life [Bailey, 1996, Getachew and Obrien, 2007, O'Connor and Eichinger, 2007, Pelphrey *et al.*, 2008, Sivakumar and Ghosn, 2009].

There are some marked differences between highway bridge loading and railway bridge loading especially on a heavy haul route. Freight trains on the heavy haul tend to be longer and this tends to increase the period within which bridges experience excitations as result of train passage. This has potential of building up the vibrations during train passage. Freight trains have high axle loads and therefore the bridge to train mass ratio is significantly higher, thus influencing the dynamic behaviour during train passage. Freight trains tend to carry dedicated goods and in the case of bulk commodities, the train loading regime is generally closely controlled and monitored. These last aspects may not be the case on highway bridges where there is a wide range of vehicle classes carrying various goods, with random arrival times and headway distances or on mixed freight rail lines where loads are not high.

1.2 Structural Performance Functions

The performance of bridges in current Bridge Management Systems (BMS) is determined from condition index and load rating [Ryall, 2010]. The condition index is obtained from condition rating which evaluates the level of material deterioration which includes corrosion, de-lamination and cracking. While material deterioration can affect safe loads that a bridge can carry, this part is separately evaluated through proof load tests and load rating which are discussed in Chapter 2.

The structural performance of bridges and other structures at design stage is based on reliability theory. Reliability is defined as the ability of a structure to

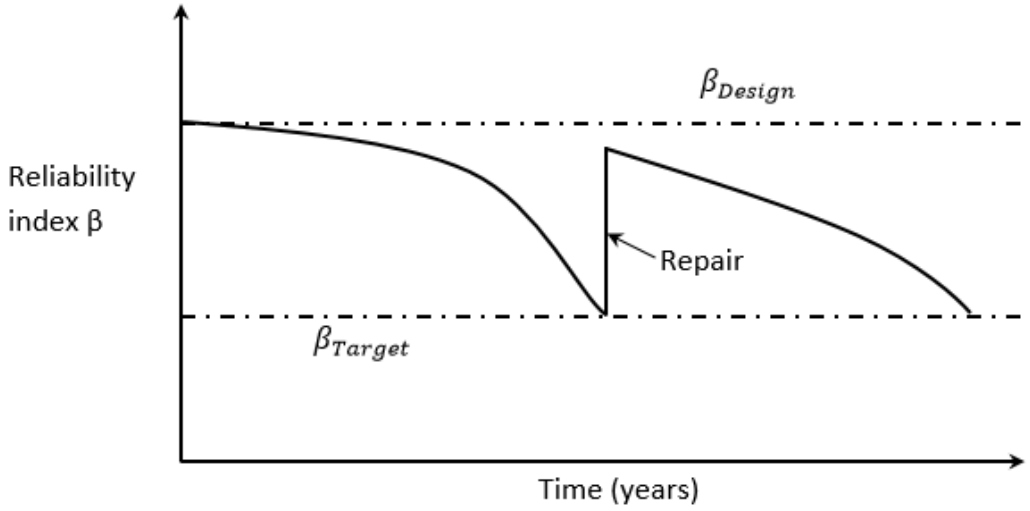

Figure 1.1: Structural performance over time

fulfil specified requirements for which it is designed during the working life [Holicky, 2009]. The requirements hence forth referred to as performance requirements include ability to carry loads, limits on deflections or vibrations and geometry so as to carry traffic. These performance requirements are normally introduced as limit state equations. During the design life of a bridge, the performance measure usually expressed as a reliability index β is non increasing at best if no modifications or maintenance is done as illustrated in Fig 1.1. The reliability index over time may decrease as a result of material deterioration and increases in traffic loads.

Structural reliability is concerned with the calculation and prediction of limit state violation of a structure at any stage during its life [Melchers, 1999]. Limit states are conditions that separate structure states as satisfactory or unsatisfactory. Limit states are divided into ultimate and serviceability limit states. Ultimate limit states include fatigue, flexure and stability. Serviceability limit states include vibrations and cracks. Reliability is defined in terms of probability of a limit state violation. A limit state violation occurs when the resistance capacity of a structure is exceeded by the load applied on it as expressed equation 1.1:

$$G(S,R) = R(t) - S(t) \leq 0 \tag{1.1}$$

where $R(t)$ is resistance function, $S(t)$ is the load, both assumed to vary with time and hence forth written as R and S respectively and $G(S, R)$ is the limit state function. The probability that an event happens that leads to a limit state violation is the probability of failure p_f given in equation 1.2:

$$p_f = P(R - S \leq 0) \tag{1.2}$$

Now if a basic reliability problem is considered where a load effect, S is resisted by load resistance, R which have joint probability density function $f_{RS}(r, s)$ where r and s are realisations of the resistance and load respectively then equation 1.2 is modified into equation 1.3:

$$p_f = \int_D \int f_{RS}(r, s) dr ds \tag{1.3}$$

where D is the failure domain as defined by the limit state. For a generalised case where $G(\mathbf{X})$ is the limit state function and $\mathbf{X}$ is the vector of relevant basic variables, the probability of failure is given as:

$$p_f = P[G(X) \leq 0] = \int \cdots \int_{G(X) \leq 0} f_X(x) dx \tag{1.4}$$

where $f_X(x)$ is the joint probability density function for the n-dimensional vector X of basic variables. The solution for equation 1.4 requires the use of numerical methods. A simplified case is obtained for two independent and normal variables for load and resistance which when applied to equation 1.3 yields:

$$p_f(t) = P[G(\mathbf{X}) \leq 0] = \Phi \left[\frac{-(\mu_R - \mu_S)}{({\sigma^2}_R + {\sigma^2}_S)} \right] = \Phi(-\beta) \tag{1.5}$$

where the parameter β is the reliability index, μ_R and μ_S represent the mean resistance and loads while σ_R^2 and σ_S^2 are the variance in resistance and load respectively.

1.2.1 Structural assessment of bridges

There are differences between bridge design and evaluation of an existing bridges. The first difference is that the random variables such as live and dead loads, bridge geometry and material strengths assumed in the design stage are only realised during the construction stage. On the other hand during operation , the statistical

characteristics of these variables can be obtained through inspections, tests and bridge monitoring. The second difference is in the time varying effects brought about by material deterioration or changes in loads arising from increase in traffic volume or regulatory changes in allowable axle load limits [Cremona, 2011, Yi, 2014]. These differences render structural performance checks based on design codes inappropriate as there is need to incorporate information about the material properties and structural behaviour gained during construction and operation of a structure.

Traditional methods of bridge assessment have combined material level evaluation and load rating to determine safe loads that a bridge can carry [Au *et al.*, 2005, Bhattacharya *et al.*, 2005, Wang *et al.*, 2011, Vinayagamoorthy and Tsang, 2014]. Material level evaluation is used to determine if a structural component has deteriorated and quantify the level of deterioration. This information is then used to reduce the resistance capacity of a component. Load rating is generally obtained by computing a rating factor which is a ratio of load carrying capacity to live loads on a given bridge.

Recently, guidelines for structural assessment of existing bridges have been proposed. These guidelines closely mirror the reliability-based bridge design methods [Brühwiler *et al.*, 2012, Cremona and Poulin, 2017]. These methods start with simple checks or checks of structural performance by using design code guidelines. This approach is suitable for undamaged bridges. If the level of structural performance is unsatisfactory, semi-probabilistic methods based on the partial factor format adopted in most codes is applied after updating the resistance and load factors. The updated factors take into account any defects and deterioration identified during inspection. The load factors are equally updated based on available data to obtain site specific or route specific load models. Probabilistic methods directly apply reliability theory to evaluate limit states requiring mode detailed modelling of loads and resistance after updating to account for site specific loads, resistances and deterioration. An illustration of the full probabilistic method together with an updating technique for relevant

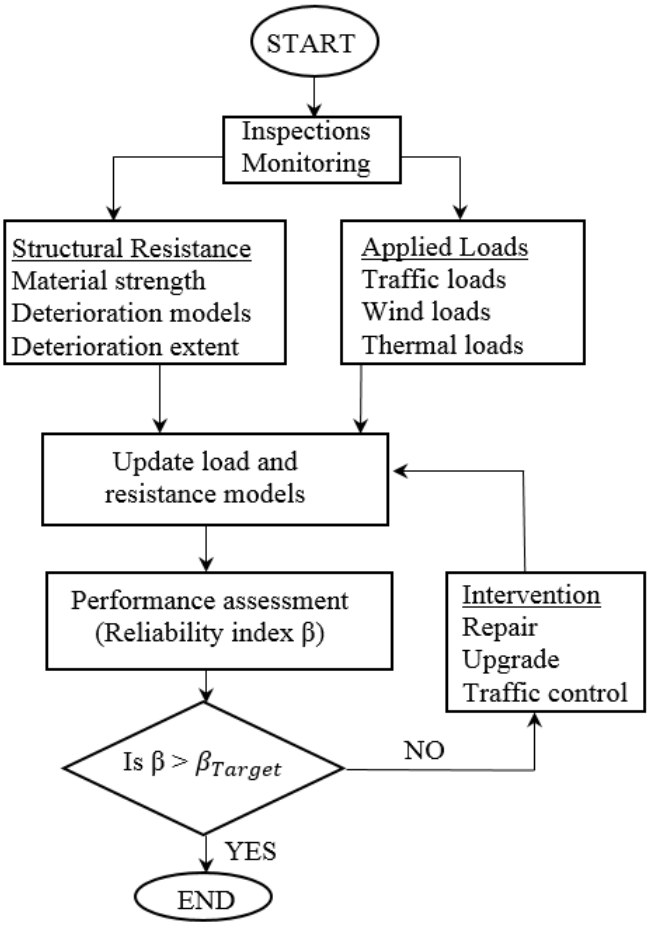

Figure 1.2: Bridge structural assessment framework [Kabani *et al.*, 2013]

variables is shown in Figs 1.2 and 1.3.

While a reliability based approach has to include both the resistance and loading aspects of the generic limit state equation as given in equation 1.1, it is generally acknowledged that there is greater uncertainty in live loading on bridges. This has lead to more focussed efforts especially in highway bridge applications to adjust design load models using site-specific traffic data to generate live models that can be used for structural assessment particularly in load rating factors [Bailey, 1996, Au *et al.*, 2005, Pelphrey *et al.*, 2008, Ghosn *et al.*, 2012].

There has been limited corresponding work on railway bridges other than in evaluation of fatigue evaluation. Research undertaken by the International Union of Railways showed that the live load model (LM 71) later adopted in

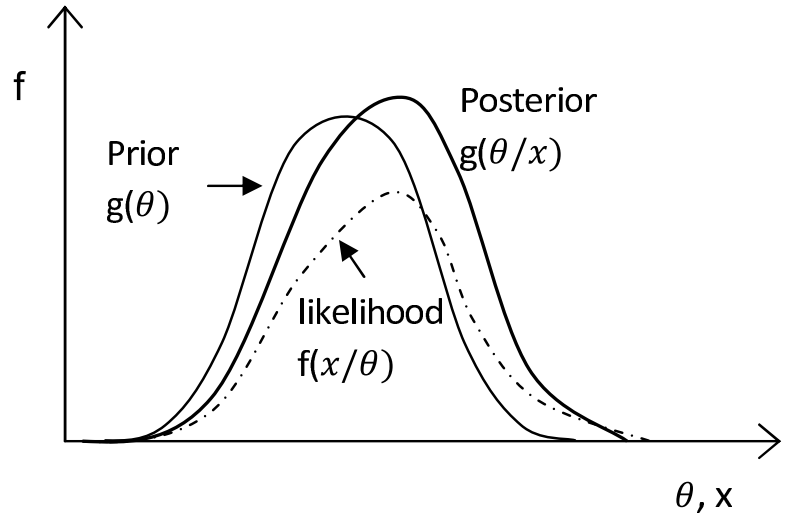

Figure 1.3: Bayesian updating of bridge resistance and loads

Eurocode was inadequate for traffic on international lines in Europe [EERI-D192/RP3, 1994]. Tobias *et al.* [1996] also showed that traffic on freight lines in the United States of America resulted in load effects close to and in some cases exceeding the load provisions of the Cooper E80 loads or the alternative loading. James [2003] studied load effects from traffic loads in Sweden on beam type bridges. However, this study was limited in scope to the mid span moment of simply supported beam type bridges of spans between 4m to 30m. Furthermore the study assumed no distribution of axle loads over rail and the dynamic response was limited to analytical study based on moving force with no modification for train mass. The study considered step change in traffic loading resulting from an increase in axle loads. The latter aspect has been analysed in highway bridge applications where an increase in axle loads generally leads to changes in axle configurations and axle spacing which alters the load effects envelopes as will be seen in Chapter 6.

In South Africa, there are two dedicated rail line corridors dedicated to heavy haul operations. These include the coal line with 26 tonne axle loads and iron ore line with 30 tonne axle loads [Kuys, 2009]. In addition, the operating trains on the iron ore with length of 4.1 km are some of the longest operational trains in the world. This research addresses some of the important factors required to formulate site-

specific loads that account for such high loads.2

1.3 Research objectives

Traffic loads on bridges vary in volume and composition over time and this has necessitated a need to review the current South Africa Transport Services railway bridge live model and investigate its suitability for use in bridge assessment. The investigation of load models and formulation of assessment live load models requires the use of weigh-in-motion datasets, instrumentation and monitoring of bridge responses and statistical tools. The objectives of this research are as follows:

1. Investigate through analytical methods and field measurements the frequency-time evolution of beam type bridges on heavy haul line arising from passage heavy axle train loads.

2. Investigate through analytical methods and field measurements the dynamic amplification factor of beam type bridges on heavy haul line arising from passage heavy axle train loads moving at constant and varying speeds.

3. Carry out a deterministic study of load effects from heavy-haul wagon axles and identify potential load effects and span lengths where the South African Railway live load model is exceeded for beam type bridges.

4. Carry out a probabilistic study of load effects from heavy-haul wagon axles and identify potential load effects and span lengths where the South African Railway live load model is exceeded for beam type bridges.

5. Carry out a probabilistic study of bridge load effects from heavy-haul wagon axles taking into account traffic volume growth and spatial dependence in axle loads.

1.4 Research contributions

This research contributes to the ongoing effort to formulate site specific live loads that can be used within the reliability based partial factor methods for structural assessment of bridges on heavy-haul rail lines. Currently this subject area is largely dominated by applications to site specific or route-specific live loads for highway bridges. Railway bridges on dedicated heavy haul lines are subjected to very high loads that are assumed to adversely impact their service life. This research carried out through analytical and field studies contributes to understanding of dynamic response of bridges subjected to high loads and the associated dynamic amplifications that arise. A continuous box-girder bridge on the South African heavy-haul rail line was instrumented in order to obtain dynamic strain response during train passage. Static vertical live load effects are computed based on weigh-in-motion data. A comparison of extrapolation techniques at selected return levels is made. Lastly the effect of traffic volume growth on return levels is investigated. In addition, the effect of dependence of axle loads arising from wagon load distribution on bogies and train loading is investigated.

1.5 Research Scope

The following are the limitations:

1. The probabilistic study is limited to short and medium span bridges with span length between 5m and 50m on the heavy haul.

2. The structural resistance of bridges and updating of structural resistance through bridge defect identification and material deterioration will not be done.

3. Existing weigh-in-motion (WIM) system data will be used for assessment load model formulation. This WIM system and data is managed separately by the railway operator.

4. A limited number of cross sections are instrumented with strain gages for field measurements study. These cross-section locations were chosen to allow monitoring of vibrations and crack growth.

1.6 Thesis outline

The thesis document is presented in 9 chapters exploring different aspects of the research undertaken. Chapter 1 gives the research motivations, problem statement, research objectives and research scope.

Chapter 2 provides a review of railway bridge live loads, showing the factors that influence static and dynamic bridge response and how they relate to bridge live loading models. Structural assessment techniques are reviewed as well as the use and formulation of live loads for assessment of bridges.

Chapter 3 presents the methods used to carry out this study. These include the instruments used and sensor layouts on the bridge that formed the case study. A summary of tools for modal parameter extraction and frequency-time evolution study are presented as these form the basis of field measurements and analytical studies presented in subsequent chapters.

Chapter 4 investigates the vibration of single and multi-span bridges on simple supports. The natural frequencies of such structural systems are obtained. The changes in frequency resulting from moving trains on multi-span bridges is investigated using both analytical and field measurement study. Chapter 5 builds on Chapter 4 by computing dynamic amplification factors based on an analytical moving force on beam formulation with modification of bridge frequency due to presence of added mass. The dynamic amplification factors are also computed based on measured strains at selected points on the case study bridge.

Chapter 6 presents a deterministic study of the heavy haul freight loading on beam-type structures. The deterministic study sheds light on potential areas and load effects that may be of interest for assessment purposes. Chapter 7

investigates the probabilistic loads based on weigh-in-motion data using classical extreme value theory. Three techniques that include the normal distribution, Bayesian method and block maxima are used to estimating loads at desired return levels under the assumption of no traffic growth and independence of axle loads.

Chapter 8 revisits the basic assumptions of independence between axle loads and uses an auto-regressive model to account for dependence of axle loads for wagons. The effect of such dependence firstly on extreme value distribution parameters and on return load levels is investigated. Traffic growth in terms of traffic volume increase based on historical data is included in the study. The effects of traffic growth on distribution parameters and return levels is investigated. Finally the combined effects of traffic volume growth and axle dependence are investigated.

Chapter 9 presents the main research conclusions and suggests areas for future research.

References

'BS EN 1991-2:2003', "Actions on strcutures part2: Traffic loads on bridges," Standard, British Standards Institution.

Cooper T., "Train loadings for railroad bridges," *Transactions of the American Society of Civil Engineers*, 31(1); 174–184, 1894.

Bailey S.F., *Basic principles and load models for the structural safety evaluation of existing road bridges*, Ph.D. thesis, EPFL, 1996.

Tobias D.H., Foutch D.A. and Choros J., "Loading spectra for railway bridges under current operating conditions," *Journal of Bridge Engineering*, 1(4); 127–134, 1996.

Melchers R.E., *Structural Reliability Analysis and Prediction*, John Wiley and Sons Ltd, 2 edition, 1999.

Bailey S.F., Antille S., Beguine P., Imhof D. and Bruhwiler E., "Niveau de securite requis pour l'evaluation de ponts-routes existants," *OFROU*, 2002.

James G., *Analysis of traffic load effects an railway bridges*, Ph.D. thesis, Royal Institute of Technology, 2003.

Au A., Lam C., Agarwal A.C. and Tharmabala B., "Bridge evaluation by mean load method per the canadian highway bridge design code," *Canadian Journal of Civil Engineering*, 32(4); 678–686, 2005.

Bhattacharya B., Li D., Chajes M. and Hastings J., "Reliability-based load and resistance factor rating using in-service data," *Journal of Bridge Engineering*, 10(5); 530–543, 2005.

Getachew A. and Obrien E.J., "Simplified site-specific traffic load models for bridge assessment," *Structure and Infrastructure Engineering: Maintenance, Management, Life-Cycle Design and Performance*, 3(4); 303–311, 2007.

O'Connor A. and Eichinger E.M., "Site-specific traffic load modelling for bridge assessment," *Proceedings of The Institution of Civil Engineers-Bridge Engineering*, 160; 185–194, 2007.

Pelphrey J., Higgins C., Sivakumar B., Groff R.L., Hatman B.H., Charbonneau J.P., Rooper J.W. and Johnson B.V., "State-specific lrfr live load factors using weigh-in-motion data," *J. Bridge Engineering ASCE*, 13(4); 339–350, 2008.

Sivakumar B. and Ghosn M., "Collecting and using weigh-in-motion data in LRFD bridge design," *Bridge Structures: Assessment, Design and Construction*, 5(4); 151–158, 2009.

Kuys, "Ore Line Capacity Expansion: Conceptual Design of the Railway Line to Increase Capacity," *International Haevy Haul Conference Proceedings*, 2009.

Holicky M., *Reliability analysis for structural design*, Sun Press, Stellenbosch, 2009.

Ryall M.J., *Bridge Management*, 2 edition, 2010.

Das P., "Bridge management objectives and methodologies," *Bridger Management 3: inspection, maintenance, assessment and repair*, 1–7, 2010.

Calgaro J.A. and Tschumi M.and Gulvanessian H., *Designers' Guide to Eurocode 1 - Actions on Bridges EN 1991-2, EN 1991-1-1, -1-3 to -1-7 and EN 1990 Annex A2*, ICE Publishing, 2010.

Wang N., O'Malley C., Ellingwood B.R. and Zureick A.H., "Bridge rating using system reliability assessment. i: Assessment and verification by load testing," *Journal of Bridge Engineering*, 16(6); 854–862, 2011.

Cremona C., *Structural Performance: Probability-based Assessment*, John Wiley and Sons Ltd, London, 1 edition, 2011.

Hayward A.C., "Train loads on bridges 1825 to 2010," *The International Journal for the History of Engineering & Technology*, 81(2); 159–191, 2011.

Ghosn M., Sivakumar B. and Miao F., "Development of state-specific load and resistance factor rating method," *Journal of Bridge Engineering*, 18(5); 351–361, 2012.

Cremona C., *Structural Performance: Probability-based Assessment*, John Wiley & Sons, 2012.

Brühwiler E., Vogel T., Lang T. and Lüchinger P., "Swiss standards for existing structures," *Structural Engineering International*, 22(2); 275–280, 2012.

Kabani M., Moyo P. and alexander M., "Challenges in reliability based bridge life-cycle management," in "Proc., Eleventh Int. Conf. on Structural Safety and Reliability, ICOSSAR2013. Deodatis G, Ellingwood BR, and Frangopol DM, eds. Boca Raton, FL: CRC Press, Taylor & Francis Group," 4733–4738, 2013.

Hayward A.C.G., "Train loading on bridges since stephenson's rocket," in "Proceedings of the Institution of Civil Engineers-Bridge Engineering," volume 167, 326–337, Thomas Telford Ltd, 2013.

Yi E.Z., chapter 14: Steel Bridge Evaluation and Rating, 351–379, CRC Press, Taylor & Francis Group, 2014.

Vinayagamoorthy M. and Tsang R., chapter 15: Concrete Bridge Evaluation and Rating, 381–441, CRC Press, Taylor & Francis Group, 2014.

Cremona C. and Poulin B., "Standard and advanced practices in the assessment of existing bridges," *Structure and Infrastructure Engineering*, 13(4); 428–439, 2017.

ERRI-D192/RP2, "Comparison of present and future rail traffic on international

lines with uic 71 loading based on deterministic calculation," Utrecht, April 1994.

EERI-D192/RP3, "Comparison of the effects of current and future rail traffic on international lines with the effects from uic 71 loading on a probabilistic basis," Utrecht, December 1994.

Chapter 2

BRIDGE LIVE LOADS FOR STRUCTURAL ASSESSMENT: A REVIEW

2.1 Introduction

Traffic loads on rail lines both in terms of traffic volumes and axle loads have progressively increased over the years since the advent of rail transportation due to increase in economic activities and technological advances in locomotive power. Railway traffic routes classified as heavy-haul lines are operated in several countries including South Africa. Heavy haul operations are competitive options on lines that mostly carry unit commodities in bulk such as metal ores. These operations have managed to achieve high tonnage in freight through a combination of higher axle wagons and longer trains made possible by technological improvements in locomotive power as well as distributed power systems. International Heavy Haul Association defines a heavy haul line as one that satisfies at least two of the following:

1. A line that operates trains or combinations of trains in that is at least 5,000 tonnes.
2. A line with an annual haulage of at least 20 million tonnes over a distance of at least 150 km.
3. A line operating with rail cars with axle loads of 25 tonnes or more

The South African heavy haul lines are operated by Transnet Freight Rail. These lines comprise of the coal line connected to the east coast while the iron ore connects to the west coast. The iron ore line which has heavier axle loads of 30 tonnes is narrow gage line that covering a distance of 861 km. The freight on the iron line has steadily increased from 18 million tonnes per annum in 1978 to the current freight tonnage above 60 million tonnes per annum. This increase in freight tonnage has been achieved through the adoption of longer trains and increasing axle loads from original 26 tonnes to the current 30 tonnes.

Traffic loads are one of the principal loads on railway bridges and in design these loads are further broken down as static live loads, dynamic impact load resulting from rapid application of force from moving traffic, rocking forces due to the effect of rail profile and wind on moving traffic and the longitudinal forces due to changes in speed of traffic during crossing [Unsworth, 2010, Pipinato and Patton, 2016]. In design codes for railway bridges, the shear and moment load effects are obtained through a combination of point loads and uniform loads that are formulated to simulate load effects on bridges. Design live loads such as South African Transport Services [1983] do not represent any idealized locomotive. South African Transport Services [1983] is based on the International Union of Railways (UIC) load model LM71 with appropriate adjustments to account for the higher axle loads. Currently, bridges on the American heavy haul lines are designed to Cooper E80 load which is based on the initial Cooper Loads that are based on coupled locomotive engines followed by wagon load [Cooper, 1894, Unsworth, 2009].

In many countries, heavy haul freight is carried on lines with bridges that were originally designed for lower axle loads than currently experienced. Indian Rail upgraded their freight rail from 22 tonne axle loads to 25 tonnes axle loads to improve their profitability [Martland, 2009]. In China, the ShuoHuang rail line was originally designed for 25 tonnes and is currently in the experimental phase of introducing 30 tonne axle wagons [Ma *et al.*, 2017]. However such increases in axle loads can potentially increase tear and wear as well as maintenance and

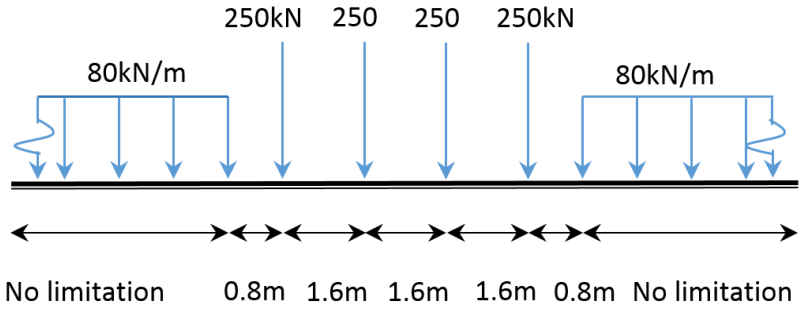

Figure 2.1: UIC Load Model 71

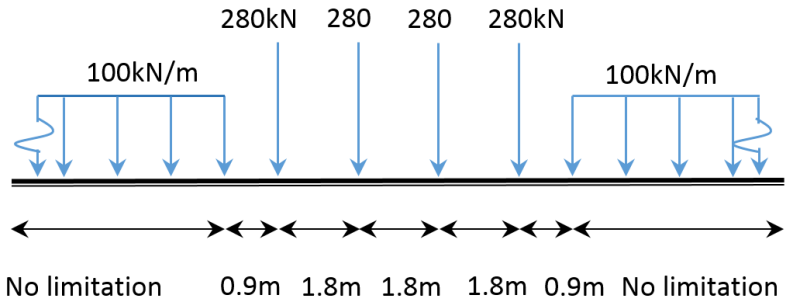

Figure 2.2: SATS 1983 Notional Loading

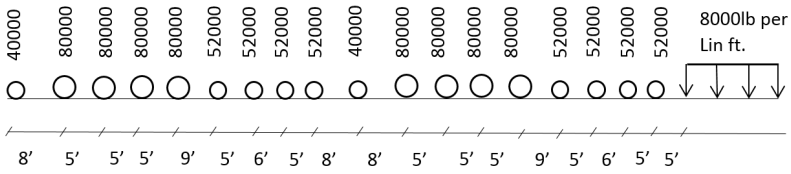

Figure 2.3: Cooper E80 loading

repair costs of ageing bridges on freight lines. The heavier trains induce higher stress cycles especially in short span bridges thus reducing their fatigue life while longer trains increase number of stress-cycles. The increase in axle loads of trains on ageing bridges also reduce the inbuilt design safety margin.

Tobias and Foutch [1996] conducted measurements of the loading spectra of a total of 508 trains that consisted of unit commodity, mixed freight and inter-modal trains. The heaviest axles for the three train classifications were obtained from Coal hopper wagons for unit commodity trains, five-pack inter-modal for the inter-modal trains and four-axle mixed freight for the last category. The corresponding 95% fractal axle load for the unit commodity,

inter-modal and mixed freight wagons were 34.86, 28.13 and 32.21 tonnes respectively. An analysis was done of the shear and bending moments produced by loaded freight cars and compared with the load effects from Cooper E80 or AREA equivalent loading. The bending moments from actual traffic were in the range of 72% to 82% of the effects obtained from Cooper E80 loads for simple span lengths from 9.1m to 27.4m respectively. The shear effects on the other hand were between 74% and 102% of the Cooper E80 loading shear. Thus it was shown that the conservativeness in American Railway Bridge design live loads diminishes for simply supported bridges on freight lines diminish as span length increases.

Leighty *et al.* [2004] considered the impact of introducing heavy axle loads on short-line rail-road in Pennsylvania in the United States. A random sample of 25 bridges were drawn from a population of 1174 bridges. The population comprised of 84% steel and 4% concrete bridges with the rest being timber and masonry bridges. Out of the sample of 25, only 12 bridges could support Cooper E80 load.

These challenges arising from heavy-haul developments have led to innovations in inspection, performance assessment, maintenance or upgrade critical infrastructure such as bridges. In comparison to rail bridges, some extensive research has been conducted on highway bridges and this will be discussed where appropriate if the parameters impacting bridge structural performance apply to both rail and highway bridges. Areas of departure between rail and highway bridge arising from loading regimes are highlighted.

2.2 Chapter objectives

The objective of this chapter is to provide an overview of live loads for structural assessment of shear and moment load effects of bridges on heavy-haul rail freight lines. A review is provided on structural assessment methods, live load estimation techniques and use of site-specific data in formulate a live load models. Parallels and differences dynamic response of rail and highway bridges reviewed to identify critical parameters that influence dynamic amplification factors.

2.3 Structural assessment methods for bridges

Bridges are important components in a transport network and their structural performance if not satisfactory can be bottleneck in transportation of goods. Bridge Management Systems (BMS) have been developed to help manage bridges from the time of construction to the end of their design life. The most widely practised methods of bridge assessment are done within the framework of BMS whose basic components as shown in Fig 2.4. Examples of BMS are Pontis developed in the United States, J-BMS developed in Japan, HiSMIS developed in the United Kingdom and Struman developed in South Africa [Ryall, 2010]. A BMS will generally have an inventory module which contains all the information about the bridge such as as-built drawings, maintenance records and location. The inspection module gives the bridge inspection reports. The maintenance module gives the maintenance records while the condition module provides an assigned score of the bridge based on information from inspections and the importance of the bridge in the network. A BMS will have project specific applications such as bridge load rating or maintenance action which relate to individual bridges. Some applications on the other hand will relate to network level management where actions such as maintenance are carried out on a bridge stock [Vassie and Arya, 2008].

Several methodologies for bridge assessment have been proposed with varying degrees of complexity from material level assessment to evaluation of structural response based on proof load tests and refined reliability based analysis. In bridge management systems through the condition module, bridge evaluation is done by condition rating based largely on information from visual inspections of the bridge. The condition ratings are either done on individual bridge elements or done on bridge components such as bridge deck or superstructure [Washer, 2014]. Condition ratings are assigned on a scale of increasing deterioration and the final bridge ratings are combined into a bridge condition index that also accounts for the importance of a bridge based on its location on a network and

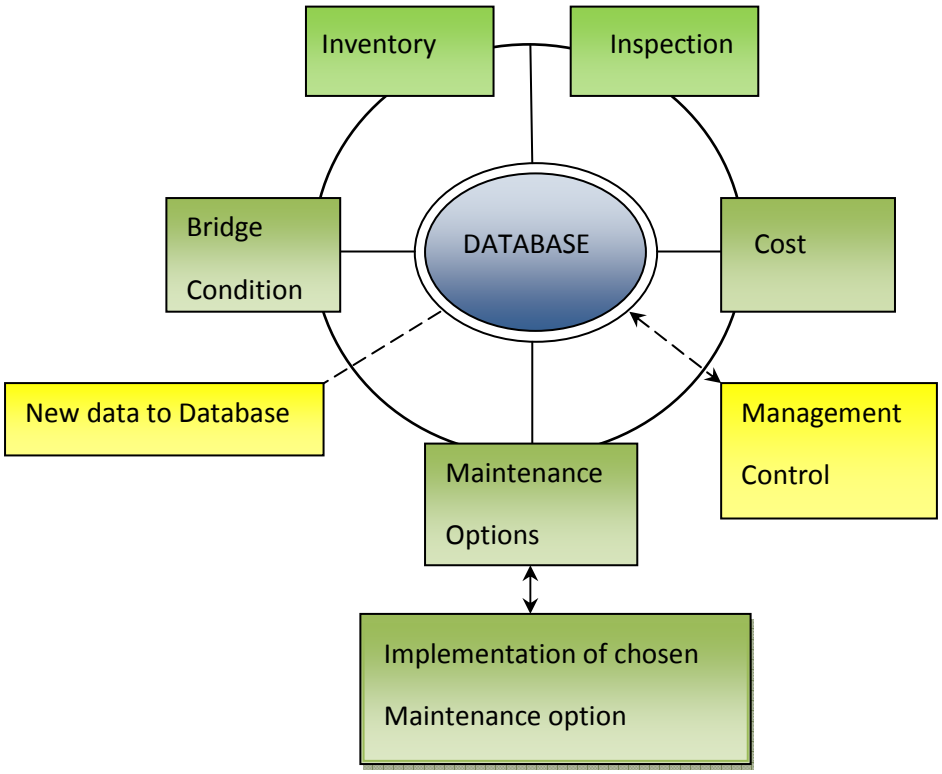

Figure 2.4: Basic components in a BMS [Ryall, 2010]

availability of possible detours [Fu and Devaraj, 2014]. The Pontis Bridge Management System provides a capability to determine transition probabilities of bridge component condition rating over time based on historical data of deterioration rates from previous inspections or from expert judgement. The South African Struman on the other hand evaluates deterioration of bridges on a 4 point system defects (D), extent (E), relevance (R) which looks at bridge safety and serviceability and urgency (U) to indicate urgency of required repair action based [Branco and Brito, 2004]. The main drawback of condition ratings is the high dependence on visual inspection data which has been shown to give low defect detection rates [Washer, 2014]. However this aspect can be addressed by use of non-destructive tests. Another drawback of condition ratings is the arbitrary scales for deterioration levels where some BMS give a scale of 1 to 5 while others give a scale of 1 to 9 in addition to sometimes subjective scores from inspectors on severity of deterioration [Fu, 2013].

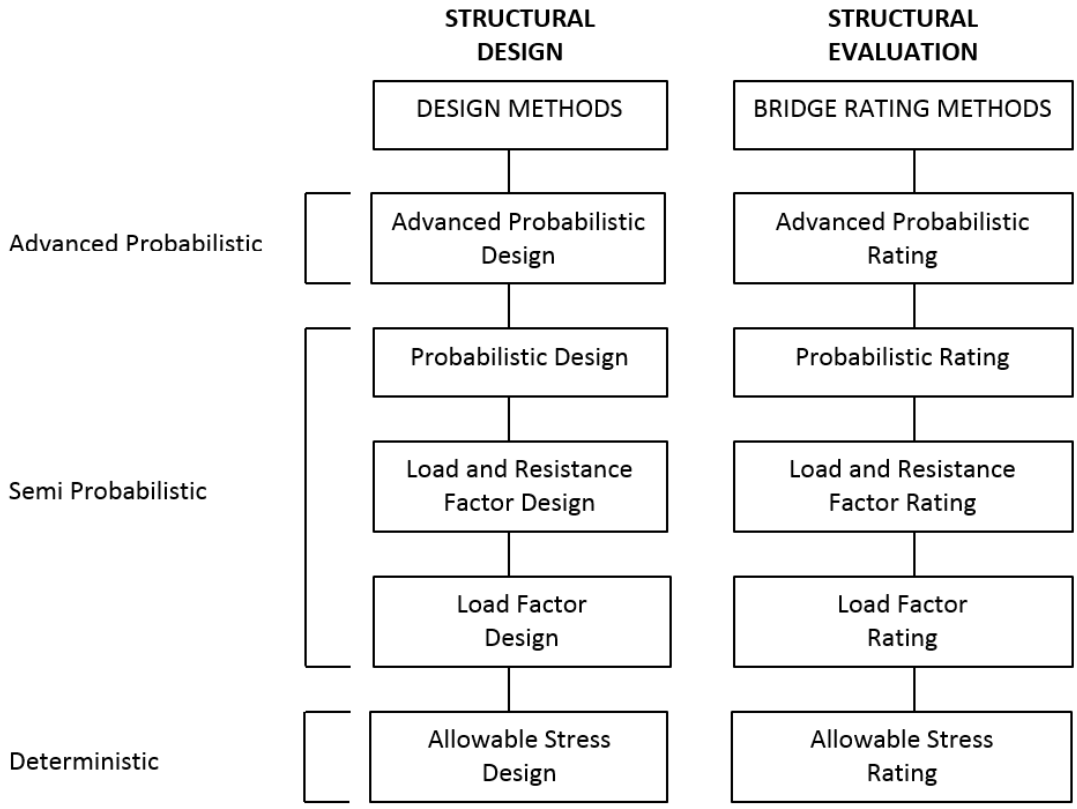

Figure 2.5: Design and rating levels (adapted from Akgül and Frangopol [2004])

While condition rating focuses on material deterioration of bridge elements, the load carrying capacity can be determined through load testing and rating. Bridge structural evaluation is usually performed after signs of damage or deterioration to bridge components have been identified from bridge condition surveys. Structural evaluation methods closely mirror those applied in design and can be classified as deterministic, semi-probabilistic or probabilistic methods depending on their treatment of uncertainties as shown in Fig 2.5. The allowable stress rating (ASR) just like allowable stress design (ASD) is a deterministic method where specified loads are supposed to induce stresses that are a fraction of the material yield stress in a structural element [Barker and Puckett, 2013]. The next level methods such as Load and Resistance Factor Rating which mirror the Load and Resistance Factor Design also known as partial factor methods are classified as semi-probabilistic methods. The formulation of partial factor methods gives deterministic expressions while probabilistic analysis is done on

input parameters to determine the load and resistance partial factors that correspond to a given level safety [Cremona and Poulin, 2017]. In addition, partial factor methods take into consideration factors such as failure modes, level of inspection and system behaviour [Allen, 1992, O'Brien *et al.*, 2005]. Higher level methods require performance requirements formulated as limit states equations. The statistical information on all variables in limits states is obtained and the probability of failure with respect to considered limit state equations is computed and checked against target values. In addition, higher level methods may consider life-cycle costs and social-economic aspects arising in the event of structural failure [O'Brien *et al.*, 2005].

Structural assessment methods based on reliability theory have been largely adopted into codes and guidelines for assessment of bridges such as Swiss Standards for existing structures [Brühwiler *et al.*, 2012]. The Swiss Standard for existing structures for example, proposes three levels of assessment starting with deterministic assessment based on the updated ratio of the structural resistance to load effects. If a structure is found deficient, a semi probabilistic method is applied that requires probability distributions of basic variables to be determined. In a full probabilistic verification, the basic variables are expressed as random variables in limit state equations for reliability analysis.

O'Brien *et al.* [2005] outlines the guidelines arising from the European Bridge Management in Europe (BRIME) project that gives 5 levels of assessment in varying degrees of complexity. Assessment level 1 is a simple bridge analysis using assessment partial factors. Level 2 assessment employs more refined analysis and material strengths based on available data are used. In level 3 assessment, site specific loading and material properties from tests of the existing structure are used. Level 4 assessment is a modification of level 3 assessment where adjustments are made to the partial factors based on expert judgement. Finally level 5 assessment is a full probabilistic analysis requiring key parameters of loading and resistance to be expressed as random variables. Similar recommendations have been propped in France for evaluation of existing

structures though on a compressed 4 level assessment scale [Cremona and Poulin, 2017]. The first level designated as Level 0 analysis is done by reviewing inspection reports to check if there are any concerns regarding a particular structure. Level 1 analysis involves the use of design standards to assess bridges that show no sign of damage or deterioration. Level 3 assessment requires the use of bridge specific data that includes material properties obtained from tests and bridge loads. This bridge specific information is used to modify partial factors. Level 4 assessment is a full reliability analysis requiring the use of probability densities of basic variables and setting an appropriate target reliability reflecting the desired level of safety.

Alternative methods of analysis that do not strictly follow the complexity progression of reliability based procedures exist. Pipinato and Patton [2016] breaks down bridge assessment into preliminary evaluation, detailed investigation, expert investigation and expert investigation. A preliminary evaluation serves the purpose of verifying the as-built drawings and document any modifications since a given bridge was built. Any forms of degradation of bridge elements are documented. A detailed investigation performs checks based on code provisions to ensure the bridge is safe which is aided by finite element models. An expert investigation involves on-site testing and dynamic analysis of the structure. Finally if a bridge is found deficient from expert investigation then non-destructive testing and design code verification are carried out followed by an updated finite element model.

Other methods outside the described framework above include load testing which can be diagnostic or proof load testing and load rating. Diagnostic load testing can be used to understand bridge structural behaviour, verify design assumptions such as transverse load distribution or estimate bridge including determining contribution of non structural elements. It can also be used to check the effect of rehabilitation measures and to check bridge performance over time. Proof load testing is used to determine if a bridge can carry prescribed factored live loads. Proof load testing is employed where structural analysis of a

bridge is deemed difficult due to levels of deterioration or lack of bridge documentation [Faber *et al.*, 2000, Branco and Brito, 2004, Lantsoght *et al.*, 2017]. Proof load testing also known as diagnostic load test does not determine the bridge ultimate load but demonstrates that the ultimate load is greater than the proof load. While proof load testing gives a better understanding of bridge response, it is time consuming and can cost as much as 6% of cost of bridge replacement [Faber *et al.*, 2000]. Load rating on the other hand gives a ratio of the structural resistance to the loads imposed on the bridge. Bridge load rating can be deterministic or probabilistic with or without the use of site specific information of the bridge being rated [Bailey, 1996].

Bhattacharya *et al.* [2005] proposed three requirements that should be satisfied by a bridge rating method. The rating should be based on a measurable concept of safety. This requirement is dependant on how the safety measure is formulated in order to accommodate uncertainties as will be seen later. The rating measure should be able to distinguish between safe and unsafe bridges with associated safety margins. This is necessary so that repair, maintenance and replacement can be prioritised within budgetary constraints faced by bridge managers. Lastly, rating should be able to accommodate the use of site information to account for uncertainties in loads and material strengths. In line with the above, bridge ratings that are performed in increasing levels of sophistication according to Allowable Stress Rating (ASR), Load Factor Resistance (LFR) or Load and Resistance Factor Rating (LRFR) methods all of which are based on the fundamental equation 2.1 given in equation 2.1 [Wang *et al.*, 2011]:

$$\gamma_{Dn} D_n + \gamma_{LL}(L + I) < C \tag{2.1}$$

where γDn, γ_{LL} are dead load and live load factors, L,I are the live load and dynamic amplification respectively while C is the resistance capacity of the component under consideration. The Rating factor RF follows from equation 2.1 and is given in equation 2.2:

$$RF = \frac{C - \gamma_{Dn} D_n}{\gamma_{LL}(L + I)} \tag{2.2}$$

where $RF \geq 1.0$ implies that a bridge can safely carry the load while $RF < 1.0$ indicates failure to meet required safety level for given live load.

The Canadian Highway Bridge Design Code (CHBDC) for bridge evaluation gives the LRFR method similar to equation 2.2 and proposes another method of rating called Mean Load Method [Au *et al.*, 2005]. The Mean Load Method rating factor is obtained from equation 2.3:

$$RF = \frac{\bar{R}\exp\left(-\beta\sqrt{V_R^2 + V_S^2}\right) - \sum \bar{D}}{\bar{L}} \tag{2.3}$$

where $\bar{R}$ is the mean resistance, $\bar{D}$ is the mean dead load, $\bar{L}$ is the mean live load effect including dynamic amplification, V_S is coefficient of variation of load, V_R is coefficient of variation of resistance and β is the target reliability index. Allen [1992] gives the main factors used in determining the target reliability β as failure mode of bridge components being sudden with or without post failure capacity, or gradual failure with warning Δ_E, importance of element in relation to bridge failure Δ_S, ease of element inspection Δ_I and traffic category Δ_{PC}:

$$\beta_1 = 3.5 - [\Delta_E + \Delta_S + \Delta_I + \Delta_{PC}] \geq 2.0 \tag{2.4}$$

The American Association of State Highway and Transportation Officials (AASHTO) ASR and LFR methods are performed for inventory and operating levels. The inventory load rating which is the rating requirement for an indefinite period which corresponds to the design safety value of $\beta = 3.5$ and the operating load rating which is rating for shorter period of 5 years corresponding to $\beta = 2.5$. In the ASR method, $\gamma_{Dn} = \gamma_{LL} = 1.0$ in equation 2.2 for both inventory and operating rating load levels. In the LFR method, $\gamma_{Dn} = 1.30$ and $\gamma_{LL} = 2.17$ for inventory rating while $\gamma_{Dn} = \gamma_{LL} = 1.3$ for operating level rating. The LRFR on the other hand specifies three rating levels which are design load, legal loads and permit loads rating. Design load rating is further broken down to inventory and operating levels [Wang *et al.*, 2011, Fu, 2013, Vinayagamoorthy and Tsang, 2014]. The AASHTO LRFR gives provision to reduce the resistance capacity of a component in equation 2.2 due to deterioration by a maximum of scaling factor

0.85 for a member in poor condition. Although Rating Factor (RF) can give the available margin of safety, the most widely adopted safety measure in limit states based design codes is reliability index (β) which was introduced in Chapter 1. Akgül and Frangopol [2004] conducted a study of 14 bridges on a road network in Colorado (United States of America) and showed that at the start of service life there is good correlation between RF and β of steel and concrete bridge girder components in flexure and shear with the exception of flexure of steel welded plate girders. The RF and β for flexure of welded plate girders were clustered with very little variability and this resulted in correlation coefficient of 0.13. Akgül and Frangopol [2004] considered the time dependent effects of resistance degradation over time and showed that RF was not an accurate measure of safety. A deteriorated 34.1m single span prestressed concrete bridge showed a reduction of 37% of RF compared to 51% reduction in β.

The load rating equation given in 2.2 allows for use of site specific data that can be used to modify partial factors while 2.3 for direct use the site-specific data. The main motivation of using site specific-data especially weigh-in-motion (WIM) data for live loads is to reduce uncertainties in modelling of traffic loads. Pelphrey *et al.* [2008] used WIM data in the State of Oregon in the United States of America to modify the AASHTO LRFR provided factors. The study investigated the effect of the length of duration for WIM data monitoring which considered 2 week and 4 week periods. An investigation of effect of seasonality on live load factors were considered. The truck events were then put in classes according to gross weight, axle group weight and length and only the top 20% in each category were used in the analysis. It was shown that there is a general drop in live load factors from recommended AASHTO LRFR of 1.80 to 1.40 for the same target uniform safety level for bridges for a 5 year rating period. The effects of seasonality were significant as there were differences in traffic between winter and summer. Seasonal variations resulted in up to 13% difference in live load factor. The difference between 2 weeks and 4 weeks monitoring period were insignificant.

Ghosn *et al.* [2012] conducted a similar study using WIM data to calibrate the LRFR partial factors for New York State. The live loads in New York were significantly higher than the live loads used for calibrating AASHTO LRFR. Thus a set of rating trucks based on WIM data were proposed. The target safety $\beta = 2.0$ was adopted based on engineering practice. The live loads from calibration process were significantly lower for all categories of permit trucks with $\gamma_L = 1.20$ for annual divisible load on multilane bridges in contrast with $1.20\gamma 1.8$ as obtained from AASHTO LRFR. This study shows that it is necessary to revise live load model as well as partial factors if significant differences with WIM data are observed.

Wang *et al.* [2011] studied 4 sample highway bridges that included a straight reinforced concrete (RC) girder bridge, a skewed RC bridge, a prestressed concrete bridge and a steel girder bridge. The tests from concrete cores showed 93% increase in strength over a 50 year period compared to the 28 day strengths specified at design. A finite element model was created and updated on basis of data from material strengths and proof load tests. This detailed model was used to obtain girder distribution factors and study shear capacity. A high degree of conservatism was observed in all bridges with at least a factor of 5.9 on design live loads. Davids *et al.* [2012] compared the load rating factors obtained by using approximate analysis methods in AASHTO with those obtained from finite element models of flat slab concrete bridges. The ratings from finite element models were between 13% to 44% higher than those obtained from AASHTO approximate methods with the lower increases observed on slabs with skew angle of less than 10.25^0 while the higher increases were from slabs with skew angle of 15^0.

Sanayei *et al.* [2015] studied the effects of transverse load distribution on the load rating of 3 span continuous slab on steel girder bridge. The load effects in the 6 longitudinal girders were first estimated using simplified two dimension (2-D) girder by girder analysis with design code based transverse load distribution coefficients. In the second method, the load distribution coefficients

were estimated from strain measurements during diagnostic load test. The updated coefficients were included in a modified method using 2-D the conventional girder analysis. The third method involved creating a finite element model and calibrating it to the strains from load test. The simple 2-D model gave the lowest result with inventory load rating of about 2.40 for interior girders. This is because this method ignores the composite action from the concrete slab as well as the stiffening effects from non structural elements such as parapets. The modified 2-D and finite element model inventory ratings were generally higher with interior girders having inventory rating above 3.50 compared to the the first method.

Load rating is simply the ratio of available structural resistance to the loads applied, thus the rating factor obtained can vary depending on the formulae applied. Au *et al.* [2005] made a comparison of the CHBDC LRFR and the Mean Load ratings for a simply supported 39.62 span bridge consisting of 3 steel box girders and composite reinforced concrete deck. The LRFR method and Mean Load methods gave ratings of 1.73 and 1.80 respectively for the live load based on coefficients and dynamic amplification from the code. The CHBDC allows for the use of coefficients from field measurements in the Mean Load method. Based on statistical parameters from measurements of live loads on site, the Mean Load method gave a higher rating of 2.83 for the same $\beta = 3.0$. Feldman *et al.* [2011] conducted a similar study on a 3 span continuous reinforced concrete bridge with end span length of 30.9m and 38.7m for the middle span. The bridge was load rated based on 62.5 tonne and 110 tonne trucks using the CHBDC LRFR and Mean Load methods. In general, the rating for flexure for interior girder was slightly higher than for exterior girders for both methods with $RF \geq 1$. The ratings based on field measurements of 135 truck events were found to be higher than those obtained by using coefficients from the code.

The literature on load rating of railway bridges for vertical live load effects besides fatigue is not as extensive as that of highway bridges. The AREMA gives a guide where railway bridge rating is done either as normal rating or maximum rating

[Unsworth, 2009, Zhou, 2014]. Normal rating determines the load level that can be carried by a bridge safely for its expected life dependant on specified speeds. Maximum rating is done for exceptional loads within speed limits. The AREMA rating approach is based on the allowable stress method which as shown in Fig 2.5 is a low level deterministic method of bridge rating.

Most of the recent research on highway bridge assessment has focused on use of WIM data to modify partial safety factors for live load. The critical characteristics of traffic that affects vertical live load factors include traffic composition, axle group weights, vehicle geometry and headway distances between vehicles [Bailey and Bez, 1999]. Pelphrey *et al.* [2008] used WIM data in the State of Oregon in the United States of America to modify the AASHTO LRFR provided factors. The study investigated the effect of the length of duration for WIM data monitoring which considered 2 week and 4 week periods. An investigation of effect of seasonality on live load factors were considered. The truck events were then put in classes according to gross weight, axle group weight and length and only the top 20% in each category were used in the analysis. It was shown that there is a general drop in live load factors from recommended AASHTO LRFR of 1.80 to 1.40 for the same target uniform safety level for bridges for a 5 year rating period. The effects of seasonality were significant as there were differences in traffic between winter and summer. Seasonal variations resulted in up to 13% difference in live load factor. The difference between 2 weeks and 4 weeks monitoring period were insignificant.

Tabatabai *et al.* [2017] conducted a study based on WIM data from Oregon in the United States to determine the severity of truck loading on simply supported bridges with span length ranging from 6.1m to 73.2m. The WIM data was collected over a period of one year with close to 6 million truck events recorded. The data was sorted into vehicle class with the most frequent being class 9 which is a 5 axle single trailer truck. Only the top 5% was considered to be important for determining extreme shear and moment load effects. A critical contribution of this study was in treatment of axle weight and axle spacing as dependent. This dependence is justified as heavy vehicles often have special axle configurations. In

the study, the effects of dependence between axle weights and axle spacing were modelled using using empirical copulas in ModelRisk® software. The extreme moments and shear were obtained from the 95% fractile to 100%fractiles with 99% chosen as design point. The 99% fractile shear and moments for class 9 trucks corresponded to 99.28% fractile of moments and 99.30% fractile for shear of all the truck classes and thus this class was used as basis for evaluating other truck load effects. The computed load effects were compared with effects from the HL-93 AASHTO LRFD design truck resulting in average live load factor of 1.60 for moments and 1.54 for shear effects.

While most of the cited research above has focused on WIM data to update highway bridge live loads, the reliability framework provides for inclusion of resistance parameters as well. O'Connor and Eichinger [2007] used site specific data to assess the load effects on a single span reinforced bridge. A WIM system was installed on the bridge over a period of 4 days with a total of 16663 truck events recorded. In this study, a series of strain gages were attached on the soffit of the deck and calibrated vehicles passed on the bridge to obtain the bridge experimental influence line. The truck data was fitted to probability distributions and Monte carlo simulation used to simulate traffic passage. Other parameters included in the study were gross vehicle weight and axle spacing. In this study, it was found that there was no correlation between gross weight and axle spacing. The characteristic load effects were obtained at 95% fractal. It was observed that the load effects with dynamic amplification included were up to 20% less than load effects from deterministic code based analysis. However the main drawback of this study was the limited duration for WIM data collection that could not have reflected the weekly, monthly or seasonal variations.

The benefits of using probabilistic approach that incorporates site-specific data have been demonstrated on highway bridges. Lauridsen *et al.* [2007] list several cases in Denmark such as the Vilsund bridge were a design code based deterministic analysis gave a maximum vehicle gross weight restriction of 40 tonnes while a probability based analysis resulted in a higher value of 100

tonnes thus saving money in terms of bridge strengthening. Similarly, a deterministic analysis of Skovdiget and Storstroem bridges showed that the remaining life was exhausted while a probabilistic study showed 15 years and 10 years reaming live respectively and thus resulting in cost saving which could have been accrued by replacing the bridges earlier.

Research on railway bridges outside fatigue assessment is not as extensive as that on highway bridges. There are differences between railway and highway traffic, the former operates on schedules and on heavy haul freight lines will mostly comprise of similar train configurations carrying unit commodities and thus producing very similar loading. Headway distances may not be a parameter of interest as railway traffic operates on train schedules. Caglayan *et al.* [2012] considered the load effect of existing rail traffic consisting of 225kN axle freight cars on component and system reliability of a girder and truss bridge in Turkey. Ambient vibration tests were conducted and the resulting natural frequencies and mode shapes used to update finite element models. A bridge load rating was first done and then reliability index obtained. The system reliability index $\beta = 5.99$ for the 40m span riveted girder bridge with current traffic was obtained which was much higher than the $\beta = 4.98$ obtained from UIC LM 71 load model. A study of a 20m long truss girder gave $\beta = 4.93$ for 21m span truss bridge with current traffic while the index $\beta = 4.06$ under UIC LM71 model loads. This study demonstrated that the conservativeness in bridges designed to load model UIC LM71 could vary depending on type of traffic, bridge type and span lengths.

A comprehensive study was conducted by the UIC on the adequacy of UIC LM71 for future traffic in Europe [ERRI Report D192/RP2, 1994, ERRI Report D192/RP3, 1994, ERRI Report D192/RP1, 1993]. The probabilistic study was done using simulated trains as formulated in [ERRI Report D192/RP1, 1993] representing European traffic based on survey from railway operators. The study considered load effects of mid span moment, support moment and support shear for single span, 2 span and 4 span beam bridges with spans ranging from 1m to 200m lengths. The study demonstrated that the load model LM71 would not be sufficient

to account for future growth of 300kN tonne axle loads on international lines.

This section shows a wide range of bridge assessment methods that are largely developed and applied to highway bridges. Traditional methods of assessing bridges rely on data collected from visual inspections as required by different bridge management systems. These inspections are used to detect and quantify damage to bridge components which is indicated by component condition rating. The load carrying capacity of a bridge is computed by reducing component resistances based on load rating and determining site specific loads. More recent assessment guidelines give assessment procedures that increase in complexity from deterministic to probabilistic methods that directly make use of material resistance and site-specific load information. Due to the variations in site specific traffic loads, protocols have been proposed on how to use weigh-in-motion data to formulate live loads or modify code based design live loads for bridges. The determination of site-specific loads for assessment and use of weigh-in-motion data is presented in section 2.4.

2.4 Determination of bridge assessment live loads

Traffic loads are one of the principal loads on railway bridges and in design these loads are further broken down as static live loads, dynamic impact load resulting from rapid application of force from moving traffic, rocking forces due to the effect of rail profile and wind on moving traffic and the longitudinal forces due to changes in speed of traffic during crossing [Unsworth, 2010, Pipinato and Patton, 2016]. The review above showed that design live loads for highway bridges are generally conservative. However, the this conservatism has not been demonstrated on railway lines especially those on freight corridors. Conservativeness in design can be justified by the increase in the safety margin of new bridges. Moreover, bridge construction and life-cycle costs have been shown to be less sensitive to the conservativeness in design codes [Calgaro *et al.*, 2010]. A comparison for two case studies of railway bridges designed based on UIC LM71 and $1.4\times$LM71 showed that there was only a small increase in

construction costs of 6% for case without traffic interference and 2% for the case with traffic interference.

Conservative loads for assessment can lead to unnecessary load restrictions on bridges and costly bridge repairs or upgrades. Recommendations for assessment live loads for railway bridges have been put forward to adjust the design live load model depending on the age of the bridge and the expected remaining life. For bridges with remaining life of 50 years, the baseline LM71 loads are applied while it is recommended that a scaling factor $\alpha = 1.33$ be applied to LM 71 loads for bridges with remaining life greater than 50 years [Calgaro *et al.*, 2010]. This latter recommendation places the live load requirements at the same level with new bridges on international lines in Europe. A significant amount of research has been conducted to show how site specific live loads can be formulated for highway bridges [O'Brien *et al.*, 2005, O'Connor and Eichinger, 2007, Brühwiler *et al.*, 2012, Cremona and Poulin, 2017]. The traffic characteristics that affect a live load model for highway bridges are vehicle gross weight, axle spacing, velocity, headway distances and presence of multiple vehicles on a bridge. Railway traffic shares some of these characteristics though other factors like headway distances may not be important as trains follow schedules. Furthermore, heavy-haul freight generally runs on dedicated rail corridors.

2.4.1 Static live loads in bridges

It is necessary to collect information on traffic characteristics to inform the live load modelling process. Protocols on collection of WIM data for use in highway live load model calibration exist and these include defining requirements for the WIM system to collect individual or group axle weights, gross vehicle weight, axle spacing, vehicle speed and time stamps for vehicle events [Sivakumar *et al.*, 2011]. Other factors to consider are site for WIM location, WIM maintenance, calibration and data quality control. WIM data is usually checked and filtered to remove events with inaccurately recorded weights or speed.

Although the need for quality accurate data can not be overstated, highway bridge

live load modelling is not very sensitive to WIM system accuracy. O'Brien *et al.* [2005] report that an accuracy level C(15) which requires 95% of measured gross vehicle weight to be within 15% of exact static weight is sufficient for load modelling purposes. O'connor and O'brien [2005] studied the impact of random error in WIM axle weight data on characteristic load effects. The load effects of interest were mid span moment of single simply supported beam and two span continuous beams as well as the support moment of continuous beam for span lengths ranging from 5m to 200m. It was shown that the shorter spans where contribution of individual axles is dominant were more sensitive to the level of accuracy of WIM data. Thus for spans less than 50m, the minimum accuracy of C(15) is required and duration of monitoring should be longer. A lesser accuracy could be used for spans above 50m and shorter WIM data duration to obtain load effects within 5% accuracy. The duration of monitoring however depends on the application whether it is load modelling for design or assessment. In applications for highway bridge load modelling, data is collected for at least a year to capture seasonal variations [Sivakumar *et al.*, 2011, Tabatabai *et al.*, 2017]. However, shorter WIM data collection durations of a week have been used to model assessment loads [O'Brien *et al.*, 2005, O'Connor and Eichinger, 2007]. In these cases, Monte carlo simulations are used to generate longer synthetic traffic streams.

The formulation of live loads for bridge design or assessment loads deals with the occurrence of rare loading situations and fall in the domain of extreme value statistics applied either to actual load effects data or simulated data of load effects. The upper tail of load effects histograms is of interest in load modelling. Let X_1,X_2,...,X_n be a sample of independent and identically distributed (iid) random variables from a parent cumulative distribution function (c.d.f) F of load effects. Then the maximum Z_n is defined as equation

$$Z_n = \max(X_1, X_2, ..., X_n) \tag{2.5}$$

The distribution of maximums F_Z is given in equation 2.6:

$$F_Z = P(Z \leq x) = \prod_{i=1}^{n} P(X_i \leq x) = F^n(x) \tag{2.6}$$

In practice, the parent c.d.f may not be known and thus equation 2.6 can not be readily applied. However, if the variables for partial maxima are renormalised some non-degenerate asymptotic distributions G can be obtained and these will belong to the following distribution families [Coles, 2001]:

$$\text{Gumbel (Type 1) } G(x) = \exp\left\{ -\exp\left[-\frac{x-\mu}{\sigma}\right]\right\}, \ -\infty < x < \infty \tag{2.7}$$

$$\text{Frechet (Type II) } G(x) = \begin{cases} 0 & x \leq b \\ \exp\left\{ -\left(\frac{x-\mu}{\sigma}\right)^{\xi}\right\} & x > b \end{cases} \tag{2.8}$$

$$\text{Weibull (Type III) } G(x) = \begin{cases} \exp\left\{ -\left[-\left(\frac{x-\mu}{\sigma}\right)^{\xi}\right]\right\} & x < b \\ 1 & x \geq b \end{cases} \tag{2.9}$$

where σ, μ and ξ are the scale, location and shape parameters respectively. The above extreme value distributions can be combined into generalised extreme value (GEV) distribution given equation 2.10:

$$G(\mu,\sigma,\psi) = \begin{cases} \exp\left\{ -\left[1+\xi\frac{x-\mu}{\sigma}\right]^{\frac{-1}{\xi}}\right\} & \xi \neq 0 \\ \exp\left\{ -\exp\left[-\frac{x-\mu}{\sigma}\right]\right\} & \xi = 0 \end{cases} \tag{2.10}$$

where μ, σ and ξ are the location, scale and shape parameters of the distribution. The shape parameter ξ determines the tail behaviour of the GEV and therefore determines the modelled extreme type distribution. The Weibull distribution is obtained when $\xi < 0$ while the Frechet type distribution is obtained when $\xi > 0$. The Gumbel distribution is obtained when $\xi = 0$. The differences in the three extreme type distributions are shown in Fig 2.6.

Similarly, if $X_1, X_2, ..., X_n$ is a sequence of iid that exceed a threshold u, then for large enough threshold, the non degenerate distribution of $(X_i - u)$ can be approximated by the Generalised Pareto Distribution density function given in equation 2.11:

$$G(\mu,\sigma,\psi) = \begin{cases} \frac{1}{\sigma}\left[1+\xi\frac{x-\mu}{\sigma}\right]^{\frac{-1}{\xi}-1} & \xi \neq 0 \\ \frac{1}{\sigma}\exp\left(-\frac{x-\mu}{\sigma}\right) & \xi = 0 \end{cases} \tag{2.11}$$

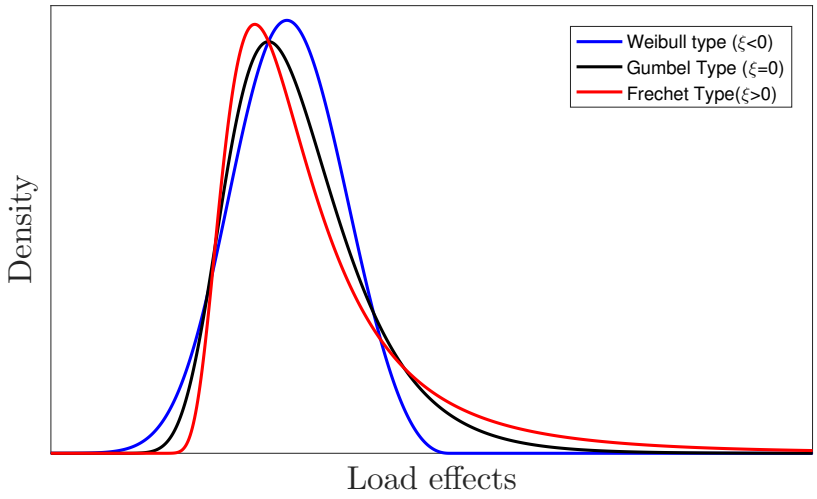

Figure 2.6: Extreme Value distributions

Applications of extreme value theory in bridge live load effects studies use two main procedures namely the peaks over threshold approach and block maxima approach. In the peaks over threshold method, a threshold is chosen and the peaks over this are fitted to a Generalised Pareto distribution. The block maxima on the other hand subdivides the period of observation into smaller non overlapping intervals and only one maximum value from each interval is selected to form a sample of maxima that are fitted to a Gumbel and Weibull distributions or to Generalised Extreme Value distributions [Coles, 2001, OBrien *et al.*, 2015]. Nowak [1994] on the other hand fitted block maxima load effects on to normal distribution and used normal probability paper for extrapolating the effects.

Comparative studies have been done of traffic load effects on bridges predicted by peak over threshold method and block maxima methods. OBrien *et al.* [2015] studied characteristic load effects generated from simulated highway traffic data on single span and 2 span continuous beams obtained extrapolation effects. It was shown that the block maxima approach which fitted load effects to normal distribution underestimated characteristic midspan moments for 15m and 35m span simply supported beams as well as support moment and support shear. The peaks over threshold method and block maxima fitted to GEV produced comparable characteristic load effects with greater variance compared to the normally fitted block maxima method. James [2003] analysed the 50 year return

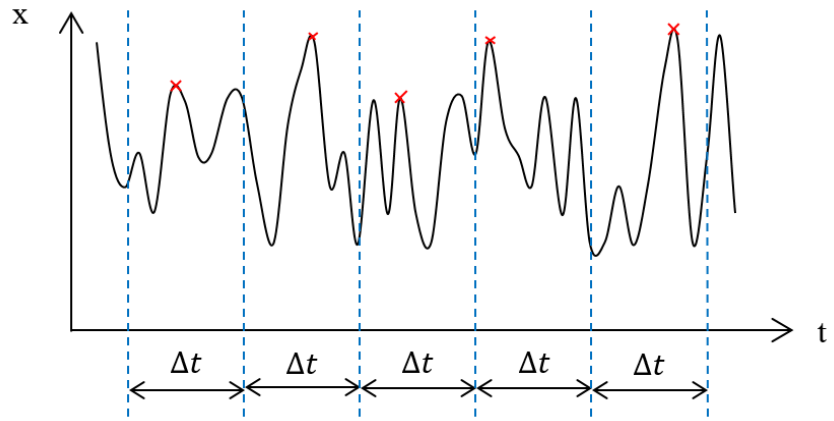

Figure 2.7: The Block Maxima approach

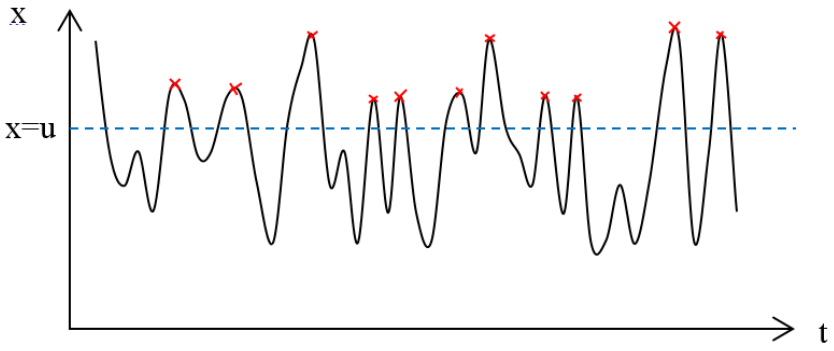

Figure 2.8: The Peak Over Threshold approach

midspan moments for simply supported railway bridges with spans ranging from 4m to 30m using the peak over threshold fitted to Generalised Pareto distribution and block maxima GEV method arising from passage of freight and passenger trains. The two approaches gave similar the mean return levels with estimated parameters suggesting either Gumbel or Weibull type tail. However there were significant differences in return levels at 95% significance level with block maxima giving much higher return levels.

In most highway bridge applications, the characteristic load effects are estimated using block maxima approach where distribution such as Gumbel or Weibull are assumed a priori before parameter estimation. Bailey and Bez [1999] used the Weibull distribution to fit highway traffic load effects of support shear, mid span moment and support moment. It was argued that extreme traffic load effects have an upper bound due to physical constraints. O'connor and O'brien [2005]

suggested that the best fit distribution for highway traffic load effects on bridges depended on span length. The Weibull type distribution showed a better fit for spans of length less than 20m and Gumbel type gave best fit for spans greater than 50m. The Weibull or Gumbel types could be used to fit load effects for spans between 20m and 50m. O'Connor and Eichinger [2007] obtained similar results when comparing the goodness of fit of Gumbel and Weibull governing distributions for midspan moments of simply supported beams of 5m, 50m and 200m spans. The study demonstrated that the Weibull distribution produced better fit for short span of 5m while Gumbel type had a better fit for longer spans. Moyo *et al.* [2004] fitted a Gumbel distribution to block maximum of bridge strains obtained from a continuous monitoring and extrapolation to obtain characteristic strains.

The prior selection of distribution can introduce modelling errors when studying load effects. In order to avoid modelling errors in choice of distribution, it has become increasingly common to adopt the Generalised Extreme value (GEV) distribution in traffic load modelling studies. Getachew and Obrien [2007] used simulated highway traffic to obtain mid span moments and end span shear on simply supported beams of span lengths between 15m and 30m. The generated daily maxima traffic were then fitted to GEV. Caprani *et al.* [2008] investigated load effects from bidirectional highway traffic on two lane short to medium span bridges where multiple occurrence of trucks cause critical loading cases. These non-identically distributed load effects were fitted to GEV in order to obtain characteristic values.

The physical quantities such as axle weights, vehicle gross weights or strains can be represented as time series. The concept of stationarity of time series which implies that the properties of a time series such as mean or variance do not change over time allow the asymptotic theory of extreme values to be applied readily. However, stationarity condition in traffic loads may be unjustified. The characteristics of traffic as well as traffic volumes change over time due to technological advances, changes in legal limits on axle loads or growth in economic activity. In order to accommodate these changes, researchers have

used extreme value distributions with time varying parameters to account for the changes in time of distribution parameters [OBrien *et al.*, 2014, Leahy *et al.*, 2016]. OBrien *et al.* [2014] considered the effect of increases in highway traffic volumes on characteristic mid span moment and shear for simply supported beam and support moment for 2 span continuous beam at 20 and 75 year return period. In order to address this, it was assumed that traffic growth within a block was negligible. With this approximation, equation 2.6 is modified as follows:

$$F_t = P(Z \leq x) = \prod_{i=1}^{n} F_i(x) \tag{2.12}$$

where $F_i(x)$ is the parent distribution for the i th block. The resulting distribution F_t can be approximated as a time varying GEV:

$$F_t \sim G(\mu(t), \sigma(t), \psi(t)) = \begin{cases} \exp\left\{ -\left[1 + \xi(t)\frac{x-\mu(t)}{\sigma(t)}\right]^{\frac{-1}{\xi(t)}} \right\} & \xi(t) \neq 0 \\ \exp\left\{ -\exp\left[-\frac{x-\mu(t)}{\sigma(t)}\right] \right\} & \xi(t) = 0 \end{cases} \tag{2.13}$$

The study showed that there is a general increase in characteristic load effects with increase in traffic volumes. The increases depend on load effect under consideration and span length. Thus for the support moment for a 15m long, 2 span continuous bridge increased by 6.9% for 75 year return period and 3% increase in annual traffic. The effect of highway traffic volume growth were more pronounced with increasing span length. The support moment for a 30m long 2 span continuous bridge increased by 9.1% in comparison to the 6.9% obtained for 15m span long bridge. The maximum load effect increase of 15.7% was obtained for support shear for the 2 span 30m long continuous beam.

Leahy *et al.* [2016] investigated the impact of growth both highway traffic volumes and gross vehicle weight (GVW) on characteristic bridge load effects. The increase in GVW was achieved by replacing lighter trucks with the next heavy class with either the same or higher number of axles based on information from 4 months of WIM measurements. This GVW increase was done for trucks less than 50 tonnes while for those above, the increase was achieved by increasing axle loads up to 20

tonnes. The study considered shear and mid span moment in simply supported bridges and central support moment for 2 span continuous beams of lengths 15m, 30m and 45m. The increases in volume and gross weight were over a service period (remaining life) of 40 years while characteristic loads levels were obtained for return period of 75 years. In order to investigate the impact on growth, a scaling α-factor was defined which normalised extrapolated effects to the Eurocode load model LM1 for highway bridges as follows:

$$\alpha = \frac{\text{Simulated 1000 year load effect}}{\text{Basic LM1 load effect}} \tag{2.14}$$

The α factors when no growth is considered were all less than 0.7 indicating conservativeness in the design load model for the site specific loads. Traffic volume increase of 2% per annum with no increase in truck weights led to an increase of 9% in load effects. In contrast, an increase in truck weights of 1% per annum with no increase in traffic volumes led to 43% increase in α. An increase of 2% in traffic volume with an increase of 1% in truck weight resulted in 48% increase in α. It was shown that the characteristic loads are more sensitive to increase in truck weight.

The multiple occurrence of trucks on bridges has been investigated by researchers. This loading case is especially important when the truck weights are correlated. The correlation can arise if trucks are operated by the same owner and are carrying similar loads. Nowak [1994] investigated the impact of correlation on shear and midspan moments of single span bridges as well as centre support moment for two span bridges of span lengths from 9m to 60m. The study considered the correlation coefficient $\rho = 0$, $\rho = 0.5$ and $\rho = 1$ at headway distances of 4.5m and 9m. It was shown that the uncorrelated case governs the one lane bending midspan moments for spans less than 24.4m for headway distance of 4.5m and thereafter the correlated case ($\rho = 1$) resulted in critical moments. When headway distance was increased to 9m, the uncorrelated case was critical up to 36.6m spans.

Railway bridge live loads from design codes may be unconservative for bridges on

dedicated freight lines. This has necessitated the need to collect weigh-in-motion data on freight lines to check the load effects against the provisions of design codes such as the South African Transport Services railway bridge loading code. Protocols on data collection, preprocessing and cleaning have been proposed for highway bridges and these largely apply for railway bridges as well. While highway load effects may not be very sensitive to random errors in data as given in the C15 data accuracy requirement, this has not been investigated for railway application. It is observed that the investigations on data accuracy requirements were based on short to medium span bridges under free flow conditions. The duration of WIM data collection for load modelling is very important in highway applications due to the variations and seasonality effects. However, this may not be critical on dedicated freight corridors where wagon loads are closely controlled. Different extrapolation methods have been applied to obtain characteristic highway loads where the normal method has been shown to be conservative for some spans. A comprehensive comparison has not been done for railway load effects. The extreme value distributions for highway load effects have been shown to be dependant on span length. It is increasingly common to use GEV for load effects modelling to avoid errors in choice of distribution prior to parameter estimation. The changes in distribution type with increase in span length have not been investigated for various load effects on railway bridges. It has also been shown that characteristic load effects on highway bridges increase with increase in traffic volume. However, the greatest increase is obtained from an increase in axle loads. Lastly, it has been shown that the effects of correlation in trucks on a bridge changes the characteristic load effects estimation although this is also dependent on span length and headway distances between the correlated trucks.

2.4.2 Dynamic live loads on bridges

The dynamic behaviour of railway bridges under moving loads is of interest when designing or assessing railway bridges. The behaviour of railway bridges under passage of trains has been a subject of research from the inception of railway

transport [Ewing, 1929, Inglis, 1934, Hayward, 2011]. It was observed that bridge response under moving railway traffic was generally more than that induced by an equivalent static load. The bridge response under these dynamic loads was influenced by several factors that include bridge and train modal parameters, presence of rail joints on the bridge and the magnitude of unbalanced masses in early locomotive engines [Ewing, 1929]. In order to account for the dynamic loads, a dynamic amplification (DA) was applied which is defined as follows:

$$DA = \frac{R_{dyn} - R_{sta}}{R_{stat}} \tag{2.15}$$

where R_{dyn} is the maximum dynamic response and R_{stat} is the maximum static response at a given location. Alternatively, a dynamic amplification factor (DAF) is defined as follows:

$$DAF = \frac{R_{dyn}}{R_{stat}} \tag{2.16}$$

Early design rules allowed to increase static load by up to 30% for 1.5m spans down to 10% for 30.5m span bridges [Hayward, 2011]. In order to explore bridge dynamic response, a brief review is provided in the next section of the critical parameters.

Dynamic amplification of bridge response under moving loads

The dynamic amplification in bridges for use in bridge evaluations can be obtained from either code based formulae, conducting bridge tests under controlled or normal traffic or from dynamic analysis of bridges of interest [Paultre *et al.*, 1992]. Extensive reviews of dynamic amplification in highway bridges and the critical factors that influence it has been done [Paultre *et al.*, 1992, Deng *et al.*, 2014]. The dynamic amplification in bridges is influenced by many factors generally grouped as bridge or vehicle related factors. Bridge related factors include bridge natural frequencies, bridge approaches, ride surface quality. The factors relating to vehicles include vehicle speed, mass, suspension and axle spacings. Dynamic amplification in codes is often based on

few of the factors such as bridge frequency, span length and surface riding quality for the sake of simplicity.

Dynamic Amplification Factors: Code Comparison

The dynamic behaviour of a bridge depends on numerous factors that include speed of traffic during bridge crossing, the irregularities of the track, the mass of the structure and and the mass of the vehicle as presented in earlier sections. Design codes however tend to provide simple formulae that use one of the many variables affecting the dynamic response and provide limits for the range of application. Design guides address the dynamics load effects problem by first determining the static load effects and applying the necessary scaling to obtain dynamic load effects. The static and dynamic load effects deflections, bending moments and shear forces in design guides are mapped onto dynamic load effects by the dynamic amplification factor. The American Railway Engineering and Maintenance-of-Way Association (AREMA) defines the dynamic amplification factor to include rocking effects RE and vehicle-structure interaction I_V effects as given in equation below [Unsworth, 2010]:

$$DAF = RE + I_V \tag{2.17}$$

The rocking effects are independent of vehicle speed and result from the vibrations of the rail wagon or locomotive about an axis parallel to its longitudinal axis. The rocking effects are not explicitly given in dynamic amplification formulae given in South African Transport Services [1983] code or the more recent Eurocode [1991]. Most design codes give dynamic amplification formulae with expressions that contain either span length or natural frequency and vehicle speed. The Eurocode proposes different formulae for carefully maintained track in equation 2.18:

$$\Omega_2 = \frac{1.44}{\sqrt{L_\Phi} - 0.2} + 0.82 \tag{2.18}$$

with $1 \leq \Omega_2 \leq 1.67$ while for track under standard maintenance computed from

equation 2.19;

$$\Omega_3 = \frac{2.16}{\sqrt{L_\Phi} - 0.2} + 0.73 \tag{2.19}$$

with $1 \leq \Omega_2 \leq 2.0$, where L_Φ is defined for different structural elements and bridge types. For a simply supported beam, L_Φ is taken as the span length while for multi span beams with number of spans greater or equal 5, then L_Φ = $1.5\times$ span length.

The South African Transport Services [1983] code gives formulae for bending moment and shear load effects and specifies the range of application in Table 2 of the code document:

$$DAF_{SHEAR} = \begin{cases} 2.00 & \text{if } L < 3.6 \\ 0.73 + \dfrac{2.16}{\sqrt{L_\Phi} - 0.2} & \text{for } 3.6 \leq L \leq 67 \\ 1.00 & \text{if } > 67 \end{cases} \tag{2.20}$$

$$DAF_{SHEAR} = \begin{cases} 1.67 & \text{if } L < 3.6 \\ 0.82 + \dfrac{1.44}{\sqrt{L_\Phi} - 0.2} & \text{for } 3.6 \leq L \leq 67 \\ 1.00 & \text{if } > 67 \end{cases} \tag{2.21}$$

where L is the span length for simply supported beams or L_Φ = $1.55\times$ span length for number of spans greater than 5. There are striking similarities in the formulae put forward by South African Transport Services [1983] and Eurocode [1991] as they both draw from the background research from the International Union of Railways.

The South African Transport Services [1983] code does not propose dynamic factors for real trains and the inbuilt conservatism in the code during its formulation may not be applicable to the changes in South African train configurations. On the other hand Eurocode [1991] proposes dynamic amplification factors to be used for actual trains in service with known speed envelops as follows:

$$DAF = \begin{cases} 1 + \varphi' + \varphi'' & \text{for track with standard maintenance} \\ 1 + \varphi' + 0.5\varphi'' & \text{for carefully maintained track} \end{cases} \tag{2.22}$$

with:

$$\varphi' = \begin{cases} \dfrac{K}{1 - K + K^4} & \text{for } K < 0.76 \\ 1.325 & \text{for } K \geq 0.76 \end{cases} \tag{2.23}$$

where

$$K = \frac{v}{2L_\Phi \times n_0} \tag{2.24}$$

and

$$\varphi'' = \frac{\alpha}{100}\left[56e^{-\left(\frac{L_\Phi}{10}\right)^2} + 50\left(\frac{L_\Phi n_0}{80} - 1\right)e^{-\left(\frac{L_\Phi}{20}\right)^2}\right] \tag{2.25}$$

and $\varphi'' \geq 0$ with:

$$\alpha = \begin{cases} \dfrac{v}{22} & \text{for } v \leq 22ms^{-1} \\ 1 & \text{for } v > 22ms^{-1} \end{cases} \tag{2.26}$$

where v, n_o and α are maximum permitted vehicle speed in ms^{-1}, first natural frequency of bridge loaded by permanent actions in Hz and speed coefficient respectively and L_Φ as previously defined.

The South African Transport Services [1983] does not provide formulae or guidance on computation of local dynamic amplification factors. The Eurocode [1991] on the other hand specifies both global dynamic amplification factors as given above and amplification factors for local stresses. The local stress amplification factor for deck slab that is part of a box girder in both transverse and longitudinal direction is computed using either equations 2.18, 2.19 or 2.22 with L_Φ taken as 3 times the deck span.

Dynamic amplification from dynamic analysis

Analytical studies of influence of various factors mentioned earlier that influence bridge dynamic response have been conducted by many researchers. These analytical studies have used various levels of idealisations in models of bridges and vehicles mostly with focus on highway bridges. While most analytical studies idealise bridges as beams, vehicles are have been treated as moving forces,

moving masses or moving sprung masses often leading to contradictory results. The moving force idealisation is the simplest as it only considers the vehicle weight and leads to closed form solutions [Johansson *et al.*, 2013]. This formulation ignores the centripetal and Coriolis forces contribution.

Chang and Lee [1994] compared dynamic amplifications from moving force, moving mass and moving sprung for different riding surface roughness and vehicle speeds from 60km/h to 100km/h on simply supported beams with spans from 25m to 100m. It was observed that all the three models gave similar amplification factors for a smooth riding surface. However for a rough riding surface, the moving force and moving mass models greatly overestimated the bending moment derived amplification factors. In contrast, Yau *et al.* [1999] made a comparison of moving load and more realistic moving sprung mass vehicle models on dynamic amplification factors and showed that the difference was insignificant. However, the sprung mass models predicted higher vertical accelerations with increasing riding surface roughness. Thus it was concluded that while moving force adequately modelled bridge response, a more refined model was needed if the focus was on vehicle response. Hamidi and Danshjoo [2010] made similar recommendations that more complicated vehicle models only increased precision in predicting vehicle response.

The influence of riding surface roughness has been widely investigated investigated by researchers. Riding surface roughness is usually modelled through the use of power density spectral functions. Humar and Kashif [1993] studied the effect of surface roughness and showed that surface roughness in bridge approaches imposed initial oscillations in vehicle on entering a bridge and this increased the amplification factors. Chang and Lee [1994] also showed that dynamic amplification increased with increasing riding surface roughness on simply supported bridges. Deng and Cai [2010] used 3 dimensional coupled bridge vehicle models to investigate dynamic amplification factors on simply supported prestressed multi-girder bridges with spans from 9.14m to 39.62m. It was shown that amplification increased with increasing surface roughness for

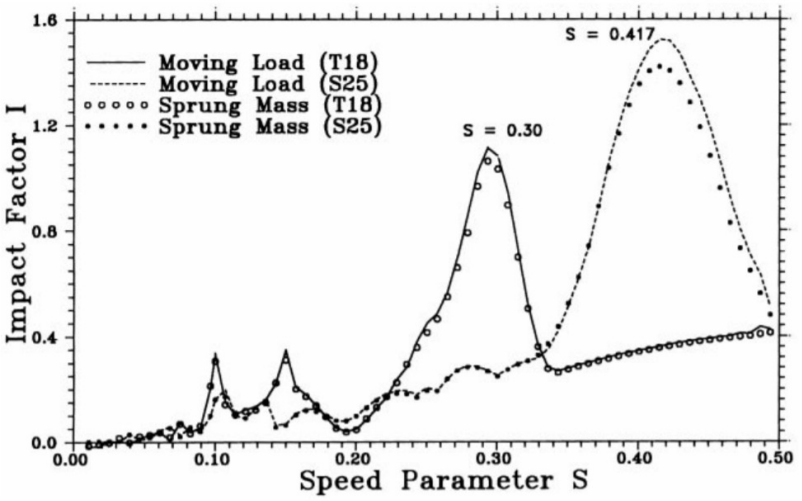

Figure 2.9: Dynamic amplification for midspan deflection of simply supported beam: different vehicle models Yau *et al.* [1999]

vehicles speeds from 30km/h to 120km/h. On the other hand Yang *et al.* [1995] found that ride surface roughness has a minor influence on deflection and bending moment moment based amplification factors while its influence was slightly greater for shear force derived amplification. Yau *et al.* [1999] also found that there was no difference between smooth and irregular surfaces on the dynamic amplification factors in simply supported and continuous beams.

Vehicle speed has long been regarded as an important factor in the dynamic response of bridges. Vehicle speed has either been studied directly or been converted into a non-dimensional speed parameter non dimensional speed S defined in equation 2.27:

$$S = \frac{\pi v}{\omega L} \tag{2.27}$$

where L is characteristic length in meters and ω is the fundamental frequency of the bridge in Hz and v the vehicle velocity in m/s. Chu *et al.* [1986] studied dynamic amplification in prestressed box girder bridges. The dynamic amplification of moments at midspan increased with increase in speed. Yang *et al.* [1995] studied the impact of vehicle speed on amplification and proposed a linear relationship between dynamic amplification and non-dimensional speed

parameter S. This linear relationship showing an increase in dynamic amplification was proposed for both shear and moments in simply supported as well as continuous beams. Wang *et al.* [1992] studied dynamic amplification in a railway truss bridge and showed that it increases with increase in speed. Deng and Cai [2010] on the other hand presented results of a study on prestressed girder bridges showing a decrease in dynamic amplification with increasing speed. Similar results were obtained from field tests by Ashebo *et al.* [2007] who found positive but weak correlation between vehicle speed and dynamic amplification factors on on an instrumented skew continuous box girder bridge. More recently Deng *et al.* [2015] conducted an analytical study of T and box girder bridges with spans 20 m and 30m for simply supported beams and 70m for continuous 3 span beams. It was shown that there was no single trend between dynamic amplification and vehicle speed.

Hwang and Nowak [1991] investigated dynamic amplification of prestressed girder bridges under increasing gross weight and speeds. The vehicles were modelled as rigid distributed mass on springs allowing both vertical rotations and pitching rotations while the bridge was modelled as a prismatic beam with road surface roughness generated from a power spectral density function. It was shown that dynamic amplification factor decreased with increase in vehicle gross weight. Humar and Kashif [1993] on the other hand considered effect of vehicle-bridge mass ratio on dynamic amplification and showed that there was in increase in maximum amplification factor as the vehicle-bridge ratio was increased from 0.1 to 1.50 for speed parameter ranging from 0 to 0.30.

Dynamic amplifications can be significantly increased due to resonance phenomenon. The occurrence of resonance depends on bridge span length, vehicle axle spacing,number of axles, bridge damping ratio and bridge natural frequency [Li and Su, 1999, Xia *et al.*, 2006]. Resonance can be caused by the periodic loading of vehicles as result of axle group spacing or can be caused by the loading rate which depends on vehicle speed. Hamidi and Danshjoo [2010] investigated the effect of the ratio of axle spacing to bridge span length for high

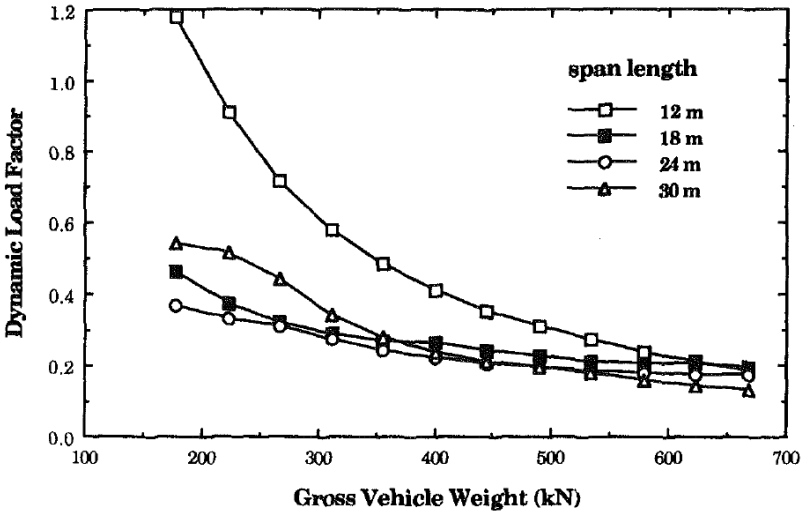

Figure 2.10: Dynamic Load factor versus Gross Vehicle Weight for Prestressed Concrete Girder Bridges Hwang and Nowak [1991]

speed trains and showed that the dynamic amplification factor increases when axle spacing to span length decreases. The loading rate on the other hand causes resonance when it equals the bridge natural frequencies [Lee *et al.*, 2012].

While the studies reviewed above focused on global amplification of bridge response, Yu *et al.* [2017] investigated local amplification factor of a simply supported box girder bridge. It was shown that global dynamic amplification was largely influenced by lower bending modes while higher bending modes had a significant influence on local amplification factors. The local amplification factors were shown to decrease linearly with increase in span length and generally greater than global amplification factors for shorter spans.

Deng and Wang [2015] investigated the influence of vehicle braking on dynamic amplification of highway bridge response. Vehicle braking increased the amplification factors by between 8.89% and 327% in comparison to vehicles moving at constant speed. The largest increase was observed for shorter span bridges when vehicle deceleration occurred in the first half of single span bridges.

Dynamic amplification from field tests

Bridge testing is a reliable way to determine dynamic amplification factors. Dynamic amplification factors can be obtained from dynamic response by appropriate application of low pass filter over dynamic response measurements to obtain equivalent static response as given in equation 2.4.2.

$$DA = \frac{R_{dyn} - R_{static}}{R_{static}} \approx \frac{R_{dyn} - R_{filtered}}{R_{filtered}} \tag{2.28}$$

where R_{dyn} is the maximum dynamic response, R_{static} is the static response and $R_{filtered}$ is the maximum static response as obtained from the filtered dynamic response.

Billing [1984] performed field tests on a total of 27 bridges consisting of 14 steel bridges with span lengths from 22m to 122m, 10 concrete bridges with span lengths 16m to 41m and 3 timber bridges of span length 5m. The test vehicles chosen to represent commercial vehicles in Canada at the time comprised of 3 axle truck with 241kN gross weight, 5 axle trucks of gross weights 391kN and 414kN and an 8 axle truck with gross weight 580kN. The instrumentation included a data acquisition system, accelerometers to acquire data for modal analysis, strain gages and displacement transducers. The static bridge responses were obtained by applying a low pass filter on the dynamic responses obtained when test vehicles were passed on the bridge at 16km/h and 48km/h. The tests confirmed findings from many analytical studies indicating that there is a reduction in dynamic amplification with increasing vehicle weight. Vehicle passage on simple span bridges mostly excited first flexural and first torsional modes while for continuous bridges a range of flexural and torsional modes were excited and the first flexural mode could not be easily identified. It was also shown that dynamic amplification from trucks two trucks with separation distance equal to bridge span was 10% to 30% higher than that obtained from single truck passage.

Ashebo *et al.* [2007] conducted tests on a skew box girder bridge where static

responses were obtained from dynamic responses by using a low-pass Butterworth filter. It was observed that heavier vehicles induce lower dynamic amplification than light vehicles. Furthermore it was shown that there is weak correlation between speed and dynamic amplification and no correlation between number of axles and dynamic amplification.

Section 2.4.2 shows that while it is accepted that dynamic load effects are greater than static load effects cased by the the same vehicle crossing a bridge, there is no agreement on the influence of the factors involved. There is agreement on dependence of resonance on vehicle speed, axle spacing and bridge natural frequency, however there is no consensus on influence of speed away from resonance speeds. There is also no agreement on analytical models for vehicles with some researchers suggesting that complex models do not increase accuracy in computing bridge response. A critical factor of importance to railway bridge application is the vehicle mass ratio as it is much higher on railway bridges. There is no consensus on effect of mass ratio on dynamic amplification although it is agreed that increased mass ratio reduces the vehicle-bridge system frequency. The most reliable method of determining dynamic amplification remains field measurements.

2.5 Concluding remarks

Traditional assessment methods have made use of condition and load rating for assessment of bridges. Load rating can be formulated to include site specific live loads as well as account for deterioration levels in bridge components. The AASHTO LRFR gives a range of modification factors to account for deterioration levels. These modification factors are at component level and do not explicitly allow for adjustments that account for failure modes, ease of inspection or system redundancy. Furthermore it has been shown that the derived RF may be poorly correlated to β in some bridges and thus is not a rational safety measure.

Protocols for use of WIM data are well established for highway applications. The requirements for WIM data accuracy have been derived for free low conditions

which is the critical loading condition for short to medium bridges. However there are departures with freight rail loading and these have not been explored. The duration of WIM monitoring on highway bridges should be long enough to capture traffic composition and and changes over different seasons. These seasonal variations may not be present on freight rail lines and the traffic composition does not change as much unless on mixed freight lines. The loading regime for freight rail is more controlled which reduces the variance between axle loads. It is also expected that there would be some level of correlation between boggies for a particular wagon and the adjacent wagon due to wagon coupling. The issue of correlation changes the traffic simulation approach as well as the block size in order to still permit the use of classical extreme value theory. While the issue of growth has been discussed in literature, a more extensive study of growth in traffic volumes in freight rail and its impact on characteristic load effects of midspan moment, support moment and shear in both single and multi-span continuous beam type bridges is lacking.

The dynamic amplification factors reviewed mostly for highway applications show some contradictory results. While most studies show a dependency with speed, it has been shown that the correlation with speed is weak. There are also contradictions on the effect of ride roughness on amplification. Most studies based on single load passage show an increase in amplifications. In contrast, the amplifications observed on simulation of train loads show that the effect is insignificant. Due to these contradictions, it is important to provide both an analytical and experimental study of amplifications during train passage.

References

International Heavy Haul Association, https://www.ihha.net/about-ihha, Accessed: 2017-10-10.

Cooper T., "Train loadings for railroad bridges," *Transactions of the American Society of Civil Engineers*, 31(1); 174–184, 1894.

Ewing J.A., "The vibrations of railway bridges: An example of co-operative

research," *Journal of the Royal Society of Arts*, 77(3989); 624–646, 1929. URL http://www.jstor.org/stable/41358216

Inglis C.E., *A Mathematical Treatise on Vibrations in railway Bridges*, Cambridge University Press, 1934.

South African Transport Services, "Bridge code," 1983.

Billing J.R., "Dynamic loading and testing of bridges in ontario," *Canadian Journal of Civil Engineering*, 11(4); 833–843, 1984.

Chu K., Garg V. and Wang T., "Impact in railway prestressed concrete bridges," *Journal of Structural Engineering*, 112(5); 1036–1051, 1986.

Eurocode C., "1: Actions on structures, part 2: Traffic loads on bridges," *Brussels: European Standard EN*, 2; 2003, 1991.

Hwang E.S. and Nowak A.S., "Simulation of dynamic load for bridges," *Journal of structural engineering*, 117(5); 1413–1434, 1991.

Paultre P., Chaallal O. and Proulx J., "Bridge dynamics and dynamic amplification factors—a review of analytical and experimental findings," *Canadian Journal of Civil Engineering*, 19(2); 260–278, 1992.

Allen D., "Canadian highway bridge evaluation: reliability index," *Canadian Journal of Civil Engineering*, 19(6); 987–991, 1992.

Wang T., Shahawy M. and Huang D., "Impact in highway prestressed concrete bridges," *Computers & structures*, 44(3); 525–534, 1992.

Humar J. and Kashif A., "Dynamic response of bridges under travelling loads," *Canadian Journal of Civil Engineering*, 20(2); 287–298, 1993.

Chang D. and Lee H., "Impact factors for simple-span highway girder bridges," *Journal of Structural Engineering*, 120(3); 704–715, 1994.

Nowak A.S., "Load model for bridge design code," *Canadian Journal of Civil Engineering*, 21(1); 36–49, 1994.

Yang Y.B., Liao S.S. and Lin B.H., "Impact formulas for vehicles moving over simple and continuous beams," *Journal of Structural Engineering*, 121(11); 1644–1650, 1995.

Bailey S.F., *Basic principles and load models for the structural safety evaluation of existing road bridges*, Ph.D. thesis, EPFL, 1996.

Tobias D.H. and Foutch D.A., "Loading spectra for railway bridges under current operating conditions," *Journal of Bridge Engineering, ASCE*, 1,No4; 127–134, 1996.

Yau J.D., Yang Y.B. and Kuo S.R., "Impact response of high speed rail bridges and riding comfort of rail cars," *Engineering structures*, 21(9); 836–844, 1999.

Li J. and Su M., "The resonant vibration for a simply supported girder bridge under high-speed trains," *Journal of Sound and Vibration*, 224(5); 897–915, 1999.

Bailey S.F. and Bez R., "Site specific probability distribution of extreme traffic action effects," *Probabilistic engineering mechanics*, 14(1-2); 19–26, 1999.

Faber M.H., Val D.V. and Stewart M.G., "Proof load testing for bridge assessment and upgrading," *Engineering structures*, 22(12); 1677–1689, 2000.

Coles S., *An Introduction to Statistical Modeling of Extreme Values*, Springer-Verlag, London, 2001.

James G., *Analysis of traffic load effects an railway bridges*, Ph.D. thesis, Royal Institute of Technology, 2003.

Akgül F. and Frangopol D.M., "Bridge rating and reliability correlation: Comprehensive study for different bridge types," *Journal of Structural Engineering*, 130(7); 1063–1074, 2004.

Branco F.A. and Brito J.d., *Handbook of concrete bridge management*, American Society of Civil Engineers, 2004.

Leighty C.A., Laman J.A. and Gittings G.L., "Heavy axle study: impact of higher rail car weight limits on short-line railroad bridge structures," *Civil Engineering and Environmental Systems*, 21(2); 91–104, 2004.

Moyo P., Brownjohn J.M.W. and Omenzetter P., "Highway bridge live loading assessment and load carrying capacity estimation using a health monitoring system," *Structural Engineering and Mechanics*, 18(5); 609–626, 2004.

Akgül F. and Frangopol D.M., "Time-dependent interaction between load rating

and reliability of deteriorating bridges," *Engineering Structures*, 26(12); 1751–1765, 2004.

Au A., Lam C., Agarwal A.C. and Tharmabala B., "Bridge evaluation by mean load method per the canadian highway bridge design code," *Canadian Journal of Civil Engineering*, 32(4); 678–686, 2005.

O'Brien E.J., Znidaric A., Brady K., González A. and O'Connor A., "Procedures for the assessment of highway structures," 2005.

Bhattacharya B., Li D., Chajes M. and Hastings J., "Reliability-based load and resistance factor rating using in-service data," *Journal of Bridge Engineering*, 10(5); 530–543, 2005.

O'connor A. and O'brien E.J., "Traffic load modelling and factors influencing the accuracy of predicted extremes," *Canadian journal of civil engineering*, 32(1); 270–278, 2005.

Xia H., Zhang N. and Guo W., "Analysis of resonance mechanism and conditions of train–bridge system," *Journal of Sound and Vibration*, 297(3-5); 810–822, 2006.

Lauridsen J., Jensen J. and Enevoldsen I., "Bridge owner's benefits from probabilistic approaches," *Structure and infrastructure engineering*, 3(4); 281–302, 2007.

Ashebo D.B., Chan T.H. and Yu L., "Evaluation of dynamic loads on a skew box girder continuous bridge part ii: Parametric study and dynamic load factor," *Engineering structures*, 29(6); 1064–1073, 2007.

Getachew A. and Obrien E.J., "Simplified site-specific traffic load models for bridge assessment," *Structure and infrastructure Engineering*, 3(4); 303–311, 2007.

O'Connor A. and Eichinger E.M., "Site-specific traffic load modelling for bridge assessment," in "Proceedings of the Institution of Civil Engineers-Bridge Engineering," volume 160, 185–194, Thomas Telford Ltd, 2007.

Vassie P. and Arya C., "Bridge management," in "ICE Manual of Bridge Engineering: Second Edition," 591–613, ICE Publishing, 2008.

Caprani C.C., OBrien E.J. and McLachlan G.J., "Characteristic traffic load effects

from a mixture of loading events on short to medium span bridges," *Structural safety*, 30(5); 394–404, 2008.

Pelphrey J., Higgins C., Sivakumar B., Groff R.L., Hatman B.H., Charbonneau J.P., Rooper J.W. and Johnson B.V., "State-specific lrfr live load factors using weigh-in-motion data," *J. Bridge Engineering ASCE*, 13(4); 339–350, 2008.

Unsworth J., chapter 7: Overview of Bridges and Structures for Heavy Haul Operations, Virginia Beach, VA: International Heavy Haul Association, 2009.

Martland C.D., chapter 2: Economics, Virginia Beach, VA: International Heavy Haul Association, 2009.

Ryall Michael J., *Bridge Management*, Elsevier, 2 edition, 2010.

Unsworth J.F., *Design of Modern Steel Railway Bridges*, CRC Press, New York, 2010.

Calgaro J., Tschumi M. and Gulvanessian H., "Designers' guide to eurocode 1: Actions on bridges: En 1991-2," Technical report, EN 1991-1-1,-1-3 to-1-7 and EN 1990 Annex, 2010.

Hamidi S.A. and Danshjoo F., "Determination of impact factor for steel railway bridges considering simultaneous effects of vehicle speed and axle distance to span length ratio," *Engineering Structures*, 32(5); 1369–1376, 2010.

Deng L. and Cai C., "Development of dynamic impact factor for performance evaluation of existing multi-girder concrete bridges," *Engineering Structures*, 32(1); 21–31, 2010.

Wang N., O'Malley C., Ellingwood B.R. and Zureick A.H., "Bridge rating using system reliability assessment. i: Assessment and verification by load testing," *Journal of Bridge Engineering*, 16(6); 854–862, 2011.

Wang N., O'Malley C., Ellingwood B.R. and Zureick A.H., "Bridge Rating Using System Reliability Assessment. II: Improvements to Bridge Rating Practices," *Journal of Bridge Engineering*, 16(6); 854–862, 2011.

Feldman L.R., Jackson K.P., Sparling B.F. and Sparks G.A., "Comparison of load rating techniques for the red deer river bridge," *Canadian Journal of Civil Engineering*, 38(10); 1072–1081, 2011.

Sivakumar B., Ghosn M. and Moses F., *Protocols for collecting and using traffic data in bridge design*, volume 683, Transportation Research Board, 2011.

Hayward A.C.G., "Train loads on bridges 1825 to 2010," *International Journal for the History of Engineering and Technology*, 81, No2; 159–191, 2011.

Caglayan O., Ozakgul K. and Tezer O., "Assessment of existing steel railway bridges," *Journal of Constructional Steel Research*, 69(1); 54–63, 2012.

Lee H.H., Jeon J.C. and Kyung K.S., "Determination of a reasonable impact factor for fatigue investigation of simple steel plate girder railway bridges," *Engineering Structures*, 36; 316–324, 2012.

Ghosn M., Sivakumar B. and Miao F., "Development of state-specific load and resistance factor rating method," *Journal of Bridge Engineering*, 18(5); 351–361, 2012.

Davids W.G., Poulin T.J. and Goslin K., "Finite-element analysis and load rating of flat slab concrete bridges," *Journal of Bridge Engineering*, 18(10); 946–956, 2012.

Brühwiler E., Vogel T., Lang T. and Lüchinger P., "Swiss standards for existing structures," *Structural Engineering International*, 22(2); 275–280, 2012.

Fu G., *Bridge Design and Evaluation: LRFD and LRFR*, John Wiley & Sons, 2013.

Johansson C., Pacoste C. and Karoumi R., "Closed-form solution for the mode superposition analysis of the vibration in multi-span beam bridges caused by concentrated moving loads," *Computers & Structures*, 119; 85–94, 2013.

Barker R.M. and Puckett J.A., *Design of highway bridges: An LRFD approach*, John wiley & sons, 2013.

Washer G., chapter 12: Nondestructive evaluation methods for bridge elements, 301–317, CRC Press, Taylor & Francis Group, 2014.

Vinayagamoorthy M. and Tsang R., chapter 15: Concrete Bridge Evaluation and Rating, 381–441, CRC Press, Taylor & Francis Group, 2014.

Zhou Y.E., chapter 14: Steel Bridge Evaluation and Rating, 351–379, CRC Press, Taylor & Francis Group, 2014.

Fu G. and Devaraj D., *Bridge Engineering Handbook:Construction and*

Maintenance, chapter 9: Bridge Management Using Pontis and Improved Concepts, 233–246, CRC Press, Taylor & Francis Group, 2014.

OBrien E.J., Bordallo-Ruiz A. and Enright B., "Lifetime maximum load effects on short-span bridges subject to growing traffic volumes," *Structural Safety*, 50; 113–122, 2014.

Deng L., Yu Y., Zou Q. and Cai C., "State-of-the-art review of dynamic impact factors of highway bridges," *Journal of Bridge Engineering*, 20(5); 04014080, 2014.

Deng L., He W. and Shao Y., "Dynamic impact factors for shear and bending moment of simply supported and continuous concrete girder bridges," *Journal of Bridge Engineering*, 20(11); 04015005, 2015.

Deng L. and Wang F., "Impact factors of simply supported prestressed concrete girder bridges due to vehicle braking," *Journal of Bridge Engineering*, 20(11); 06015002, 2015.

Sanayei M., Reiff A.J., Brenner B.R. and Imbaro G.R., "Load rating of a fully instrumented bridge: comparison of lrfr approaches," *Journal of Performance of Constructed Facilities*, 30(2); 04015019, 2015.

OBrien E.J., Schmidt F., Hajializadeh D., Zhou X.Y., Enright B., Caprani C.C., Wilson S. and Sheils E., "A review of probabilistic methods of assessment of load effects in bridges," *Structural safety*, 53; 44–56, 2015.

Leahy C., OBrien E. and O'Connor A., "The effect of traffic growth on characteristic bridge load effects," *Transportation Research Procedia*, 14; 3990–3999, 2016.

Pipinato A. and Patton R., *Innovative Bridge Design Handbook Construction, Rehabilitation and Maintenance*, chapter 19: Railway Bridges, 510–516, Butterworth Heinemann, London, 2016.

Ma Z., Zhang G., Qie L. and Pan Z., "Experimental study on track dynamic characteristics of 30t axle load in revenue service railway," in "Proc. 11th IHHA Conf," 457–463, 2017.

Yu Y., Deng L., Wang W. and Cai C., "Local impact analysis for deck slabs of

prestressed concrete box-girder bridges subject to vehicle loading," *Journal of Vibration and Control*, 23(1); 31–45, 2017.

Cremona C. and Poulin B., "Standard and advanced practices in the assessment of existing bridges," *Structure and Infrastructure Engineering*, 13(4); 428–439, 2017.

Lantsoght E.O., van der Veen C., de Boer A. and Hordijk D.A., "State-of-the-art on load testing of concrete bridges," *Engineering Structures*, 150; 231–241, 2017.

Tabatabai H., Titi H. and Zhao J., "Wim-based assessment of load effects on bridges due to various classes of heavy trucks," *Engineering Structures*, 140; 189–198, 2017.

ERRI Report D192/RP2, "Comparison of present and future rail traffic on international lines with UIC 71 loading based on deterministic calculation," Utrecht, April 1994.

ERRI Report D192/RP3, "Comparison of the effects of current and future rail traffic on international lines with the effects from UIC 71 loading on a probabilistic basis," Utrecht, December 1994.

ERRI Report D192/RP1, "Theoretical basis for verifying the present UIC 71 loading," Utrecht, March 1993.

Chapter 3

RESEARCH METHODOLOGY

3.1 Introduction

The assessment of existing bridges has been predominantly done through visual inspection to assess occurrence of damage through material deterioration and proof load testing and rating. With few exceptions, the bulk of research work has focused on assessment of highway bridges. In these applications, the assessment is generally done within a framework of a Bridge Management System. These systems through effective have the main shortcoming of determining the safety level through condition indexes which though correlated with bridge safety are not an expression of bridge reliability in line with design safety considerations. An overall reliability based assessment framework has to address the load and resistance aspects of a bridge under assessment as shown in Fig 3.1 below:

The main components of a reliability assessment framework include a module for inspections and monitoring of both the loading regime and the bridge behaviour including bridge deterioration. This module directly informs the bridge structure modelling and the formulation of an appropriate load model. Bridge loads include environmental loads from wind and temperature,water flow and traffic loads. This study focuses on the traffic loads which are dominant in design load cases and have been the subject of study by many researchers. The load model as used in bridge design addresses dynamic and static load effects separately.

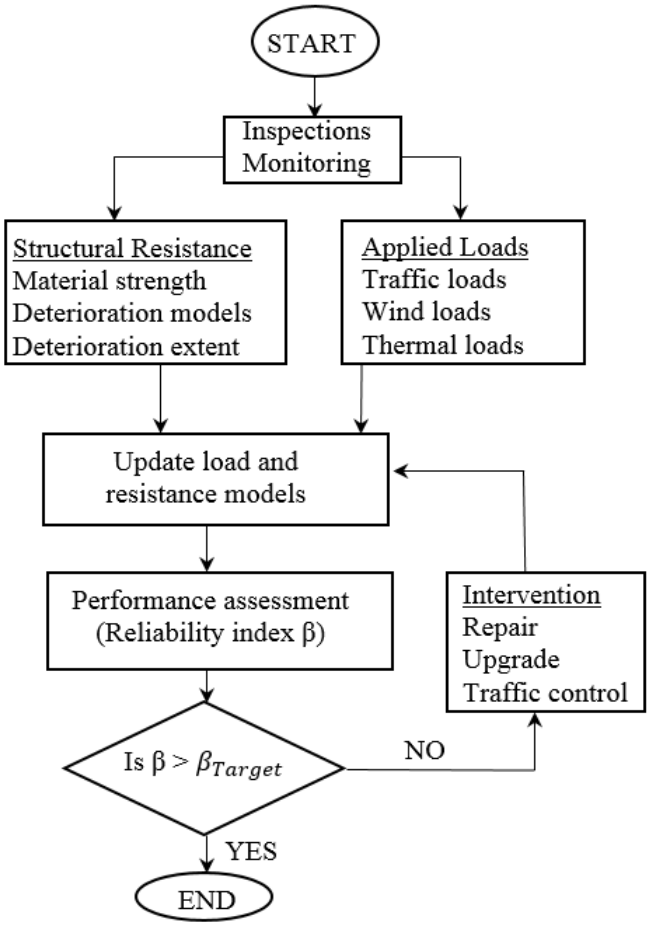

Figure 3.1: Reliability framework for assessment

This format is adopted in this research were the dynamic load effects are treated in a deterministic way while the static load effects are treated in more detailed probabilistic way. This approach has been adopted by many researchers on assessment loads for highway bridges and is very similar to the formulation of design live load modelling for bridges.

In order to formulate and update appropriate network specific traffic loads for assessment of bridges on the heavy haul line, data on traffic volumes and traffic characteristics and composition was obtained from an already existing weigh in motion system. The selected weigh in motion system described in later sections is located on the Olifants River bridge. In addition, a separate monitoring system was installed on the Olifants bridge to measure the bridge response. An overview of the South African Iron Ore line, typical freight trains and the geometry of the

Olifants Bridge are presented in the next section. This is followed by a description of the installed weigh in motion system, the structural health monitoring system and signal processing and the choice of appropriate algorithms for analysis of SHM vibration measurements. The study makes use of analytical formulations and monitoring data to formulate network specific live loads. The methodology for the analytical formulations is presented in given in relevant chapters.

3.2 Chapter Objectives

The objective of this chapter is to outline the field testing, monitoring and instrumentation of the Olifants Railway Bridge on the Iron Ore freight line in South Africa. The monitoring system is used in studying both ambient and forced vibration responses of the bridge. An overview of the Wheel Impact Monitoring Weigh-In-Motion (WIM-WIM) system used to collect data for static live load modelling. provide an overview of structural assessment of existing bridges with emphasis on formulation of live loads appropriate for use on heavy-haul rail freight lines. A summary of data processing techniques used to extract frequencies and strain based dynamic amplification factors is presented.

3.3 Olifants River Bridge

The Olifants Bridge is the longest bridge on the South African Iron Ore rail line. The ore line is a single line on 1067mm gage of length 861 km connecting the mines in Seshen to the Port of Saldahna on the west coast of South Africa as shown in Fig 3.2. The rail line traffic is predominantly made up of iron ore freight trains. The annual haulage on the ore line has increased from 18 million tonnes at its inception to over 60 million tonnes in 2014. It is this increase in traffic volumes achieved through introduction of different types of train that justified this study.

The Olifants Bridge which located at 178km from Saldahna the largest bridge on the network. The Olifants bridge is a prestressed single box girder bridge that was constructed in 1978 and has been in operation since. The bridge was constructed using incremental launching technique from one end. The bridge

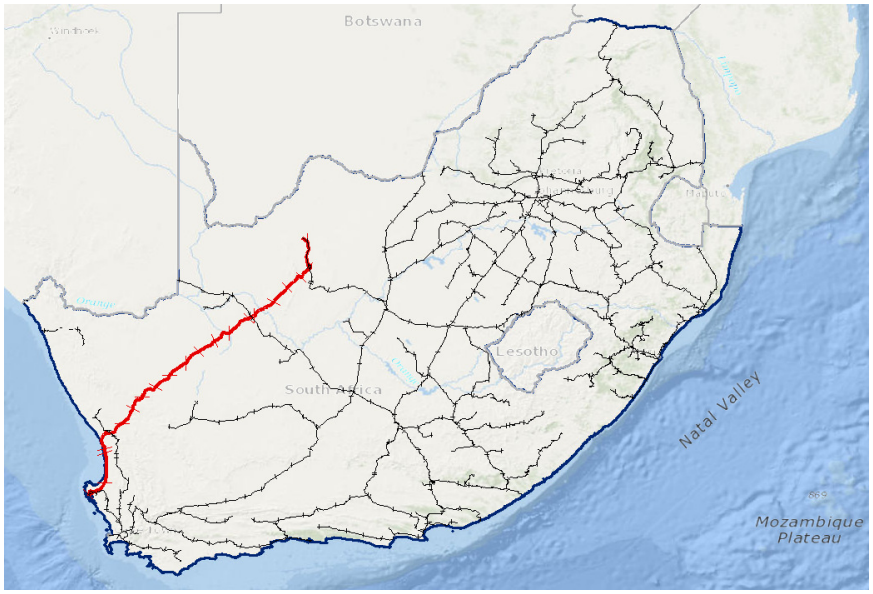

Figure 3.2: South African Iron Ore Line

bridge has a total length of 1035m made up of 23 spans of 45m length each. The bridge has three segments which include 11 span continuous segments on either end and a drop span in the middle. The superstructure is supported on piers with the tallest pier having a height of 50m. The bearing system is made up of sliding Neoprene bearings or Neoprene-Teflon and steel bearings. The overall geometry of the bridge is shown in Fig 3.3. The Olifants Bridge has two installations of monitoring systems operated separately by University of Cape Town(UCT) and TRANSNET in addition to an installed weigh-in-motion system. The data obtained from the weigh-in-motion system and the UCT operated monitoring systems are used in this research. A brief description of the weigh in motion and UCT monitoring systems is presented in the sections that follow.

3.4 Olifants Bridge WIM-WIM System

Weigh in motion systems are widely installed on roads where they are used to generate data of truck axle loads and help enforce legal axle load limits. Most of the requirements in terms of hardware performance and data requirements in highway applications can be directly applied to railway traffic. In railway traffic, the Weigh In Motion systems serve another role of Wheel Impact Monitoring due to

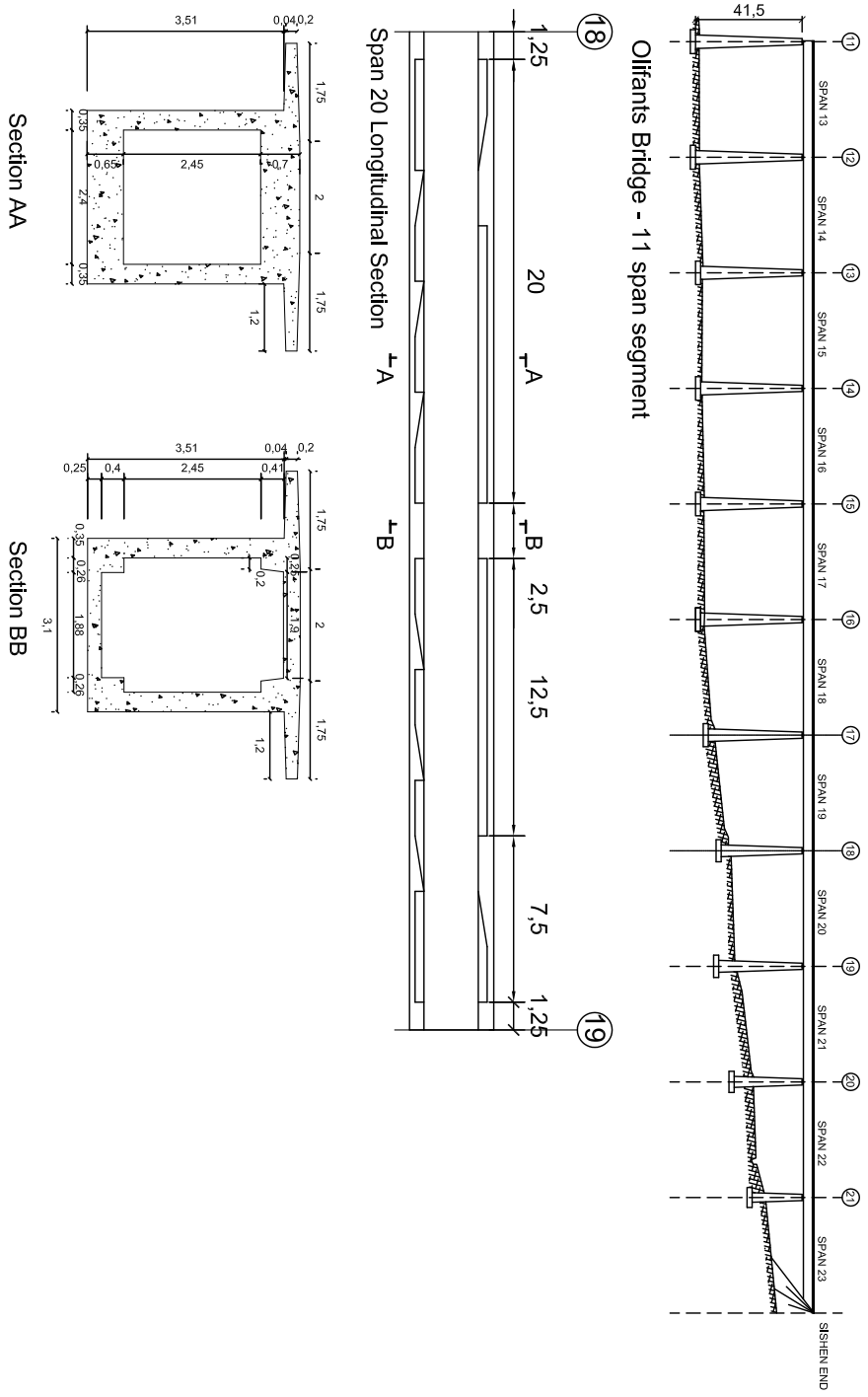

Figure 3.3: Olifants River Bridge-Elevation and sections

Figure 3.4: WIM-WIM sensors

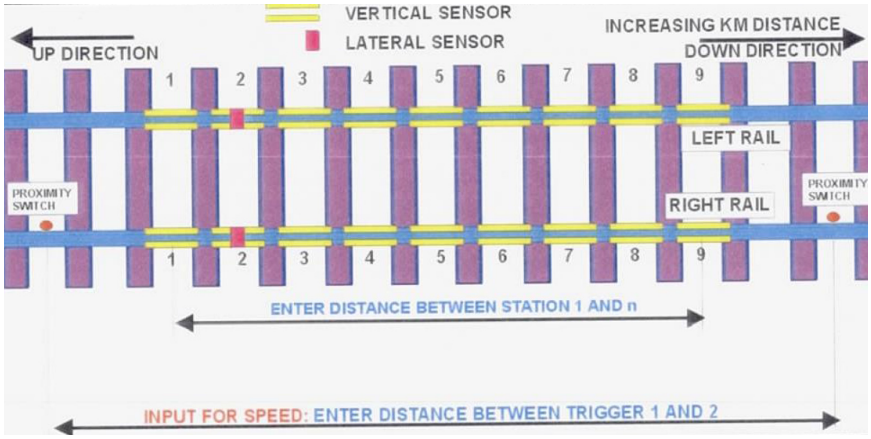

Figure 3.5: WIM-WIM sensor arrangement

wheel irregularities which have the effect of significantly increasing the dynamic loads and hence the combined functions are abbreviated to WIM-WIM. Weigh in motion systems use a range of sensors that include piezoelectric sensors, load cells or strain gauges.

The heavy haul line has two installed WIM-WIM systems namely SLK.SLK2.WIM.01 and SLK.K804.804.WIM.01 located at 175km and 804km respectively. The Olifants WIM-WIM named SLK.SLK2.WIM.01 is located on the Olifants Bridge and the data squired from this system is used in this study which also has a separate monitoring system allowing for independent event

WIM STATION	TIME	DIRECTION	TRAIN NUMBER	PARAMETER	VALUE
SLK.SLK2.L04.WIM.01	2016/03/01 07:30	Down	EMXM801403290216	Type [V]	15E
				Speed [V]	46.2
				Mass [V]	180
				Mass [V]	91.2
				Mass [V]	88.7
				Mass [B]	91.7
				Mass [B]	88.1
				Dynamic Load [A]	18.8
				Dynamic Load [A]	15.2
				Dynamic Load [A]	18.3
				Dynamic Load [A]	16.6
				Dynamic Load [A]	16.7
				Dynamic Load [A]	16.3
				Dynamic Load [A]	16.2
				Dynamic Load [A]	17.7
				Dynamic Load [A]	16.1
				Dynamic Load [A]	17.6
				Dynamic Load [A]	15.2
				Dynamic Load [A]	17

Total Mass on side each side 1

Total bogie mass

Dynamic Load per axle

Figure 3.6: WIM-WIM Typical output

identification and logging based on the bridge response. The Olifants WIM-WIM is managed by Transnet who are the freight rail operators. The system development and installation was completed in 1999. The Olifants WIM-WIM system uses up to 32 strain gauges comprising 32 channels that are sampled at 2.5kHz per channel which is sufficient to capture train speeds up to 150km/h. The requirements for WIM-WIM data to be useful in assessment load model formulation are very similar to those for design requirements which include identifying trains with all the associated locomotive and wagon types, measuring train speeds, measuring axle loads and spacings and having regular calibration for axle load determination. The Olifants WIM-WIM system uses a trigger to detect train passage and is used to determine locomotive and wagon types, the speed of each wagon as it passes over the sensor installation, dynamic wheel mass and static bogie mass. The system works by measuring the strains in the rail caused by the wheel contact force. The measured strains provide the dynamic mass while the filtered signal provides the static mass of the axle. An overview of the data output for an engine passage is shown in Fig 3.6.

Experience in highway applications show that Weigh-In-Motion measurements are affected by vehicle dynamics and approach surface profile. The accuracy of the system is therefore checked through regular calibrations. The Olifants WIM-WIM

after calibration achieves an accuracy of measurement of static wagon mass within 2% and total train mass within 0.5%. For the purposes of this research, further data checks are performed to check presence of anomalies in train events. These include checks of axle loads and train speeds. The axle loads and train speeds are regulated on the freight line. The Olifants WIM-WIM measurements are used both in the deterministic and probabilistic study of bridge loads and load effects.

3.5 Olifants Bridge Monitoring System

The Olifants Bridge was selected to be instrumented with a continuous monitoring system as part of University of Cape Town and TRANSNET research initiative aimed at understanding behaviour of the bridge and site specific loads on the ore line. The bridge has power and instruments are housed inside the box girder. The monitoring system has four subsystems of sensors for measurement of vibrations, strains, temperature and crack growth. The monitoring system was installed on span 20 which is the 4 th span from the abutment in the direction of Sishen. The choice of span 20 was based on the need to have a span where critical bridge vibration modes could be monitored as well as sections with significant crack width.

The Olifants system is based on National Instruments Compact Rio technology deployed as a master module and a slave expansion chassis connected by an ethernet cable with synchronisation modules on the slave and master module to manage the sampling clock. A schematic of the system is shown in Fig 3.7. The analytical dynamic analysis and dynamic amplification factors in this study are compared with results obtained from Olifants Bridge measurements. Thus only vibration and strain measurement systems are described in detail.

3.5.1 Strain Monitoring

The Olifants bridge strain monitoring module was implemented to capture both global and local bridge response during train passage. These measurements are to be used to inform efforts to develop finite element models of the bridge and also

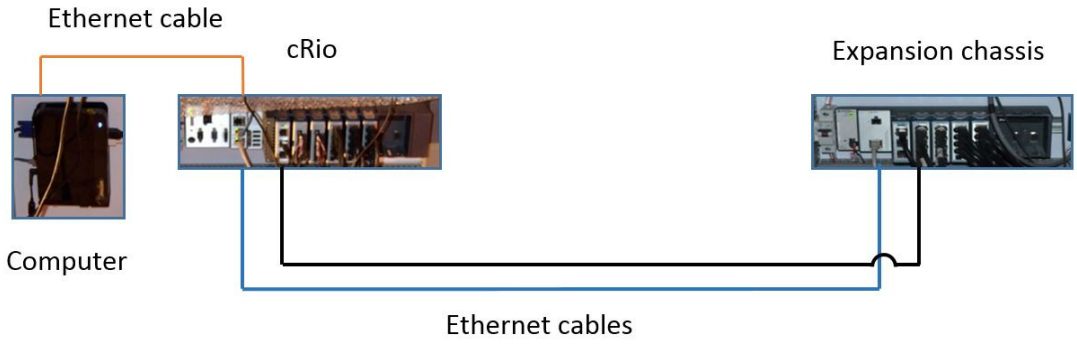

Figure 3.7: Olifants Structural Monitoring System

provide an alternative experimental method to determine load effect amplifications during train events. The later objective is part of the research effort in this study. A total of 16 strain gages are installed on the bridge. These strain gages are full bridge demountable type SLB 700A electric resistance transducers supplied by HBM. The National Instrument module for analog to digital conversion is the NI 9237 which is a 24 bit module with an inbuilt analog anti aliasing filter. The strains are logged continuously and saved in hourly files in TDMS format. In addition, event files are logged during train passage and saved with file name based on the time the event occurred. Strains are sampled at a higher rate which is decimated to 200Hz for continuous logged hourly files and to 500Hz during events.

The strain sensors are set up with a dense layout at support and mid span sections of span 20 where most sensors are aligned to capture the transverse strain variations. However, additional sensors are deployed to give the longitudinal profile as well. The overall strain sensor layout is shown in Fig 3.8 while Fig 3.9 shows a typical sensor installed on the bridge.

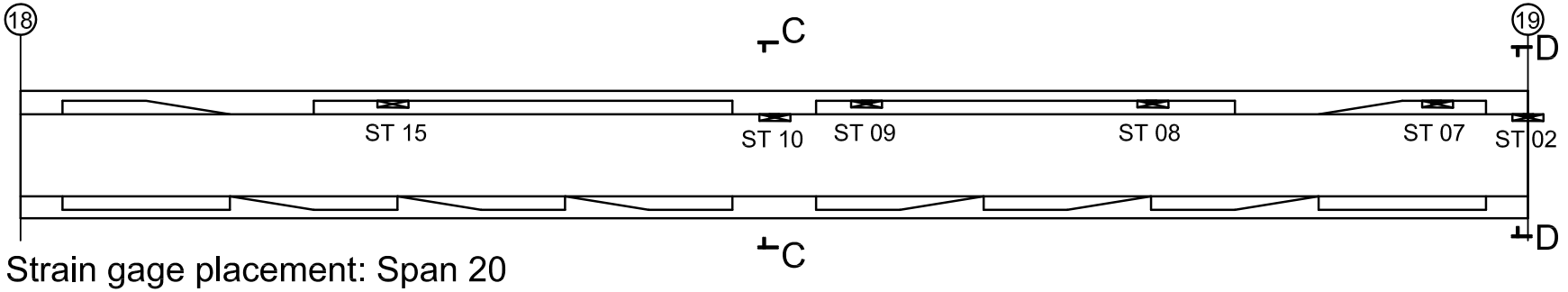

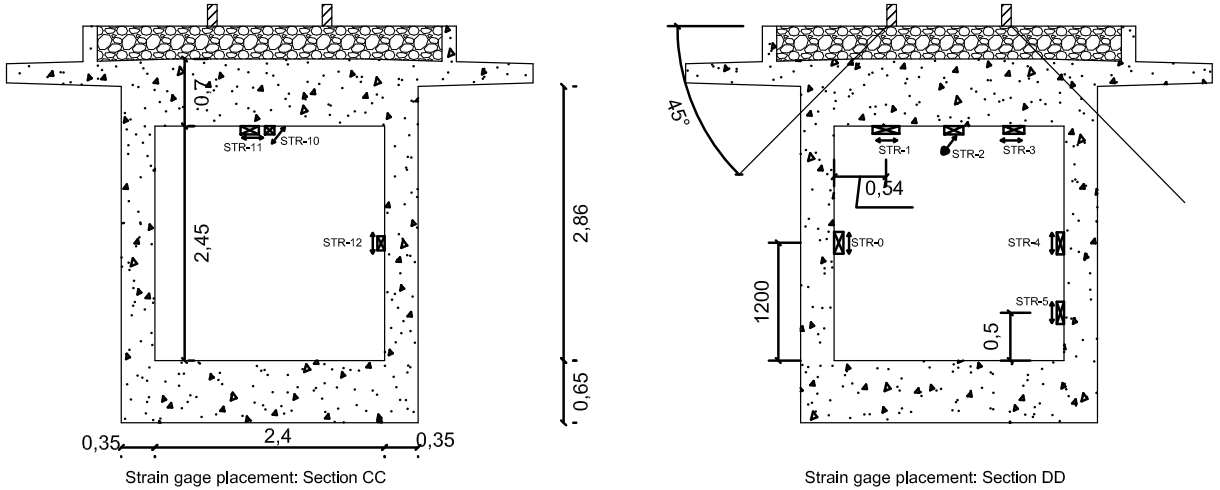

Figure 3.8: Strain measurements

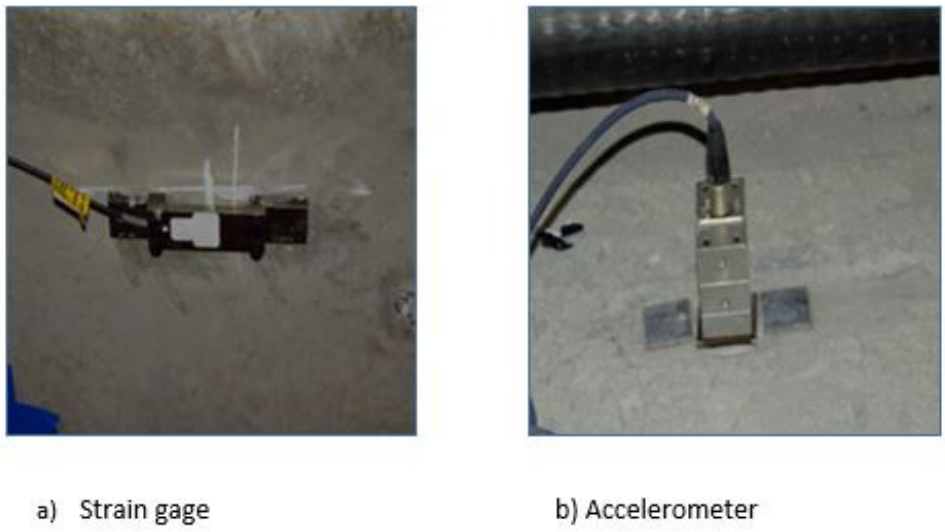

Figure 3.9: Vibration and strain transducers

The location of strain gages has to be within the zone where dynamic effects can be effectively captured. Paultre *et al.* [1992] conducted field studies of dynamic amplification factors of highway bridges and suggested a layout adopted in this study. The sensors whose measurements are used for computation of dynamic amplification have to be in the zone within 45^0 angle to avoid underestimating the dynamic affects. This is shown in Fig 3.8.

3.5.2 Vibration Monitoring

The Olifants bridge vibration module was implemented after some preliminary testing of the bridge done by Busatta and Moyo [2017]. This test that was done on spans 19 and 20 together with some analytical work of bridge mode shapes showed that it was possible to resolve a few flexural modes with the limited number of sensors deployed. A total of 8 sensors are deployed on the bridge for continuous monitoring of vibrations. The 5 accelerometers in the vertical direction to help monitor some flexural and torsional modes are shown in Fig 3.10. The accelerometers deployed are force balance Honeywell type QA 700A accelerometers. Force balance accelerometers are recommended for civil engineering structures where frequencies monitored are very low.

The vibrations analog to digital converter module is National Instrument NI-9234

Figure 3.10: Accelerometer layout

which is a 24 bit module also with inbuilt analog filter. The accelerations are logged in continuous hourly files and event files just as the case for strains. However, the vibrations are sampled at a much higher frequency of 1kHz train passage while the continuous hourly files are logged at 200Hz. The event triggers are based on the 1 second root mean square value of two of the measurements from vertical accelerometers exceeding a threshold value of $9.82m/s^2$ after which the termination is determined by the event duration length fixed to 6 minutes 30 seconds. The vibrations are squired with setting of DA coupling and mean reading for accelerometers in vertical direction under ambient conditions is $9.81m/s^2$. The event duration is based on the observed event duration during the testing phase. There have been longer events on record lasting 20 minutes during passage of slow trains. The sampling frequency of continuous hourly files is in fact more than adequate to resolve the flexural frequencies within the range of interest, thus no refinement to event end was necessary.

The overall design of monitoring software specification and implementation was done in conjunction with the local National Instruments office and implementation by Kairos Engineering Services.

3.6 Operational Modal Analysis

The vibrations measurements in this study are used to inform the analytical studies on bridge fundamental frequency and its evolution over the study period of one year and a period of one year and to provide insight into bridge behaviour during train passage. The well established set of techniques referred to as Operational Modal Analysis (OMA) are used to address the issue of extracting

modal parameters of the bridge. The techniques of OMA enable solution of the inverse problem of obtaining modal parameters from vibration measurements of a structure. A number of assumptions are made in OMA and these include [Ranieri and Fabbrochino, 2014]:

1. The system is linear and thus the system response from combination of inputs is the sum of individual outputs.
2. The structure dynamic characteristics do not change over time.
3. The sensor layout is sufficient to allow observation of modes of interest.
4. The input excitation is white noise so as to excite all modes of interest equally.

Operational Modal Analysis techniques can be grouped as method operating in frequency domain and those in time domain. Other classifications put the methods as parametric methods which aim to fit data to models and non parametric methods. A detailed presentation of these techniques is found in literature and considered outside the scope [Ranieri and Fabbrochino, 2014, Brinker and Ventura, 2015]. A brief overview is given of the two methods used in this study namely the Peak-Picking method and the Stochastic Subspace Identification method. The former method is selected for its ease of use to provide an overview of the frequency content in the measurements and the latter is chosen as it is more automated and robust for a structure with close modes. The OMA techniques were applied on the measurements using proprietor software ARTeMIS.

3.6.1 Peak-Picking Method

The Peak-Picking method is an easy to use method for obtaining natural frequencies and Operational Deflected Shapes which under certain assumptions are very close to mode shapes. The Peak-Picking method relies on the assumption of low damping and well separated modes. At the $r-th$ resonance mode, the structural response is given as:

$$\{y(t)\} \approx \{\phi_r\} q(t) \tag{3.1}$$

where ϕ_r and $q(t)$ are the mode shape and modal coordinates respectively. The correlation matrix of responses is given as:

$$[R_{yy}(\tau)] = \mathbb{E}[q_r(t+\tau)q(t)]\{\phi_r\}\{\phi_r\}^T \tag{3.2}$$

The spectral density matrix is obtained from 3.2:

$$[G_\omega] = [G_{qq}(\omega)]\{\phi_r\}\{\phi_r\}^T \tag{3.3}$$

where $[G_{qq}(\omega)]$ is the auto spectral density of modal coordinates. At resonance, any column of spectral density matrix gives the scaled mode shapes. The trace of spectral density matrix at frequency values is used to obtain peaks. The ability to determine the frequencies depends on the septation between frequencies being greater than the band with of mode under consideration.

3.7 Time-frequency analysis during train passage

The frequency-time evolution of the Olifants railway bridge is investigated. Firstly train signals are selected where the train speed was fairly constant during bridge crossing. The short time Fourier transform available through the spectrogram function in $Matlab$ is implemented to show the frequency-time pattern of the bridge.

A detailed study of the evolution of fundamental frequency is undertaken using the Complementary Ensemble Empirical Mode Decomposition (CEEMD)algorithm [Colominas *et al.*, 2014]. The CEEMD improves on the Ensemble Empirical Mode Decomposition (EEMD) which is based on the Empirical Mode Decomposition (EMD) proposed by Huang [2014]. The EEMD algorithm is used to decompose a signal into a collection of Intrinsic Mode Functions (IMF) iteratively with addition of white noise to overcome mode mixing. The overall CEEMD is implemented in the following steps:

3.8 Concluding remarks

Bridge natural frequency is used in simplified formulae provided by design codes to determine dynamic amplifications of load effects. Bridge fundamental

frequency is also used in field studies where quasi-static load effects on bridges are obtained from dynamic bridge responses by filtering dynamic effects. Bridge-vehicle systems on heavy haul rail lines under loads where the vehicle mass to bridge mass ratio is high experience reductions in frequencies of the combined system. Significant reductions in Olifants Bridge system frequencies on South African heavy haul line are observed. The derived system frequency is used in the chapter that follows as the basis for both analytical and experimental determination of amplification factors.

References

Paultre P., Chaallal O. and Proulx J., "Bridge dynamics and dynamic amplification factors—a review of analytical and experimental findings," *Canadian Journal of Civil Engineering*, 19(2); 260–278, 1992.

Colominas M.A., Schlotthauer G. and Torres M.E., "Improved complete ensemble EMD: A suitable tool for biomedical signal processing," *Biomedical Signal Processing and Control*, 14; 19–29, 2014.

Huang N.E., "Introduction to the hilbert–huang transform and its related mathematical problems," in "Hilbert–Huang transform and its applications," 1–26, World Scientific, 2014.

Ranieri C. and Fabbrochino G., *Operational Modal Analysis of Civil Engineering Structures: An Introduction and Guide for Applications*, Springer, 2014.

Brinker R. and Ventura C., *Introduction to Operational Modal Analysis*, Wiley, 2015.

Busatta F. and Moyo P., "How testing and monitoring can support heavy haul railway bridge management: The experience gained in South Africa," *11-th International Heavy Haul Conference Proceedings, Capw Town*, 599–, 2017.

Chapter 4

DYNAMIC BEHAVIOUR OF RAILWAY BRIDGES

4.1 Introduction

The dynamic behaviour of railway bridges under train loads has been the subject of research for many years and a summary of this is provided by Frỳba [1996]. It was recognised that the load effects resulting from moving trains were larger than the load effects produced by equivalent static loads. Furthermore, early steam locomotives caused high vibrations on bridges through their reciprocating unbalanced masses inducing what was referred to as hammer blows [Ewing, 1929, Inglis, 1934, Hayward, 2011]. In recent years, studies on dynamic response of railway bridges have focused on effects resonance as train speeds on high-speed rail lines have gone up exceeding 200 km/h [Yang *et al.*, 1995, Xia *et al.*, 2006]. The factors that influence dynamic response of bridges during train passage are generally grouped as bridge modal parameters, vehicle modal parameters, vehicle speed and axle spacings. Vehicle speed on a bridge is one of the key parameters for consideration which together with bridge natural frequency and vehicle axle spacing determine critical speeds at which resonance can occur. The freight on heavy-haul lines generally operate trains at much lower speeds thus key factors arising train-bridge interaction which are discussed in sections below are of interest in the analysis.

Dynamic response of railway bridges can obtained from formulae given in design

codes, from performing field measurements of bridge response or by performing a dynamic analysis of the bridge. The code based approach may be conservative and may not be appropriate for assessment. In the current chapter, the key parameter of bridge natural frequency and train-bridge natural frequencies are investigated using an analytical procedure and field measurements. Analytical studies of bridges under traffic loads employ various levels of idealisations for the bridge and vehicles depending on the study objective. Analytical studies of railway bridges use the beam idealisation where span to depth ratios are greater than 10 where shear deformations are negligible in line with the Euler-Bernoulli beam theory. Memory *et al.* [1995] investigated the impact of beam idealisation on natural frequency and found it was within 6% of estimate from field measurement. The beam idealisation is used for single track bridges with no skew where the flexural modes are critical. Chu *et al.* [1986] used a beam bridge model to investigate dynamic amplification factors caused by passage of freight cars on prestressed bridges. Hamidi and Danshjoo [2010] used a beam bridge model to investigate the influence of vehicle speed and axle spacing on bridge response. Other researchers have used finite element models to create more 3-dimensional bridge models [Deng and Cai, 2010].

Vehicle idealisations for bridge dynamic analysis are classified as moving force, moving mass or moving sprung mass. Moving force idealisations allow for closed form solutions to be obtained and generally show the main characteristics of the moving load problem. However, moving force formulations have the main drawback of ignoring the centripetal and Coriolis effects arising from the moving masses [Dugush and Eisenberger, 2002, Ouyang, 2011]. More complex moving load models make use of sprung masses that allow for several degrees of freedom to be included. Such complex models give better prediction in moving vehicle response with little improvements in prediction of bridge response behaviour [Yau *et al.*, 1999].

Railway bridges are subjected to distributed loads that are significantly large in proportion to bridge self weight in comparison to highway bridges. Heavy-haul

rail lines are operated in many parts of the world and are characterised by loads above 25 tonnes per axle and longer trains in order to optimally transport bulk commodities such as mineral ores. In order to understand the dynamic response of bridges on these lines, it is important to study their behaviour under ambient excitations and under train loads. The associated bridge response under train loads has to account for the vehicle-bridge mass ratio which has been shown to influence the dynamic response as well as the resulting dynamic amplifications [Humar and Kashif, 1993]. While there is no generally consensus of effect of increased mass on dynamic amplification factors as reviewed in Chapter 2, it is accepted that presence of trains on a bridge can change the frequency of the train-structure system [Ewing, 1929, Fryba, 1999, Li *et al.*, 2003].

Li *et al.* [2003] showed that increasing the mass of a moving sprung mass system on simply supported beam-type bridges lowers the frequency of vehicle-bridge system. Furthermore, increasing the stiffness of the sprung moving mass increases the natural frequency of the combined system as compared to the bridge natural frequency. In simply supported beam bridges the natural frequency of combined vehicle-bridge system has been shown to oscillate passage of a train consisting of equally spaced sprung masses. Mao and Lu [2011] investigated the resonance criteria of single span simply supported railway bridges under increasing train-bridge mass ratio and showed that the critical speed for resonance reduced due to reduction in resonance frequency by up to 10% for mass ratio between 1 and 2.50. Cantero and OBrien [2013] showed that frequency in vehicle-bridge interaction models is non stationarity and is of relevance in determining the displacements and accelerations of bridges during train passage.

4.2 Chapter Objectives

In this chapter the natural frequency which shows how sensitive a structure is to dynamic loading is investigated based on Euler-Bernoulli beam and compared with frequency estimates from field measurements. The analytical study is

limited to frequencies for single span, 2 and 4 span continuous beams as these beams are used throughout the study. The first contribution in this chapter is a generalised derivation for frequency evolution of a multi-span continuous beam on simple supports under moving loads. The second contribution is a field study of frequency-time evolution on bridges on heavy-haul line where train to bridge linear mass ratios are high.

4.3 Free vibration of beam bridges

Bridge natural frequencies and mode shapes are necessary when studying bridge behaviour under dynamic loading. In design codes, the natural frequency is often given in formulae for computing dynamic amplification factors.

4.3.1 Experimental studies and empirical formulae

Extensive field measurements have been undertaken to determine bridge natural frequency and to fit empirical formulae that allows the prediction of fundamental frequency. Billing [1984] reports a study of 24 highway bridges as part of an extensive field testing program in Canada. The tested bridges consisted of 14 steel bridges with spans from 22m to 122m and concrete bridges with spans from 16m to 41m. A plot of the logarithm of first flexural frequency versus span length showed a linear relation with an increase in span length resulting in a reduction of first flexural frequency. There was no attempt to fit an empirical formula due to the small sample size. Paultre *et al.* [1992] presented a review of bridge dynamics that included an empirical formulae obtained by fitting data from field testing of 883 bridges:

$$f_0 = 82L^{-0.9} \tag{4.1}$$

where f_0 is the first flexural frequency and L is the span length. The BS EN 1991-2:2003 gives similar formulae of flexural frequency in formulae for impact formulae. The upper limit for flexural frequency is given as:

$$\eta_0 = 94.76L_{\Phi}^{-0.748} \tag{4.2}$$

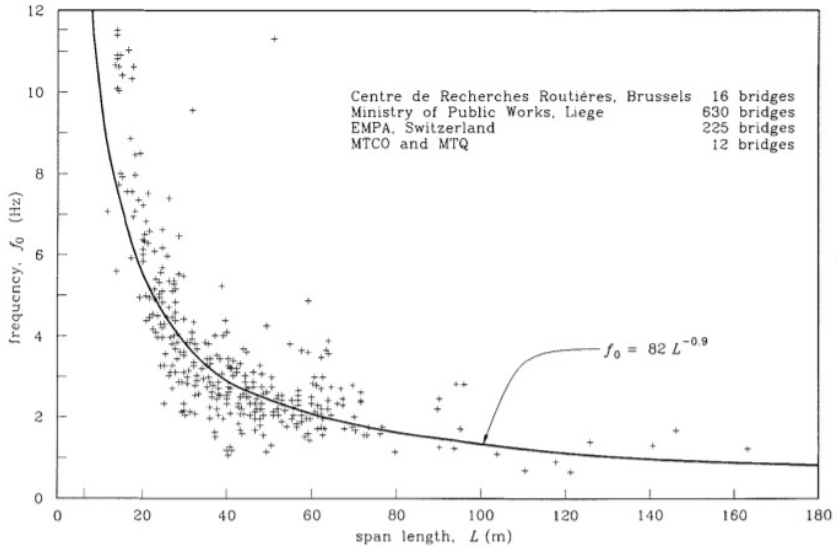

Figure 4.1: First flexural frequency versus span length [Paultre *et al.*, 1992]

and lower limit is given as:

$$\eta_0 = \begin{cases} \dfrac{80}{L_\Phi} & 4 \leq L_\Phi \leq 20 \\ 23.58 L_\Phi^{-0.592} & 20 < L_\Phi \leq 100 \end{cases} \tag{4.3}$$

were η_0 is the first flexural frequency and L_ϕ is the characteristic span length that is dependent on number of spans.

4.3.2 Analytical studies

Many bridges show beam type behaviour and therefore their global behaviour in analytical studies has been approximated using the Euler-Bernoulli beam theory [Inglis, 1934, Yang *et al.*, 1995, Fryba, 1999]. Euler-Bernoulli beam theory assumes that the beam cross section rotation and distortion due to shear are negligible compared to translation and deformation due to bending. These assumptions hold for beams with span to depth ratio greater than 10 [Rao, 2007]. In this section, the general beam equation is presented and mode-shapes as well as nondimensionalised frequencies for single, 2, 4 and 11 span continuous beams obtained.

The equation for transverse vibration of beams can be derived from energy or equilibrium considerations and the latter approach is adopted here. Consider a

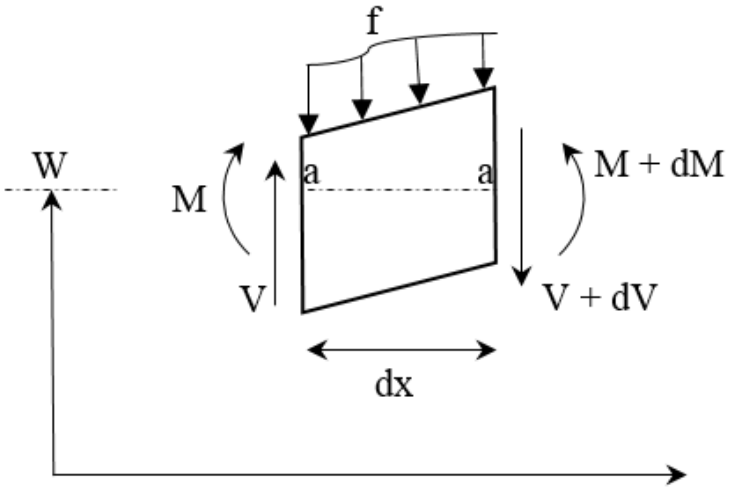

Figure 4.2: Beam bending under dynamic load

segment of an beam of arbitrary cross-section $A(x)$ under a load varying both in time and space $f(x,t)$ resulting in moments $M(x,t)$, $M(x,t)+dM(x,t)$ and shears $V(x,t)$,$V(x,t)+dV(x,t)$ in Fig 4.2 (see derivation from Thomas [1972], Rao [2007]) with the independent variables x,t dropped for brevity. Based on equilibrium considerations:

$$-(V+dV)+fdx+V=\rho A(x)\frac{\partial^2 W}{\partial t^2} \tag{4.4}$$

$$(M+dM)-(V+dV)dx+f\frac{(dx)^2}{2}-M=0 \tag{4.5}$$

where $dV=\frac{\partial V}{\partial x}dx$ and $dM=\frac{\partial M}{\partial x}dx$

$$\frac{\partial V}{\partial x}+f=\rho A(x)\frac{\partial^2 W}{\partial t^2} \tag{4.6}$$

$$\frac{\partial M}{\partial x}-V=0 \tag{4.7}$$

Substituting Eq 4.7 into equation 4.6:

$$-\frac{\partial^2 M}{\partial x^2}+f=\rho A(x)\frac{\partial^2 W}{\partial t^2} \tag{4.8}$$

Now $M = EI\frac{\partial^2 W}{\partial x^2}$, where E,I are Youngs modulus and moment of inertia respectively. Substituting this in equation 4.8, the equation for transverse vibration is obtained:

$$\frac{\partial^2}{\partial x^2}\left[EI\frac{\partial^2 W}{\partial x^2}\right]+\rho A(x)\frac{\partial^2 W}{\partial t^2}=f \tag{4.9}$$

Free vibration of single span simply supported beams

When free vibrations are considered, equation 4.9 is solved by separation of variables with $f = 0$.

$$W(x,t) = \phi(x)q(t) \tag{4.10}$$

Substituting 4.10 into equation 4.9 with $f = 0$ and simplifying:

$$\frac{d^2q(t)}{dt^2} + \omega^2 q(t) = 0 \tag{4.11}$$

$$\frac{d^4\phi(x)}{dx^4} - \Theta^4\phi(x) = 0 \tag{4.12}$$

where Θ is given below and ω is circular frequency.

$$\Theta^4 = \frac{\rho A\omega^2}{EI} \tag{4.13}$$

The solution to equation 4.12 is the characteristic function of the general form:

$$\phi(x) = A\cosh(\Theta x) + B\sinh(\Theta x) + C\cos(\Theta x) + D\sin(\Theta x) \tag{4.14}$$

where A,B,C and D are mode shape constants and Θ as given before. For a simply supported beam, the support conditions restrict translation and the bending moment vanishes.

$$\phi(0) = 0;\ \frac{d^2\phi(0)}{d^2x} = 0 \tag{4.15}$$

Applying 4.15 for a simply supported single span beam in 4.12 gives:

$$A = C = 0 \tag{4.16}$$

Similarly, the boundary conditions at support on L are given:

$$\phi(L) = 0;\ \frac{d^2\phi(L)}{d^2x} = 0 \tag{4.17}$$

Applying 4.17 for a simply supported single span beam in 4.12 gives:

$$\begin{aligned} B\sin\Theta L + D\sinh\Theta L = 0 \\ -B\sin\Theta L + D\sinh\Theta L = 0 \end{aligned} \tag{4.18}$$

A non trivial solution is obtained by setting determinant of equations 4.18 to zero:

$$\sin \Theta L \sinh \Theta L = 0 \tag{4.19}$$

The non trivial solution for 4.19 is obtained when:

$$\Theta L = n\pi, , \; n = 1, 2, ... \tag{4.20}$$

The displacement normalised mode shape ϕ of these beams is easily obtained as given below:

$$\phi_n = sin(\Theta_n x) \tag{4.21}$$

where n is the mode shape number, x is the length along the beam length.

Free vibration of continuous beams on simple supports

An investigation of free vibration of a continuous beam is done based on an analytical solution based on an eigen stiffness matrix first proposed by Hayashikawa and Watanabe [1981]. Consider continuous beam on simple supports with i spans as shown in Fig 4.3. The general solution is given in equation 4.46 where i denotes the span number and n is the mode associated with a given solution:

$$\phi_{n,i}(x) = A_{n,i} \cosh(\Theta_n x) + B_{n,i} \sinh(\Theta_n x) + C_{n,i} \cos(\Theta_n x) + D_{n,i} \sin(\Theta_n x) \tag{4.22}$$

where $A_{n,i}$,$B_{n,i}$,$C_{n,i}$ and $D_{n,i}$ are mode shape constants. Continuity requirements are enforced to obtain deflected shapes for given Θ values. For intermediate spans continuity requirements in slope and moments of adjacent spans and the displacement constraints at support leads to the following requirements:

$$\left.\frac{d\phi_{n,i}(x)}{dx}\right|_{x=L_i} = \left.\frac{d\phi_{n,i+1}(x)}{dx}\right|_{x=0}$$
$$\left.\frac{d^2\phi_{n,i}(x)}{d^2x}\right|_{x=L_i} = \left.\frac{d^2\phi_{n,i+1}(x)}{d^2x}\right|_{x=0} \tag{4.23}$$

$$\phi_{n,i}(x)_{x=L_i} = \phi_{n,i}(x)_{x=0} = 0$$

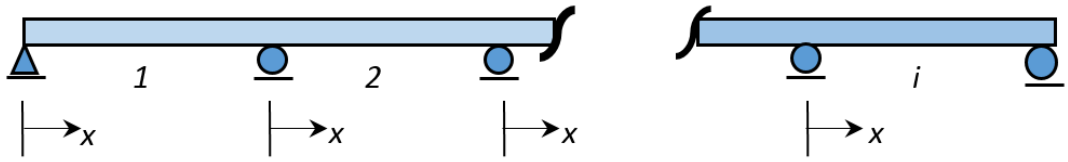

Figure 4.3: Continuous simply supported beam

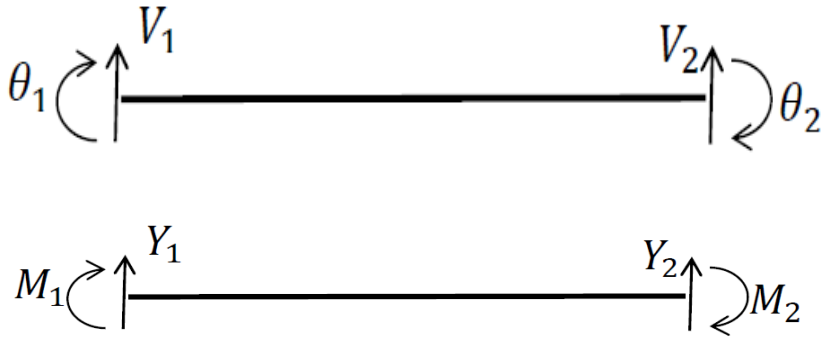

Figure 4.4: Displacements and end forces signs

where $x = L_i$ is the end of ith span and $x = 0$ is the start of of a span. The first and last supports have no moments and displacement is restrained. More general boundary conditions can be applied but are not considered in this chapter [Fertis, 1995, Johansson *et al.*, 2013].

Hayashikawa and Watanabe [1981] formulated the eigen stiffness matrix for a continuous beam based on imposed boundary conditions and the eigen values can be obtained after assembled matrix for the bridge and boundary conditions enforced. The eigen matrix for given span is given based on the conversion in Fig 4.4:

$$\begin{bmatrix} Y_1 \\ M_1 \\ Y_2 \\ M_2 \end{bmatrix} = \begin{bmatrix} k_{11} & k_{12} & k_{13} & k_{14} \\ & k_{22} & k_{23} & k_{24} \\ & & k_{33} & k_{34} \\ & \text{SYM.} & & k_{44} \end{bmatrix} \begin{bmatrix} V_1 \\ \theta_1 \\ V_2 \\ \theta_2 \end{bmatrix} \tag{4.24}$$

Table 4.1: Continuous beam natural frequency(λ)

Spans	Mode number										
	1	2	3	4	5	6	7	8	9	10	11
1	3.14	6.28	9.42	12.57	15.71	18.85	21.99	25.13	28.27	31.42	34.56
2	3.14	3.93	6.28	7.07	9.42	10.21	12.57	13.35	15.71	16.49	18.85
4	3.14	3.39	3.92	4.46	6.28	6.55	7.07	7.59	9.42	9.69	10.21
11	3.14	3.18	3.28	3.45	3.62	3.82	4.03	4.23	4.42	4.58	4.69

where

$$
\begin{aligned}
k_{11} &= G(\sin\lambda\cosh\lambda + \cos\lambda\sinh\lambda;\\
k_{12} &= \frac{-G(\sin\lambda\sinh\lambda)}{\Theta};\\
k_{13} &= -G(\sin\lambda + \sinh\lambda);\\
k_{14} &= \frac{G(\cos\lambda - \cosh\lambda)}{\Theta};\\
k_{22} &= \frac{G(\sin\lambda\cosh\lambda - \cos\lambda\sinh\lambda)}{\Theta^2};\\
k_{24} &= \frac{-G(\sin\lambda - \sinh\lambda)}{\Theta^2};\\
G &= \frac{EI\Theta^3}{1-\cos\lambda\cosh\lambda)};
\end{aligned}
\tag{4.25}
$$

$k_{33} = k_{11}; k_{23} = -k_{14}; k_{34} = -k_{12}; k_{44} = k_{22}$

and $\lambda = \Theta/L$ and L is the respective span length. The equation 4.24 above can be written as:

$$\{F\} = [K]\{U\} \tag{4.26}$$

The eigen values are computed from equation:

$$det|\mathbf{K}| = 0 \tag{4.27}$$

The non dimensioanlised frequencies λ of beams with uniform cross section and equal spans on simple supports is obtained by solving the equation 4.27 numerically using $Matlab$ and are presented in Table 4.1. The corresponding displacement normalised mode shapes are given in Figs 4.5 to 4.6.

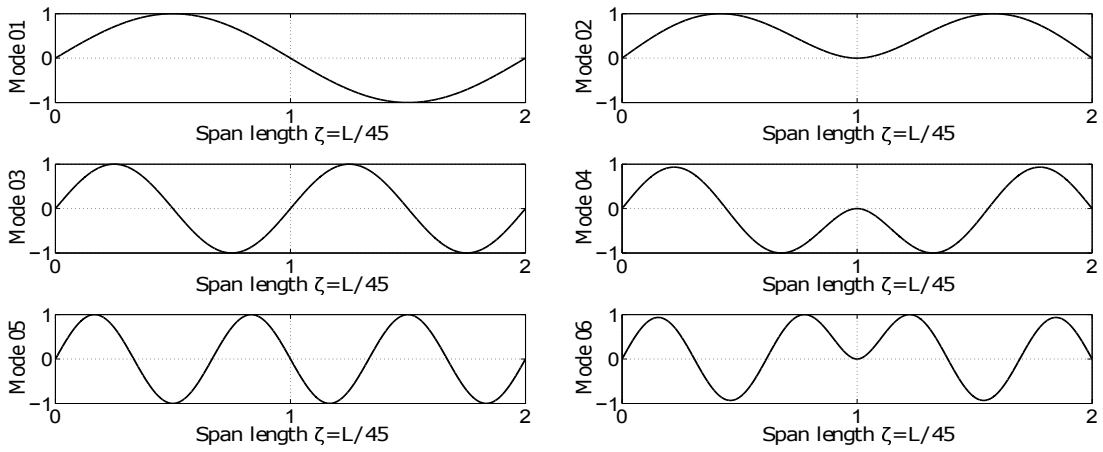

Figure 4.5: 2 span beam mode clusters

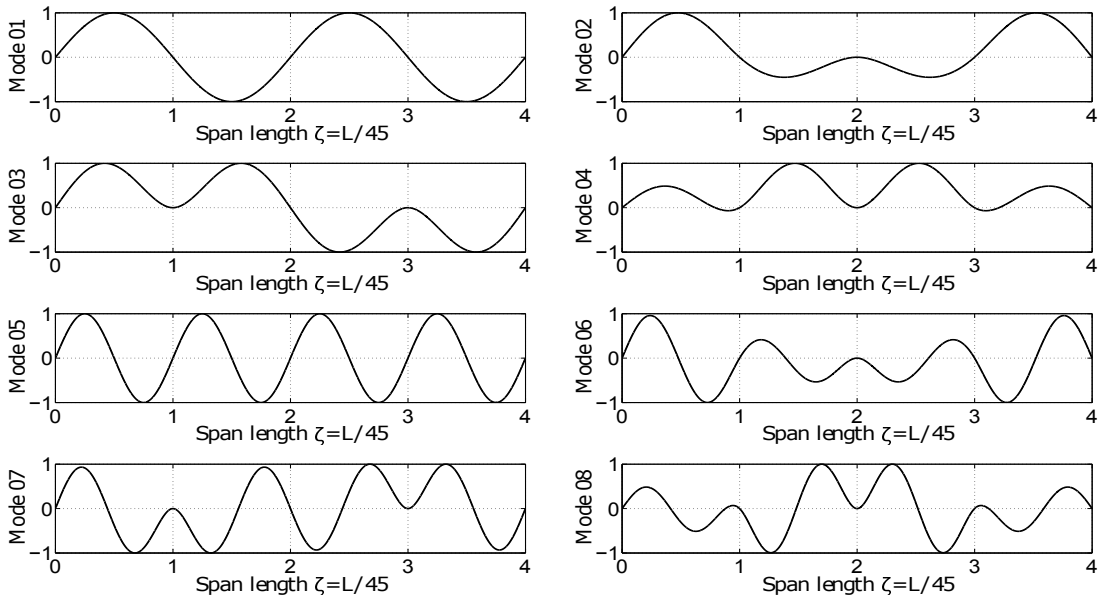

Figure 4.6: 4 span beam mode clusters

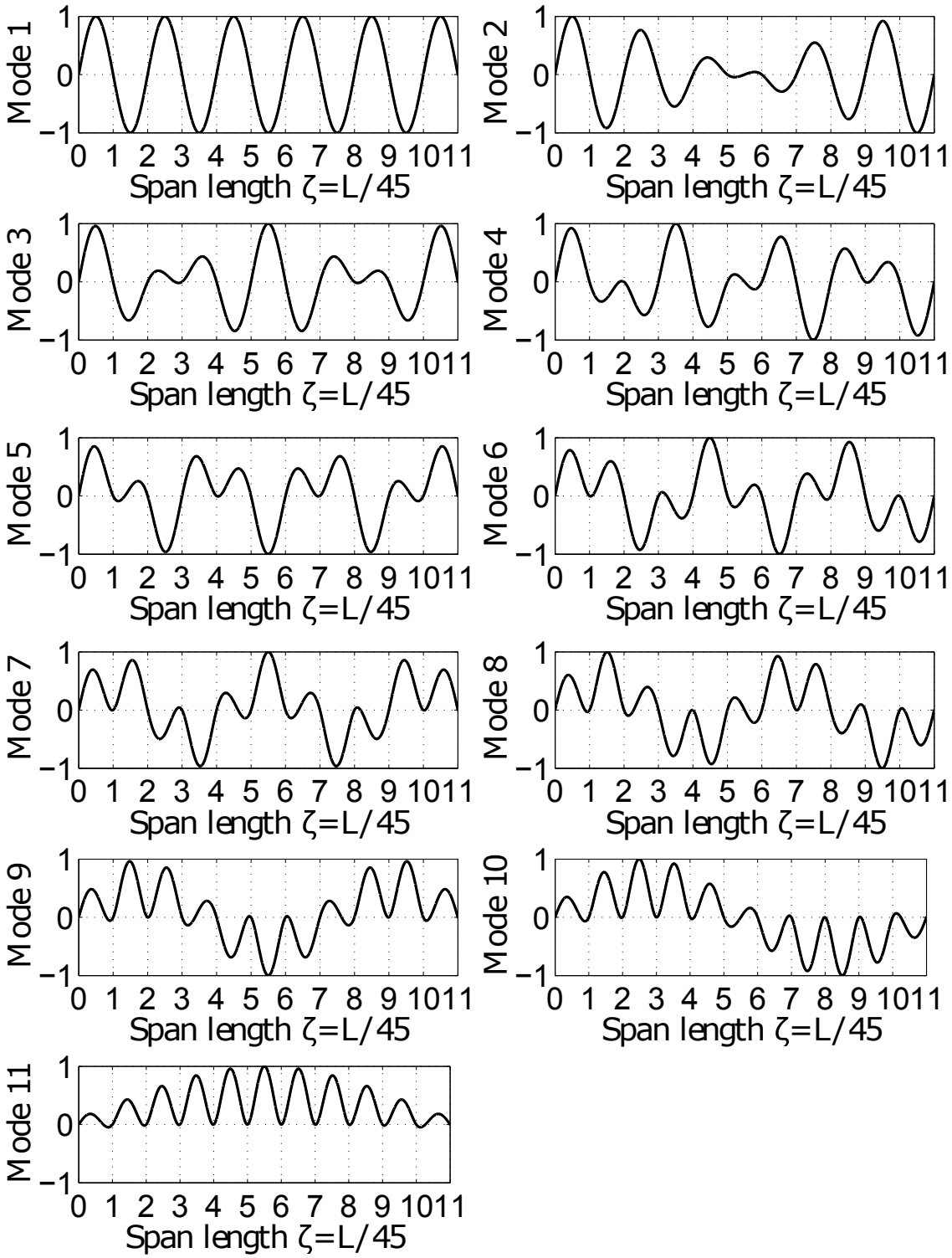

Figure 4.7: 11 span beam mode clusters

4.4 Frequency of beam bridges with added masses

The vibration of railway bridges during train passage has been of interest to researchers over the years. It is generally recognised that the modal parameters of vehicle-bridge system are non stationary during vehicle passage [Ewing, 1929, Fryba, 1999]. The two main cases of stationary sprung and moving masses on beam type bridges have been investigated with main focus on frequency of combined sprung mass-bridge systems. Kukla and Posiadala [1994] investigated beams with stationary sprung masses using Green functions. Although this method is an exact formulation, the main drawback is that it is not easily implemented in efficient computer codes. GÜRGÖZE [1998] used the assumed-modes and lagrange multiplier compute natural frequencies of beams with sprung mass attachments. Cha [2001] formulated a more computationally method that can be applied to obtain natural frequencies of a beam with multiple attachments as given by equation 4.28 (derivation in Cha and Wong [1999], Cha [2001]):

$$\omega = \Big\{ \prod_{i=1}^{N} (K_i - \omega^2 M_i) \Big\} \det[\mathbf{B}] = 0 \tag{4.28}$$

where K_i,M_i are diagonal elements in stiffness and mass matrix respectively, ω is circular frequency and N is the number of modes in the expansion. The elements of the $S \times S$ matrix [B] where s is the number of attached sprung masses are given by

$$b_{ij} = \sum_{i=1}^{N} \frac{\phi_r(x_i)\phi_r(x_j)}{K_r - \omega^2 M_r} + \frac{1}{\sigma_i}\delta_i^j, \ i,j = 1,....S \tag{4.29}$$

where δ_i^j is the Kronecker delta and $\phi_r(x_i)$ is the r th mode function at attachment position x_i and σ_i is given below:

$$\sigma_i = \frac{k_i m_i \omega^2}{\omega^2 m_i - k_i} \tag{4.30}$$

where k_i,m_i are the attached spring and masses respectively. The equation 4.28 can be efficiently programmed and when attached masses are not positioned at nodes of mode shapes corresponding to frequencies of interest the equation

reduces to:

$$\det[\mathbf{B}] = 0 \tag{4.31}$$

The vehicle-bridge systems that include effects of motion have been investigated. Mao and Lu [2011] considered the effect of added vehicle mass on critical speeds for resonance to occur. The investigation was done using finite element model of short span fixed-fixed and simply supported beams under passage of sprung masses. It was observed that the critical speeds reduced for vehicle mass ratios above 1 by approximately 10% due to a reduction in bridge-vehicle fundamental frequency. There was no significant reduction of critical speed for mass ratios below 1.

Cantero and OBrien [2013] investigated the influence of vehicle-bridge mass and frequency ratios on combined system fundamental frequency for simply supported beam type bridges. A general patten was observed in analytical studies using sprung masses where combined system fundamental frequency reduced in comparison to unloaded bridge fundamental frequency if vehicle frequency was higher than bridge frequency. In contrast when vehicle frequency was less than bridge fundamental frequency, there was an increase in combined system fundamental frequency. More recently Cantero *et al.* [2017] conducted both analytical and field testing of bridges under stationary and moving vehicles. The bridges tested were 3 span bridge and a single span bridge with fundamental frequencies of 3.5Hz and 3.13 Hz respectively. The 3 span bridge was tested by having a 3 axle 26 tonne truck drive at craw speed of 13 km/h/h to excite the bridge while minimising the dynamic effects of uneven ridding surface or loading frequency from axle spacing. There was an increase in bridge frequency from 3.5 Hz to 3.63 Hz during train passage. The single span bridge on the other hand was tested with vehicle at selected stationary positions. There was an increase in bridge frequency from 3.13 to 3.5Hz during the test.

The above studies mostly demonstrated the effects of vehicle mass on the bridge but did not propose formulae between unloaded and loaded bridge frequencies.

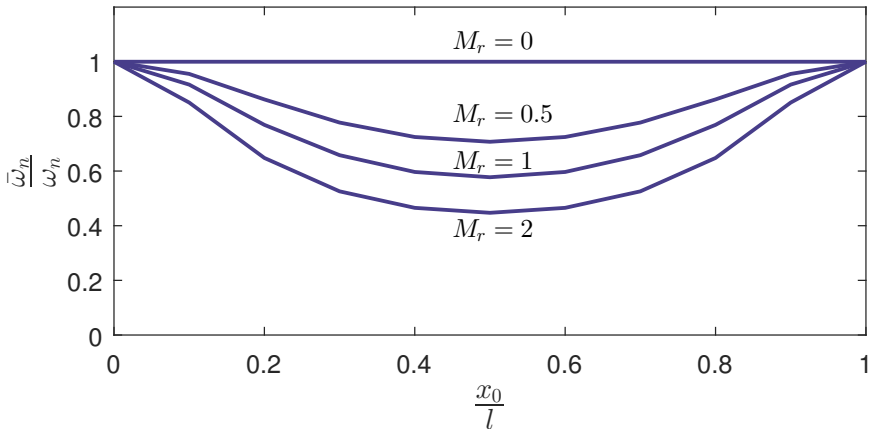

Figure 4.8: Frequency variation of loaded beam

Fryba [1999] proposed some approximate formulae that account for increased mass on the bridge:

$$\bar{\omega} = \omega\sqrt{\frac{\mu}{\bar{\mu}}} \tag{4.32}$$

where $\bar{\omega}$ and $\bar{\mu}$ are frequency and mass per unit length of loaded bridge respectively while ω and μ are frequency and mass per unit length of unloaded bridge. Fryba [1999] derived an approximate equation for computing the frequency of a loaded beam taking into account the contribution of the added mass given below:

$$\bar{\omega}_n = \frac{\omega}{\sqrt{1 + \frac{2m_w}{m_b}\sin^2\frac{n\pi x_0}{L}}} \tag{4.33}$$

where m_w is the moving mass, m_b is mass of the bridge, L is the total length and x_0 is the force location. A parametric solution for different ratios of moving mass to the bridge mass and at different moving mass locations is reported by Fryba [1999] with typical plots shown in Fig 4.8 for selected vehicle to bridge mass ratios M_r. The fundamental frequency reduction is maximum when the moving mass is located at mid span. An examination of equation 4.32 shows that it does not explicitly show the relation between system frequency and location of moving vehicle on particular bridge. This aspect is addressed by equation 4.33 which is applicable to a single span simply supported beam.

The frequency of beams loaded with stationary sprung masses has been investigated in literature. It is generally recognised that the presence of

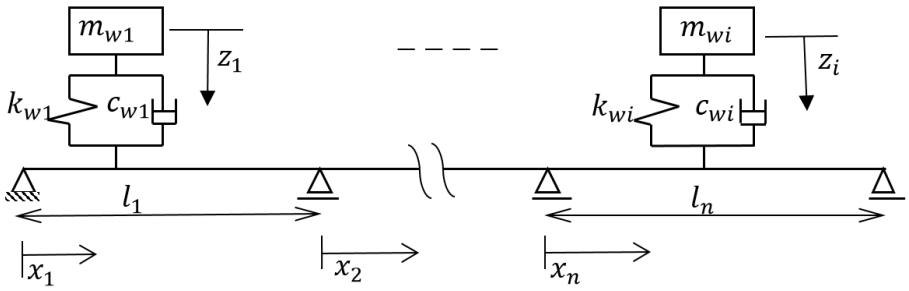

Figure 4.9: Continuous beam with sprung masses

additional mass on the bridge reduces natural frequency of the combined bridge-train system [Ewing, 1929, Fryba, 1999]. In order to study the frequency-time evolution of beams under moving loads, it is necessary to consider the inertial effects from the masses and therefore equation 4.9 is reformulated by replacing the forcing function. Consider an Euler-Bernoulli beam carrying sprung masses as shown in Fig 4.9. The governing equation for such a system is given as:

$$EI\frac{\partial^4 W(x,t)}{\partial x^4} + c_b\frac{\partial W(x,t)}{\partial t} + m_b\frac{\partial^2 W(x,t)}{\partial t^2} = P(t)\delta(x - vt) \tag{4.34}$$

where the subscript b represents beam parameters with m_b and c_b is the bridge mass and damping respectively,W is bridge vertical displacement,v is vehicle speed across the bridge, and the forcing function $P(t)$ is given below:

$$P(t) = \sum_{i=1}^{N}\left[m_{wi}g - m_{wi}\frac{\partial^2 W(x,t)}{dt^2} + c_{wi}\left(\frac{dz_i}{dt} - \frac{du_i}{dt}\right) + k_{wi}\left(z_i - u_i\right)\right] \tag{4.35}$$

where the subscript w represents moving mass parameters with m_w, c_w and k_w are the vehicle mass, damping and stiffness respectively and u_i is the bridge displacement at point of contact with mass m_{wi}. As a first approximation, the Coriolis and centripetal forces are ignored. Utilising the mode expansion representation of deflected bridge shape:

$$W(x,t) = \sum_{n=1}^{\infty}\phi_n(x)q(t)_n \tag{4.36}$$

where $\phi_n(x)$ is the nth the mass normalised vibration mode of the bridge and $q(t)$ are generalised generalised coordinates. Substituting in above, multiplying by $\phi(x)$

and making use of orthogonality conditions:

$$\frac{d^2q_n(t)}{dt^2} + 2\omega_n\xi_n\frac{dq_n(t)}{dt} + \omega_n^2 q_n(t) = P(t)\phi(vt) \tag{4.37}$$

The dynamic equilibrium of the sprung mass is given as:

$$m_{wi}\ddot{z} + k_i(z_i - W(x,t)) = 0 \tag{4.38}$$

The equations above are coupled and have been solved numerically. However, Li *et al.* [2003] proposed an approximate formula that is extended here for continuous beams. The equation above can be rearranged assuming a train of moving masses each with mass m_w, damping c_w and stiffness k_w:

$$\begin{aligned}\left[1 + m_w\sum_{i=1}^{N}\phi_i^2(vt)\right]\ddot{q}_n(t) + \left[2\xi_n\omega_n + c_w\sum_{i=1}^{N}\phi_i^2(vt)\right]\dot{q}_n(t) \\ + \left[\omega_n^2 + k_w\sum_{i=1}^{N}\phi_i^2(vt)\right]q_n(t) = p_n(t)\end{aligned} \tag{4.39}$$

where

$$\begin{aligned}p(t) = \sum_{i=1}^{N}\phi_i(vt)\Bigg[m_{wi}g - m_{wi}\sum_{k=1}^{\infty}\phi_k(vt)\ddot{q} + c_s(\frac{dz_i}{dt} - \frac{du_i}{dt}) \\ +k_i(z_i - u_i)\Bigg]\end{aligned} \tag{4.40}$$

The combined frequency of the system incorporating only moving mass can be computed as:

$$\bar{\omega}_n^2(t) = \frac{\omega_n^2 + k_{wi}\sum_{k=1}^{N}\phi_k^2(vt)}{1 + m_{wi}\sum_{k=1}^{N}\phi_k^2(vt)} \tag{4.41}$$

Li *et al.* [2003] presented a similar equation for frequency-time evolution of a single span simply supported bridge during passage of trains. The approximate equation 4.41 is a more general form that can be applied to multi-span bridges with different boundary conditions, provided the coefficients in the mode shape function $\phi(vt)$ can be obtained. The bridge frequency during massage of train depends on the train mass and the stiffness of the train suspension system. As the frequency is a key parameter in determining bridge response, the updated frequency $\bar{\omega}_n$ includes both the effects of mass and stiffness where the increases in mass tends to lower the combined system frequency while the increased vehicle stiffness increases the

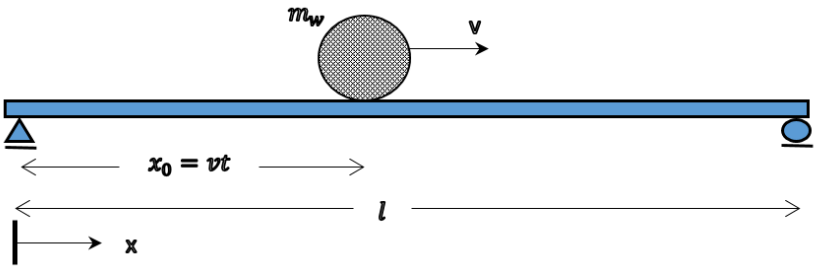

Figure 4.10: Simply supported beam with moving mass

stiffness.

4.4.1 Frequency of loaded simply supported single span beams

The frequency-time evolution for simply supported beams under a single moving mass has been widely investigated and is reported in literature.

A generalisation of the frequency reduction for a simply supported beam can be obtained by from equation 4.41 and Eq 4.46 with A,B and C terms in $\phi(vt)$ vanishing. The mode shape function for a simply supported beam is obtained from equation 4.42.

$$\phi(x) = \sin \frac{n\pi x}{l} \tag{4.42}$$

where n,x and l are the mode number, the location and the beam length respectively. In the generalised equation 4.41, the mode shape is mass normalised and the location is defined as:

$$\phi(vt) = \sqrt{\frac{2}{m_b l}} \sin \frac{n\pi vt}{l} \tag{4.43}$$

where v and t are velocity and time respectively with $0 \leq vt \leq l$ which is the location of the mass on the bridge and m_b is the bridge linear mass density. Thus substituting equation 4.43 in 4.44

$$\bar{\omega}_n^2(t) = \frac{\omega_n^2 + \dfrac{2k_{wi}}{m_b l} \sum\limits_{k=1}^{N} \sin^2 \dfrac{n\pi vt}{l}}{1 + \dfrac{2m_{wi}}{m_b l} \sum\limits_{k=1}^{N} \sin^2 \dfrac{n\pi vt}{l}} \tag{4.44}$$

The approximate formula in equation 4.44 is a further development of equation 4.33 to include the effects of springs in the case of sprung masses. The moving

mass approximation will generally underestimate the loaded bridge frequency as the springs in the vehicles have a general effect of increasing the frequency. Li *et al.* [2003] derived a similar equation for frequency-time evolution of a simply supported beam. The frequency obtained for a train of moving masses oscillates with time due to the time variation of modal mass as the moving masses move along the beam.

4.4.2 Frequency-time evolution of continuous beams

The frequency-time evolution for a continuous beam on simple supports is obtained from equation 4.41 with mass normalised modeshape $\phi(vt)$. Unlike the case of simply supported beams where the mode shape changes as the mass moves across the beam, it is expected that the mode shapes for continuous beams change during the time when the train only partially loads the bridge. However during the time when the bridge is fully loaded, the mode shapes can be assumed to be approximately the same with the free vibration case. Thus the generalised equation:

$$\bar{\omega}_n^2(t) = \frac{\omega_n^2 + k_{wi} \sum_{k=1}^{N} \phi_k^2(vt)}{1 + m_{wi} \sum_{k=1}^{N} \phi_k^2(vt)} \tag{4.45}$$

where

$$\phi_{n,i}(x) = A_{n,i}\cosh(\Theta_n x) + B_{n,i}\sinh(\Theta_n x) + C_{n,i}\cos(\Theta_n x) + D_{n,i}\sin(\Theta_n x) \tag{4.46}$$

where $A_{n,i}$,$B_{n,i}$,$C_{n,i}$ and $D_{n,i}$ are mode shape constants for the nth mode at the i th span.

4.5 Olifants River Bridge: Case study

The Olifants River Bridge whose geometry and monitoring system has been described in detail in methodology is used for the case study where analytical values are compared with estimates from measured vibrations. The free vibrations of the continuous span are investigated first based on measurements from the continuous monitoring system on span 20. This is followed by a study

on the frequency evolution of of the bridge during train passage.

The geometric and material properties assumed are Youngs modulus $E = 40GPa$ for concrete, moment of inertia $I = 9.58m^4$ and density of concrete $\rho = 2500kg/m^3$ and bridge superstructure linear density along the length $12379kg/m$. These values are not based on any material testing as this has not been possible. They are based on information from construction drawings of required strength for concrete and from available literature on concrete material properties.

The bridge is located on the iron ore line carries a with traffic being primarily empty and loaded freight trains carrying mostly iron ore and in some cases manganese. Typical trains consists of 342 wagons of type CR-13 and and 8 Type 15E locomotive engines operating under a distributed power system. The wagons have two bogies each with 2 axles and static load of 30 tonnes per axle when loaded and 5 tonnes when empty. The main locomotive engine type 15E has 2 bogies each consisting of 3 axles that have 21 tonne static axle loads. The details of the traffic load composition and train types are presented in chapters on load models. However for this study, the linear mass of the empty and loaded bogies is included which is $2040kg/m$ and $12245kg$ respectively. The loaded trains constitute about 88% of the linear mass density when bridge is fully loaded and 15%.

4.5.1 Bridge free vibrations

Ambient vibration measurements on span 23 from continuous monitoring data was selected for a period just before a train event. A plot of power density spectra in Fig 4.11 shows limited number of flexural modes with fundamental vertical mode at 4.09Hz. The natural frequencies of multi-span beams with equal span length exhibit close and clustered frequencies with cluster size equal to number of spans as shown in earlier section. There is a high degree of mode coupling as seen in Fig 4.3 of the mode shapes.The plotted mode shapes shows that displacements of modes 1,2,6 and 8 are coupled with modes 1 and 7 being dominant in the instrumented span. The displacements of modes 3,4 5,9,10 and 11 are also coupled with modes 4,10 and 11 are also coupled with modes 4, 10

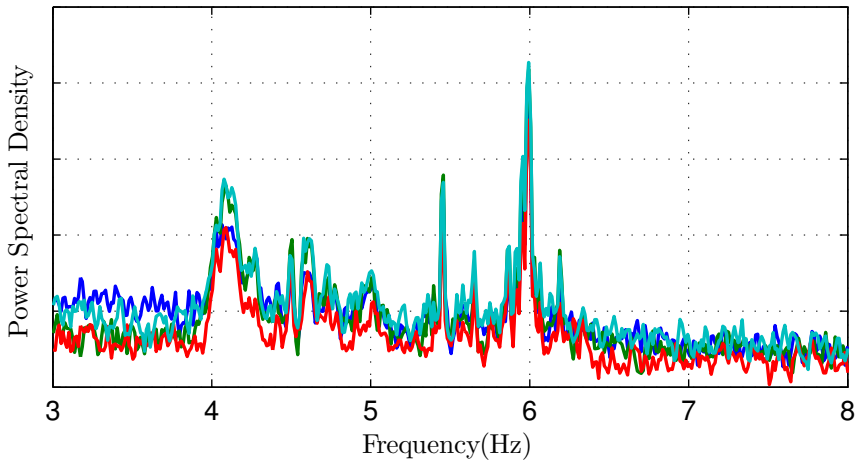

Figure 4.11: Power Spectral Density of vertical vibrations

and 11 being dominant.

The first 11 frequencies of flexural modes of the girder are obtained from equation 4.27 using $Matlab^R$ and are presented in Table 4.2. The natural frequencies are extracted over a period of one year shown in Fig below. There is no observed trends or seasonal effects in the natural frequency during the period under study. The current instrumentation arrangement can be used to effectively track frequencies over time but due the nature of the structure, it is not possible to validate the modes based on these measurements alone. A separate study has been was conducted to estimate the bridge modal parameters and observe their evolution over a period of time [Busatta and Moyo, 2017]. The tracked modes show no variations due to daily, weakly or monthly temperature over a period of 6 months.

4.6 Frequency evolution during train passage

The system frequency evolution of Olifants Bridge is investigated using the approximate analytical equation as well as vibration measurements of the bridge during train passage. The analytical investigations are performed for 60 wagon train moving masses with mass equal to an empty and loaded wagon. The existing freight trains on the ore line are much longer than 60 wagons. The choice of 60 wagons for simulations is to have a train long enough to have the

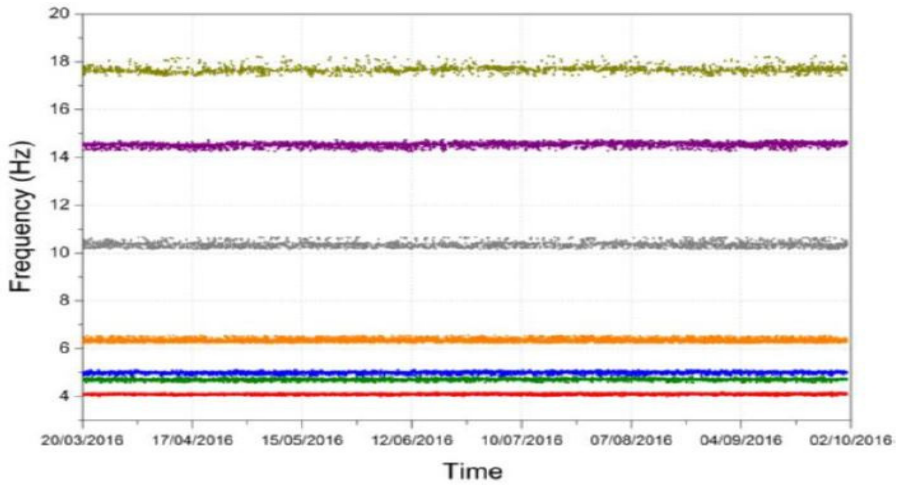

Figure 4.12: Tracking of natural frequencies [Busatta and Moyo, 2017]

who bridge loaded so as to provide insight into the bridge frequency evolution. The experimental study on the other hand is based on measurements of loaded train event identified from WIM-WIM data. The trains selected for this study are the long 342 wagon empty and loaded trains as they provide a longer measurement period allowing for better frequency resolution of the signal.

4.6.1 Frequency evolution based on analytical formulation

The frequency evolution from passage of 60 wagon empty and loaded train masses on the 45m drop span bridge is shown in Fig 4.13 to Fig 4.16. There are greater oscillations in the higher frequencies due to changes in modal mass as moving mass moves along the beam. However it is also observed that there are lower frequency high amplitude oscillations observed in frequencies corresponding to higher modes alongside the high frequency low amplitude oscillations. There is also an increase in the frequency of the low frequency oscillations for flexural frequencies corresponding to higher modes.

There is a general reduction in fundamental frequency during passage of 5 wagon masses. This reduction is from the additional non-structural mass which changes the modal mass without changing the system stiffness. The reductions in frequency are less clear for higher frequencies largely due to the low frequency high amplitude oscillations.

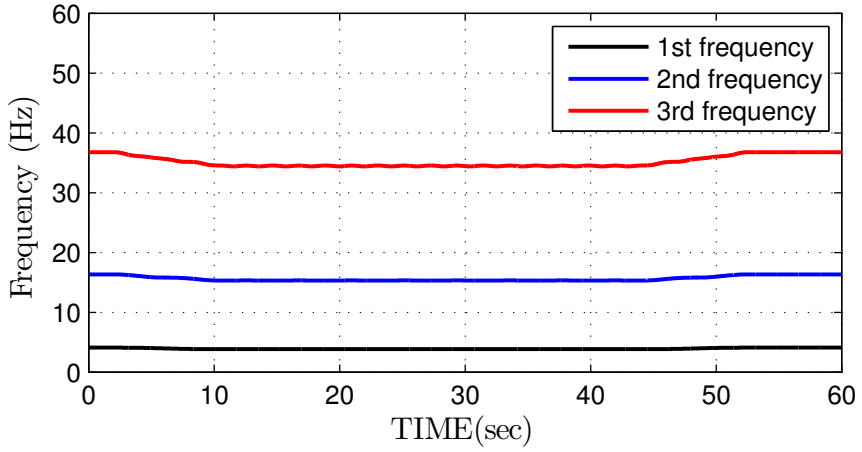

Figure 4.13: Frequency-time evolution of simply supported bridge during empty train passage

Table 4.2: Bridge-Train system frequencies

Vertical Mode	f_n (Hz)	Bridge-train system f_E(Hz)	f_L(Hz)
1	4.09	3.83	3.03
2	4.18	3.92	3.09
3	4.46	4.18	3.30
4	4.88	4.57	3.61
5	5.43	5.09	4.02
6	6.05	5.67	4.46
7	6.72	6.30	4.97
8	7.42	6.96	5.49
9	8.09	7.58	5.99
10	8.68	8.14	6.42
11	9.10	8.53	6.73

Note: f_n=bridge natural frequency
f_L is loaded train-bridge system frequency
f_E is empty train-bridge system frequency

The frequency evolution of the bridge segment with all 11 spans loaded is shown in Fig 4.15 and Fig 4.16. The oscillations in frequency observed earlier for simply supported span occur only as the train enters and leaves the bridge. The frequency oscillations are negligible during when the time the bridge is fully loaded. The reductions in natural frequency are observed for both empty and loaded train cases with system frequencies summarised in Table 4.2. During the train event, the fundamental flexural frequency reduces by 3.4% and 16.6% for the empty and loaded trains respectively.

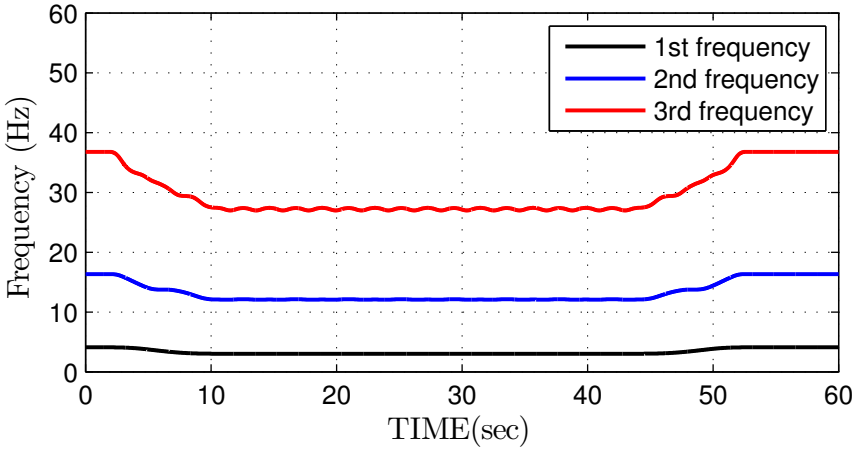

Figure 4.14: Frequency-time evolution of simply supported bridge during loaded train passage

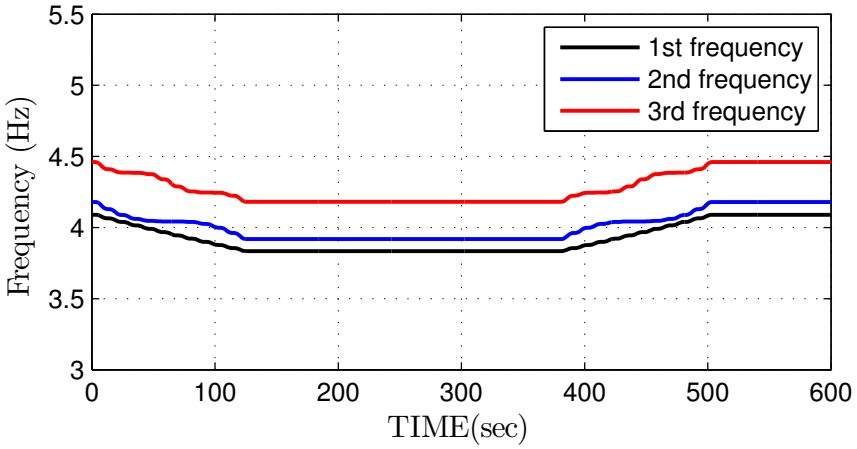

Figure 4.15: Frequency-time evolution of 11 span simply supported bridge during empty train passage

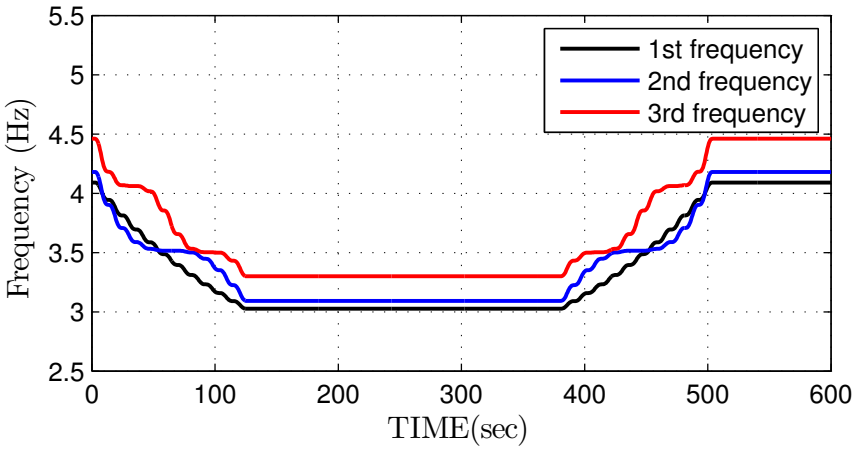

Figure 4.16: Frequency-time evolution of 11 span simply supported bridge during loaded train passage

4.6.2 Frequency evolution based on bridge vibration measurements

Vibration measurements of Olifants Bridge during train passage were used to study the frequency evolution. Selected trains were chosen from WIM-WIM data from month of June 2016. The longest trains consisting of 340 wagons and 6 locomotive with estimated total length of 4km whose vibrations were selected. A typical vibration measurement is presented in Fig 4.17. A preliminary analysis was done using the spectrogram function with a kaiser window in $Matlab$ to plot time-frequency evolution of the whole event. The closely banded frequencies of the combined system are observed in Fig 4.18 which seem consistent with the analytical derivations that showed clustered modes. A compromise is made between time and frequency resolution by the selection of window size and it is observed that modes with less power are not resolved. However, it is observed that there is a clear reduction in natural frequency. However for loaded freight rail where the train to bridge mass ratios are high, reductions in combined frequency of 16% have been observed. A simplified equation based on the moving mass formulation can be used to obtain the combined system frequencies during loaded train events.

The vibration signal was first filtered to eliminate modes higher than 12Hz and a Complete Ensemble Empirical Mode Decomposition (CEEMD) procedure is applied to the measurements and the lowest frequency is shown in Fig 4.19. The resulting modes are then analysed using the Hilbert transform with the instantaneous frequency obtained after differentiating the phase. CEEMD does not resolve the lower clustered frequency modes sufficiently well, however the reduction of frequency over time can be clearly observed from the filtered instantaneous frequency plot. The behaviour of the combined system is quite complex and the frequency decreases slowly to 3.45Hz thereafter starts to increase. While the overall fundamental frequency reduces to 3.45Hz which is predicted within 2% of the frequency obtained from equation 4.41.

The frequency time evolution gradient for the analytical formulation is very

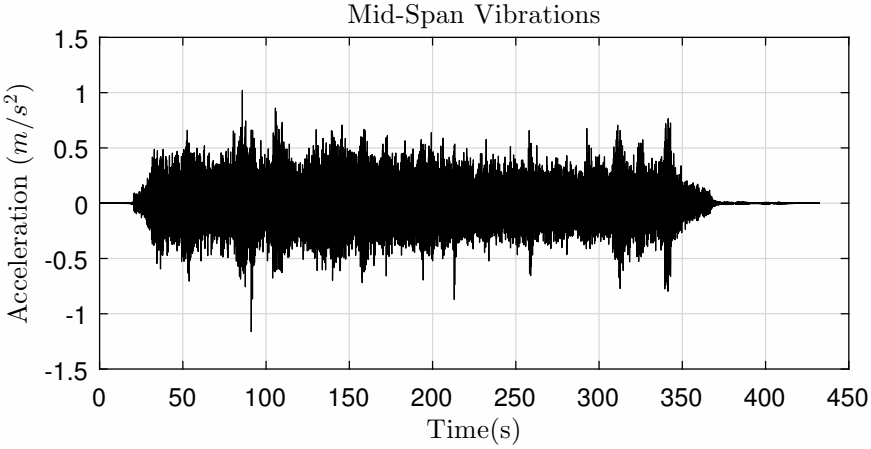

Figure 4.17: Typical vibration measurement during train passage

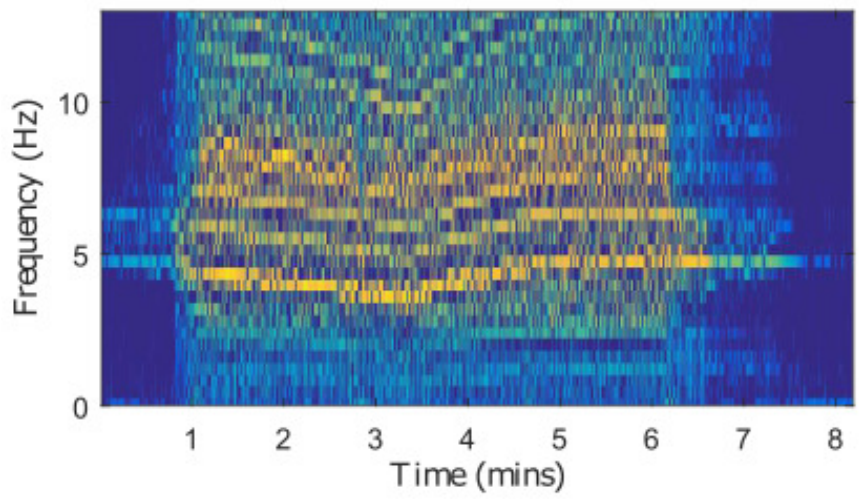

Figure 4.18: Frequency-time loaded

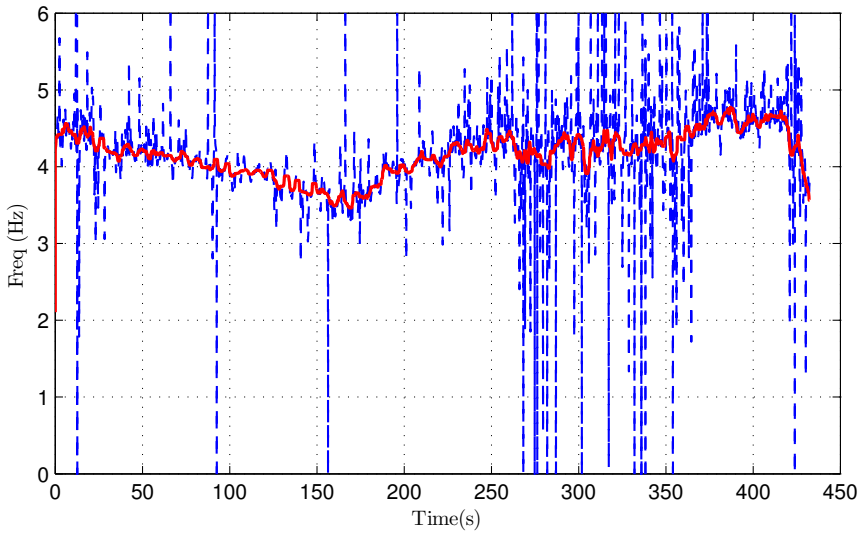

Figure 4.19: Instantaneous Frequency- Loaded train

different from that obtained from field measurements despite the agreement in minimum frequency values. The behaviour of combined systems is complex. Actual train wagons are generally modelled with many degrees of freedom to allow pitch and yaw. The suspension systems constitute several primary and secondary springs and dampers with potential to introduce non-linearities in dynamic behaviour. Furthermore, the bridge system can be more complex than the idealisation when piers and different bearing systems are taken into account. This could be some of the factors that could have influenced the frequency evolution

4.7 Concluding remarks

Bridge natural frequency is used in simplified formulae provided by design codes to determine dynamic amplifications of load effects. Bridge fundamental frequency is also used in field studies where quasi-static load effects on highway bridges are obtained from dynamic bridge responses by filtering dynamic effects. Bridge-vehicle systems on heavy haul rail lines under loads where the vehicle mass to bridge mass ratio is high experience reductions in frequencies of the combined system. Significant reductions in Olifants Bridge system frequencies on South African heavy haul line are observed. While the differences in minimum fundamental frequency obtained from approximate formula and the estimate from field measurements is small, there are significant differences in the overall pattern. The analytical solution shows a rapid decrease with frequencies remaining fairly constant for the period the bridge is fully loaded and thereafter the frequency increases to the unloaded bridge frequency. The field measurements show that this decrease is gradual and the frequency does not remain at minimum value for the duration of train passage. The derived system frequency is used in the chapter that follows as the basis for both analytical and experimental determination of amplification factors.

References

BS EN 1991-2:2003, "Actions on strcutures part2: Traffic loads on bridges," Standard, British Standards Institution.

Ewing J.A., "The vibrations of railway bridges: An example of co-operative research," *Journal of the Royal Society of Arts*, 77(3989); 624–646, 1929.
URL `http://www.jstor.org/stable/41358216`

Inglis C.E., *A Mathematical Treatise on Vibrations in railway Bridges*, Cambridge University Press, 1934.

Thomas W.T., *Theory of Vibrations with Applications*, Prentice-Hall Inc, N.J, 1972.

Hayashikawa T. and Watanabe N., "Dynamic behavior of continuous beams with moving loads," *Journal of the Engineering Mechanics Division*, 107(1); 229–246, 1981.

Billing J.R., "Dynamic loading and testing of bridges in ontario," *Canadian Journal of Civil Engineering*, 11(4); 833–843, 1984.

Chu K., Garg V. and Wang T., "Impact in railway prestressed concrete bridges," *Journal of Structural Engineering*, 112(5); 1036–1051, 1986.

Paultre P., Chaallal O. and Proulx J., "Bridge dynamics and dynamic amplification factors-a review of analytical and experimental findings," *Candian Journal of Civil Engineering*, 19; 260–278, 1992.

Humar J.L. and Kashif A.M., "Dynamic response of bridges under travelling loads," *Canadian Journal of Civil Engineering*, 20; 287–298, 1993.

Kukla S. and Posiadala B., "Free vibrations of beams with elastically mounted masses," *Journal of Sound and Vibration*, 175(4); 557–564, 1994.

Memory T., Thambiratnam D. and Brameld G., "Free vibration analysis of bridges," *Engineering Structures*, 17(10); 705–713, 1995.

Yang Y.B., Liao S.S. and Lin B.H., "Impact formulas for vehicles moving over simple and continuous beams," *J. of Structural Engineering ASCE*, 121 No 11; 1644–1650, 1995.

Fertis D.G., *Mechanical and Structural Vibrations* , John Wiley and Sons, Inc, 1995.

Frỳba L., *Dynamics of railway bridges*, Thomas Telford Publishing, 1996.

GÜRGÖZE M., "On the alternative formulations of the frequency equation of a bernoulli-euler beam to which several spring-mass systems are attached in-span," *Journal of sound and vibration*, 217(3); 585–595, 1998.

Yau J.D., Yang Y.B. and Kuo S.R., "Impact response of high speed rail bridges and riding comfort of rail cars," *Engineering structures*, 21(9); 836–844, 1999.

Cha P. and Wong W., "A novel approach to determine the frequency equations of combined dynamical systems," *Journal of Sound and Vibration*, 219(4); 689–706, 1999.

Fryba L., *Vibration of Solids and Structures under Moving Loads*, Thomas Telford, London, 3 edition, 1999.

Cha P., "Natural frequencies of a linear elastica carrying any number of sprung masses," *Journal of sound and vibration*, 247(1); 185–194, 2001.

Dugush Y.A. and Eisenberger M., "Vibrations of non-uniform continuous beams under moving loads ," *Journal of Sound and Vibration*, 254(5); 911–926, 2002.

Li J., Su M. and Fan L., "Natural frequency of railway girder bridges under vehicle loads," *Journal of Bridge Engineering*, 8(4); 199–203, 2003.

Xia H., Zhang N. and Guo W., "Analysis of resonance mechanism and conditions of train-bridge system," *Journal of Sound and Vibrations*, 297; 810–822, 2006.

Rao S.S., *Vibrations of Continuous Systems*, John Wiley & Sons, 2007.

Hamidi S.A. and Danshjoo F., "Determination of impact factor for steel railway bridges considering simultaneous effects of vehicle speed and axle distance to span length ratio," *Engineering Structures*, 32(5); 1369–1376, 2010.

Deng L. and Cai C., "Development of dynamic impact factor for performance evaluation of existing multi-girder concrete bridges," *Engineering Structures*, 32(1); 21–31, 2010.

Mao L. and Lu Y., "Critical speed and resonance criteria of railway bridge response to moving trains," *Journal of Bridge Engineering*, 18(2); 131–141, 2011.

Ouyang H., "Moving-load dynamic problems: A tutorial (with a brief overview)," *Mechanical Systems and Signal Processing*, 25(6); 2039–2060, 2011.

Hayward A.C.G., "Train loading on bridges since Stephenson's Rocket,"

Proceedings of Institution of Civil Engineers-Bridge Engineering, 167 IssueBE4; 326–337, 2011.

Johansson C., Pacoste C. and Karoumi R., "Closed-form solution for the mode superposition analysis of the vibration in multi-span beam bridges caused by concentrated moving loads," *Computers & Structures*, 119; 85–94, 2013.

Cantero D. and OBrien E.J., "The non-stationarity of apparent bridge natural frequencies during vehicle crossing events," *FME transactions*, 41(4); 279–284, 2013.

Cantero D., Hester D. and Brownjohn J., "Evolution of bridge frequencies and modes of vibration during truck passage," *Engineering Structures*, 152; 452–464, 2017.

Busatta F. and Moyo P., "How testing and monitoring can support heavy haul railway bridge management: The experience gained in South Africa," *11-th International Heavy Haul Conference Proceedings, Capw Town*, 599–, 2017.

Chapter 5

DYNAMIC AMPLIFICATION OF RAILWAY BRIDGES

5.1 Introduction

The response of railway bridges under traffic loads has been the subject of research for many years. This is largely for historical reasons when early locomotive steam engines were generally heavier than wagons and their unbalanced masses caused vibration problems from the hammer blow action [Inglis, 1934, Hayward, 2011]. Improvements in locomotive design have reduced the hammer blow action. However, the rapid application of loads due to passage of vehicles on bridges induces dynamic loads that are generally larger than those induced by equivalent static loads. The dynamic load effects have become significant due to trains moving at higher speeds thus most of current research on dynamic response of railway bridges has focused on mitigating resonance effects and ensuring passenger comfort [Yang *et al.*, 1995, Xia *et al.*, 2006]. It was shown in Chapter 4 that natural frequency of moving vehicle-bridge systems is time varying, depending on vehicle location as well as the uncoupled mass and frequencies of the vehicle and bridge. This is significant on heavy haul rail bridges where the vehicle-bridge mass ratios is much higher than in highway bridges.

In design, dynamic load effects are determined by applying scaling factors such as Dynamic Amplification (DA), Dynamic Amplification Factor (DAF) and Dynamic

Increment (DI) already presented in Chapter 2 and given below for convenience. The Dynamic Amplification gives the increment arising from dynamic effects as a fraction of static load effects as expressed in equation 5.1:

$$DA = \frac{R_{dyn} - R_{sta}}{R_{sta}} \tag{5.1}$$

where R_{dyn} is the maximum dynamic response and R_{sta} is the maximum static response. Dynamic Amplification Factor (DAF) obtained from equation 5.2:

$$\begin{aligned} DAF &= \frac{R_d}{R_s} \\ &= 1 + DA \end{aligned} \tag{5.2}$$

Dynamic Increment (DI) on the other hand is defined in terms of displacement as follows:

$$DI = \frac{\text{Maximum deflection induced by moving vehicle}}{\text{Maximum deflection induced by static vehicle vehicle}} \tag{5.3}$$

The dynamic response of bridges can be obtained from static load effects using any of factors defined in equations 5.1 to 5.3. The presentation in this chapter will be limited to dynamic amplification (DA). In assessment and strength evaluation of existing bridges, Paultre *et al.* [1992] proposes three methods for obtaining the dynamic amplification. These methods include computing dynamic amplifications based on design code provisions, performing dynamic analysis and bridge testing under controlled traffic to obtain dynamic and quasi-static bridge responses.

5.2 Chapter Objectives

The objective of this chapter is to present analytical study of beam type bridge response dynamic amplification followed by a field study of dynamic amplifications of multi-span girder bridge on the heavy haul. The first contribution in this study is to incorporate the effects of high vehicle-bridge mass ratio in computation of dynamic amplification. This is accounted for by allowing the frequency reductions as obtained in Chapter 4. The second key contribution to estimate flexural dynamic amplification factors of a continuous girder bridge under heavy-haul traffic based on field measurements. The final contribution of this chapter is to determine through the use of field

measurements the influence of changes in train speed during bridge crossing on dynamic amplification factors.

5.3 Dynamic Amplification

Dynamic amplification depends on vehicle and bridge modal parameters as well as vehicle speed, axle spacing, condition of the bridge approaches and ride surface roughness. A review of the individual effect of each of the factors above shows conflicting observations as shown in Chapter 2. Beam models are widely employed in analytical studies while more complex 3 dimensional models have been used in numerical studies [Yang *et al.*, 1995, Fryba, 1999, Deng and Cai, 2010]. While beam models can not be used to represent spatial variations in the transverse direction, they enable simple closed form solutions of bridge response to be obtained. Memory *et al.* [1995] showed that beam models will give a natural frequency within 5% of that estimated from vibration measurements of existing bridges. Beam type elements have been used in finite element models to study vehicle-bridges interaction effect on evolution of combined system frequency [Cantero *et al.*, 2017].

The influence of riding surface roughness on dynamic amplification is another area where studies have produced conflicting results as highlighted in Chapter 4. The influence of riding surface is also affected by the choice of vehicle model. Chang and Lee [1994] found that is no difference in dynamic amplification between moving force, moving mass and moving sprung mass on smooth riding surface while moving mass and moving force overestimate dynamic amplification on highway bridges with rough riding surface. However Majka and Hartnett [2009] showed using a 3 dimensional bridge and train models that the effect of ride surface roughness was negligible. There is equally no consensus on influence of vehicle models on bridge response dynamic amplification. Yau *et al.* [1999] investigated bridge responses caused by moving force and moving sprung mass vehicle models and concluded that the difference was not significant. Hamidi and Danshjoo [2010] showed that while differences in bridge response

due to different vehicle models were negligible, there were significant differences in vehicle response. Thus it was recommended that complicated vehicle models were required if vehicle response was of interest.

5.3.1 Analytical Study

Analytical solutions use the moving force vehicle idealizations to study bridge dynamic response largely due to its simplicity in obtaining closed form solutions [Inglis, 1934, Fryba, 1999, Johansson *et al.*, 2013]. The moving force problem is not strictly a moving load problem as it ignores the inertial effects of the moving masses [Ouyang, 2011]. However, it is a starting point for the modified solution presented here as closed form solutions that apply to both simply supported beams and continuous beams on simple supports. Johansson *et al.* [2013] presented closed form solutions for continuous 3 span beam bridges with different boundary conditions subjected to moving force. This study employs a moving force formulation on beam type bridge with additional mass accounted for by the reduced vehicle-bridge natural frequencies. The effects of riding surface and bridge model are not considered as part of this study.

The transverse vibration of a beam based on Euler-Bernoulli beam theory has already been derived and is presented here. If a simplified model of moving force and damping are included the vibration of a uniform cross sectional beam can be determined from equation below:

$$EI\frac{\partial^4 W(x,t)}{\partial x^4} + c\frac{\partial W(x,t)}{\partial t} + \rho A\frac{\partial^2 W(x,t)}{\partial t^2} = N\delta(x-ut) \tag{5.4}$$

where E is elastic modulus, I is moment of inertia, ρ is density,A is the cross sectional area $W(x,t)$ is the vertical displacement at time t. Given the modal expansion of $W(x,t)$, equation 5.4 multiplied by $\phi(x)$ and simplified using orthogonal relationships below:

$$W(x,t) = \sum_{j=1}^{\infty} \phi(x)_j q(t)_j \tag{5.5}$$

$$m\int_0^L \phi_n(x)\phi_j(x)dx = \delta_{nj}\ \ EI\int_0^L \phi_n(x)\frac{\partial^4\phi_j(x)}{\partial x^4}dx = \omega_n^2\delta_{nj}\ \ j,n=(1,2,...)\ \ c = 2m\omega_n\xi_n \tag{5.6}$$

$W(x,t) = \phi(x)q(t)$ where $w(x)$ are the vibration modes and $q(t)$ are the generalised coordinates then equation 5.4 can be expressed as follows:

$$\frac{d^2q(t)}{dt^2} + 2\omega_n\xi_n\frac{dq(t)}{dt} + \omega_n^2 q(t) = N\phi(v) \tag{5.7}$$

where $v = ut$

The deflection response of interest can be obtained from equation 5.7 though a duhamel integral or Laplace transform. Closed form solutions have been presented using the Laplace transform and this approach is adopted here [Johansson *et al.*, 2013]. Taking the transform of equation 5.7 and simplifying:

$$\mathscr{L}\{q\} = \frac{\dot{q}(o) + (s + 2w_n\xi_n)q(o)}{Y_1} + \frac{\mathscr{L}\{P\phi\}}{Y_1} \tag{5.8}$$

where

$$\mathscr{L}\{Pw\} = \frac{PB\Theta v}{Y_2} + \frac{PD\Theta v}{Y_3} + CP\left(\frac{s}{Y_2} - \frac{s}{Y_3}\right)$$

$$Y_1 = s^2 + 2w_n\xi + \omega_n^2$$

$$Y_2 = s^2 - (\Theta v)^2$$

$$Y_3 = s^2 + (\Theta v)^2$$

$\dot{q}(o)$ and $q(o)$ are initial conditions.

The inverse transform of equation 5.8 is obtained and computations performed.

$$q_{n,i}(t) = Q1 + B_{nj}Q2 + D_{nj}Q3 + C_{nj}P(Q4 - Q5) \tag{5.9}$$

where B_{nj}, C_{nj} and D_{nj} are mass normalised constants for nth mode and on span j; $Q1$ is a constant giving the initial conditions while $Q2$, $Q3$, $Q4$ and $Q5$ are given below:

$$Q1(t) = \frac{(\dot{q}(o) + 2\xi q(0)\omega_n)\sin\left(t\sqrt{\omega_n(2\xi_n + \omega_n)}\right) + q(0)\sqrt{\omega_n(2\xi_n + \omega)}\cos\left(t\sqrt{\omega_n(2\xi + \omega_n)}\right)}{\sqrt{\omega_n(2\xi + \omega_n)}}$$

$$Q2(t) = -P\frac{\left(e^{-\Theta_n vt}\sqrt{\omega_n(2\xi_n + \omega_n)} - e^{-\Theta_n vt}\sqrt{\omega_n(2\xi_n + \omega_n)} + 2\Theta_n v\sin\left(t\sqrt{\omega_n(2\xi_n + \omega_n)}\right)\right.}{2(-(\Theta_n v)^2 + \omega_n^2 + 2\xi\omega)\sqrt{\omega_n(2\xi_n + \omega_n)}}$$

$$Q3(t) = P\Big(\frac{\sin(\Theta_n vt)}{-(\Theta_n v)^2 + \omega_n^2 + 2\xi\omega_n} - \frac{\Theta_n v \sin\left(t\sqrt{\omega_n^2 + 2\xi\omega_n}\right)}{(-(\Theta_n v)^2 + \omega_n^2 + 2\xi\omega_n)\sqrt{\omega_n^2 + 2\xi\omega_n}}\Big)$$

$$Q4 = P\frac{-\cos\left(t\sqrt{\omega_n(2\xi+\omega)}\right) - \cos(\Theta_n vt}{-(\Theta v)^2 + \omega_n^2 + 2\xi\omega_n}$$

$$Q5 = P\frac{e^{-\Theta_n vt}\Big(e^{2\Theta_n vt} - 2e^{\Theta_n vt}\cos\Big(t\sqrt{\omega_n(2\xi+\omega)}\Big) + 1\Big)}{2(\Theta_n v)^2 + 2\omega_n^2 + 4\xi\omega_n}$$

The beam deflection at any point for any given combination of moving point forces can be obtained through back substitution into the modal expansion equation 5.5.

Dynamic amplification in simply supported beam under moving forces

The dynamic amplification of simply supported beams under a single moving load is widely discussed in literature and is easily obtained in closed form Inglis [1934], Humar and Kashif [1993], Yang *et al.* [1995]. However, the formulation above is easily applied to both simply supported and continuous beams. The deflection of a continuous beam at any given location resulting from train loads with N point loads is obtained by the summation of the individual point load effects as given below:

$$W(x,t) = \sum_{j=1}^{\infty} \phi(x)_j q(t)_j \tag{5.10}$$

where $W(x,t)_p$ is deflection from point load obtained from 5.5 and 5.9 at time t and (t) is given as:

$$q(t) = \begin{cases} Q1(t) + D_n Q3(t) & \text{for } t \le L/v \\ Q_{free}\exp(-\xi w_n t) & \text{for } t > L/v \end{cases} \tag{5.11}$$

$$Q1(t) = \frac{(\dot{q}(o) + 2\xi q(0)\omega_n)\sin\Big(t\sqrt{\omega_n(2\xi_n+\omega_n)}\Big) + q(0)\sqrt{\omega_n(2\xi_n+\omega)}\cos\Big(t\sqrt{\omega_n(2\xi+\omega_n)}\Big)}{\sqrt{\omega_n(2\xi+\omega_n)}}$$

$$Q3(t) = P\Big(\frac{\sin(\Theta_n vt)}{-(\Theta_n v)^2 + \omega_n^2 + 2\xi\omega_n} - \frac{\Theta_n v \sin\left(t\sqrt{\omega_n^2 + 2\xi\omega_n}\right)}{(-(\Theta_n v)^2 + \omega_n^2 + 2\xi\omega_n)\sqrt{\omega_n^2 + 2\xi\omega_n}}\Big) \tag{5.12}$$

$$Q_{free} = \frac{(\dot{q}(t_L) + 2\xi q(t_L)\omega_n)\sin\left(t\sqrt{\omega_n(2\xi_n + \omega_n)}\right) + q(t_L)\sqrt{\omega_n(2\xi_n + \omega)}\cos\left(t\sqrt{\omega_n(2\xi + \omega_n)}\right)}{\sqrt{\omega_n(2\xi + \omega_n)}}$$

where $q(0)$ and $\dot{q}(o)$ are displacement and velocity terms when a load arrives on the bridge while $q(t_L)$ and $\dot{q}(t_L)$ are displacement and velocity terms when a load leaves the bridge at time t_L. It is assumed for this study that the initial conditions on the bridge prior to loading are $q(0) = 0$ and $\dot{q}(o) = 0$. However the conditions when a load leaves the bridge are very different and these conditions decay with time through the logarithmic decrement as a result of the assumed damping ξ given in 5.11.

A comparison of dynamic amplification of moving single load and train loads of magnitude 294kN is done for a 45m simply supported beam with EI of $3.9 \times 10^{11} N - m^2$), $\rho A = 12000kg$ and $\xi = 0.025$. These dimensions are chosen as in previous case study to match the geometry of Olifants viaduct, the axle loads of the loaded trains and the estimated bridge damping. The dynamic amplification of single load on simple supported beam is similar to that reported by Yang *et al.* [1995] with a maximum value of 0.77 as shown in Fig 5.1. However, the train load of 25 wagons with axle spacing corresponding to wagon CR-13 shows some departure from the amplification from point load. The peaks are more distinct and do not necessarily align with those obtained from the moving single load. The general rise for single load occurs at speed parameter $S_1 = 0.2$ while the train load rise is at $S_1 > 0.3$.

The fundamental frequency of the beam with geometric parameters given above is 4.1Hz. The speed parameter S_1 used in Fig 5.1 corresponds to a speed v range of $0km/h$ to $1380km/h$ which is outside the range of practical interest. The range of interest for Olifants Bridge is below $80km/h$ which corresponds to $S_1 = 0.06$. In this speed range, the dynamic amplification for both single loads and train loads

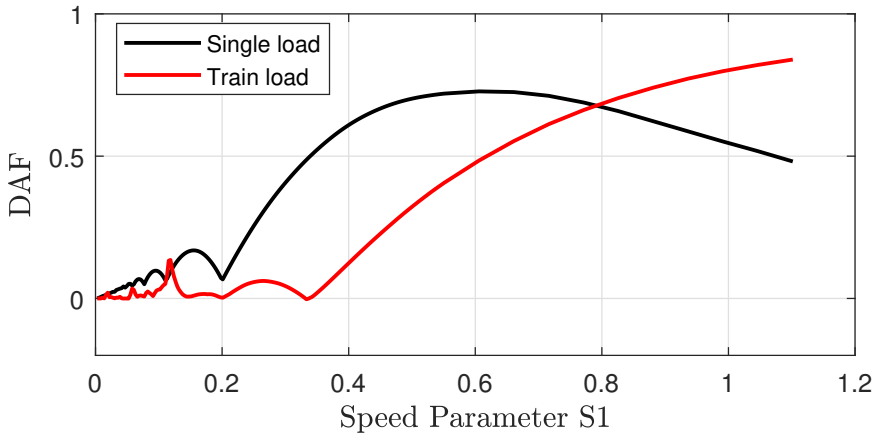

Figure 5.1: Dynamic amplification-Single span

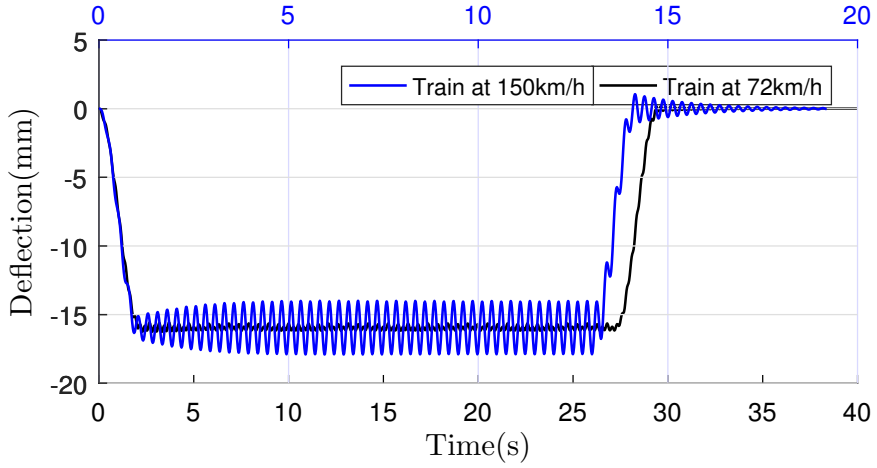

Figure 5.2: Dynamic amplification-Single span

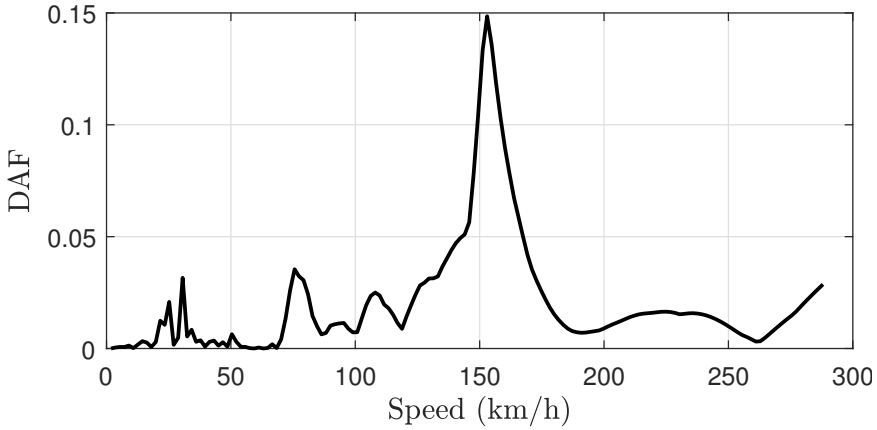

Figure 5.3: Dynamic amplification-Single span

is below 0.2, with train loads being significantly lower at less than 0.1. The study of amplification of deflections on continuous beams under train loads is limited to the speed ranges up to resonance speeds.

The dynamic response of bridges under passage of actual traffic is more complicated than the moving load simplification presented above and research in the area has produced often contradictory results. Real vehicles can be idealised as sprung masses and therefore trains are idealised as a series of sprung masses [Fryba, 1999]. Yau *et al.* [1999] investigated the moving load and the sprung mass cases on simply supported beams and showed than there is no difference in dynamic amplification for the speed range investigated $S_1 < 0.5$. Hwang and Norwak [1991] investigated the effects of truck gross weight on dynamic amplification factor and showed that there was a decrease with increasing gross weight. Humar and Kashif [1993] showed that the overall bridge response depends on the vehicle speed, vehicle to bridge frequency ratio and vehicle to bridge mass ratio. Thus for $S_1 \leq 0.15$, there is a reduction in amplification with increasing mass ratio for a frequency ratio less than 0.4 and an increase for frequency ratio between 0.4 and 0.8.

Dynamic amplification in continuous beams under moving forces

Dynamic amplification of continuous beams on simple supports can be readily computed from equation 5.9 and 5.5 which represent the general form of the solution. Continuous beams with equal spans and uniform section on simple supports unique characteristics of having close modes. In addition, the dynamic amplifications may vary from one span to the next. In this study, the 11 span segment of Olifants is considered and the moving load is implemented in $Matlab^R$ based on the equations formulated in previous section. The convergence rate for the 30 wagon train load is slow and up to 121 modes were included in the computation. For this reason, only deflection based amplification factors are presented and these are generally assumed to be close to moment based factors.

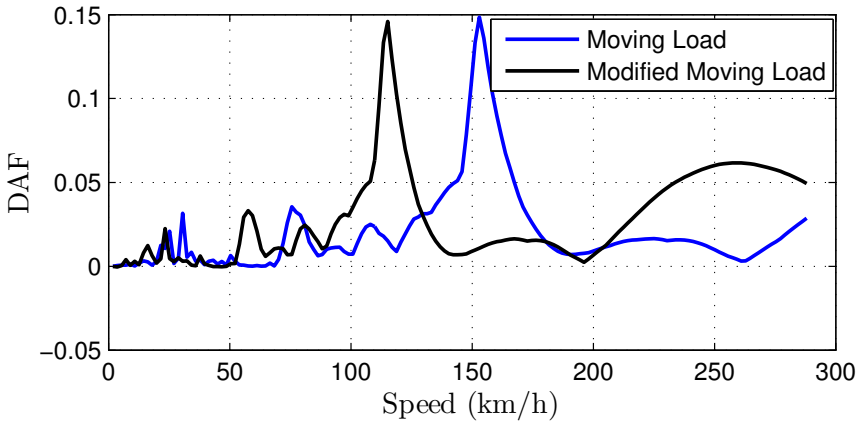

Figure 5.4: Comparison of moving load and moving mass amplification

In Chapter 4, the effects of the frequency ratio and mass ratio were shown to have an effect on the modal mass and modal stiffness of the combined vehicle-bridge system respectively. A higher vehicle stiffness tends to increase the bridge natural frequencies while higher mass ratios tend to reduce the bridge frequencies. A simulation of moving load and a modified moving load formulation based on reduced frequencies for loaded trains-bridge system on Olifants Bridge is shown in Fig 5.4. There is a slight shift of the resonance peaks when the reduced frequency is used in the simulation of bridge response. This shift has been reported in moving mass problem where it is attributed to bridge period elongation [Yang *et al.*, 2004]. However as established from previous chapter, the effect of sprung masses on combined system frequency can also lead to an overall increase in frequency and thus a reduction in period. This latter effect would shift the peaks to the right as opposed to the present case. The speed parameters S_1 for the moving moving mass and moving load are different at a given speed v due to these differences in frequencies.

A uniform section equal span continuous simply supported beam-type bridge will experience higher moments and deflections in the first span. A comparison of dynamic amplification factors of first and fourth spans of Olifants bridge is undertaken. The fourth span from the end which is span 20 is selected for study as this span is instrumented and provides the basis for comparison with experimentally determined dynamic amplification factors. The bridge response is

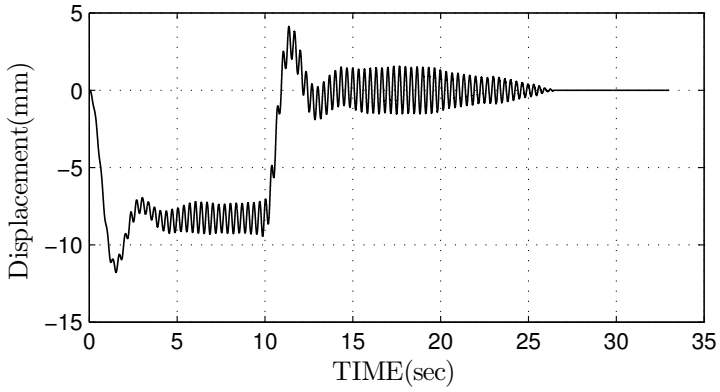

Figure 5.5: Span 23 midspan deflection (Train speed at 108km/h)

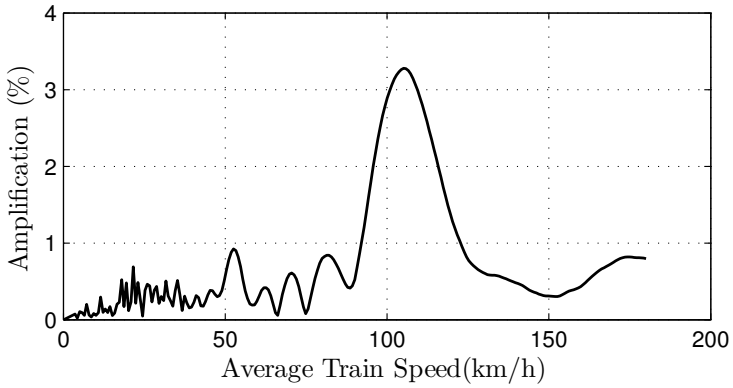

Figure 5.6: Dynamic Amplification (Span 23)

calculated for various speeds at increments of 0.36km/h up to speeds above resonance. The midspan deflection for span 20 is shown in Fig 5.7 at train speed of 108km/h with induced vibrations contributing significantly to the response. The deflection is maximum when train enters and leaves a span of interest as seen in the graphs. There are also significant vibrations immediately after train leaves a given span.

The bridge dynamic amplification based on deflections at mid span of span 20 was computed for a range of velocities assuming damping $\xi = 0.02$ and are shown in in Fig 5.8. The dynamic amplifications are significantly higher above 100km/h speeds where resonance conditions are dominant from the close frequencies. The amplifications below 50km/h are lower than 5% and significantly less than measured values for loaded trains for 40km/h to 50km/h speed range. The current operational train speeds when crossing of less than 60km/h are

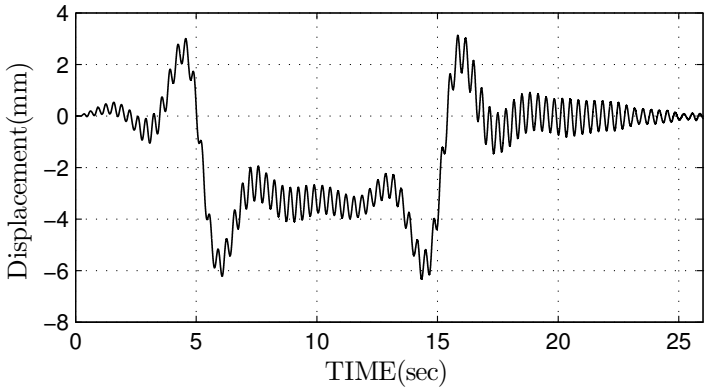

Figure 5.7: Span 20 midspan deflection(Train at 108km/h)

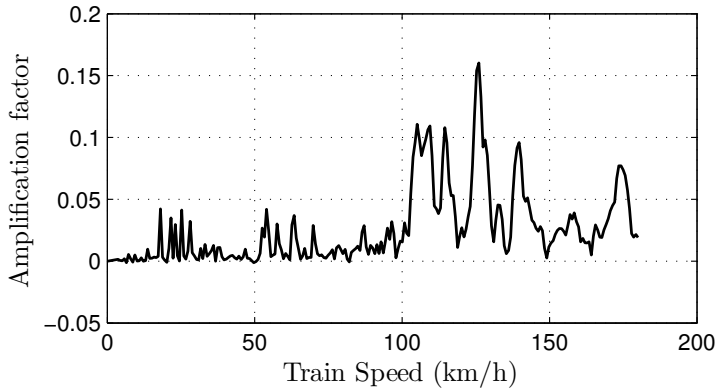

Figure 5.8: Dynamic Magnification(Span 20)

associated amplification factor of less than 5%.

The dynamic amplifications for other inner spans are computed and are very much similar to span 23. The deflection and amplifications for span 23 are shown in Fig 5.5 and Fig 5.6. The defections and hence moments for span 23 are greater than for other spans. The dynamic amplification however is much lower even though the higher moments make the section critical for assessment. The amplification for end span does not have multi-peaks for the individual resonance frequencies and it appears the cancellation effects are significant.

The dynamic amplifications obtained for the Olifants bridge are comparable to the empirically derived dynamic amplification formulae specified in South African Transport Services [1983] for 45m span. The agreement between the moving force and code based formulae could be a result of low frequency global modes being

more dominant in comparison to the higher frequency modes that are excited due to surface and wheel irregularities. The higher frequency modes are especially significant when computing local dynamic amplification response [Yu *et al.*, 2017].

Resonance and cancellation phenomenon

Resonance has been studied in railway bridges and largely confined to high speed rail bridges. The resonance effects in bridges on low speed high axle load networks such as heavy-haul rail lines has not been reported. It has been established in Chapter 4 that heavy axle train loading can significantly lower train-bridge system frequency and thus lowering the threshold for resonance to occur as the mechanisms involved depend among other factors on bridge frequency. The heavy haul trains tend to be longer and this provides sustained periodic loading that can lead to vibrations building up. An overview of resonance and cancellation expressions derived for high speed applications are presented here.

The phenomenon of resonance on heavy-haul bridges simulated in previous sections is presented in Figs 5.9 and 5.10. The bridge deflection resulting from passage of a single axle is shown in Fig 5.9 with the vibration decay as the load leaves the bridge. Successive spaced loads passing on the bridge lead to the accumulation of the free vibrations that build up causing higher vibration amplitudes as shown in Fig 5.10. The magnitude of the vibrations in a train loading case depend on the bridge damping, the number of loads, the bridge frequency and loading rate [Li and Su, 1999]. The mechanisms of resonance depend on the loading intervals leading to periodic loading, the speed of the vehicles on the bridge and the excitations caused by track irregularities and wheel hunting movements [Xia *et al.*, 2006]. The first two mechanisms are presented in this study.

The passage of a load on a bridge causes vibration transients that can build up if more successive loads pass. Thus the first resonance mechanism loading

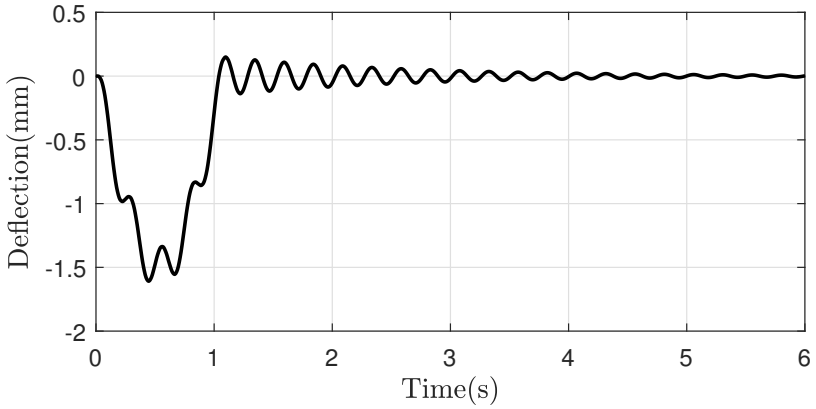

Figure 5.9: Midspan deflections during single load passage at 150km/h

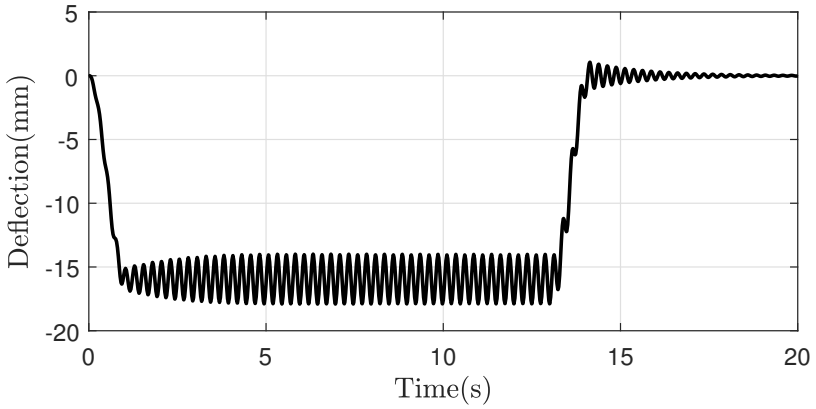

Figure 5.10: Midspan deflections at during train load passage at 150km/h

interval equals the bridge natural frequency and the critical velocity expressed mathematically in equation 5.16 is given below [Xia *et al.*, 2006]:

$$V_{cr} = 3.6\frac{f_{bn}d_v}{i} \text{ for } (n = 1, 2, ..., i = 1, 2, ...) \tag{5.13}$$

where V_{cr} is the critical velocity in km/h, f_{bn} is the bridge natural frequency and d_v is the axle or bogey spacing.

The second condition for resonance depends on the loading rate and has been derived for a simply supported beam as given below [Xia *et al.*, 2006]:

$$V_{cr} = 7.2\frac{f_{bn}L_b}{i} \text{ for } (n = 1, 2, ...) \tag{5.14}$$

where V_{cr} is the critical velocity in km/h, f_{bn} is the bridge natural frequency and L_b is the axle or bogey spacing.

The vibration cancellation phenomenon is the opposite of resonance and tends to

suppress the vibrations and is therefore desirable. The cancellation conditions are presented here for completeness. The first cancellation condition depends on individual load passage on a bridge and is given in equation 5.15 as proposed by [Xia *et al.*, 2013]:

$$V_{canc} = \begin{cases} 7.2\dfrac{f_{bn}L_b}{2i-1} & \text{for } (n = 1,3,5,...,i = 1,2,3... \text{ but } n \neq 2i-1) \\ 7.2\dfrac{f_{bn}L_b}{2i} & \text{for } (n = 2,4,6,...,i = 1,2,3... \text{ but } n \neq 2i) \end{cases} \tag{5.15}$$

The second cancellation condition deals with the suppression effect of train loads and is therefore dependent on the axle or boggey spacing [Xia *et al.*, 2013]:

$$V_{canc} = 7.2\frac{f_{bn}L_{ch}}{2i-1} \text{ for } (n = 1,2,...) \tag{5.16}$$

where L_{ch} is either boggey or axle spacing.

A summary of resonance and sub-resonance speeds estimation based on the first 11 bridge natural frequencies and axle load group spacing of 9.68m is given in Table 5.1.

Table 5.1: Critical Train Speeds

Vertical Mode	f_n (Hz)	f_L (Hz)	Critical Speed (km/h) V_R	V_{SR}
1	4.09	3.03	108	54
2	4.19	3.09	110	55
3	4.47	3.30	117	59
4	4.90	3.61	128	64
5	5.44	4.02	143	71
6	6.06	4.46	159	79
7	6.74	4.97	177	88
8	7.43	5.49	195	98
9	8.11	5.99	213	107
10	8.70	6.42	228	114
11	9.12	6.73	239	120

Note: f_n=bridge natural frequency
f_L is bridge-loaded train system frequency,
V_R is resonance speed
V_{SR} is sub resonance train speed.

A comparison of Table 5.1 and Fig 5.8 shows that not all resonant peaks show due to the phenomenon of cancellation. The case of multi-span continuous beams is

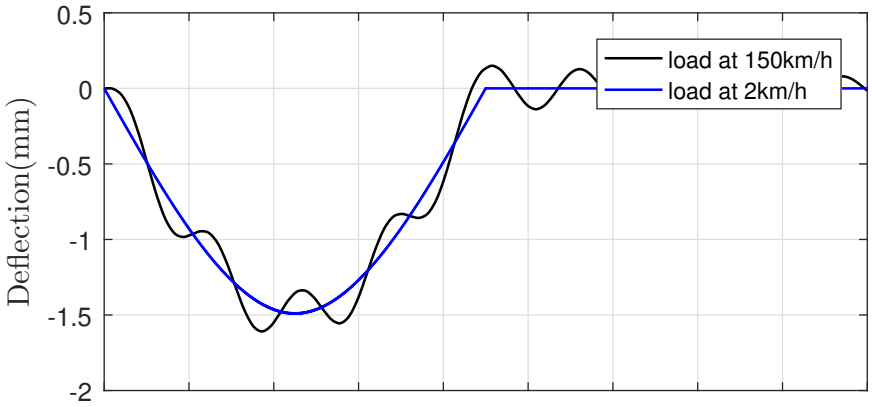

Figure 5.11: Deflection time history during single load history

complicated by the clustered frequencies. However, some cancellation speeds are estimated for the speeds 100km/h, 122km/h, 133km/h 143km/h and 153km/h in the speed range of interest. These cancellation speeds have an effect on the matching resonant frequencies or those very close.

5.3.2 Experimental estimation of dynamic amplification

Bridge tests under controlled traffic are the most reliable means of measuring dynamic amplification. This can be done by having a vehicle pass on the bridge at crawl speed less than 15 km/h/h to represent the static load effects which are then used as a reference for the dynamic load effects as shown in Fig 5.11. However, a more convenient technique has been proposed that makes use of the dynamic response to compute the dynamic amplification in highway bridges [Paultre *et al.*, 1992] and this will be adapted for application to railway bridges where dynamic amplification factors for the Olifants Bridge will be determined. The proposed method assumes that the static load effects can be derived from dynamic effects through filtering out the dynamic response as given in equation 5.17.

$$DA = \frac{R_{dyn} - R_{static}}{R_{static}} \approx \frac{R_{dyn} - R_{filtered}}{R_{filtered}} \tag{5.17}$$

where R_{dyn} is the maximum dynamic response, R_{static} is the static response and $R_{filtered}$ is the maximum static response as obtained from the filtered dynamic response.

Strain measurements

The total strain at a given point at a time $t)$ in a loaded uncracked concrete structure is composed of elastic $\varepsilon(t)_e$, creep $\varepsilon(t)_{creep}$, shrinkage $\varepsilon(t)_{sh}$ and thermal $\varepsilon(t)_{th}$ components as given in equation 5.18:

$$\varepsilon(t) = \varepsilon(t)_e + \varepsilon(t)_{sh} + \varepsilon(t)_{creep} + \varepsilon(t)_{th} \tag{5.18}$$

The elastic strain $\varepsilon(t)_e$ depends on the applied load and is obtained immediately upon load application. When a concrete structure is loaded at less than 40% of its ultimate strength, the induced strains are elastic and are thus lost upon load removal. Shrinkage strains ε_{sh} are strains from volume changes arising as a result of movement of moisture in and out of concrete and the chemical reactions in cement paste that include hydration. In addition, thermal shrinkage follows as concrete mass loses heat of hydration and starts to contract as a result. Chemical and thermal shrinkage are collectively referred to as endogeneous shrinkage as opposed to the more significant drying shrinkage caused by movement of moisture. Creep is the strain increase due to sustained stress. Creep depends on both concrete mix characteristics, environmental factors and applied stress related factors such as time from load application. The thermal strains are generated from uniform temperature changes and differential temperature changes of a structure.

Creep increases at a decreasing rate with about 50% occupying in first 3 months and 90% in first 3 years [Ranzi and Gilbert, 2010]. Shrinkage strains comprise of irreversible strains and the reversible strains if concrete is wetted as shown in Fig 5.13. In this study, the bridge was instrumented with strain gages 38 years after construction. The changes in creep strains due to self weight and prestress are therefore negligible. Similarly, the only significant changes shrinkage strains are those resulting from drying and wetting cycles associated with the different seasons. The significant strains are expected to be mainly elastic strains due to train loads and thermal strains from temperature changes.

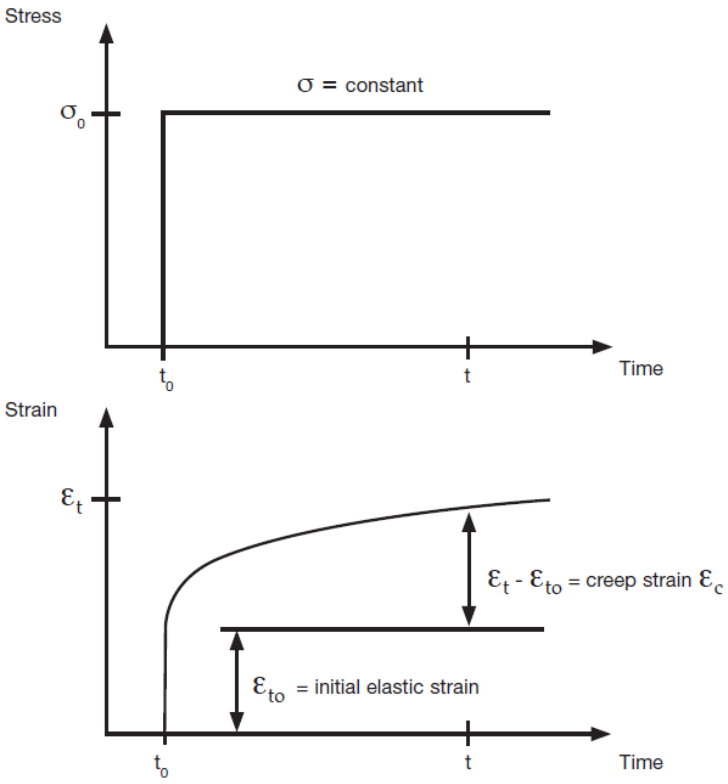

Figure 5.12: Creep Alexander and Beushausen [2009]

Dynamic amplification based on strains

Paultre *et al.* [1992] gives the general characteristics of the band pass filter required to obtain the static load effects from the dynamic response time history. The finite impulse response (FIR) filter should have a passband of $v/L\ Hz$ where v is vehicle velocity and L is shortest span length of the bridge while the cut-off frequency is the bridge fundamental frequency. The pass band frequency as proposed above can be is formulated for highway application where the duration of passage is small. In railway applications where long trains are involved, the specified pass band above would filter out even the static load effects as these occur at lower frequency due to a longer event duration.

The Olifants fundamental natural frequency was obtained from the vibration measurements under ambient vibration in previous chapter and estimated to be 4.09Hz. Busatta and Moyo [2017] has shown that the Olifants fundamental frequency does not display any trends or seasonality and thus will be assumed to

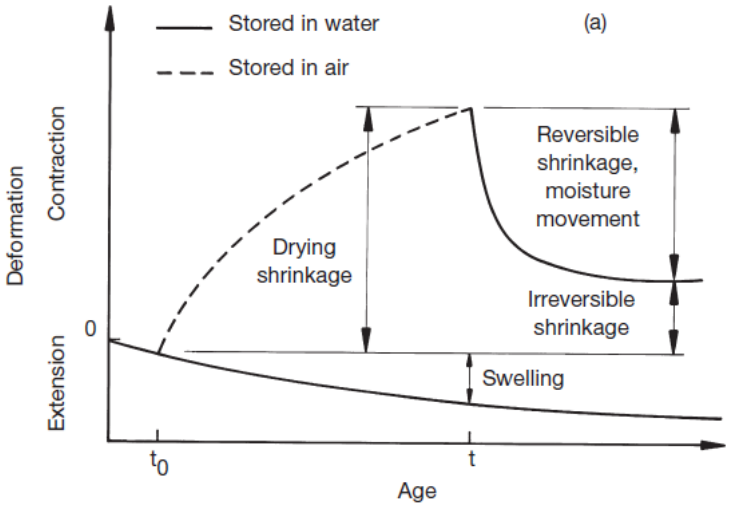

Figure 5.13: Shrinkage Alexander and Beushausen [2009]

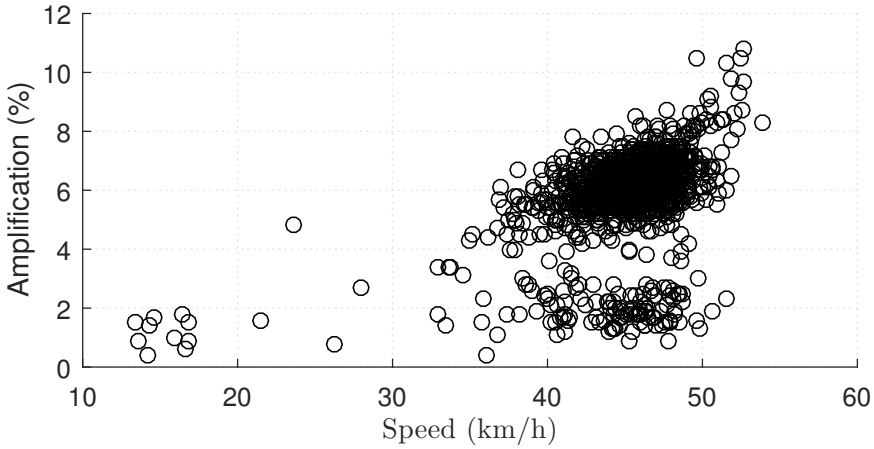

Figure 5.14: Plot of DA of midspan strain against speed obtained from loaded trains

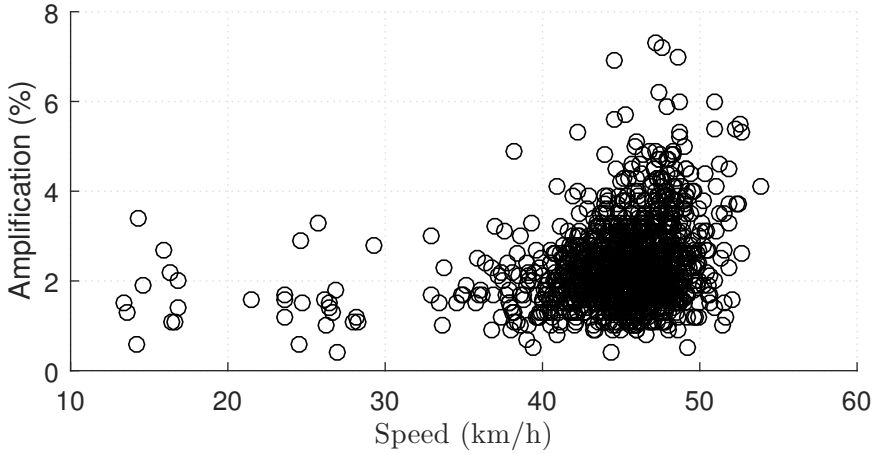

Figure 5.15: Plot of DA of support section strain against speed obtained from loaded trains

be stationary for this study. However, due to the train mass being significant, an estimate of fundamental train-bridge system frequency of $3.45Hz$ as proposed in

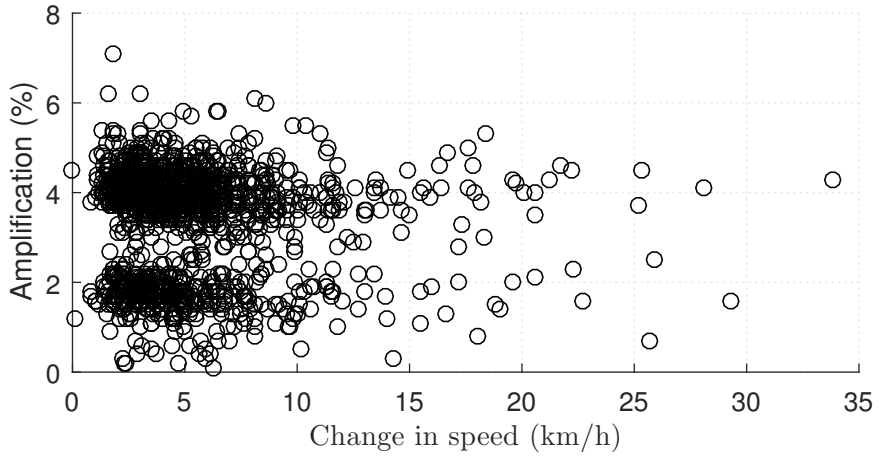

Figure 5.16: Plot of DA midspan section strain against speed obtained from empty trains

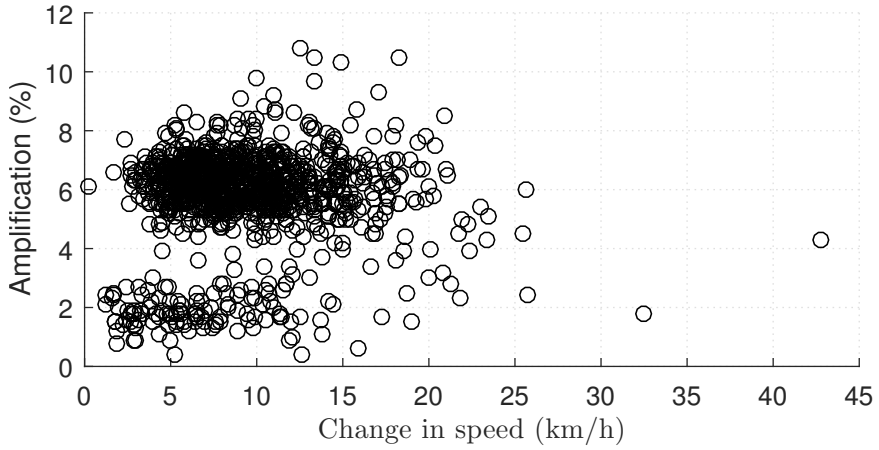

Figure 5.17: Plot of DA against change in speed caused by loaded trains (June2016 to April 2017 period)

previous chapter is used as the cut-off frequency. A low pass filter with cut off frequency of $3.45Hz$ for loaded train-bridge system frequency and $3.95Hz$ is implemented in $Matlab^R$ to analyse a total of 1174 loaded train events and 1372 empty train crossing events that occurred in period from June 2016 to March 2017. Due to the large variation of bridge-train mass ratios of 0.14 for empty trains and 0.88 for loaded trains, the train events logged are separated between loaded and empty train events in order to compute the dynamic amplification factors.

A comparison of Fig 5.14 and Fig 5.15 shows that dynamic amplifications even for flexural response as obtained from strains in longitudinal direction depend on location of interest. The midspan strains show relatively higher amplification

with most events having amplification between 6% to 8% while the maximum of 11% was obtained. The support section amplification on the other hand are much smaller with mean of 2% and maximum of 8%. Differences between dynamic amplification factors for sagging and hogging moments have been reported by Deng *et al.* [2015] on highway bridges where hogging moment amplifications where larger than sagging moment amplification factors. However the opposite is observed here in the case of a continuous bridge on heavy-haul line. A comparison of dynamic amplifications from loaded trains in Fig 5.14 and empty trains in Fig 5.16 show a marginal decrease in the case of empty trains. The effect of increase in vehicle mass has been considered in previous studies where it was shown that an increase in mass leads to reduction in amplification factors in highway bridge applications [Hwang and Norwak, 1991, Ashebo *et al.*, 2007]. However the field data for a continuous data presented above show an increase in amplification factor envelop with increase in train gross mass.

The effect of vehicle acceleration and deceleration on highway bridges has not been widely studied while the effect on heavy-haul bridges has to the author's knowledge not been studied. Deng and Wang [2015] showed that the dynamic amplification is greater by 300% when vehicle deceleration is introduced on a good road surface compared to where a vehicle crosses at constant speed. The majority of trains cross the Olifants Bridge at between 40km/h and 50km/h average speed and most trains experience a change in speed of up to 15 km/h. While the actual acceleration is not computed, a plot of dynamic amplification and maximum speed change for the train events is shown in Fig 5.17. The plot shows two clusters for the amplification factors with increasing scatter for change of speed above 10 km/h. The highest values of dynamic amplification factors are obtained for change of speed greater than 10 km/h even though there are fewer points to draw conclusions from in this zone.

5.4 Concluding remarks

Dynamic amplification factors for a continuous 11 span bridge are computed based on an analytical procedure using moving force idealization. The effects of the increased mass that lead to a shift in the peak response have been incorporated in the moving force formulation by using the modified bridge frequency. This results lowering of critical speeds for resonance and sub-resonance peaks and thus shifting the peaks towards lower speeds. The analytical procedure shows that the dynamic amplification induced by loaded trains is higher in the inner span 20 than the end span 23. However, the moments are more critical in the end span where the dynamic amplification is less than 4% while in span 20 the amplification considerably greater at 15% at resonance speeds. The computed amplification factors within the imposed speed limits on the bridge are 1% for end span and 5% for inner span 20. The code based dynamic amplification for 45m span continuous bridge are comparable to the computed analytical values showing that the contribution from wheel and surface irregularities which excite higher frequency modes are not the dominant factor at such span lengths.

The dynamic amplification factors estimated from strain measurements show that the factors estimated from midspan measurements are marginally greater than those obtained from measurements on the support. Although there is great scatter in the results, the highest amplification factors were obtained at speeds between 50km/h and 60km/h close to computed sub-resonance peaks. The amplification factors for loaded trains were greater than those for empty trains. Although this observation is contrary to some results in literature, the shifts in resonance peaks are a possible explanation for higher dynamic amplifications from passage of loaded trains. An examination of analytical and experimental methods in this study show that the analytical method greatly underestimates the dynamic amplification factors. The field measurements give a maximum of 12% for midspan strain based factors in contrast with 5% from analytical

method for loaded trains and observed speeds. However, there is a lot of scatter and clustering in the estimated dynamic amplifications from field measurements. The cause of scatter and clustering was not identified in this study. A possible reason for the scatter could be the wheel irregularities having a greater influence on bridge local response in upper deck strain measurement.

Vehicle acceleration or deceleration have been shown to significantly increase dynamic amplification on highway bridges. In this study, the maximum change in speed as opposed train accelerations were obtained from weigh-in-motion data logs. The effect of changes in train speed on dynamic amplification does not show any clear trends. The maximum dynamic amplifications from midspan strain measurements were obtained for speed change magnitudes between 10km/h to 15km/h while the hogging factors had maximums between 5km/h and 10km/h.

The dynamic load effects are usually treated in a deterministic framework in design codes and no attempt is made here to consider a probabilistic framework. The next chapters shift the focus to the static load effects on the heavy haul.

References

Inglis C.E., *A Mathematical Treatise on Vibrations in railway Bridges*, Cambridge University Press, 1934.

South African Transport Services, "Bridge code," 1983.

Hwang E.S. and Norwak A., "Simulation of dynamic loads for bridges ," *J. Structural Engineering ASCE*, 117(5); 1413–1434, 1991.

Paultre P., Chaallal O. and Proulx J., "Bridge dynamics and dynamic amplification factors-a review of analytical and experimental findings," *Candian Journal of Civil Engineering*, 19; 260–278, 1992.

Humar J. and Kashif A., "Dynamic response of bridges under travelling loads," *Canadian Journal of Civil Engineering*, 20(2); 287–298, 1993.

Chang D. and Lee H., "Impact factors for simple-span highway girder bridges," *Journal of Structural Engineering*, 120(3); 704–715, 1994.

Memory T., Thambiratnam D. and Brameld G., "Free vibration analysis of bridges," *Engineering Structures*, 17(10); 705–713, 1995.

Yang Y.B., Liao S.S. and Lin B.H., "Impact formulas for vehicles moving over simple and continuous beams," *Journal of Structural Engineering*, 121(11); 1644–1650, 1995.

Yau J.D., Yang Y.B. and Kuo S.R., "Impact response of high speed rail bridges and riding comfort of rail cars," *Engineering structures*, 21(9); 836–844, 1999.

Li J. and Su M., "The resonant vibratio for a simply supported girder bridge under high-speed trains," *Journal of Sound and Vibrations*, 224(5); 897–915, 1999.

Fryba L., *Vibration of Dolids and Structures under Moving Loads*, Thomas Telford, London, 3 edition, 1999.

Yang Y.B., Yau J.D. and Wu Y.S., *Vehicle-Bridge Interaction Dynamics With Applications to High Speed Railways*, World Scientific, Singapore, 2004.

Xia H., Zhang N. and Guo W., "Analysis of resonance mechanism and conditions of train–bridge system," *Journal of Sound and Vibration*, 297(3-5); 810–822, 2006.

Ashebo D.B., Chan T.H. and Yu L., "Evaluation of dynamic loads on a skew box girder continuous bridge part ii: Parametric study and dynamic load factor," *Engineering structures*, 29(6); 1064–1073, 2007.

Alexander M. and Beushausen H., "Deformation and volume change of hardened concrete," *Fulton's concrete technology*, 111–144, 2009.

Majka M. and Hartnett M., "Dynamic response of bridges to moving trains: A study on effects of random track irregularities and bridge skewness," *Computers & Structures*, 87(19-20); 1233–1252, 2009.

Hamidi S.A. and Danshjoo F., "Determination of impact factor for steel railway bridges considering simultaneous effects of vehicle speed and axle distance to span length ratio," *Engineering Structures*, 32(5); 1369–1376, 2010.

Deng L. and Cai C.S., "Development of dynamic impact factor for performance evaluation of existing multi-girder concrete bridges," *Engineering Structures*, 32; 21–31, 2010.

Ranzi G. and Gilbert R.I., *Time-dependent behaviour of concrete structures*, CRC Press, 2010.

Ouyang H., "Moving-load dynamic problems: A tutorial(with brief overview)," *Mechanical Systems and Signal Processing*, 25; 2039–2060, 2011.

Hayward A.C.G., "Train loading on bridges since Stephenson's Rocket," *Proceedings of Institution of Civil Engineers-Bridge Engineering*, 167 IssueBE4; 326–337, 2011.

Johansson C., Pacoste C. and Karoumi R., "Closed-form solution for the mode superposition analysis of vibration in multi-span beam bridges caused by concentrated moving loads," *Computers and Structures*, 119; 85–94, 2013.

Xia H., Li H., Guo W. and De Roeck G., "Vibration resonance and cancellation of simply supported bridges under moving train loads," *Journal of Engineering Mechanics*, 140(5); 04014015, 2013.

Deng L., He W. and Shao Y., "Dynamic impact factors for shear and bending moment of simply supported and continuous concrete girder bridges," *Journal of Bridge Engineering*, 20(11); 04015005, 2015.

Deng L. and Wang F., "Impact factors of simply supported prestressed concrete girder bridges due to vehicle braking," *Journal of Bridge Engineering*, 20(11); 06015002, 2015.

Cantero D., Hester D. and Brownjohn J., "Evolution of bridge frequencies and modes of vibration during truck passage," *Engineering Structures*, 152; 452–464, 2017.

Busatta F. and Moyo P., "How testing and monitoring can support heavy haul railway bridge management: The experience gained in South Africa," *11-th International Heavy Haul Conference Proceedings, Capw Town*, 599–, 2017.

Yu Y., Deng L., Wang W. and Cai C., "Local impact analysis for deck slabs of prestressed concrete box-girder bridges subject to vehicle loading," *Journal of Vibration and Control*, 23(1); 31–45, 2017.

Chapter 6

DETERMINISTIC LIVE LOAD MODELLING FOR HEAVY-HAUL RAIL BRIDGES

6.1 Introduction

Railway bridges are critical infrastructure in any transport system and are generally designed for a life above 100 years. During this design life, the bridges are subjected to changes in traffic volumes and traffic composition largely resulting increased axle loads and design changes in locomotive and wagon configuration. Railway bridge design live loads are formulated to take account of these changes and be relevant for a wide range of bridge types as possible. Railway bridge load models generally consist of uniform distributed loads and point loads and are of the format proposed by Cooper [1894] or more recent format proposed by International Union of Rail [UIC Leaflet 702OR, 2003]. The design load models are formulated to give bridge load effects due to current and predicted future traffic. Their accuracy depends on current and predicted vehicle gross weights, axle loads, axle spacing, headway between vehicles during bridge crossing, proportion of heavy vehicles in traffic and bridge length [Bailey and Bez, 1999, Miao and Chan, 2002].

Bridges are regularly inspected to assess their condition based on observed deterioration and damage. Where observed deterioration is deemed to compromise the load carrying capacity of a bridge, structural performance

assessment is conducted usually using codified live load models. Increasingly it is recognized that codified live loading is not representative of live loading experienced by a given bridge and this has necessitating site site specific live loading. Structural health monitoring systems and weigh in motion systems are now commonly used for live load and structural performance assessment [Sivakumar and Ghosn, 2012].

Several guidelines have been formulated for use in evaluation of bridges as reviewed in Chapter 2. The evaluation of existing structures provides a stepwise increment in analysis complexity for bridge assessment from deterministic, semi probabilistic to a full probabilistic assessment. Although the partial factor methods in design codes give deterministic equations relating load effects and load resistances, they include factors determined from a full probabilistic analysis and are thus referred to as semi-probabilistic methods. Deterministic analysis of load effects is usually a starting point in assessment and in this chapter the traffic loads were considered as deterministic based on the design capacity of freight wagon axle loads and the specified locomotive axle loads.

Deterministic analysis of bridge load effects by general rail traffic was conducted in Europe as part of a study to check the adequacy of rail traffic load models in Eurocode [ERRI Report D192/RP2, 1994]. However, studies with focus on heavy-haul railway bridge infrastructure are generally lacking. Hewson *et al.* [2017] performed a deterministic study on the effect of increasing wagon axle loads on the South African Iron Ore line from 30 tonnes to 36 tonnes. This study focused on the effects of load increase on rail, sleepers and ballast on the assumption that the other infrastructure can carry the increased loads.

6.2 Chapter Objectives

The objective and contribution of this chapter is to provide a deterministic assessment of beam type bridges on heavy haul line based on current wagon loads operating on the South African Iron Ore line. A comparison is made of the static load effects of current trains on the Iron Ore line, load effects effects

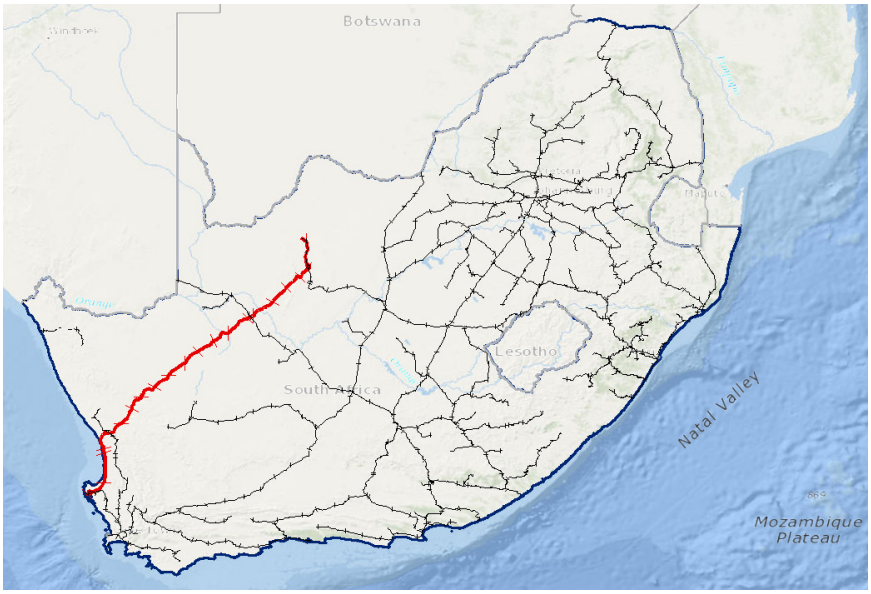

Figure 6.1: The Heavy Haul Iron Ore rail line

predicted by South African Transport Services Bridge Code (1983) herein referred to as SATS1983 and the Swedish Iron Ore Load model. The Swedish Iron Ore model is chosen for comparison as it is specified for the Iron Ore Freight railway line similar to the Saldhana-Sishen line. A second contribution is to check the adequacy of the baseline South African railway bridge live load model against the prevailing traffic on heavy-haul rail line and identify areas that could potentially have lower safety margins in a detailed probabilistic analysis.

6.3 South African Iron Ore Traffic

There are two main heavy haul lines in South Africa, namely the coal line to the East Coast of South Africa and the Iron Ore line from Sishen to Western Port at Saldhana. The heavy haul Iron Ore line consisting of a single 1067mm was built in 1978 and been in operation for close to 40 years now. The geographic location with the heavy haul highlighted is shown in Fig 6.1. The Iron Ore line is electrified with 50kV AC and has 19 loops over its entire length. In the early phase of operation the traffic on the line consisted of wagons with 26 tonnes per axle loads and annual haulage of 18 million tonnes per annum (mtpa) and this has increased to over 60 mtpa to satisfy the global demand for iron ore [Kuys,

Figure 6.2: Train crossing Olifants Bridge

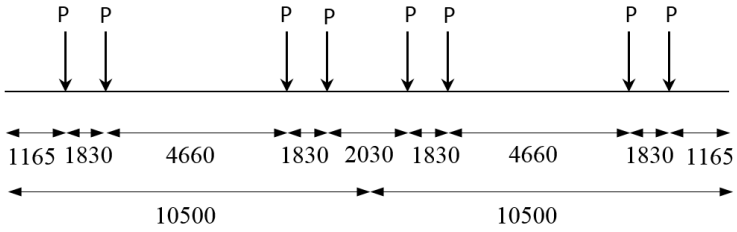

Figure 6.3: CR13 wagon axle spacing

2009]. In order to achieve this high haulage level, the rail operators (TRANSNET) have introduced new wagons with self steering bogeys capable of carrying up to 30 tonne axle loads. Longer trains have been introduced that have a total of 342 wagons composed of 114 wagon sets and 4 consist of locomotive engines equipped with Radio distributed power. Typical engines and wagon layout for the 342 wagon trains are shown in Fig 6.5 to Fig 6.6.

The current traffic on the rail line consists mostly of 4 types of trains whose characteristics for the period from June 2016 to March 2017 are shown in Table 6.1. The more common longer trains with up to 342 type CR-13 or type CR-14 wagon trains operate in two configurations powered either by 5 electric locomotive engines types 15E or 6 engines comprising of 4 Type 15E engines and 2 type 43D locomotives operating under a distributed power system. These longer trains carry Iron Ore and have the heaviest axle loads on the freight line.

Figure 6.4: Type 15E locomotive

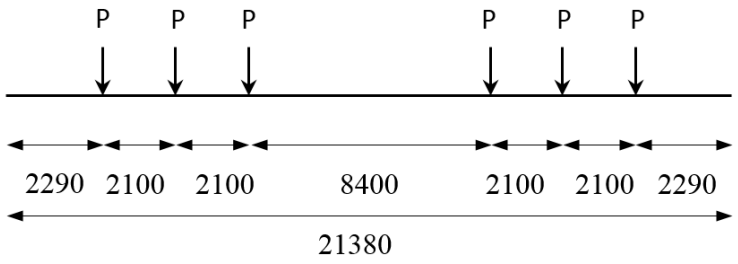

Figure 6.5: 15E engine axle spacing

The loads for empty type CR-13 and type CR-14 is shown in Fig 6.7 with a mean of 5 tonnes per axle. The loaded wagon types CR-13 and type CR-14 have mean axle loads around 29 tonnes as shown in Fig 6.8 and a maximum design capacity of 30 tonnes per axle. The distribution of axle loads for the locomotive engines shows a bimodal distribution as a result of the main engines in use which include type 15E with 19 tonne axle loads and 34D400 or type 43D diesel engines with a mean of 21 tonnes and 29 tonnes per axle respectively as shown in Fig 6.9. The trains consisting of 114 wagon to 223 wagon are normally powered by 2 type 15E and a 43D locomotive while trains with less than 114 wagons are powered by two diesel-electric locomotives which are type 34D400. The shorter trains comprise a small fraction of the freight traffic when haulage volumes are considered. These trains generally use different wagons of type CR-6, CR-9 and CR-10 and CR-17. These sets of wagons have two bogies with two axles per bogie and when loaded have 20 tonnes per axle while empty wagons have 4.4 tonnes per axle.

The traffic loads obtained in this section are used to obtain bending moments and

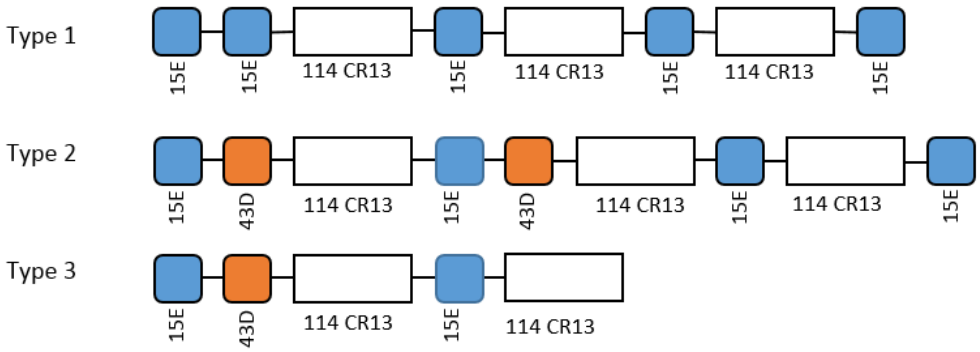

as

Figure 6.6: Iron Ore Line train consists

Table 6.1: Train events characteristics

Train Consists	Number (events)	Number (engines)	Wagons (min)	Wagons (max)
T1	385	5	338	343
T2	495	6	348	343
T3	106	3	114	223
T4	173	2	12	114
OTHER	90	MIN=1 MAX=6	0	225

shears in a deterministic analysis. The study will be limited to the heavier long trains with the load effects compared to South African code provision. The next section presents a review of live loading as presented in design codes.

6.4 Rail Traffic Load Models

Railway bridges are subjected to a range of loads that include environmental loads such as wind loading and temperature, live loads arising from passage of traffic and the self weight of the bridge structure. Live load is the one of the dominant actions on many bridges besides self weight. Other loads arising from passage of rail traffic include longitudinal acceleration and deceleration forces and lateral action from wheel hunting and rocking. Live load is generally derived from static load effects and through appropriate dynamic amplification factors the dynamic load effects are derived. Dynamic impact factors have already been discussed in Chapter 5 while the longitudinal forces from acceleration and braking together

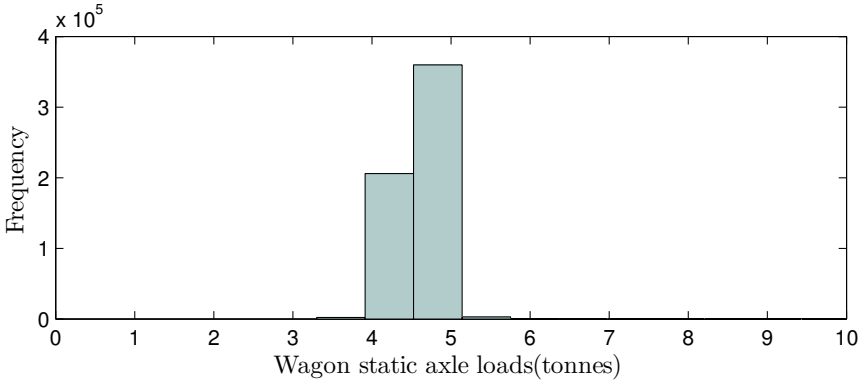

Figure 6.7: Empty wagon static axle loads

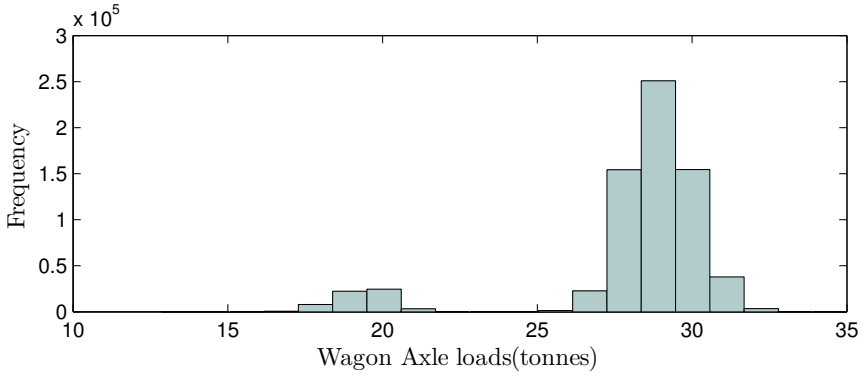

Figure 6.8: Loaded wagon static axle loads

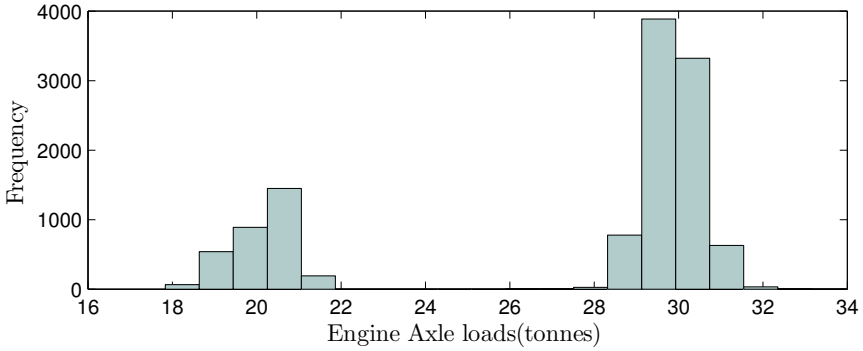

Figure 6.9: Locomotive static axle load

with collisions are outside the scope of this research.

From the dawn of railway traffic, bridge engineers averaged static trainloads for a given train length to produce a uniformly distributed load for bridge design. However, railway load restrictions on bridges were specified in terms of locomotive gross weight and axle loads as steam locomotives were generally much heavier than wagons [Hayward, 2011]. Cooper [1894] proposed a bridge standard loading based on coupled double locomotive engines and a uniform load trailing it. The

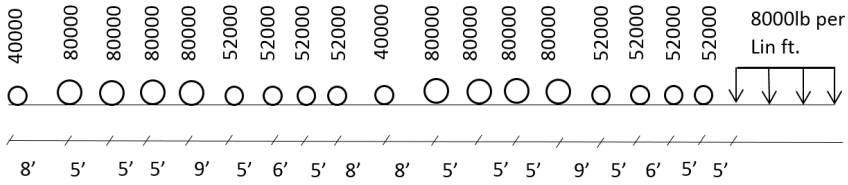

Figure 6.10: Cooper E80 loading

Cooper loading was the basis of the Railway Availability RA1 loading units in BS 153:1923. Cooper E in the format of Cooper E80 shown in Fig 6.10 is the railway bridge loading standard used in the United States of America while a similar metric version of the load is used in Australia [Cooper, 1894, O'Connor and Shaw, 2000, Unsworth, 2010].

More recent design codes such as South African Transport Services [1983] and 'BS EN 1991-2:2003' are based on the International Union of Railways load models. Design loads no longer represent specific locomotive or wagon loads and axle spacings but provide envelopes of bridge load effects for a wide range of bridges at a safety level determined by a given return period.

6.4.1 UIC Load Model 71

International Union of Railways Load Model 71 herein referred to as UIC LM71 is the basis of the Eurocode LM71 and the much earlier BS 5400 loading code which is the reference code for South African Transport Services [1983]. The load model is formulated for use on standard gage rail does not represent any specific train but is formulated to cover existing and predicted future train load effects on bridges. UIC LM71 suggests a longitudinal distribution of point loads with 50% carried by sleeper directly below the load and 25% carried by each of the side sleepers.

The UIC LM71 is used to determine static load effects and consists of 250kN points loads in addition to uniformly distributed load as shown in Fig 6.11. The loading given in UIC LM 71 is characteristic load and can be modified depending on client requirements. The loading is to be applied to achieve the most adverse effect with the relieving part ignored. The characteristic loads in railway loading codes do are not derived from 95% fractal but are based on notional loads. On

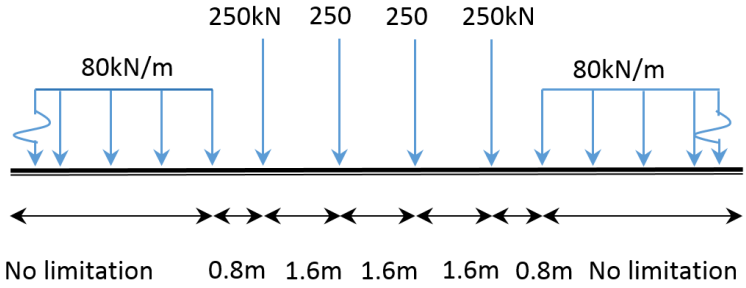

Figure 6.11: UIC Load Model 71

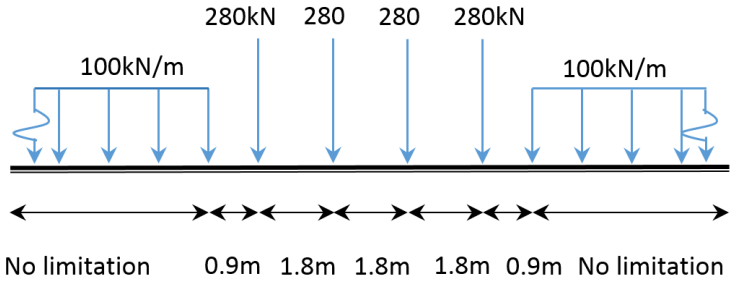

Figure 6.12: SATS 1983 Notional Loading

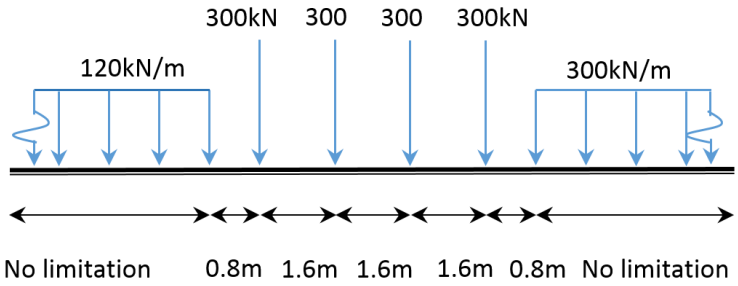

Figure 6.13: Swedish Iron Ore Loading

International lines in Europe, LM 71 is increased by a factor of 1.33 resulting in what are referred to as 'classified vertical loads' [Calgaro *et al.*, 2010]. For bridge assessment applications, LM 71 can be modified depending on the estimated remaining life of a given bridge . Bridges with residual life less than 50 years are assessed using LM71 without scaling, while bridges with residual life greater than 50 years are assessed using LM71 multiplied by 1.33 [O'Connor and Shaw, 2000, Calgaro *et al.*, 2010].

A deterministic analysis of LM71 for heavy freight load in Europe showed that LM71 was deficient for bending moment of simply supported span bridges and recommendation of scaling loads by factor 1.25 was made [ERRI Report

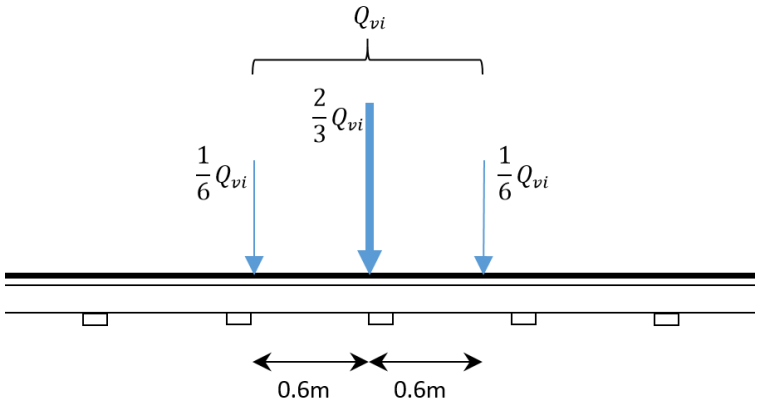

Figure 6.14: Load distribution used in SATS 1983 live load

D192/RP2, 1994]. The bending at support for 2 span beams was exceeded by 36% and 29% at spans of 65m and 200m respectively. The freight wagons governing the load effects envelop used in the study had axle loads between 250kN and 275kN.

6.4.2 South Africa Railway Bridge Code

The general format of UIC LM71 is the basis of SATS 1983 NR loading with modifications to the axle spacings, point and distributed loads to reflect local conditions [South African Transport Services, 1983, O'Connor and Shaw, 2000]. The 250kN point loads are increased to 280 kN, the uniformly distributed load is increased to 100 kN/m while the point load spacings are adjusted as shown in Fig 6.12. The longitudinal distribution of the loads over sleepers specifies $2/3$ rd for the sleeper directly under the load while the adjacent sleepers carry $1/6$ th each as shown in Fig 6.14. While SATS 1983 bridge code generally give higher load effects than UIC LM71, a comparison of mid-span bending moment for simply supported beam assuming similar lateral load distribution on sleepers shows that from 3m to 6m span lengths, the predicted load effects are similar and in some cases slightly less than the load effects from UIC LM71 as shown in Figs 6.15. However, the support shear from SATS 1983 live load are greater than the UIC LM71 for the whole span range as shown in 6.16.

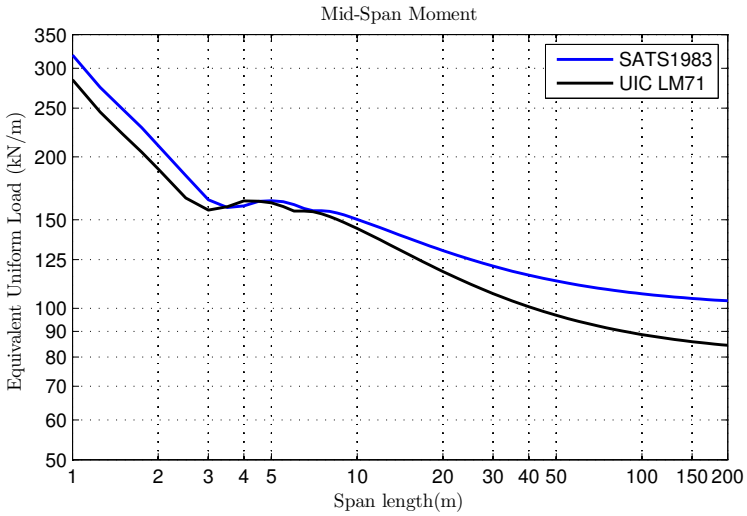

Figure 6.15: Comparison of mid-span moment

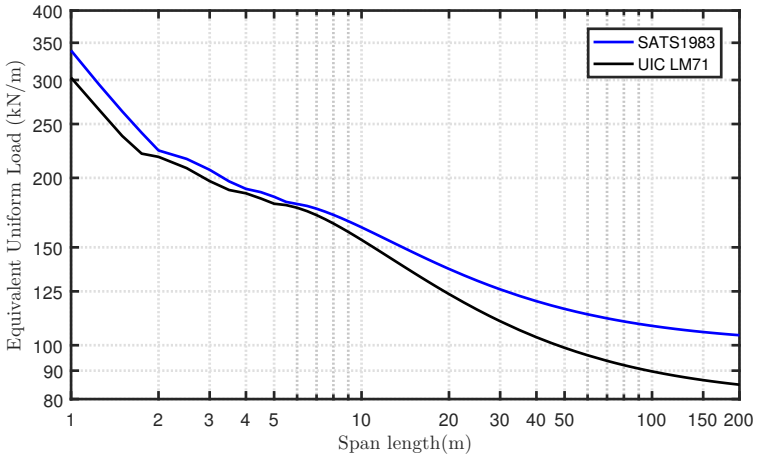

Figure 6.16: Comparison of support shear

6.4.3 The Swedish Iron Ore Load Model

The Swedish Iron Ore Load Model presented here for comparison with South African loads on heavy haul is an adaptation of UIC LM71. The loading is for use on iron ore which is the reason for a comparison while it must be noted that the SATS 1983 code is applied on narrow gage rail. The point loads are increased to 300kN point loads allow for higher axle loads whose load effects are dominant in short spans while the distributed load of 120kN/m allows for high gross weights distributed as uniform loads. The spacings for the loads is unchanged from the UIC LM71.

6.5 Simulation procedure

The beam types investigated in this study to determine the load effects of bending moments and shear at critical selected points include single span, 2 span and 4 span beams. The mid span sagging moment and end span shear which are critical for single span beams were investigated. The load effects for continuous multi span beams on the other hand included midspan sagging moment for the first span, first interior support hogging moment and shear. Only the case of equal spans is considered for multi span beams and the number of spans was limited to 4 while the span length was from 1m to a maximum of 200m. A summary of the relevant influence lines is given in Table 6.2. The study is limited to a maximum of 4 spans as the contributions to load effects at points of interest is negligible beyond 4 spans as seen in influence lines 6 to 8 in Table 6.2.

The train used in the deterministic study is based on the longest train in South Africa modified to represent the possible load effects induced by the train types listed in Table 6.1. The train configuration has an engine at one end and middle section with wagons and the whole configuration was $2 \times 15E + N \times CR13$ wagons $+$ $2 \times 15E + N \times CR13$ wagons where N is the number of wagons. The number of wagons for simulated train is dependent on the total bridge length as each of the wagon sets' length is equal to the span length with a minimum of 21 m length. The axle loads for locomotive engine type 15E has static axle load of 30 tonnes while CR-13 type wagon used in this simulation has a specified maximum axle load of 30 tonnes. The axle loads used here are slightly higher than the observed mean values from WIM-WIM as they are based maximum wagon axle loads and were chosen on the basis of the available wagon and locomotive engine drawings. The axle and bogie spacing distances for wagons are smaller than those for the locomotive engines and this lead to wagons producing the critical loading cases in short spans.

The code based loading is applied to obtain the maximum load effects and therefore any relieving load on an influence line is ignored. However, the full influence line is

Table 6.2: Influence Lines

No.	Description	Influence line
1	Midspan moment Simply supported beam	
2	Support Shear Simply supported beam	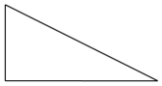
3	Midspan moment 2 span continuous beam	
4	Support moment 2 span continuous beam	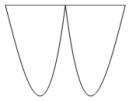
5	Support shear 2 span continuous beam	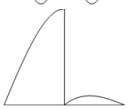
6	Midspan moment 4 span continuous beam	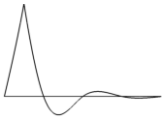
7	Support moment 4 span continuous beam	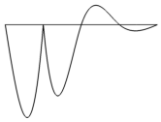
8	Support shear 4 span continuous beam	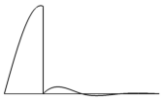

applied for existing traffic loading cases and maximum load effects are obtained. The load effects (LE) are computed from equation 6.1:

$$LE = \sum_{n=1}^{N} w_i A_i \tag{6.1}$$

where N is the number of axles, w_i is the distributed axle load and A_i is the corresponding area under the influence line as provided in Table 6.2. An equivalent distributed load (EUL) required to produce the obtained maximum load effects at point of interest is computed and is the basis of the comparison that follows.

In the study that follows, the Swedish Iron Ore LM are applied to narrow gage (1065mm) rail lines for comparison with SATS 1983. Furthermore, the

longitudinal distribution of point loads is assumed to be on 3 sleepers, $1/3$ rd on central sleeper while the two adjacent sleepers each carry $1/6$ th as specified in the SATS1983 code. Most studies on bridge loading consider the loading effects of shear at support for single span beams or first interior support shear for continuous beams. Similarly the moments are obtained from midspan of first span and first interior support for continuous spans. The influence lines used in this study are as shown in Table 6.2. The simulation was done using $Matlab^R$.

6.6 Deterministic Load effects

The generated mid span support moments for single span beam and first span of 2 span continuous beams and 4 span continuous beams corresponding to influence lines 1,3 and 6 in Table 6.2 are shown in Figs 6.17 to 6.19. The Swedish Iron Ore loads consistently produce higher loads than the SATS1983 or the current exiting SA Iron Ore trains. However the difference is much smaller in the range below 3m spans where the axle load effects are dominant. The midspan moment produced by current traffic for the simply supported beam for span lengths above 20m can be obtained by simply averaging converting the gross weight to a uniformly distributed load. The bending moment from existing traffic based on the maximum carrying capacity of the existing wagons exceeds the moments produced by the unfactored loads from SATS1983 for spans greater than 60m. The existing traffic midspan moment for a 2 span beam exceeds the SATS1983 unfactored moments at spans greater than 50m while the moments from existing traffic on a 4 span beam are all below the code provisions. This observation is as a result of the reliving effects for the simulated traffic being significant for the 4 span beam compared to the other beam types.

The interior span moment for 2 span continuous beam and 4 span continuous beam are shown in Figs 6.20 to 6.20 respectively. In general, the load effects from existing train traffic for a 2 span beam are very close to those obtained from the unfactored SATS 1983 loads for span lengths less than 20. The load effects from existing traffic are exceeded beyond 20 m span lengths. The interior span moment

for the 4 span beam displays a similar pattern to the 2 span beam with load effects from existing traffic being higher than SATS 1983 unfactored loads above 50 m span lengths.

A plot of the shear load effects for the different beams is shown in Fig 6.22 to Fig 6.24. All the beam types exhibit a similar pattern with respect to shear load effects produced by existing traffic. The existing traffic load effects on single span simply supported beams exceeds the unfactored SATS1983 load effects for spans greater than 40m. The shear load effects for 2 span and 4 span beams are very similar and this is explained by the influence lines 5 and 8 as given in Table 6.2. The existing load effects for both 2 span and 4 span continuous beams exceed the SATS 1983 load effects for spans greater than 30m.

The load effects from actual traffic are normalised by the effects obtained from SATS 1983 Code and presented in Figs 6.25 to 6.26. The Swedish Iron Ore loading code is deemed to be too conservative to be used for assessment on South African heavy-haul line as observed in Figs 6.17 to 6.24. A comparison of midspan moments shows that moments resulting from actual traffic are greater than those obtained from the unfactored SATS 1983 code for spans less than 3m. The bending moment is shorter spans is dominated by individual axle loads and the existing axle loads of 30 tonnes are greater than the South African Transport Services [1983] specified axle loads of 280kN. However, the effects from distributed load become significant at longer spans. The normalised mid span bending moments for a simply supported beam above 50m spans are the dominant effects as shown in Fig 6.25.

The normalised shear load effects are very close and show a very similar pattern. However, the shear for a single simply supported beam is slightly higher for span length less than 10m while above this span length, the dominant effects are from a 2 span beam. The differences are not considered significant. The normalised first interior support moment shown in Fig 6.26 show sightly different trends for the two beam types. The interior support moments for 2 span beam are

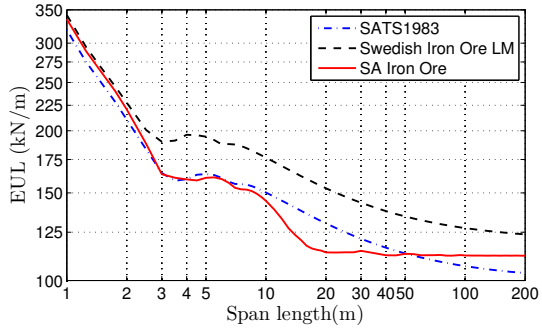

Figure 6.17: Simple support midspan moment

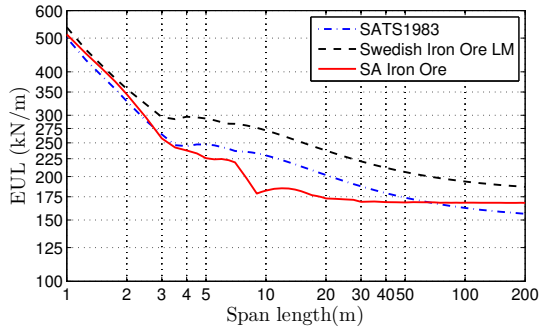

Figure 6.18: Mid span moment-2span beam ComparisonSV

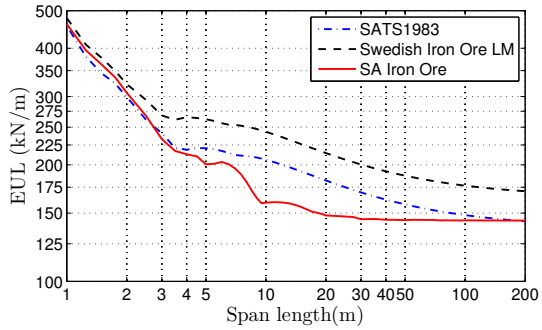

Figure 6.19: Mid span moment-4span beam

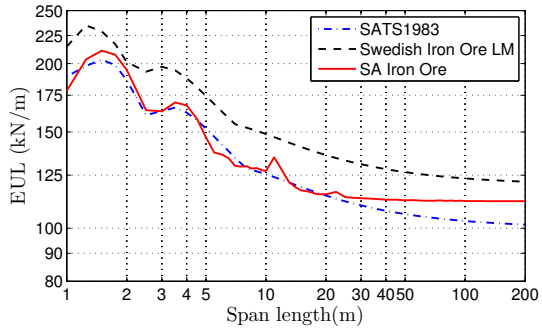

Figure 6.20: Interior support moment-2span beam

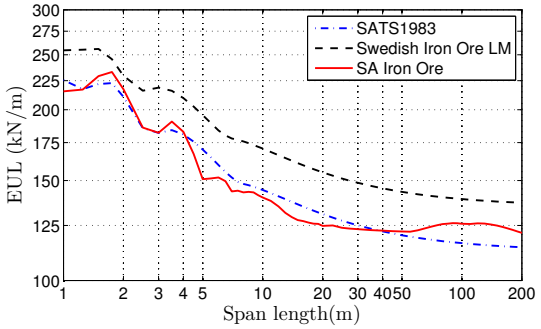

Figure 6.21: Interior span moment-4span beam

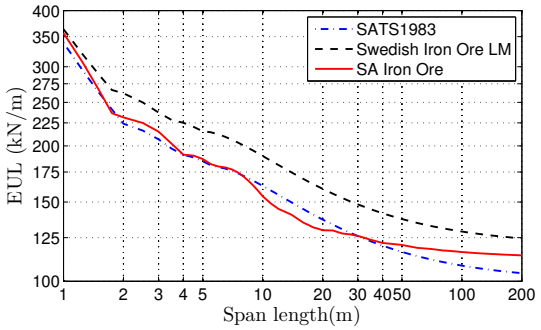

Figure 6.22: Simple support shear

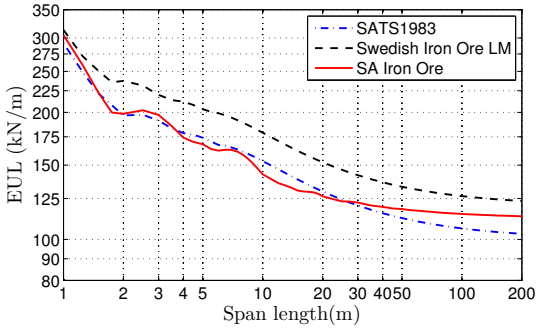

Figure 6.23: Interior support shear-2span beam

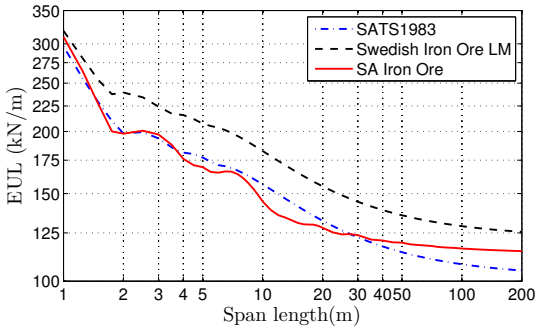

Figure 6.24: Interior span shear-4span beam

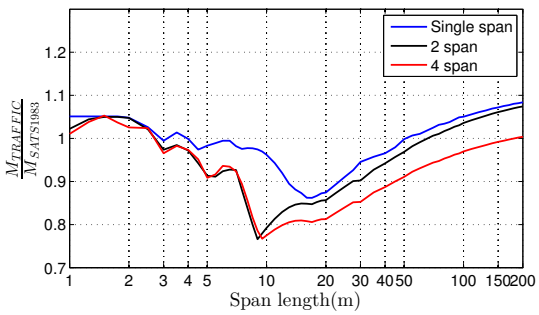

Figure 6.25: Comparison of normalised mid-span moments

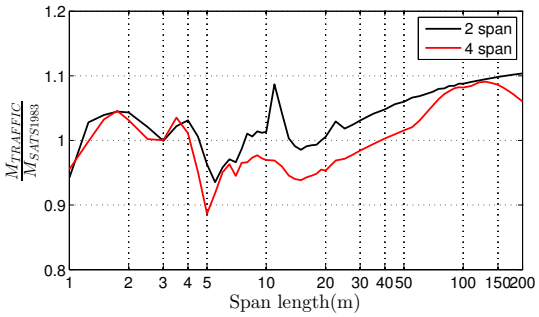

Figure 6.26: Comparison of normalised interior support moments

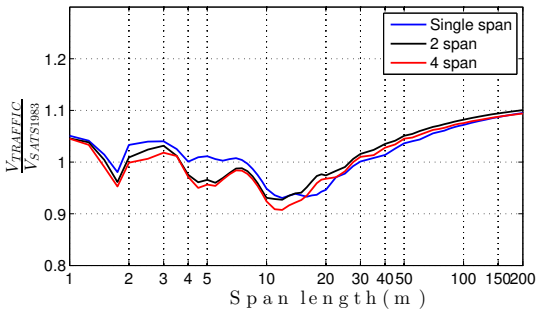

Figure 6.27: Comparison of normalised interior support shear

dominant as the moments are additive for any load configurations covering all spans. A comparison of all the normalised load effects shows that the 2 span interior support moment is dominant with existing traffic load effects being greater than the SATS 1983 code for span length above 8m.

6.7 Concluding remarks

Bridge design load models are generally conservative when used for assessment. The vertical live load models as given in UIC LM 71 and SATS 1983 code give characteristic loads which are assumed to represent the 95% fractile of loads on lines for design purposes. Although SATS 1983 vertical live load model uses higher point loads and uniformly distributed loads than the UIC LM71 model, the induced load effects in simply supported beams of span lengths between 3m and 7m are not significantly different. This is due to the increase in distance between point loads adopted in SATS 1983.

The South African Iron Ore line has operated wagons with 30 ton axle load

capacity. Due to increases in axle loads from 26 tonnes to the current 30 tonnes on heavy haul, SATS 1983 characteristic live load model may be unconservative based on a deterministic analysis for spans below 3m and above 50 m for single and multi-span beams. The load effects for simply supported beams show that the SATS 1983 model is only conservative for span lengths between 8m and 30m for support shear. The current traffic induces greater mid span moments in single span beams with support lengths between 5m and 50m while the support moments for 2 span beam type bridges are generally unconservative except for span lengths between 4m and 7m. In general, SATS 1983 live load model gives lower load effects for shorter spans where the individual axles are dominant as these have loads higher than the point loads provided in the design code. The load effects from traffic are also greater for longer spans where the effects are larger than the uniform load component provided in the design code.

While a deterministic study shows areas of that may be deficient, a comprehensive assessment load has to include the variability in axle loads and recalibrate live load factors. The live loads from WIM-WIM system show that the loads vary within the range from 26 tonnes to 32 tonnes. A probabilistic approach to modelling load effects is undertaken in Chapter 7.

References

'BS EN 1991-2:2003', "Actions on Structures Part 2: Traffic Loads on bridges," Standard, British Standards Institution.

Cooper T., "Train Loadings for Railroad Bridges," *Transactions of the American Society of Civil Engineers*, 31, Part 1; 174–184, 1894.

South African Transport Services, "Bridge code," 1983.

ERRI Report D192/RP2, "Comparison of present and future rail traffic on international lines with uic 71 loading based on deterministic calculation," 1994.

Bailey S.F. and Bez R., "Site specific probability distribution of extreme traffic action effects," *Probabilistic Engineering Mechanics*, 14; 19–26, 1999.

O'Connor C. and Shaw P.A., *Bridge Loads: An international perspective*, Spon Press, London, 2000.

Miao T.J. and Chan T.H.T., "Bridge live load models from WIM data," *Engineering Structures*, 24; 1071–1084, 2002.

UIC Leaflet 702OR, "Static loading diagrams to be taken into consideration for the design of rail structures on lines used by international services," 2003.

Kuys W., "Ore line capacity expansion: Conceptual design of the railway line to increase capacity," in "Proc. 9th IHHA Conf," 941–949, 2009.

Unsworth J.F., *Design of Modern Steel Railway Bridges*, CRC Press, New York, 2010.

Calgaro J., Tschumi M. and Gulvanessian H., *Designers' Guide to Eurocode 1 - Actions on Bridges EN 1991-2, EN 1991-1-1, -1-3 to -1-7 and EN 1990 Annex A2*, ICE Publishing, 2010.

URL http://app.knovel.com/hotlink/toc/id:kpDGEABE01/designers-guide-eurocode/designers-guide-eurocode

Hayward A.C.G., "Train Loads on Bridges 1825 to 2010," *International Journal for the History of Engineering and Technology*, 81, No2; 159–191, 2011.

Sivakumar B. and Ghosn M., "Collecting and using Weigh-in-Motion data in LRFD bridge design," *Bridge Structures: Assessment, Design and Construction*, 5(4); 151–158, 2012.

Hewson D.J., Gräbe P.J. and Shaw F.J., "Ore line capacity expansion: Conceptual design of the railway line to increase capacity," in "Proc. 11th IHHA Conf," 472–479, 2017.

Chapter 7

PROBABILISTIC LIVE LOADS FOR ASSESSMENT OF HEAVY-HAUL BRIDGES

7.1 Introduction

Railway bridges experience material deterioration as well as changes to traffic volumes and composition during their design life. These changes can severely compromise the safety level of a bridge as well as the ability to satisfy the primary function of allowing the passage of traffic. Railway bridges are regularly inspected and assessed during their service life to ensure their structural performance remains satisfactory. The assessment of bridges involves material assessment that usually focuses on checking for signs and deterioration or damage to the bridge through condition surveys. These assessments are largely based on visual inspections supplemented with non destructive testing to finally determine the bridge condition index which is taken as a performance measure. The structural performance is obtained by load rating of bridges. Bridge load rating is obtained from proof load tests where the bridge is subjected to a known load and resulting deformations limited to the elastic response region. Proof load tests have the main draw back of not being an accurate representation of actual bridge traffic.

Recently there has been focus on assessment of bridges largely due to the ageing infrastructure in many countries coupled with constraints on maintenance

budgets. The assessment of bridges is fundamentally different from bridge design and the main difference is in the treatment of uncertainties and the service life under consideration. It is recognised that design loads are inherently conservative and formulated to be applicable to a wide range of structures and can not be applied to evaluate existing structures. Live loads for bridges which include both static and dynamic loads from traffic together with bridge dead weight form part of critical load combinations in both assessment and design applications. Design loads are computed based on extreme value theory with return periods raging from 75 years to 1000 years depending on design code under application. In AASHTO, the bridge design service life of 75 years coincides with the load return period while in Eurocode the return period which is a measure of safety is 1000 years.

An existing structure on the other hand has remaining service life that is lesser than design life. In addition the material properties, geometric parameters and loading of an existing structure can be obtained and may deviate significantly from design assumptions. Several guides propose a stepwise increment in analysis complexity performed during assessment from deterministic to fully probabilistic [Melchers, 1999, Cremona and Poulin, 2017]. A deterministic study of load effects has already been presented in Chapter 6 where it is shown that the unfactored load model given in South African Transport Services [1983] may be marginally unconservative for evaluating interior support hogging moments due to existing traffic. A deterministic analysis ignores the randomness in the loads and thus a probabilistic framework is needed to better understand the load effects.

Cremona and Poulin [2017] suggest that for undamaged bridges, a conservative assessment using design guides can be performed. When a design code check yields unsatisfactory performance, a semi probabilistic analysis requiring material tests and loads to recalibrate partial factors is done. The recent practice in highway bridges assessment has been to use weigh-in-motion data to quantify uncertainties in the live load model and therefore recalibrate load models or partial safety factors so that they reflect route specific or site specific conditions

while maintaining the required level of safety [Nowak *et al.*, 1993, Getachew and Obrien, 2007, Sivakumar and Ghosn, 2012, Cremona and Poulin, 2017].

In evaluation of characteristic and design load effects, three main approaches have been widely used namely monte-carlo simulation, the classical methods of block maximum (BL) and peak over threshold (POT) for extreme value analysis have been applied to measured or computed effects. Monte-carlo simulation has been used either to obtain characteristic loads or to supplement data where monitoring period was short. Monte-carlo simulation generally requires more computational resources. Tabatabai *et al.* [2017] fitted weigh in motion data to multi-modal histograms and used empirical copula functions and monte-carlo simulation to obtain characteristic loads. O'Connor and Eichinger [2007] used experimentally obtained influence lines to obtain bridge moments. The block maximum approach and monte carlo were used to compute characteristic values. The daily maximum load effects were fitted to both Gumbel and Weibull distributions. Moyo and Brownjohn [2004] fitted a Gumbel distribution to block maximum of bridge strains obtained from a continuous monitoring and extrapolation to obtain characteristic strains was done on Gumbel paper. Nowak *et al.* [1993] used traffic gross-weight data to compute load effects of simply supported bridges. Characteristic load effects were obtained by plotting load effects data of daily block maximums on normal distribution paper and extrapolated to required return period.

This study presents assessment traffic static loads based on weigh-in-motion data from the South African iron ore heavy haul line. Extreme load effects based on assumption of stationarity in traffic volume and composition are obtained for 50 year return reference period. The freight traffic characteristics and general load effects simulation procedure are presented in the sections that follow.

7.2 Chapter Objectives

The main objective of this chapter is to present a probabilistic analysis of heavy-haul rail loads based on route specific weigh-in-motion data. The first

contribution is to compare various extrapolation techniques given block maxima load effects from beam-type bridges on heavy haul. Variations of extrapolated load effects due to choice of technique have been reported on highway bridge applications under free flow conditions. The second contribution is an investigation of variation distribution shape factors against increasing span length for heavy haul bridges. This will give some indication of any possible departures if a distribution is chosen a priori when studying load effects. The third contribution focusses on checking the sensitivity of predicted load effects to choice of return period for bridges on heavy haul. This last aspect is relevant as there is greater control in loading regimes for freight trains on dedicated heavy-haul lines.

7.3 Extreme value prediction

The formulation of live loads for bridge design or assessment loads deals with the occurrence of rare loading situations during the bridge design life. The analysis and prediction of these tail end live loads is based on classical extreme value theory. Applications of extreme value theory in load effects studies use two main procedures namely block maxima approach and the threshold exceedance approach. This study is limited to the block maxima approach generally adopted in extreme load effects studies. A summary of underlying extreme value theory applicable to the univariate case is presented here while more detailed mathematical treatment can be found in several texts [Galambos *et al.*, 1982, Castillo, 1988, Coles, 2001].

Let X_1,X_2,...,X_n be a sample of independent and identically distributed (iid) random variables from a parent cumulative distribution function (c.d.f) F. Then the maximum Z_n and W_n are defined as below:

$$\begin{aligned} Z_n &= \max(X_1, X_2, ..., X_n) \\ W_n &= \min(X_1, X_2, ..., X_n) \end{aligned} \tag{7.1}$$

The distribution of maximums or minimums F_Z and F_W can be obtained:

$$\begin{aligned} F_Z &= P(Z \leq x) = \prod_{i=1}^{n} P(X_i \leq x) = F^n(x) \\ F_W &= P(W \geq x) = \prod_{i=1}^{n} P(X_i \geq x) = (1 - F(x))^n \end{aligned} \tag{7.2}$$

Similarly, the density function $f(x)_z$ for extremes can be obtained by differentiating equation 7.3:

$$f(x)_z = nF^n(x)f(x) \tag{7.3}$$

When the number of samples n tends to infinity, the partial maxima F_Z degenerates to the cases in equation 7.4:

$$F_Z = F^n(x) \xrightarrow{n\to\infty} \begin{cases} 0 & \text{if } x < x^F \\ 1 & \text{if } x \geq x^F \end{cases} \tag{7.4}$$

In practice, the parent c.d.f for the random variables of interest may not be known and thus equation 7.3 can not be readily applied. However, if the variables for partial maxima are renormalised some non-degenerate asymptotic distributions can be obtained from the extremal types theorem [Coles, 2001]:

If there exists a sequence of constants $a_n > 0$ and b_n such that

$$P\left\{\frac{Z_n - b_n}{a_n} \leq z\right\} \to G(x) \text{ as } n \to \infty \tag{7.5}$$

where G is a non-degenerate distribution function, then G belongs to one of the following families:

$$\text{Gumbel (Type 1) } G(x) = \exp\left\{ -\exp\left[-\frac{x-\mu}{\sigma}\right]\right\}, \ -\infty < x < \infty \tag{7.6}$$

$$\text{Frechet (Type II) } G(x) = \begin{cases} 0 & x \leq b \\ \exp\left\{ -\left(\frac{x-\mu}{\sigma}\right)^{\xi}\right\} & x > b \end{cases} \tag{7.7}$$

$$\text{Weibull (Type III) } G(x) = \begin{cases} \exp\left\{ -\left[-\left(\frac{x-\mu}{\sigma}\right)^{\xi}\right]\right\} & x < b \\ 1 & x \geq b \end{cases} \tag{7.8}$$

where σ, μ and ξ are the scale, location and shape parameters respectively. The Gumbel and Weibull types are widely selected to model extreme load effects on

highway bridges. The Weibull type distribution imposes an upper limit and this is desirable if the underlying mechanism under study has a limit. The Frechet type distribution has a heavy upper tail and is not used in extreme load effects prediction as it leads to overestimates of effects.

The concept of domains of attraction for distribution of maximums follows from equation 7.2. For the non degenerate case after transformation with constants a_n and b_n, a c.d.f $F(x)$ is belongs to the domain of attraction of c.d.f $G(x)$ if equation 7.9 is satisfied [Castillo, 1988]:

$$\lim_{n\to\infty} G(a_n + b_n x) = \lim_{n\to\infty} F^n(a_n + b_n x) = G(x) \tag{7.9}$$

The commonly used distributions for random variables of interest in engineering such as Normal, Exponential and Log-normal distributions have the domain of maximums attraction to the Gumbel distribution. The rate of convergence of the Normal to the Gumbel distribution is generally slow [Dey *et al.*, 2016]. The Gumbel, Weibull and Frechet type distributions have maximums domains of attractions as Gumbel, Weibull and Frechet distributions respectively a situation referred to as max-stable [Castillo, 1988, Coles, 2001]. Max-stability is achieved if X_1,X_2,...,X_n are i.i.d samples drawn from c.d.f G and $max(X_1, X_2, ..., X_n)$ have the same distribution.

In highway bridge load effects studies, data of maximum daily load effects are fitted to either Gumbel or Weibull distributions. The initial distribution choice can introduce modelling errors prior to parameter estimation. The generalised extreme value (GEV) distribution combines the three extreme type distributions described earlier and can be used to address the uncertainty in distribution choice. The GEV is given equation 7.10:

$$G(x) = \exp\left\{ -\left[1 + \xi\frac{x-\mu}{\sigma}\right]^{\frac{-1}{\xi}} \right\} \tag{7.10}$$

where μ, σ and ξ are the location, scale and shape parameters of the distribution. The shape parameter ξ determines the tail behaviour of the GEV and therefore determines the modelled extreme type distribution. The Weibull distribution is

obtained when $\xi < 0$ while the Frechet type distribution is obtained when $\xi > 0$. The Gumbel distribution is obtained when $\xi = 0$.

7.3.1 Model selection

Statistical model selection considers the critical selection of the distribution type to represent the distribution of load effects maxima for a given bridge or route. Previous studies on highway bridge applications have assumed the distribution to be either Gumbel or Weibull types and focused on parameter estimation [Moyo and Brownjohn, 2004, O'Connor and Eichinger, 2007]. The choice of a model can be made based on theoretical understanding of the problem or using statistical methods based on available data. O'Connor and Eichinger [2007] has shown that the distribution that best represents the load effects on a highway bridge depends on span length and the load effects under consideration. Weibull distribution resulted in a better fit of gross weight data for short span bridges (span $\leq$ 5m) as it assumes an upper limit that is consistent in the physical limits on gross weight.

Probability plots are among the common graphical techniques employed check the validity of the selected model to fit a given dataset [Castillo, 1988, Coles, 2001]. The probability plot is obtained by transforming the observed variable and the probability such that the empirical c.d.f becomes a straight line. Given a $x_1 \leq x_2 \leq,...,\leq x_n$ as samples drawn from c.d.f F then the empirical c.d.f is defined as [Castillo, 1988]:

$$F_E(x) = \frac{i}{n+1} \text{ for } x_i \leq x \leq x_{i+1} \tag{7.11}$$

The probability plot is obtained from points as given in equation 7.12 [Coles, 2001]:

$$\left\{(F_E(x), \frac{i}{n+1}) \text{: i = 1,..n}\right\} \tag{7.12}$$

The most commonly applied probability plots in loads and load effects studies for highway bridges are the normal, Weibull and Gumbel plots. The normal plot has been applied directly to extrapolate the load effects as given in equation 7.3. Given

a normal random variable, the p.d.f is given as:

$$F_N(x;\mu,\sigma) = \Phi(\frac{x-\mu}{\sigma}) \tag{7.13}$$

and the reduced variate is obtained:

$$\eta = \frac{1}{\sigma}u - \frac{\mu}{\sigma} \tag{7.14}$$

where

$$u = h(x) = x \tag{7.15}$$

The Gumbel distribution already presented earlier is given here:

$$G(x) = \exp\left\{ -\exp\left[-\frac{x-\mu}{\sigma}\right]\right\} \tag{7.16}$$

The reduced variate is given as equation 7.17:

$$\eta = \log[-\log(F(x))] \tag{7.17}$$

where

$$u = h(x) = x \tag{7.18}$$

Finally the Weibull distribution is given:

$$G(x) = \exp\left\{ -\left[-\left(\frac{x-\mu}{\sigma}\right)^{\xi}\right]\right\} \quad x \leq \mu, \beta > 0 \tag{7.19}$$

the reduced variates are given:

$$\eta = -\log[-\log(F(x))] \tag{7.20}$$

where

$$u = -log(\mu - x) \tag{7.21}$$

7.3.2 Parameter estimation

Once a distribution has been chosen on the basis of techniques above, distribution parameters can be estimated using various methods such as Least Squares, Maximum-Likelihood Method or Probability-Weighted Moments. The Maximum-Likelihood Method is used in this study and is presented here

[Castillo, 1988, Coles, 2001]. Parameter estimation was obtained using the ismev package in R [Hefferman and Stephenson., 2016].

For an i.i.d data set $X = X_1, X_2, ..., X_n$ from a p.d.f $f(x;\theta)$ and c.d.f $F(x;\theta)$ where θ is the parameter space, the likelihood function is given as:

$$L(\theta|x) = \prod_{i=1}^{n} f(x;\theta) \tag{7.22}$$

The likelihood function estimates the model with the highest probability based on the data. The log-likelihood is often used in computations derived from taking logarithm of equation 7.22

$$l(\theta|x) = \sum_{i=1}^{n} \log f(x;\theta) \tag{7.23}$$

The maximum likelihood point estimate can be obtained if it satisfies the following equations:

$$\frac{\partial l(\theta|x)}{\partial \theta} = 0 \tag{7.24}$$

subject to:

$$\frac{\partial^2 l(\theta|x)}{\partial \theta^2}\Big|_{\theta=\theta_1(x)} < 0 \tag{7.25}$$

where $\theta_1(x)$ is solution from equation 7.24.

7.3.3 Bayesian approach

In parameter estimation, it is assumed that given the random realisations of maxima $\boldsymbol{X}$ that are from a c.d.f $F(\theta)$ the parameter θ though unknown is fixed and thus parameter estimation reduces to a procedure that finds the values of θ that maximise the likelihood function. Under the Bayesian approach, the parameters θ are assumed to be random. The Bayesian theorem expressed in terms of $prior$ distribution $f(\theta)$ and $posterior$ distribution $f(\theta|x)$ is given in equation 7.26:

$$f(\theta|x) = \frac{f(\theta)f(x|\theta)}{\int_\theta f(\theta)f(x|\theta)d\theta} \tag{7.26}$$

where the prior $f(\theta)$ distribution provides information on θ from the $prior$ distribution and the data x.

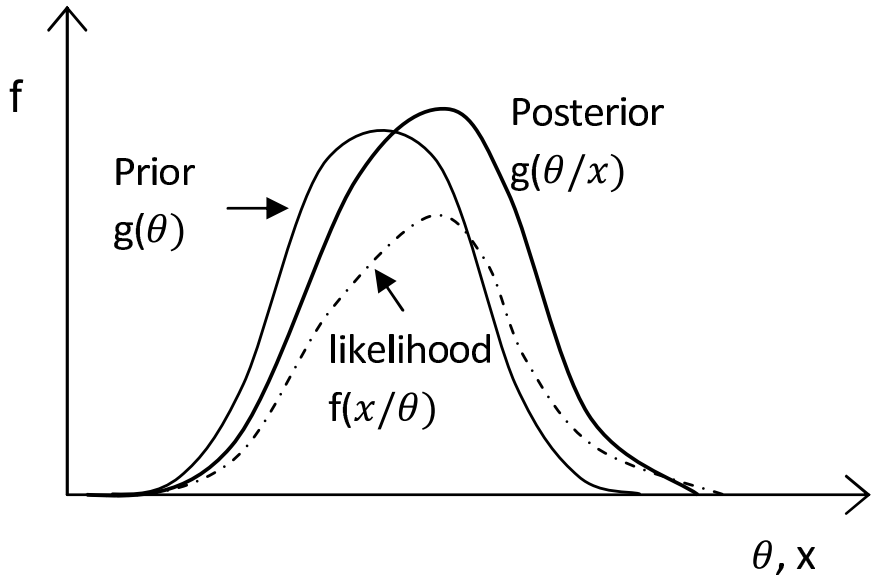

Figure 7.1: Bayesian framework update

The computation of the normalising integral in the numerator of equation 7.28 is done generally done through Markov-Chain Monte Carlo (MCMC) algorithm. However in this study, integration is performed as implemented in R package $revdbayes$ which is based on ratio of uniforms method of sampling the posterior [Northrop, 2017]. Wakefield *et al.* [1991] generalised the ratio of uniforms method of sampling with focus of improving its efficiency with a generalisation for multivariate distribution given below:

Theorem 1. *Suppose h is a positive integratable function over χ a subset of $\boldsymbol{R}^k$. Suppose further that the variables $(u, v_1, ..., v_k)$ are uniformly distributed over:*

$$C_h(r) = \left\{(u, v_1, ..., v_k) : 0 < u \leq \left[h\left(\frac{v_1}{u^r}, ..., \frac{v_k}{u^r}\right)\right]^{\frac{1}{rk+1}}\right\}$$

where $r \geq 0$. Then $\boldsymbol{x} = (x_1, ..., x_k)$ where $\boldsymbol{x_i} = v_i/u^r$ has density $\dfrac{h(\boldsymbol{x})}{\int h(\boldsymbol{x})}$.

The region sampled is restricted to the regions where $C_h(r)$ is bound in a k-dimensional rectangle. Provided that h is bounded and $x_i^{rk+1}(h((x))^r$ is bounded, $i = 1, 2, ..., k$ the enclosing rectangle is defined such that:

$0 < u < a(r)$

$b_i^- \leq v_i(r) \leq b_i^+(r)$, $i = 1, ..., k$

where

a(r) = $\sup_\chi [h(\boldsymbol{x})]^{r/(rk+1)}$

$b_i^-(r) = \inf_{\chi_i^-} x_i[h(\boldsymbol{x})]^{r/(rk+1)} i = 1, ..., k$

$b_i^+(r) = \sup_{\chi_i^+} x_i[h(\boldsymbol{x})]^{r/(rk+1)} i = 1, ..., k$

with $\chi_i^- = \{\boldsymbol{x} \in \chi : x_i \leq 0\}$, and $\chi_i^+ = \{\boldsymbol{x} \in \chi : x_i \geq 0\}$ The acceptance probability $p_a(r,k)$ is the ratio of the volume of $C_h(r)$ relative to the enclosing k-dimensional rectangle as given in equation 7.27:

$$p_a(r,k) = \frac{\int h(\boldsymbol{x}) d\boldsymbol{x}}{(rk+1)a(r) \prod_{i=1}^{k} (b_i^-(r) - b_i^+(r))} \tag{7.27}$$

The choice of priors allows for inclusion of past experiences and expert opinion into the determination of posterior distribution. The inclusion expert opinion makes the posterior distribution. However in the absence of information, the priors can be formulated as non informative. Coles [2001] used non informative priors to determine parameters for GEV of maxima of annual sea levels. The prior density function assumes independence in μ, ξ and ϕ of the form:

$$f(\theta) = f(\mu, \phi, \xi) = f_\mu(\mu) f_\phi(\phi) f_\xi(\xi) \tag{7.28}$$

where $f_\mu(\mu)$, $f_\phi(\phi)$ and $f_\xi(\xi)$ are normal density functions of zero mean.

7.3.4 Characteristic loads and return periods

Characteristic loads are live loads that correspond to an expected level of safety of bridges. The expected level of safety is generally expressed as a fractile of the annual loads. For dominant variable actions such as traffic live loads, the 'BS EN 1991-2:2003' defines a characteristic load as the load that is only exceeded 2% of the times in a year alternatively defined to 98% fractile. This corresponds to an event with a return period of 50 years. The design loads are however determined as loads with 0.1% chance of exceedance in a year alternatively defined to 99.9% fractile. The design level fractile corresponds to an event with a return period of 1000 years. The Load and Resistance Factor Design code live load factors are based a extrapolating load effects to the bridge design life of 75 years. In this study, the load effects are obtained for the 50 year and 1000 year return level.

7.3.5 Characteristic loads for heavy-haul bridges

Live loads on bridges have been determined based on extreme value theory using block maximum methods. The applications of the block maxima method either fits the maximums to Gumbel type or the Generalised Extreme Value GEV [James, 2003, O'Connor and Eichinger, 2007, OBrien *et al.*, 2015]. Design live loads have also been obtained by fitting the maxima data to a normal distribution and then extrapolated to the required return level [Nowak *et al.*, 1993]. More recently, the Bayesian method has been applied to extreme value analysis of both weather and live loads for bridges [Coles, 2001, OBrien *et al.*, 2015].

The block maxima method divides the duration of data collection into equal intervals that are non overlapping. The block size in traffic live load effects on bridges studies is generally chosen to correspond to the natural time durations such as a day. of a day. In weather studies, the block may be monthly or yearly maxima. Let X_1, X_2, ... be random variables from c.d.f F. The block maxima is defined as [Ferreira *et al.*, 2015]:

$$\tilde{X} = \max_{(i-1)m<j<im} X_j \tag{7.29}$$

where $m = 1, 2, ...$ and $i = 1, 2, ...k$ such that the observations are divided into k blocks. Under some appropriate transformation, a non degenerate distribution which is GEV can be obtained:

$$G(x) = \begin{cases} \exp\left(-\left(1 + \xi\frac{x-\mu}{\sigma}\right)^{\frac{-1}{\xi}}\right) & \text{if } \xi \neq 0 \\ \exp\Big(-\exp\big(-\frac{x-\mu}{\sigma}\big)\Big) & \text{if } \xi = 0 \end{cases} \tag{7.30}$$

where μ, σ and ξ are the location, scale and shape parameters of the distribution determined using any of the parameter estimation methods listed earlier. While fitting data to GEV eliminates the errors that may arise by first assuming any of the extreme type distributions, it has been pointed out that this approach rarely fits to the Gumbel type as it is just once case in the parameter space.

The block maxima of traffic load effects have also been fitted to normal distributions and raised to required return level based on equation 7.2. For data

fitted to a normal distribution, the maxima under appropriate normalising constants approaches asymptotic distribution as Gumbel type which is referred to as its domain of attraction [Castillo, 1988].

The Bayesian method is not widely applied in prediction of extreme traffic load effects on bridges. However, it has been demonstrated to yield predictions comparable to other methods with reduced variance in predicted characteristic values [OBrien *et al.*, 2015]. The Bayesian framework is especially attractive in that it allows expert judgement through the choice of information priors to be included in the computation of extreme loads.

The principle of tail equivalence allow that only a fraction of the upper quantile samples are used for distribution identification and parameter estimation. Sivakumar and Ghosn [2012] suggests using the top 5% of gross weight data to be fitted to normal distribution for determination of extreme load effects. OBrien *et al.* [2015] used the top 30% data of maximum daily load effects to determine the extreme value distribution of annual maximums. In this study, the weekly maximums representing 5% of the simulated dataset of load effects used. The maximum likelihood approach is widely used in parameter estimation.

7.4 Heavy-haul traffic based on WIM-WIM system

An overview of freight traffic on the heavy haul iron line was briefly presented in Chapter 6 while omitting the necessary details for a probabilistic study. The axle loads obtained from WIM-WIM dataset from January 2016 to August 2016 are best described as multi-modal distributions with each mode corresponding to different wagon or locomotive axle times as summarised in Fig 7.2 below. The first mode centred around 5 tonnes is composed of empty wagons of types CR-6, CR-9, CR-13 and CR-14. The WIM WIM does not identify individual wagons and thus these wagon types were obtained through a query to the railway operator. The peak around 20 tonnes is composed of loaded type CR-6, CR-9 and CR-10 used for transporting manganese and diesel locomotive engines type 34D400 which are used to power the shorter trains. The loaded iron ore wagons type CR-13 and type

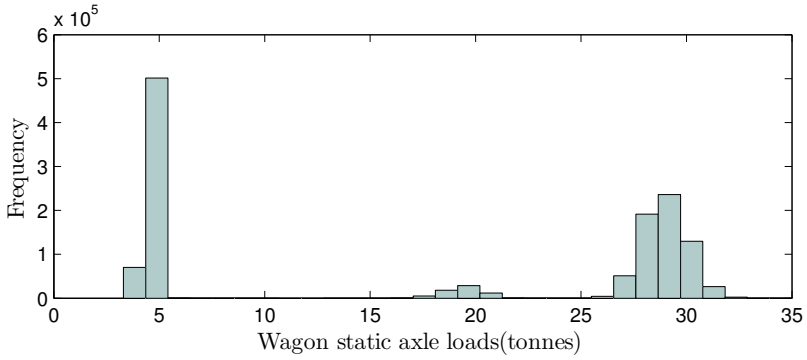

Figure 7.2: South African Iron Ore axles

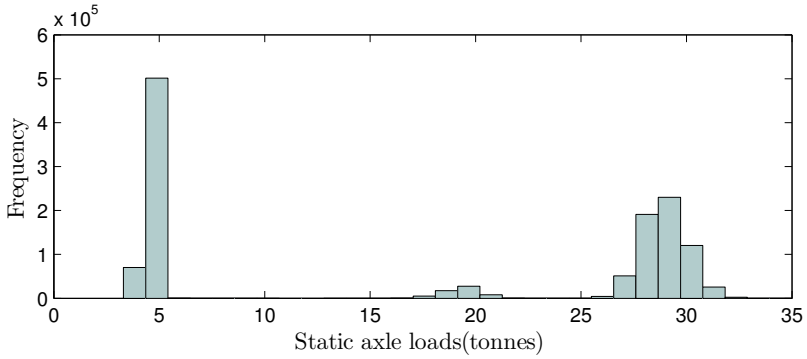

Figure 7.3: Freight line wagon axle loads

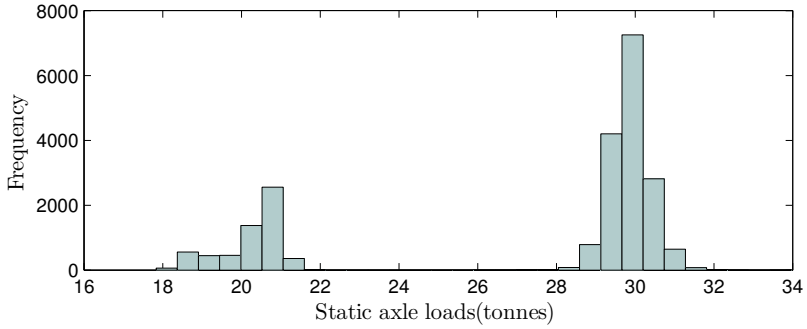

Figure 7.4: Freight line locomotive axle loads

CR-14 as well as locomotive engines types 15E and 43D make up the third peak centred around 28 tonnes. The locomotive and wagon loads are separated and shown in Fig 7.3 and 7.4 respectively.

Traffic load models are normally based on the higher axle loads observed. Thus from the axles observed above, only the iron ore loaded trains are considered which comprise of 342 wagon trains hauled by Type 15E locomotive engines. These trains as seen from the previous chapter form the bulk of the trains and are the ones used for transportation of Iron Ore. The wagons and engines are fitted to normal

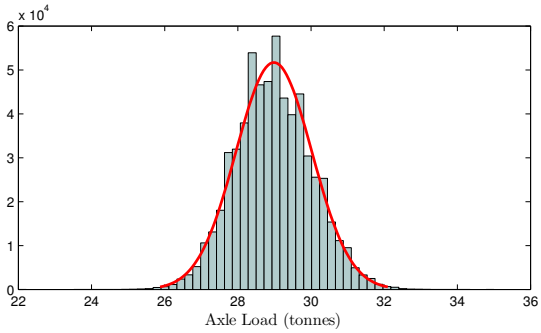

Figure 7.5: Loaded wagon distribution

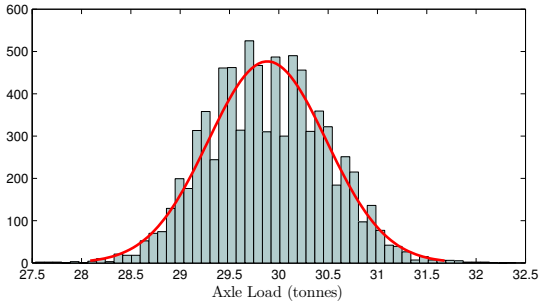

Figure 7.8: Locomotive engine distribution

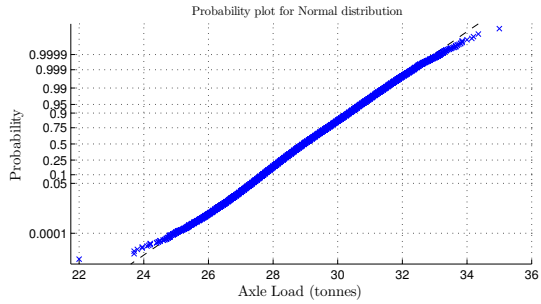

Figure 7.6: Wagon axle probability plot

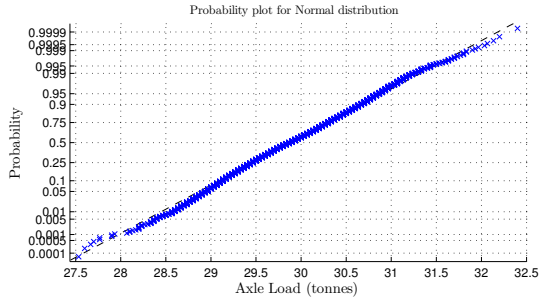

Figure 7.9: Locomotive axle probability plot

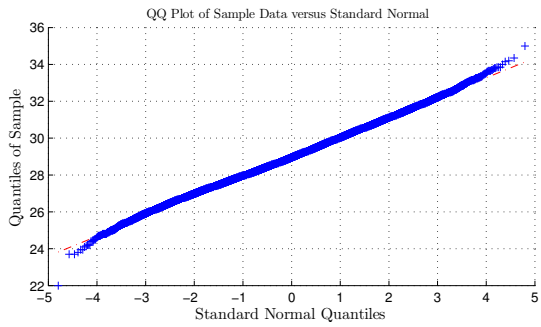

Figure 7.7: Wagon axle quantile plot

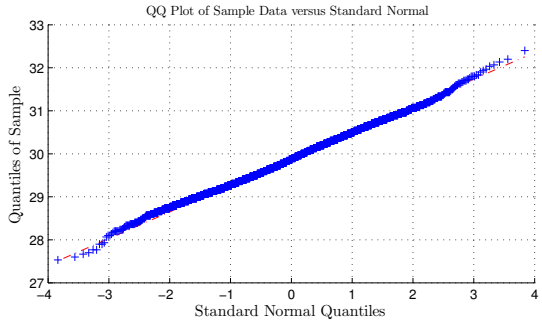

Figure 7.10: Locomotive axle quantile plot

distribution and the model checks indicate that it is a reasonable choice for wagon and locomotive gross weight.

The probability plots and the quantile plots of the engine show linear trends confirming that a normal distribution is an acceptable choice. The type CR-13 and CR-14 wagons axles have a mean of of 28.99 tonnes and standard deviation of 1.04 tonnes while the locomotive type 15E engines have a mean of 29.88 tonnes and standard deviation of 0.60 tonnes. The WIM-WIM system does not collect axle spacing data. The variations in axle spacing within a wagon type is expected to be negligible so is treated as deterministic variable.

Table 7.1: Influence Lines

No.	Description	Influence line
1	Midspan moment Simply supported beam	
2	Support Shear Simply supported beam	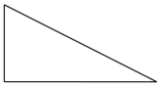
3	Midspan moment 2 span continuous beam	
4	Support moment 2 span continuous beam	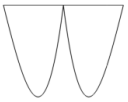
5	Support shear 2 span continuous beam	
6	Midspan moment 4 span continuous beam	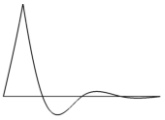
7	Support moment 4 span continuous beam	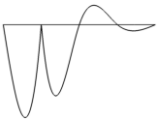
8	Support shear 4 span continuous beam	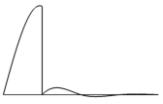

7.5 Probabilistic load effects simulation

The static load effects of on 3 beam type bridges namely single span simply supported beam, 2 and 4 span continuous bridge are computed. The load effects of interest include mid span bending moment, first interior support moment and first interior support shear. The relevant influence lines at selected locations are given in Table 7.1 presented earlier. The load effects LE are computed from equation below:

$$LE = \sum_{n=1}^{N} w_i A_i \tag{7.31}$$

where N is the number of axles, w_i is the distributed axle load and A_i is the corresponding area under the influence line.

The area under the influence lines is the same as in the deterministic cases as the span lengths assume assigned deterministic values. However, the axle loads are generated as independent and identically distributed (iid) random variables representing the individual train axle loads at a spacing level corresponding to the wagon types. The train configuration in the simulation had two engines at one end and middle section with wagons. The train configuration in the simulation is $2 \times 15E$ engines + $114 \times CR13$ wagons + $15E$ engine + $114 \times CR13$ wagons + $15E$ engine + $114 \times CR13$ wagons.

A probabilistic study is done based on load effects from simulated train axle loads. The density function of axle loads is based on weigh-in-motion data over a period of 7 months (210 days). OBrien *et al.* [2015] compared several probabilistic methods of extrapolating load effects to desired return period and showed that the accuracy of the extrapolation is largely influenced by the number of days of available data. It was shown that simulated data for a period of 1000 days gave extrapolated return values whose mean was more accurate compared to that obtained from 200 days of day. A total of 8 trains per day are simulated over a period of 156 weeks and weekly maximum load effects for single span simply supported and 2 span bridges at locations in Table 7.1 were obtained. The simulated weekly maxima representing approximately 2% of the data is extrapolated after fitting to GEV, the normal distribution and using the Bayesian inference. The obtained extrapolated values are normalised by South African Transport Services [1983] bridge loading code for comparison.

7.6 Results and discussion

In this section, the results obtained from 3 different extrapolation techniques of block maxima data using normal distribution fitting, GEV maximum likelihood parameter estimation and GEV Bayesian parameter estimation are presented and discussed. The normal distribution fitting and extrapolation of block maxima fits weekly maxima to a normal distribution and the extrapolations done according to equation 7.2. A typical density function obtained for midspan moment of a 5m

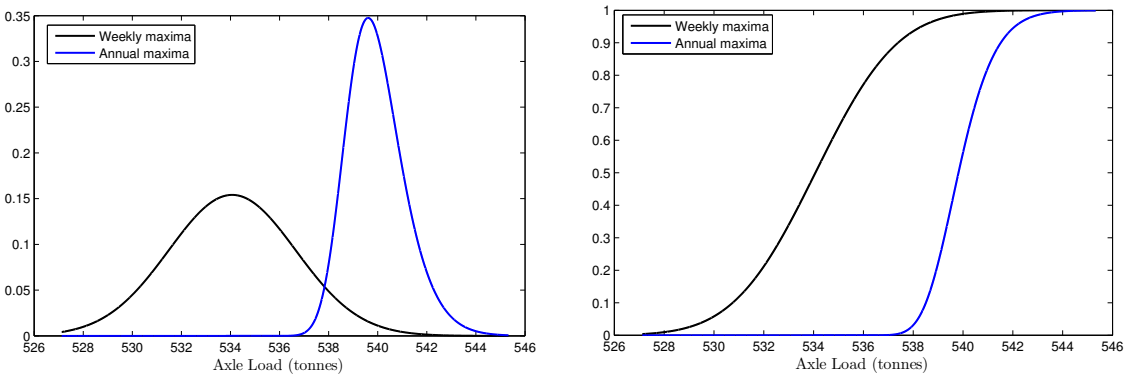

Probability density Cumulative density

Figure 7.11: Extrapolation of bending moment for 5m span beam

span simply supported beam is shown in Fig 7.11 and this is done for all beam spans and beam types under consideration. The annual maxima cumulative distribution is used to obtain the loads at 98% and 99.9% fractiles which correspond to 1 in 50 and 1 in 1000 year levels respectively.

The second approach uses weekly maxima load effects fitted to GEV with parameter estimation done using the maximum likelihood method outlined in Section 7.3.2. The simulated weekly maxima and fitted GEV are plotted on Gumbel probability paper with reduced variate ν given in equation 7.32:

$$\eta = -log(-log(F(x))) \tag{7.32}$$

where $F(x)$ is probability of non exceedance. For a return period of 50 years gives a reduced variate $\eta = 7.86$ and the corresponding load effects level is extracted. Typical plots on Gumbel paper are presented in Fig 7.12 for a 20m span simply supported beam and a 20m continuous 2 span beam showing both weekly maxima data and fitted distribution.

The Bayesian inference is done to estimate the distributions of the parameters for GEV as outlined earlier. Diffuse priors with mean $\mu = 0$, variance $\sigma = 10000$ and shape factor $\xi = 100$ were set. This was done for all the beams and typical plots are shown in Fig 7.13 for the 5m span simply supported beam mid span moment weekly maxima. The values for return level corresponding to desired safety level

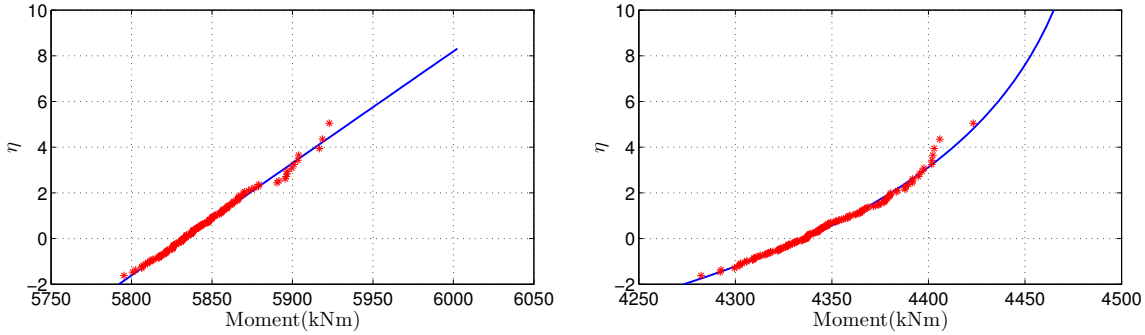

Simply supported beam 2 span beam

Figure 7.12: Plots of mid span moment on Gumbel paper for 20m span beams

are given in equation 7.33.

$$z_p = \begin{cases} \mu - \dfrac{\sigma}{\xi}[1 - (-\log(1-p))^{-\xi}] & \text{for } \xi \neq 0 \\ \mu - \sigma \log(-log(1-p)) & \text{if } \xi = 0 \end{cases} \tag{7.33}$$

where p is the probability of exceedance derived from a given period. The inference of parameters is performed on weekly maxima and thus assuming a 52 week long year, the required probability for a 50 year period is obtained from $\frac{1}{50\times 52} = 3.846 \times 10^{-4}$.

A comparison of the extrapolated load effects for the three methods is done for the load effects of mid span moment and first support shear return level for 100 years for the single span and 4 span continuous beams at various span lengths. The predicted values normalised by South African Transport Services [1983] load effects for simple supported beam and a 4 span continuous beams are shown in Tables 7.2 to 7.3 with the rest of results presented in appendix. The three methods of extrapolating extreme values give comparable values. A closer analysis shows that the normal extrapolation gives results that are marginally lower than those obtained from Bayesian and GEV methods. The normal method approaches the Gumbel distribution as its asymptotic distribution and thus is expected to give slightly higher values than the GEV and Bayesian which all fit to a Weibull distribution. This can however be explained by the slower convergence to the Gumbel distribution.

The Bayesian inference and fitting block maxima to GEV through maximum

Table 7.2: Comparison of normalised mid-span moments

Span length	Simply supported			4-span continuous		
(m)	Normal	Bayesian	GEV BL	Normal	Bayesian	GEV BL
5	1.06	1.08	1.08	1.02	1.03	1.04
10	1.02	1.03	1.03	0.82	0.82	0.83
15	0.92	0.93	0.93	0.84	0.84	0.85
20	0.91	0.92	0.92	0.83	0.84	0.84
25	0.94	0.95	0.95	0.86	0.86	0.86
30	0.98	0.98	0.98	0.87	0.87	0.87
35	0.98	0.99	0.99	0.88	0.89	0.89
40	0.98	0.99	0.99	0.90	0.90	0.90
45	1.00	1.00	1.00	0.91	0.91	0.91
50	1.01	1.02	1.02	0.92	0.92	0.92

Table 7.3: Comparison of normalised first support shear

Span length	Simply supported			4-span continuous		
(m)	Normal	Bayesian	GEV BL	Normal	Bayesian	GEV BL
5	1.09	1.10	1.10	1.03	1.04	1.03
10	1.00	1.01	1.01	0.98	0.98	0.98
15	0.99	0.99	0.99	0.96	0.97	0.97
20	1.00	1.01	1.01	0.99	1.00	1.00
25	1.01	1.01	1.01	1.00	1.00	1.00
30	1.02	1.03	1.03	1.02	1.02	1.02
35	1.03	1.03	1.03	1.02	1.03	1.02
40	1.04	1.04	1.04	1.03	1.04	1.04
45	1.04	1.04	1.04	1.03	1.04	1.04
50	1.05	1.05	1.05	1.04	1.05	1.05

likelihood methods all give the additional information on the shape parameter which is used to determine the extremal distribution type. The Gumbel and Weibull type distributions have been used to obtain traffic loads for highway bridges. O'Connor and Eichinger [2007] showed that the Weibull provided a better fit to highway bridge load effects for shorter span bridges while the Gumbel was chosen for medium span bridges. The variation of shape factor for given load effects over a range of spans is investigated with a typical graph shown in Fig 7.14 with additional plots provided in appendix. The investigated load effects and beam types show that a Weibull type distribution better describes the load effects for all span lengths and beam types. A Weibull type distribution accounts for the constraints on the maximum load that can be transported in

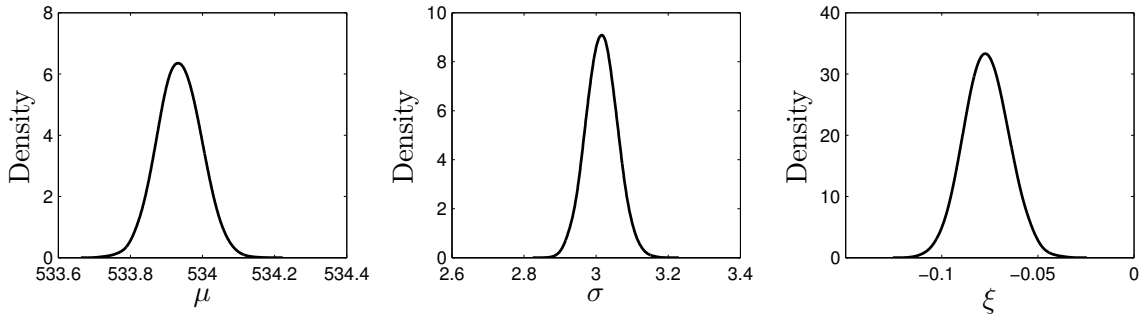

Figure 7.13: GEV Parameter distributions for mid-span moment (5m span)

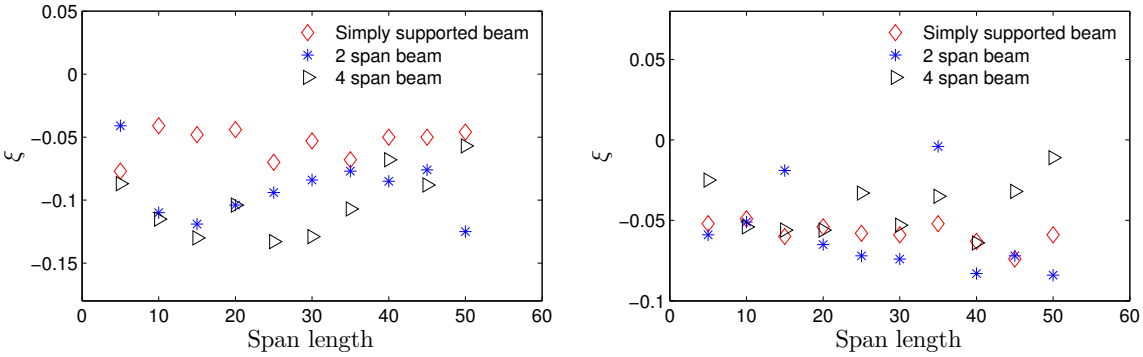

Mid-span moment Shear effects

Figure 7.14: Variation of shape factor with span length

the wagons. The bending moment effects for a simply supported beam generally approach a Gumbel distribution compared to the other beam types while this is not observed on the plot of the shear load effects. The shear load effects do not display a particular trend with increase in span length. Furthermore, there is considerable scatter in shape parameter for simply supported beam and the 2 span continuous beam shear and midspan moments.

The characteristic load and design loads already described earlier are investigated at 50 year and 1000 year return levels corresponding to the reduced variates $\nu = 7.86$ and $\nu = 10.86$ on Gumbel paper as shown in Fig 7.15 for the midspan moment of a 2 span continuous beam. The difference in moments at these return levels is less than 1 % as shown from selected load effects in Table 7.4 and therefore the observations from 1000 year return levels are equally applicable to the 50 year level case. This observation is can be explained as the fitting methods on a GEV either directly though parameter estimation of block maxima or through Bayesian

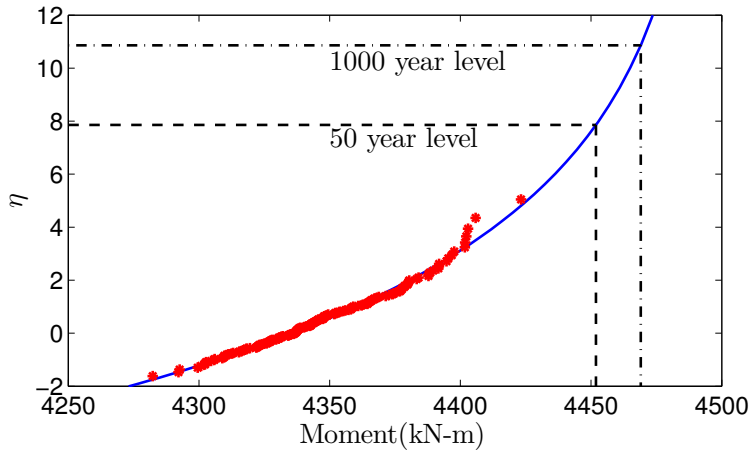

Figure 7.15: 2 span mid moment return levels (20m span)

inference end up with a Weibull distribution. However, this observation holds for load effects obtained using the normal distribution extrapolation. A more likely explanation is the loading controls applied on freight wagons as observed from the small variance in axle loads consequently resulting in lower values for scale parameter in GEV. Similar small differences in load effects between 1 in 100 year and 1 in 1000 year are reported in literature [ERRI Report D192/RP3, 1994].

The 1000 year load effects for various beam types and span ranges from 5m to 50m are normalised with the South African Transport Services [1983] Notional Load. The daily load effects based on average axle loads are obtained for the beams and normalised to SATS 1983 NR code for comparison. A comparison of mid span moments for all beam types corresponding to influence lines 1, 3 and 6 in Table 7.1 shows that for span length below 10m, the axle loads are more dominant leading to higher ratios when compared to SATS 1983 NR loading. The governing mid span bending moments at 1000 years return levels are obtained from simply a supported beam with span length of 5m with a factor of 1.10 to the SATS 1983 NR. This ratio is likely to be higher for span lengths below 5 m where individual axles as opposed to bogies act. The daily average for simply supported beams shows the inherent conservatism in computing mid span moments based on SATS 1983 NR loading when applied to heavy haul lines.

The support shear load effects show a similar pattern where the ratio increases

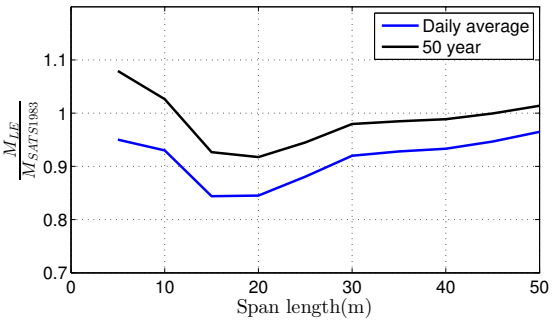

a1: Simply supported (Moment)

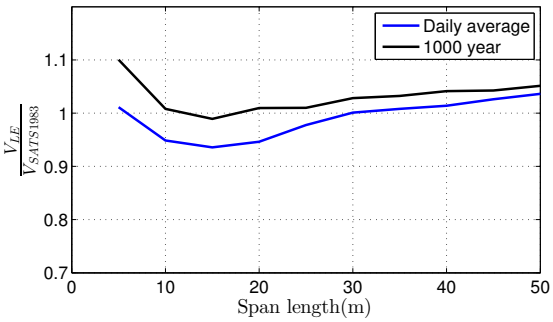

b1: Simply supported (Shear)

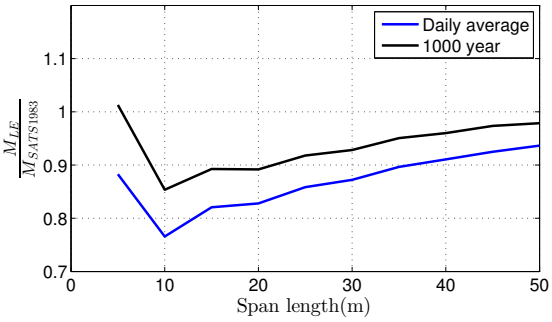

a2: Two span beam (Moment)

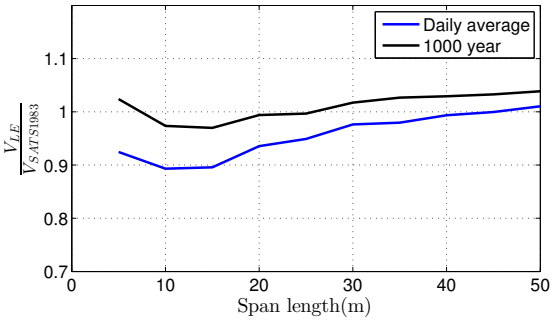

b2: Two span beam (Shear)

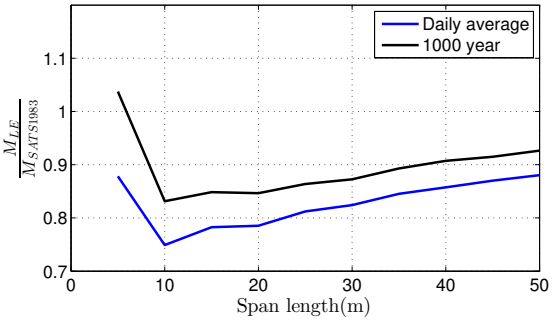

a3: Four span beam (Moment)

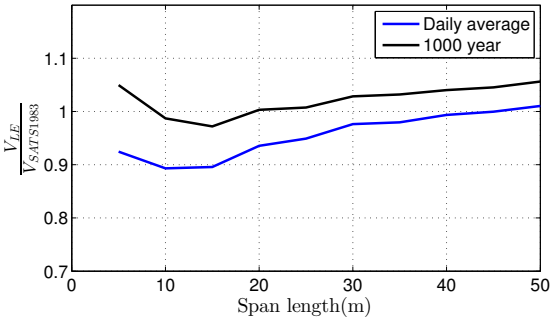

b3: Four span beam (Shear)

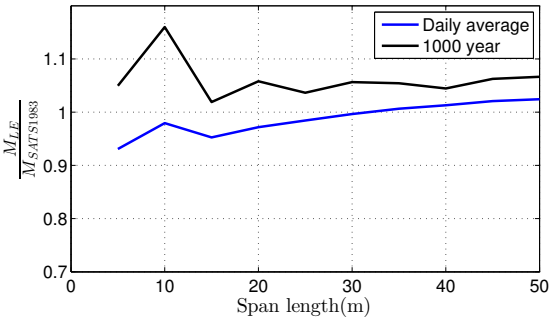

a4: Two span beam(Supp Moment)

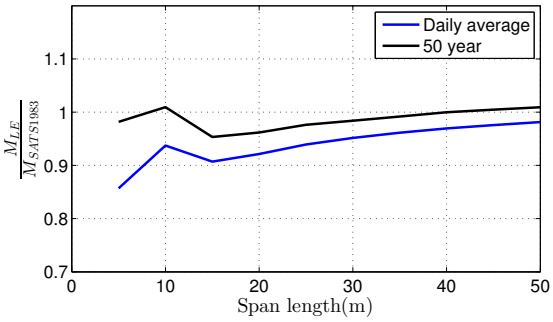

b4: Four span beam (Supp moment)

Figure 7.16: Comparison of 1000 year SATS 1983 NR normalised load effect

Table 7.4: Comparison of 50 year and 1000 year level mid-span moments

Span (m)	Simply supported beam Return Level (years)			4-span continuous Return Level (years)		
	50	1000	diff(%)	50	1000	diff(%)
5	551.7	556.2	0.2	407.2	408.9	0.3
10	1927.7	1944.8	0.2	1214.5	1223.8	0.3
15	3598.3	3626.2	0.2	2606.9	2622.1	0.2
20	5975.7	6018.8	0.2	4373.9	4405.5	0.2
25	9230.5	9275.5	0.1	6713.7	6747.6	0.1
30	13371.6	13446.0	0.1	9471.6	9520.4	0.1
35	17875.8	17957.6	0.1	12877.8	12949.0	0.1
40	23021.4	23146.2	0.1	16723.9	16858.6	0.1
45	29022.9	29168.3	0.1	21053.4	21188.4	0.1
50	35913.7	36094.9	0.1	25952.3	26147.5	0.1

The values in table are obtained from Block maxima fitted to GEV and are in kN-m

as the length is less than 10m or greater than 15m. The smaller spans are greatly influenced by variations in individual bogie groups or individual axles where greater variations are expected. The longer spans on the other hand are influenced by the linear distribution of the traffic load along the longitudinal axis of the bridge. The variations in distributed load are lesser for longer spans and thus the difference between daily average load effects and the effects at 1000 years narrows with increasing span length. The dominant shear effects for the span range considered are experienced at 5m span length with a factor of 1.1.

The internal support moments show a very different pattern where there is a reduction either side of 10m span length. The wagon length corresponds to 11m and thus the maximum load effects are obtained when the bogies of a wagon are at mid spans of adjacent spans. There is a marginal increase in support span moment with increasing span length beyond 15m. The daily load effects ratios increase with increasing span beyond 15m and the difference narrows with the 1000 year return event. The dominant effects for support moment at 1000 year level are obtained for a 2 span continuous span with span length of 10m resulting in a factor of 1.15.

In general the normalised load effects for 2 span continuous beams are larger than corresponding load effects of a 4 span continuous beam of the same span length. This is caused by the relieving effects that result from applying the simulated traffic loads over the whole influence lines as opposed to the code application which ignores the relieving part of the influence lines.

7.7 Concluding remarks

It is necessary to account for route specific traffic characteristics in formulating live loads for bridge assessment. The traffic composition on the South African heavy haul iron ore line consists mostly of 342 wagon trains with axle loads significantly higher than other trains. The 342 wagon trains account for 70% of the number of loaded trains on line and a much greater freight tonnage.

Different extrapolation techniques were used to obtain load effects from the same block maxima data. It was shown that the normal, GEV and Bayesian extrapolation methods give load effects within 1% of each other with the normal extrapolation being marginally on the lower end. This observation holds across beam types and span lengths from 5m to 50m. Although the GEV allows for all the three extreme type distributions, an analysis based on available weigh-in-motion data of axle weights show that the fitted distributions using Bayesian and Maximum Likelihood Estimate for all load effects for the span ranges are all Weibull type. On the other hand it is known that the domain of attraction for the normal distribution is Gumbel type. The extrapolated loads are less sensitive to increase in return period beyond 50 years and this is explained by the controls in wagon loading leading to small variance. This aspect is significant as return period is a measure of safety target when determining design values for loads.

The load effects obtained from this trains over a 1000 year return period are greater than the loads from SATS 1983 NR loading by a factor of 1.15 but much less than the specified design live load factor of 1.6 specified in South African Transport Services [1983]. The dominant load effects for assessment are shear at spans less

than 5m and interior support moments at span length of 10m.

In Chapter 8 effects of traffic volume growth from available historical data and spatial dependence in wagon axle loads are investigated.

References

'BS EN 1991-2:2003', "Actions on strcutures part2: Traffic loads on bridges," Standard, British Standards Institution.

Galambos T.V., Ellingwood B., MacGregor J.G. and Cornell A., "Probability Based Load Criteria: Assessment of Current Design Practice," *J. Structural Engineering ASCE*, 108 ST5; 959–977, 1982.

South African Transport Services, "Bridge code," 1983.

Castillo E., *Extreme Value Theory in Engineering*, Academic Press, Inc, London, 1 edition, 1988.

Wakefield J.C., Gelfand A.E. and Smith A.F.M., "Efficient generation of random variates via the ratio-of-uniforms method," *Statistics and Computing*, 1(2); 129–133, 1991.

URL `https://doi.org/10.1007/BF01889987`

Nowak A., Nassif H. and DeFrain L., "Effect of truck loads on bridges," *Journal of Transportation Engineering, ASCE*, 119(6); 853–867, 1993.

Melchers R.E., *Structural Reliability Analysis and Prediction*, John Wiley and Sons Ltd, 2 edition, 1999.

Coles S., *An Introduction to Statistical Modeling of Extreme Values*, Springer-Verlag, London, 2001.

James G., *Analysis of traffic load effects an railway bridges*, Ph.D. thesis, Royal Institute of Technology, 2003.

Moyo P. and Brownjohn J.M.W., "Highway bridge live loading assessment and load carying capacity estimation using health monitoring system," *Structural Engineeringand Mechanics*, 18(5); 609–626, 2004.

Getachew A. and Obrien E.J., "Simplified site-specific traffic load models for

bridge assessment," *Structure and Infrastructure Engineering: Maintenance, Management, Life-Cycle Design and Performance*, 3(4); 303–311, 2007.

O'Connor A. and Eichinger E.M., "Site-specific traffic load modelling for bridge assessment," *Proceedings of The Institution of Civil Engineers-Bridge Engineering*, 160; 185–194, 2007.

Sivakumar B. and Ghosn M., "Collecting and using Weigh-in-Motion data in LRFD bridge design," *Bridge Structures: Assessment, Design and Construction*, 5(4); 151–158, 2012.

Ferreira A., De Haan L. *et al.*, "On the block maxima method in extreme value theory: Pwm estimators," *The Annals of statistics*, 43(1); 276–298, 2015.

OBrien E.J., Schmidt F., Hajializadeh D., Zhou X.Y., Enright B., Caprani C.C., Wilson S. and Sheils E., "A review of probabilistic methods of assessment of load effects in bridges," *Structural safety*, 53; 44–56, 2015.

Dey D., Roy D. and Yan J., *Extreme Value Modeling and Risk Analysis: methods and Applications*, 1–20, Chapman & Hall/CRC: Boca Raton, Florida, 2016.

Hefferman J.E. and Stephenson. A.G., *ISMEV: An Introduction to Statistiacl Modeling of Extreme Values*, 2016, r package version 1.41.

Northrop P.J., *revdbayes: Ratio-of-uniform sampling for bayesian Extreme value analysis*, 1 edition, 2017, R package version 1.3.1.
URL `https://CRAN.R-project.org/package=revdbayes`

Cremona C. and Poulin B., "Standard and advanced practices in the assessment of existing bridges," *Structure and Infrastructure Engineering*, 13, No4; 428–439, 2017.

Tabatabai H., Titi H. and Zhao J., "WIM-based assessment of load effects on bridges due to various classes of heavy trucks," *Engineering Structures*, 140; 189–198, 2017.

ERRI Report D192/RP3, "Comparison of the effects of current and future rail traffic on international lines with the effects from UIC 71 loading on a probabilistic basis," Utrecht, December 1994.

Chapter 8

EFFECTS OF AXLE LOAD SPATIAL DEPENDENCE AND TRAFFIC GROWTH ON HEAVY-HAUL BRIDGE LIVE LOADS

8.1 Introduction

Structural performance assessment and maintenance of bridges has gained attention largely due to the ageing infrastructure in many countries coupled with constraints on maintenance budgets. It is acknowledged that bridges undergo material deterioration as well as changes to traffic volumes and composition during their design life and these factors affect their structural performance. The wide adoption and installation of weigh-in-motion (WIM) systems on many transport networks has provided data to quantify uncertainties in the live load models thus enabling the recalibration of load models to reflect route specific or site specific conditions while maintaining the required level of safety [Nowak *et al.*, 1993, Getachew and Obrien, 2007, Sivakumar and Ghosn, 2012].

In Chapter 7, classical extreme value theory was applied to obtain load effects at various return periods under the assumption that axle loads are stationary and that they are independent and identically distributed. Decisions on changes in axle loads are determined by railway operator and generally require introduction of different wagon types which may have different axle spacing or configuration. The wagon types on heavy-haul changed from capacity of 26 tonne to the current 30 axle wagons in the year 2000 [Hewson *et al.*, 2017]. The stationarity of axle

loads which is formally defined in Section 8.3 is assumed since it is not correct to assume growth in axle loads without changing wagon types. The stationarity in axle loads therefore only admits increase in freight volumes by increasing the number of trains running or train consists. In the previous chapter, route specific loads where obtained by fitting axle loads to distributions and assessment loads computed without accounting for the traffic growth.

The effect of growth in axle loads and traffic volumes has been investigated for highway bridges. OBrien *et al.* [2014] investigated single span and 2 span beams and showed that traffic volume growth of 3% increased load effects by 6.9% for 75 year return level. Leahy *et al.* [2016] considered growth in both traffic volume and axle load of highway bridges with 40 year remaining period. The study showed in increase in load effects of 9% for annual traffic volume growth of 3% and no growth in axles. However, an annual growth of 1% for axle loads over 40 year period resulted in 43% increase in load effects. The growth in axle loads was achieved through replacement of lighter vehicles with heavy vehicles of a higher class with either the same or different axle configurations identified from weigh-in-motion data.

The asymptotic theory of extreme values has been applied to the evaluation of load effects on bridges under the assumption that the traffic loads are independent and identically distributed random variables [O'Connor and Eichinger, 2007, OBrien *et al.*, 2014, Leahy *et al.*, 2015, OBrien *et al.*, 2015, Tabatabai *et al.*, 2017]. However most physical phenomena with data collected as time series show some dependence. The extreme value of dependent time series has been applied widely in hydrology and climate studies. The most commonly addressed dependence arising from clustering of correlated events is addressed by careful choice of block size or threshold [Coles, 2001]. This ensures that the obtained block maxima or threshold exceedance are independent. However, for bridge load effects there is an additional dependence that can arise during traffic events where multiple trucks may have correlated weights. The loads in multiple truck occurrences are may be correlated due to similarities in loads of trucks

from same operator or truck axle configurations. In formulating highway bridge live model for the LRFD, Nowak and Hong [1991] assumed that every 50th truck was followed by another truck whose load was partially correlated and that every 100th truck was followed by another truck whose weight was fully correlated. The occurrence of multiple trucks with correlated loads has been shown to be a critical loading condition for negative moments in 2 span continuous bridges [Nowak and Hong, 1991]. Sivakumar and Ghosn [2012] reports that 6.7% traffic events from WIM data in the United States are multiple truck events and 3.3% of those multiple truck events have completely correlated weights. It has been shown that under given conditions such as stationarity and weak dependence, the extreme values converge to either Frechet, Gumbel and Weibull distributions [Coles, 2001].

This study presents assessment traffic static loads based on weigh-in-motion data over a period of one year from the South African iron ore heavy haul line. A comparison of extreme value load effects normalised to the South African Transport Services [1983] bridge code load effects is made. The generated traffic based on assumption of independent and identically distributed random wagon loads as well was weakly dependent wagon loads is passed on selected influence lines for single span and 2 span continuous bridges. Extreme load effects based on assumption of stationarity in traffic volume and composition are obtained for remaining life of 50 years and return period of 100 years.

8.2 Chapter Objectives

The objective of this chapter is obtain load effects for beam-type bridges on heavy-haul railway line that account for traffic volume growth and axle dependencies. The first contribution of this study is to examine the sensitivity of heavy-haul traffic volume growth on return levels of load effects on beam-type bridges. The second contribution is an investigation of effect of axle load dependencies on return levels of loads on heavy-hail rail line.

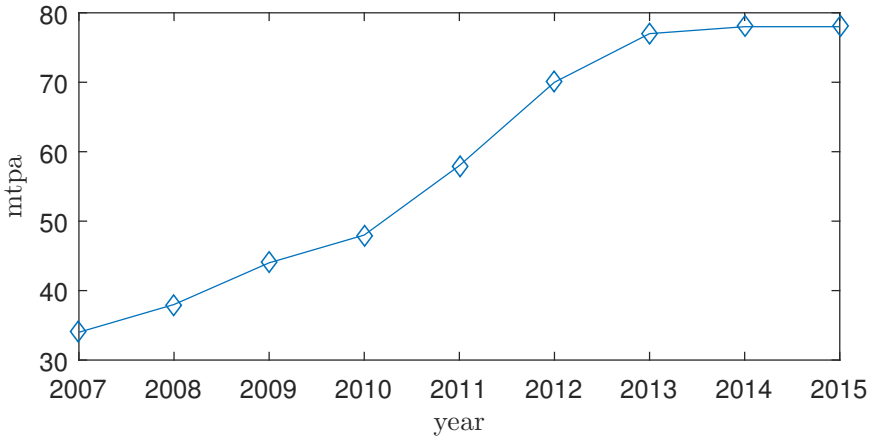

Figure 8.1: Annual freight in million tonnes per annum (mtpa)

8.3 South African Iron Ore Traffic

During the 40 years of operation of the Iron Ore freight line, there have been changes in traffic volumes and axle loads brought about by the increased demand for Iron Ore and advances in locomotive technology. The total tonnage hauled per year from 2007 to 2015 in Fig 8.1 shows the volume increase twofold. However when the whole operation period is considered, there has been a four fold increase in volume with an average increase of 4% per annum. The increase in freight tonnage has been achieved through an increase in the year 2000 of axle loads from 26 tonnes to 30 tonnes per axle, introduction of longer trains and an increase average daily freight traffic. However, this analysis of effects of growth will only consider increase in number of trains [Kuys, 2009, Hewson *et al.*, 2017]. Increases in axle loads result in a step change in axle loading data and is only instituted after careful studies on the capacity of other existing rail infrastructure.

8.3.1 Stationarity in axle loads

The time series of the iron ore train axle load obtained over a period from January 2016 to August 2016 is shown in Fig 8.4 and 8.3. In developing the loading model for the simulated train traffic, the stationarity and dependence structure of axle load time series is investigated. Stationarity is important for the limit distributions in presented in Chapter 7 to hold. A series $X_1, X_2, ...$ of random variables is said

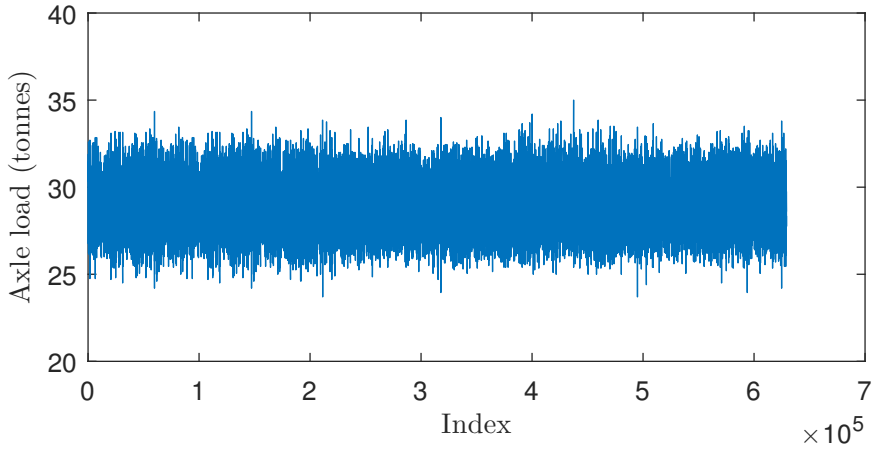

Figure 8.2: Axle loads from January 2016 to September 2016

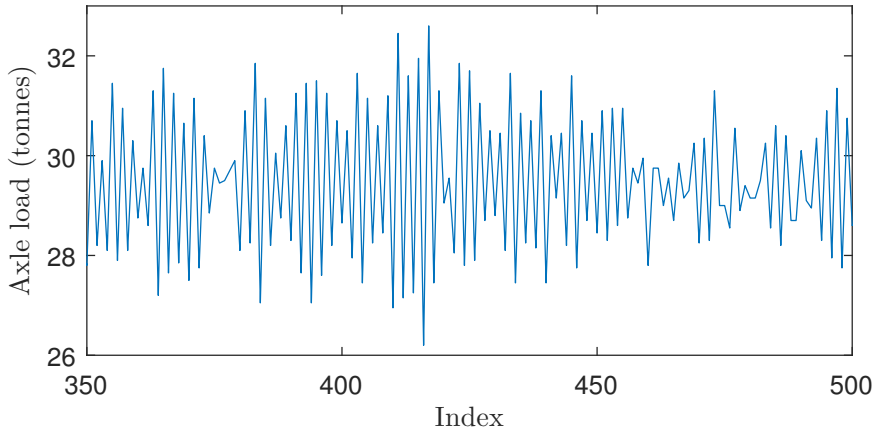

Figure 8.3: Axle load time series structure

to be strictly stationary if it satisfies the two conditions below [Galambos, 1978]:

1. $P(X_j < x) = F(x)$ for each j.

2. For any positive integer s; $F_{i(k)}(x_1, x_2, ..., x_k) = F_{i(k)+s}(x_1, x_2, ..., x_k)$.

The above conditions imply that the properties of the series are not affected by changes in time. In general, time series need not be strictly stationary for limit laws to be applied. For weakly stationarity condition, the mean and variance must be constant [Mills, 2015]. A visual assessment of plotted axle loads in Fig 8.4 shows no sign of trends in the mean value.

The traffic load simulation is done on the basis of stationarity in axle loads with growth in haulage volumes arising from increase in number of trains. The current volume of 8 trains per day increases to 57 trains per day in line with the observed

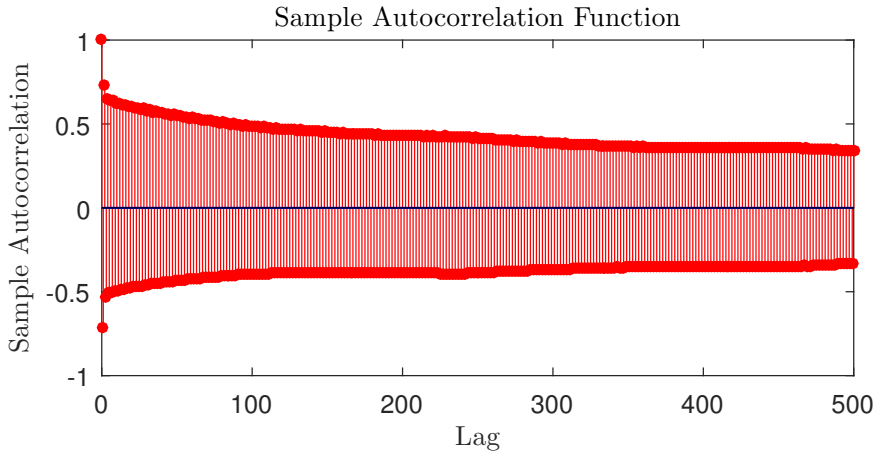

Figure 8.4: Autocorrelation of axle loads

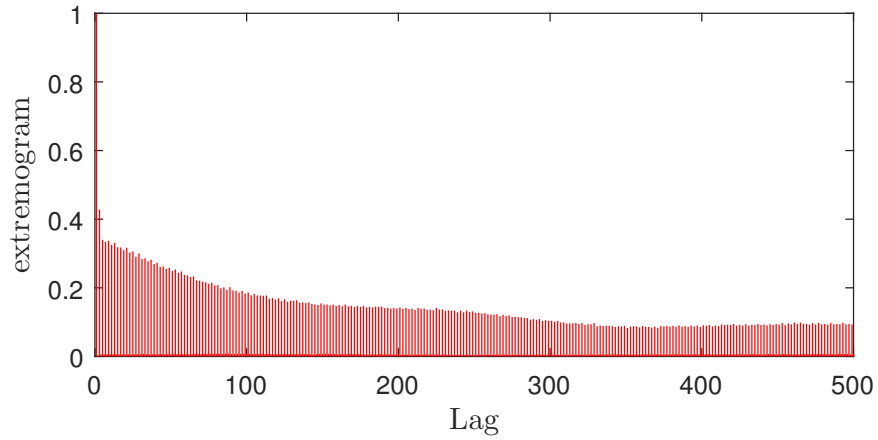

Figure 8.5: extremogram of axle loads

historical increase of 4% per annum. The feasibility of such an increase for the remaining life of bridges is not considered. Stationarity in time series is assessed through root tests based on autoregressive or moving average polynomials where a root equal to unity suggests that the data series is not stationary [Mills, 2015]. The unit root tests that include augmented Dickey-Fuller test and the Phillips-Perron test packages in R were applied to the dataset comprising of 8 months time series of axle loads data of loaded trains [Trapletti and Hornik, 2017]. These tests showed the axle loads to be stationary.

8.3.2 Dependence in axle loads

Autoregressive (AR) models are widely used to model correlated data in a time series analysis. The AR model is adopted as there is no need for differencing

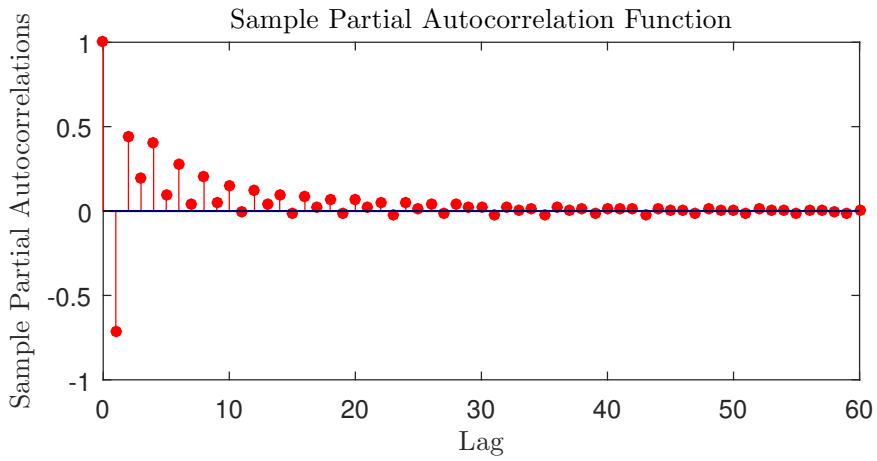

Figure 8.6: Partial correlation of axle loads

operations to convert the series to a stationary one. Autoregressive models arise when a realisation of a value in a time series depends on previous realisations. The cause of dependence in this case can be explained since axles that comprise a bogey for a wagon give rise to values that are not entirely independent from each other. The axles for a particular wagon will have loads that have some relation and so too are the axle loads for adjacent wagons. The relation between axles is best shown by the autocorrelation and partial autocorrelation plots at different lags as shown in Fig 8.4.

The general AR(m) model is written as:

$$x_t = a_t + \sum_{n=1}^{m} \phi_n x_{t-n} \tag{8.1}$$

where x_{t-n} is the realisation at lag n while $\phi_(n)$ and a_t are constants. The axle load data was fitted to an autoregressive model using $Matlab$ with the resulting model having the equation 8.2

$$x_t = 12.2164 + -0.6062x_{t-1} + 0.2669x_{t-2} + 0.3605x_{t-3} + 0.4588x_{t-4} \\ +0.0986x_{t-5} + N(0, 0.3422) \tag{8.2}$$

The order of the AR model is determined from the plot partial correlation in plot 8.6. The autocorrelation between axle loads during multiple truck events does

not give a good measure of dependence of extreme axle loads which is dependence between events in the tail of the distribution. Davis *et al.* [2013] propose a different measure for dependence in the tail region as given in equation 8.3:

$$\gamma_{AB}(h) = \lim_{n\to\infty} n\text{cov}\Big(\boldsymbol{I}_{\{a_n^{-1}X_0\in A\}}, \boldsymbol{I}_{\{a_n^{-1}X_h\in B\}}\Big) \quad , h \geq 0. \tag{8.3}$$

where (a_n is a sequence of normalising constants, A, B are fixed bounded sets and $X_0 \in a_n A$ and $X_h \in a_n B$ are extreme events which are h lags apart. Equation 8.3 is implemented in an R package and a plot of axle load data is shown in Fig 8.5. The upper tail dependence in axle loads is weak as observed in the extremogram plot.

8.4 Extreme value prediction

Extreme value theory has been applied in determining design loads in form of return levels and frequency of occurrence in terms of return periods in structural engineering applications. The classical asymptotic theory of extreme values is discussed in terms of independent and identically distributed random variables and applications to dependent series.

8.4.1 Non stationary GEV traffic loads

The general block maxima method has been described in Chapters 7 and 2 where it was applied through fitting to GEV through the maximum likelihood method of parameter estimate or the Bayesian inference and also by extrapolation on normal distribution paper. The theoretical framework to accommodate the non stationarity and dependence is presented here. The non stationarity considered here refers to changes in traffic volumes and not axle loads.

In the stationary case, the limiting non degenerate distribution if it exists converges to either Frechet, Gumbel or Weibull distributions. The Gumbel, Weibull and Frechet type distributions can be combined into the Generalised Extreme Value (GEV) distribution:

$$G(x;\theta) = \begin{cases} \exp\left(-\left(1+\xi\dfrac{x-\mu}{\sigma}\right)^{\frac{-1}{\xi}}\right) & \text{if } \xi \neq 0 \\ \exp\Big(-\exp\big(-\dfrac{x-\mu}{\sigma}\big)\Big) & \text{if } \xi = 0 \end{cases} \tag{8.4}$$

where μ, σ and ξ are the location, scale and shape parameters of the distribution given as constants. In the non stationary case, the traffic volume changes within a block are negligible while the traffic volume changes between blocks is significant. The GEV for non stationary case is thus given as:

$$G(x:\theta(t)) = \begin{cases} \exp\left(-\left(1+\xi(t)\frac{x-\mu(t)}{\sigma(t)}\right)^{\frac{-1}{\xi(t)}}\right) & \text{if } \xi(t) \neq 0 \\ \exp\left(-\exp\left(-\frac{x-\mu(t)}{\sigma(t)}\right)\right) & \text{if } \xi(t) = 0 \end{cases} \tag{8.5}$$

where $\mu(t), \sigma(t)$ and $\xi(t)$ are linearly varying with time as given below:

$\mu(t) = \mu_0 + \alpha_\mu(t)$

$\sigma(t) = \sigma_0 + \alpha_\sigma(t)$

$\xi(t) = \xi_0 + \alpha_\xi(t)$

The fundamental equation for the extreme distribution of based on block data of a stationary distribution can readily be extended to the non stationary case as shown in equation 8.6:

$$F_W = P(W \geq x) = \prod_{i=1}^{n} F(x:\theta(t)) \text{ for non stationary distribution } F(x:\theta(t)) \tag{8.6}$$

8.4.2 Extremes for dependent series

The asymptotic theory developed for independent and identically distributed random variables can be applied to time series with some dependence provided conditions such as strong mixing, condition $D(u)$ and m-dependence are satisfied. The strong mixing condition for a sequence X_n is satisfied if [Castillo, 1988]:

$$|P(A \cap B) - P(A)P(B)| \xrightarrow{j\to\infty} 0 \tag{8.7}$$

where A is event generated by $(X_1, X_2, ..., X_n)$ and B is generated by $(X_{n+j}, X_{n+j+1}, ...)$ for any value of n. The condition $D(u)$ follows from the strong mixing condition and is given as presented in De Haan and Ana [2007].

Let l and p be positive integers. For any random vector $X_1, ..., X_p$ with joint distribution $F_{1,...,p}$, the condition $D(u_n)$ is said to hold if for any integers

$1_1 < .... < i_p < j_1 < .... < j_p \leq n$ for which $j_1 - i_p \leq l$ we have

$$|F_{i_1,...,i_p,j_1,...,j_p}(u_n) - F_{i_1,...,i_p}(u_n)F_{j_1,...,j_p}(u_n)| \leq x_{n,l} \tag{8.8}$$

where $x_{n,l} \to 0, n \to \infty$ for some sequence $l = l_n = o(n)$.

The autoregressive models of finite order satisfy the strong mixing condition and the condition $D(u_n$ and thus realisations from generated time series can be treated with the asymptotic theory of extremes for independent variables. This conclusion is given in theorem below [Castillo, 1988]:

Theorem 2. *Let X_N be a stationary sequence and let $\{a_n\}$ and $\{b_n\}$ be two sequences of real numbers such that:*

$$\lim_{n\to\infty} P[X_{n:n} \leq a_n + b_n x] = G(x)$$

If a sequence $\{u_n = a_n + b_n x\}$ satisfies the $D(u_n)$ for each x, then $G(x)$ is one of the three limit distributions for the independent case.

Bhattacharya [2008] has shown that the distribution of maxima under the iid assumption is to the right of the distribution of maxima of a stationary dependent process. More formally, for a sufficiently high threshold u_n where n is finite number of samples, M_n and $\tilde{M}_n$ are maxima for iid and stationary dependent sequences respectively:

$$P[M_n \leq u_n] > P[\tilde{M}_n \leq u_n] \tag{8.9}$$

for every u_n such that $0 < F(u_n) < 1$; and in the limit:

$$\tilde{G}(a + bx) > G(a + bx), \quad 0 < \theta < 1 \tag{8.10}$$

where $\tilde{G}$, G are cumulative distribution functions for stationary dependent and iid case respectively, a, b are normalising constants and θ is extremal index defined as the reciprocal of the mean limiting cluster size above a threshold. From equation 8.10, the assumption of independent and identically distributed variable is a conservative estimate.

8.5 Simulation procedure

The study progresses from the case where axle loads are independent and identically distributed to where some correlation in the wagon axle loads is introduced. The independent axle case is case is simulated using a normal random generator while for the dependent case, the WIM-WIM data is fitted to an autoregressive model of order 5 on the basis of equation 8.2. The AR5 model is able to account for correlation between the 4 wagon axles and an additional axle on the adjacent wagon. Simulated trains are then generated using both methods assuming no growth in traffic and passed on the selected bridge influence lines to obtain the load effects. The technique for computing load effects is based on the same procedure. For a remaining service life of 50 years used in this study, the return periods are obtained corresponding to 1000 year level. Thereafter growth in traffic volumes from 56 trains per week to 398 trains per week in the 50th year is generated for the dependent and independent cases.

8.6 Load effects study

The results of effects of axle load dependence and the effects of traffic growth on assessment loads is investigated here. The effects of dependence and growth are investigated separately and finally coupled for a more realistic assessment load as presented in the sections that follow.

8.6.1 Effects of weak dependence

The weekly maximum load effects for a single simply supported beam and a two span continuous beam are shown in Figs 8.7-8.8. A comparison of shear and moments show that a fitted GEV load effects from weak dependant axle loads leads to a shift in the location parameter μ resulting in reductions in extrapolated loads. The shape factor changes for selected load effects such as the mid span moment for single span beam shown in Fig 8.7. The weak dependant axle load case shows a shift from Gumbel type to Weibull type distribution for the simply supported mid span bending moments effects. However the shape factor shift

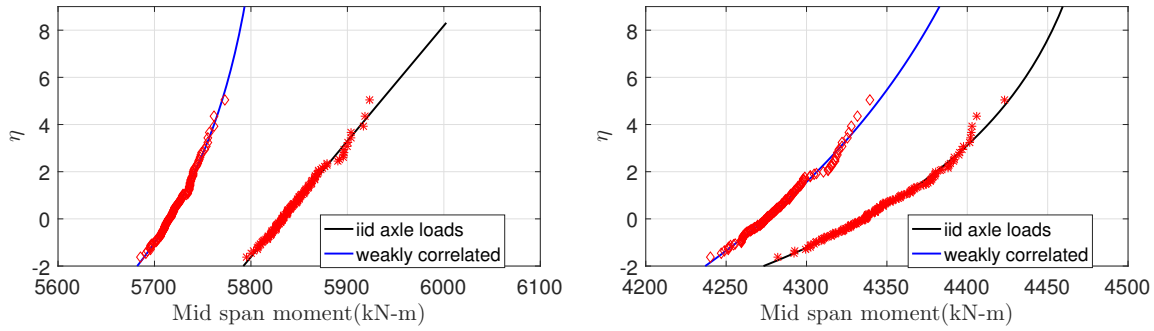

a1:Simply supported a2: Two span beam

Figure 8.7: Comparison of midspan moment (20m span length)

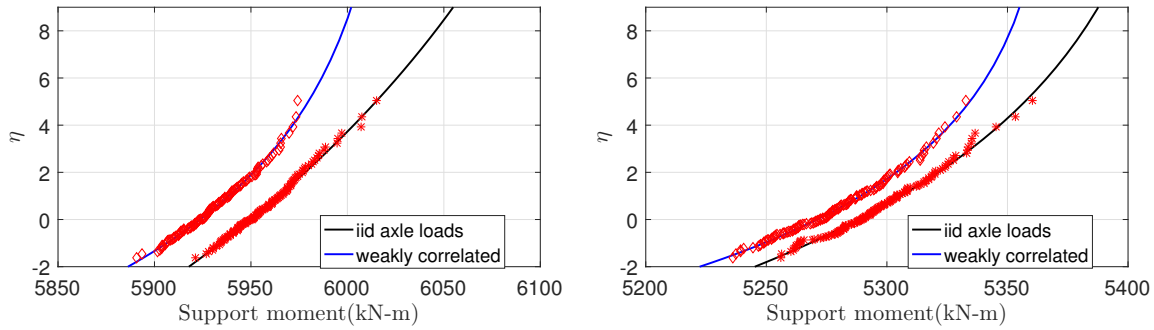

a2: Two span beam a2: Four span beam

Figure 8.8: Comparison of support moment (20m span length)

observation is not of a general nature across different spans, load effects or beam types as shown in additional plots in appendices.

The simulated load effects for independent and identically distributed (iid) and the autoregressive (AR) cases for span length ranges from 5m to 50m and normalised by SATS 1983 load effects are presented in Figs 8.9 to 8.10. The average daily train load effects based on average train axle loads are also presented for comparison. The normalised average daily load effects show the conservatism in SATS 1983 NR load model as shown in the deterministic study. The normalised load effects are higher for bridge length less than 10m for mid span moments and support shear. The lowest effects are observed between 10 and 15m span length for load effects with the exception of interior support span moments. The general pattern observed in the figures shows that the load effects for dependent axle loads are less than that obtained from trains with independent axle loads and the difference

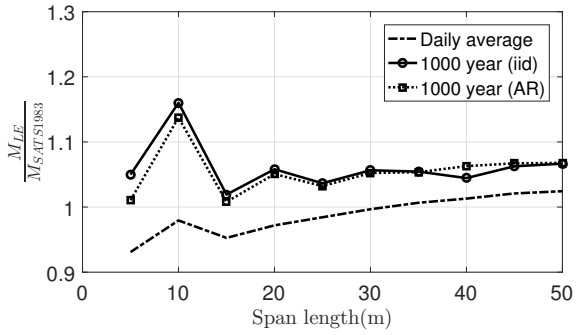

a1:Two span

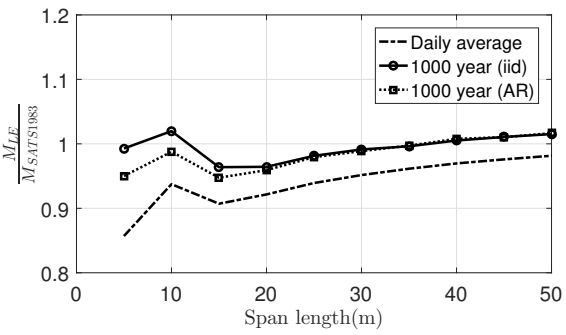

a2: Four span beam

Figure 8.9: Factored support moment

is particularly pronounced at shorter span lengths.

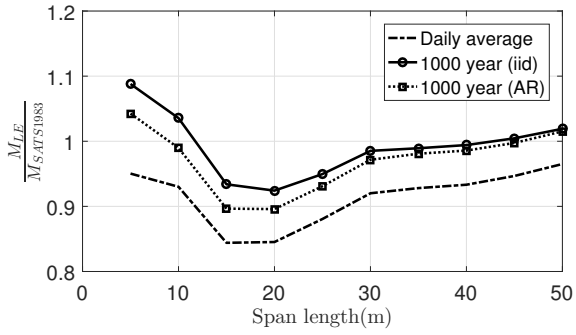

a1:Simply supported

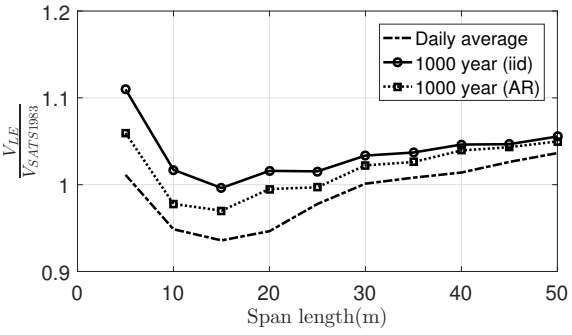

b1:Support shear

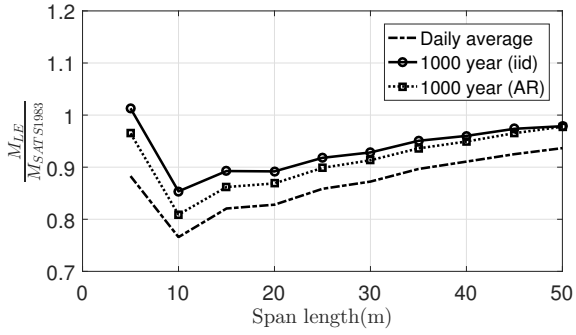

a2:Two span

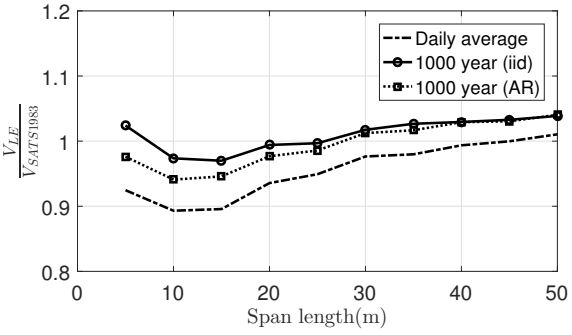

b2:Two span

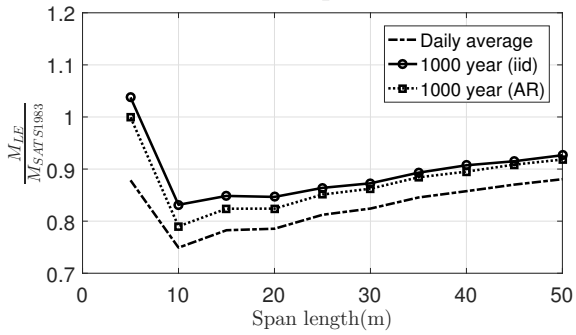

a3:Four span

Figure 8.10: Factored mid-span moment

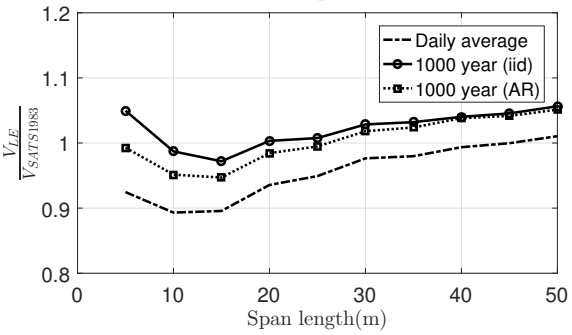

b3:Four span

Figure 8.11: Factored support shear

The assessment loads effects at 1000 years levels for iid case on simply supported beams are within a factor of 1.12 of SATS NR at a span length of 5m while the normalised loads are much less at longer spans. The extrapolated 1000 year load effects levels for both AR and IID case converge at 50m length. The difference between the daily and 1000 year shear effects reduces with increasing span lengths as the distributed load from the axles approaches the mean value. The trends observed for simply supported beams across span length for the simply supported beam case is replicated for the 2 span and 4 span continuous beam load effects of mid span bending moment and first interior support shear.

The interior support moments for 2 span and 4 span continuous beams give a critical loading envelop for all the load cases considered, with the normalised factor of 1.15 as in previous chapter. There is convergence between the iid and AR cases from span length of 20m with only marginal differences at shorter spans. The critical maximum support moment occurs at span length of 10m and this corresponds with the wagon length.

8.6.2 Effects of traffic volume growth

The effects of traffic growth on assessment loads is investigated based on iid generated axle loads with train traffic growth at 4% per annum. In the case of stationary traffic volume (0% traffic volume growth) the computations for characteristic and assessment load were based on return period of 50 years and 1000 years respectively. However, the case of non stationary traffic volume requires the remaining service life to be defined. The service life for a new bridge is set between 75 years and 120 years depending on design code applied. The remaining life on the other hand takes into account the time that the structure has been in operation and the design service life. The analysis in this section assumes a remaining life of 50 years. Thus the traffic volume is incremented at 4% from 56 trains per week to a total 398 trains per week in the 50th year. The desired safety level is set in the return period which extrapolates the effects after 50 years of traffic increase to the 1000 year return level.

Traffic growth results in changes in distribution parameters over time as shown in Fig 8.12. The variation of GEV parameters for weekly maximum moment and shear of a 5m simply supported beam is shown in Fig 8.13. Growth has the overall linear increase of the location parameter μ over time and this is expected to increase the 1000 year load effects. The shift in location parameter is observed for both shear and moment load effects and across different beam types as shown in Figs 8.13 and Fig 8.14.

There is a general linear decrease in scale parameter σ over time as a result of traffic growth with the exception observed in the shear load effects of a 5m span beam shown in Fig 8.14. The scale parameter for the 2 span beam of span length of 5m does not show any particular trend and no attempt was made to fit a higher order polynomial to the data. The shape parameter ξ does not show a general trend with time. Although the shape parameter does not give a general trend cross span lengths, beam types and load effects, there is no physical explanation to allow a distribution change from either Weibull and Gumbel types to Frechet type distribution as observed in Fig 8.14.

The return levels of load effects is computed from equation 7.2 and 8.6 for the stationary and non stationary cases having fitted the block data using the Maximum Likelihood or Bayesian methods described in Chapter 7. The GEV parameters μ and σ were treated as non stationary linear functions while the shape parameter ξ taken as stationary. The current weekly traffic volume of 56 trains is used as the lower bound while the traffic growth of 4% to a total of 397 trains in the 50th year is provided as an upper bound case. A typical plot of mid span bending moment for a 30m span simply supported beam is shown on Gumbel paper in Fig 8.15.

The comparison of load effects for stationary and non stationary traffic for selected shear and support bending moments is summarised in Table 8.1. The effects of traffic volume growth on heavy haul has a negligible effect on assessment loads with an increase under 1%. This is consistent with the modest

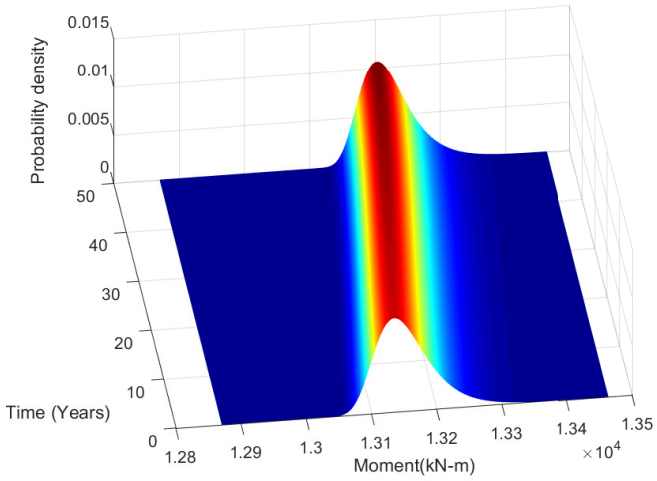

Figure 8.12: Traffic growth GEV pdf for simply supported beam

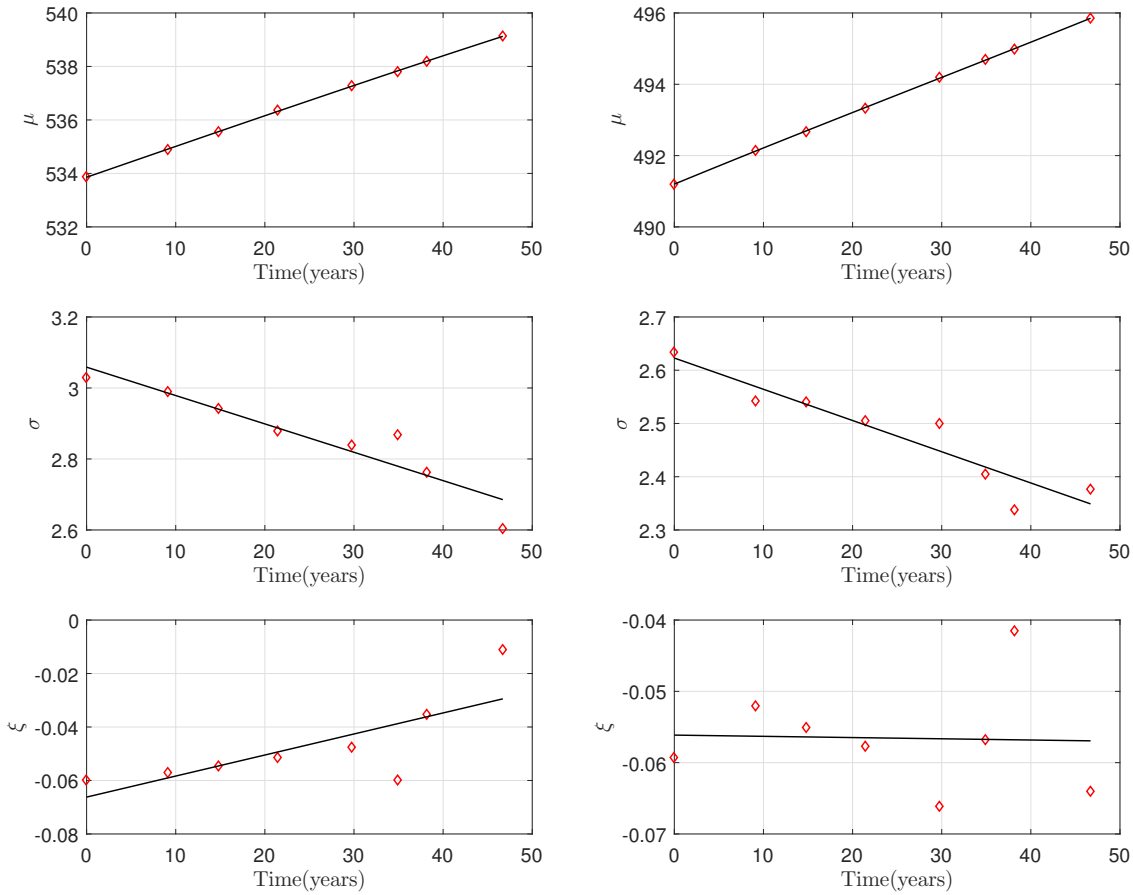

Mid span moment Support shear

Figure 8.13: Changes in GEV parameters for 5m long simply supported beam at 4% annual traffic growth

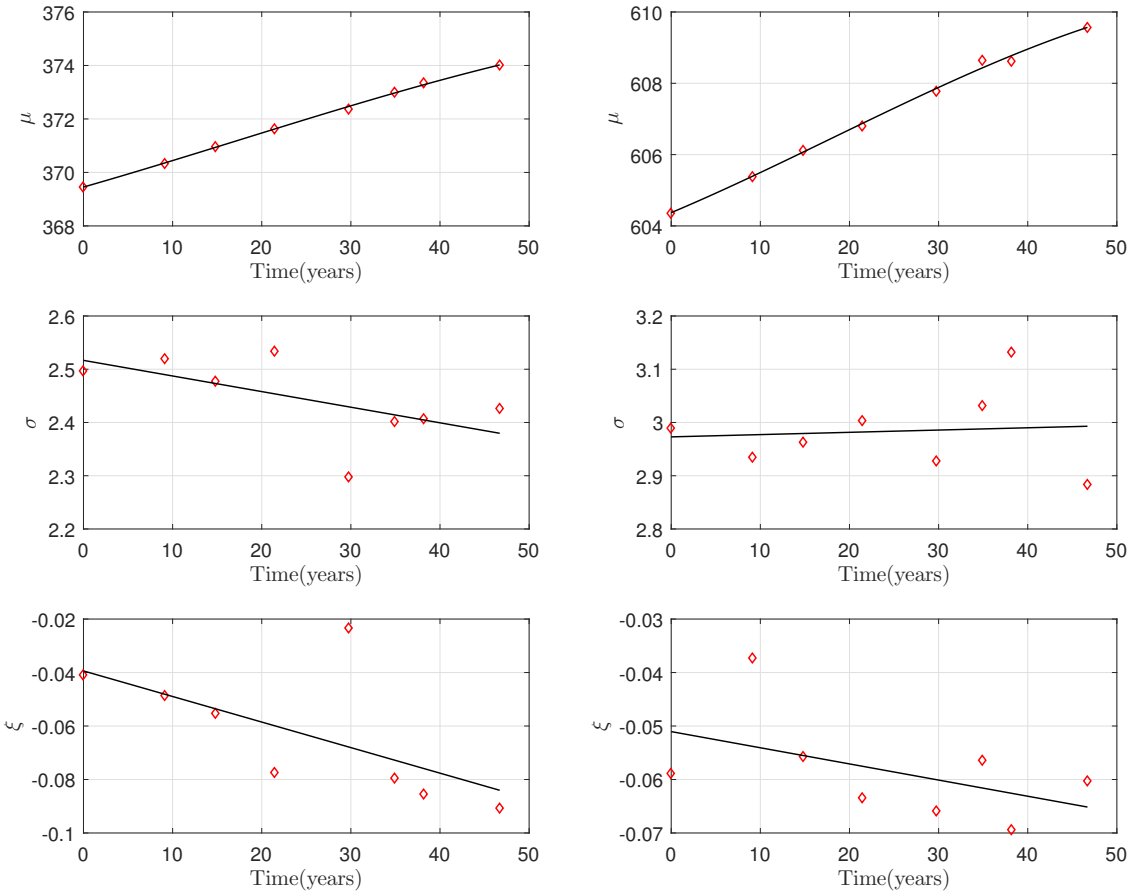

Figure 8.14: Changes in GEV parameters for 5m long 2 span beam at 4% annual traffic growth

increases in location parameter over time of less than 1 % for all the cases considered. Additional tables for traffic growth are presented in appendices.

8.6.3 Combined effects of traffic volume growth and axle dependence

The analysis of the GEV parameters show that the assessment loads for evaluating moments and shear of beam type bridges on the Iron Ore line are more sensitive to the effects of axle dependence than increases in traffic volumes of the current long train configuration. The axle dependence effects are more pronounced at short spans and the effects become negligible at span length above 20m. Traffic increases of about 4 % of the current volume only result in a maximum of 0.7% increase in load effects. The upper bound curve showing 397 trains per week over the whole service life shows a marginal increase in traffic.

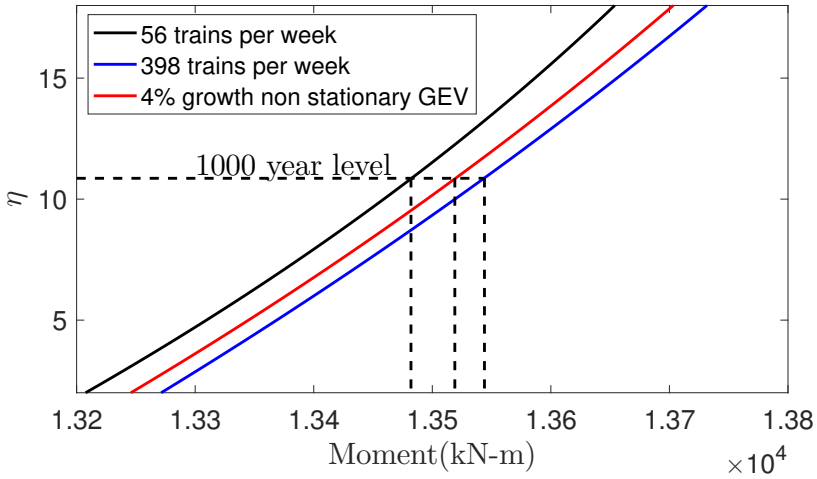

Figure 8.15: Comparison for stationary and non stationary GEV for simple 30m span beam moment

Table 8.1: Comparison of stationary and non stationary and 1000 year level load effects

Span (m)	Simply supported beam Mid-span moment(kN-m)			2-span continuous Mid-span moment(kN-m)		
	0% Growth	4% Growth	diff(%)	0% Growth	4% Growth	diff(%)
5	560	562	0.3	392	394	0.6
10	1946	1959	0.7	1223	1224	0.0
15	3615	3624	0.2	2680	2690	0.4
20	6021	6036	0.2	4515	4534	0.4
25	9337	9343	0.1	6936	6936	0.0
30	13460	13496	0.3	9797	9807	0.1
35	17881	17891	0.1	13260	13296	0.3
40	23145	23178	0.1	17054	17075	0.1
45	29150	29222	0.2	21615	21667	0.2
50	36050	36110	0.2	26651	26661	0.0

8.7 Concluding remarks

Assessment loads were generated based on WIM data while considering the internal time series structure and growth estimated from available records. While haulage volumes can increase as a result of changes to permitted maximum axle loads, this study focussed on the effects of increasing traffic volume on assessment loads. The axle dependence was modelled by autoregressive series and traffic growth through non stationary *GEV* parameters. Assessment loads for the heavy haul have been shown to be more

sensitive to the weak dependence than to traffic growth over the remaining service life of 50 years. The increase in return levels of load effects is less than 1% for traffic volume growth of 4% over a period of 50 years in contrast to the much higher values between 6% and 9% reported on highway bridges for 3% traffic volume growth over 40 year period. Assessment loads that account for some wagon axle dependence have lower return values of load effects than loads effects where axle loads are independent which is consistent with theory.

References

Galambos J., *The Asymptotic Theory of Extreme Order Statistics*, John Wiley Sons, New York, 1 edition, 1978.

South African Transport Services, "Bridge code," 1983.

Castillo E., *Extreme Value Theory in Engineering*, Academic Press, Inc, London, 1 edition, 1988.

Nowak A.S. and Hong Y.K., "Bridge live-load models," *Journal of Structural Engineering*, 117(9); 2757–2767, 1991.

Nowak A.S., Nassif H. and DeFrain L., "Effect of truck loads on bridges," *Journal of transportation engineering*, 119(6); 853–867, 1993.

Coles S., *An Introduction to Statistical Modeling of Extreme Values*, Springer-Verlag, London, 2001.

De Haan L. and Ana F., *Extreme Value Theory: An introduction*, Springe Science & Business Media, 2007.

Getachew A. and Obrien E.J., "Simplified site-specific traffic load models for bridge assessment," *Structure and Infrastructure Engineering: Maintenance, Management, Life-Cycle Design and Performance*, 3(4); 303–311, 2007.

O'Connor A. and Eichinger E.M., "Site-specific traffic load modelling for bridge assessment," *Proceedings of The Institution of Civil Engineers-Bridge Engineering*, 160; 185–194, 2007.

Bhattacharya B., "The extremal index and the maximum of a dependent stationary

pulse load process observed above a high threshold," *Structural Safety*, 30(1); 34–48, 2008.

Kuys, "Ore Line Capacity Expansion: Conceptual Design of the Railway Line to Increase Capacity," *International Haevy Haul Conference Proceedings*, 2009.

Sivakumar B. and Ghosn M., "Collecting and using Weigh-in-Motion data in LRFD bridge design," *Bridge Structures: Assessment, Design and Construction*, 5(4); 151–158, 2012.

Davis R.A., Mikosch T. and Zhao Y., "Measures of serial extremal dependence and their estimation," *Stochastic Processes and their applications*, 123(7); 2575–2602, 2013.

OBrien E.J., Bordallo-Ruiz A. and Enright B., "Lifetime maximum load effects on short-span bridges subject to growing traffic volumes," *Structural Safety*, 50; 113–122, 2014.

Leahy C., OBrien E.J., Enright B. and Hajializadeh D., "Review of HL-93 Bridge Traffic Load Model Using an Extensive WIM Database," *Journal of Bridge Engineering*, 20(10); 04014115, 2015.

OBrien E.J., Schmidt F., Hajializadeh D., Zhou X.Y., Enright B., Caprani C.C., Wilson S. and Sheils E., "A review of probabilistic methods of assessment of load effects in bridges," *Structural safety*, 53; 44–56, 2015.

Mills T.C., *Time Series Econometrics: A Concise Introduction*, Palgrave texts in econometrics, Palgrave Macmillan, 2015.

Leahy C., OBrien E. and O'Connor A., "The effect of traffic growth on characteristic bridge load effects," *Transportation Research Procedia*, 14; 3990–3999, 2016.

Hewson D.J., Gräbe P.J. and Shaw F.J., "Ore line capacity expansion: Conceptual design of the railway line to increase capacity," in "Proc. 11th IHHA Conf," 472–479, 2017.

Trapletti A. and Hornik K., "tseries: Time series analysis and computational finance," *Structural safety*, 2017, r package version 0.10-42.

URL `https://CRAN.R-project.org/package=tseries`

Tabatabai H., Titi H. and Zhao J., "WIM-based assessment of load effects on

bridges due to various classes of heavy trucks," *Engineering Structures*, 140; 189–198, 2017.

Chapter 9

CONCLUSIONS AND RECOMMENDATIONS

9.1 Introduction

The work in this thesis focuses on live loads for beam-type bridges on heavy-haul lines with particular emphasis on South Africa iron ore line. The study considers the mid span moments for single span simple supported beams, 2 span simply supported and 4 span simply supported continuous beams. In addition, the study considered shear at support and first interior support for continuous beam-type bridges subjected to South African heavy-haul loads. The main aims of this research are restated as:

1. Investigate through analytical methods and field measurements the frequency-time evolution of beam type bridges on heavy haul line arising from passage heavy axle train loads.

2. Investigate through analytical methods and field measurements the dynamic amplification factor of beam type bridges on heavy haul line arising from passage heavy axle train loads moving at constant and varying speeds.

3. Carry out a deterministic study of load effects from heavy-haul wagon axles and identify potential load effects and span lengths where the South African Railway live load model is exceeded for beam type bridges.

4. Carry out a probabilistic study of load effects from heavy-haul wagon axles

and identify potential load effects and span lengths where the South African Railway live load model is exceeded for beam type bridges.

5. Carry out a probabilistic study of bridge load effects from heavy-haul wagon axles taking into account traffic volume growth and spatial dependence in axle loads.

In order to achieve the objectives above, a combination of analytical and field studies were undertaken. An approximate method for frequency-time evolution for moving mass systems on continuous multi-span bridges was derived and implemented in Matlab. In order to investigate the dynamic amplification factors for beam-type bridges subjected to trains with high linear train to bridge mass ratios, a modified moving load method was implemented which accounted for the reductions in combined train-bridge system. A deterministic analysis was done on basis of maximum wagon design capacity and the load effects obtained from passing the simulated loads on relevant influence lines. Analytical models that account for random nature of axle loads were used to study the load effects. Finally the effects of growth in traffic volumes and axle load spatial dependence were considered in computing load effects.

The field study was limited to the Olifants River Bridge which is a continuous prestressed box girder bridge. The bridge is instrumented with strain gauges, accelerometers, crack meters and thermocouples. The field study focussed on measured accelerations and strains. The frequency-time evolution during train passage was obtained using spectrogram function in Matlab as well as using the Complimentary Empirical Ensemble Mode Decomposition technique in order to obtain the evolution of fundamental flexural frequency. The strain measurements were used to compute dynamic amplification factors for both loaded and unloaded trains. The deterministic and probabilistic analysis of static load effects was carried out using data from a weigh-in-motion system currently installed on the bridge and managed by the railway operator.

9.2 Research findings

In relation to the objectives listed above, the analytical and field investigation of live loads on heavy-haul made a number of findings in relation to bridge dynamic response and static live load effects. The reduction of bridge frequency bridge under heavy loads is an important aspect for consideration for bridges on heavy-haul railway lines. A simplified 2 dimensional beam model with moving masses can be used to give an estimate within 12% of the estimate from field vibration measurements of continuous beams. The approximate formula from analytical method considered a continuous span with an approximate formula giving a 26% reduction in fundamental frequency from 4.09Hz to 3.03Hz. On the other hand estimates from field vibration measurements showed reduction of 16% reduction to 3.45Hz. The approximate formula underestimates the frequency as the stiffening contribution from train suspension system is ignored in a moving mass approximation.

Dynamic amplification factors for a continuous 11 span bridge are computed based on an analytical procedure using moving force idealization while accounting for frequency reductions induced by loaded trains. The analytical procedure shows that the dynamic amplification induced by loaded trains is higher in the inner span 20 than the end span 23. However, the moments are more critical in the end span where the dynamic amplification is less than 4% while in span 20 the amplification considerably greater at 15% at resonance speeds. The computed amplification factors within the imposed speed limits on the bridge are 1% for end span and 5% for inner span 20. The amplification factors obtained from field strain measurements on an 11 span bridge where much higher with maximum of 12% for midspan strain based factors in contrast with 5% from analytical method for loaded trains. The dynamic amplifications are higher for heavily loaded trains than empty trains with maximum values obtained within the speed range from 50km/h to 60km/h. The increased train-bridge mass ratio results in a greater reduction of the critical sub-resonance velocity for loaded trains in comparison to empty trains.

The changes in train speed during bridge crossing does not significantly affect dynamic amplification factors. However, it was observed that maximum dynamic amplifications from midspan strain measurements were obtained for speed change magnitudes between 10km/h to 15km/h in contrast with amplification factors for support section which had maximum values for changes in speed between 5km/h and 10km/h.

A deterministic study of static load effects shows that South African Transport Services [1983] live model is unconservative for shear for simply supported beams of lengths below 8m and above 30m. The current heavy-haul traffic induces greater mid span moments in single span beams with span lengths between 5m and 50m while the support moments for 2 span beam type bridges are generally unconservative except for span lengths between 4m and 7m. In general, South African Transport Services [1983] live load model gives lower load effects for shorter spans where the individual axles are dominant as these have loads higher than the point loads provided in the design code. However, the probabilistic study shows that design load effects obtained from trains for a 1000 year return period are greater than the loads from SATS 1983 NR loading by a factor of 1.15 which is much less than the specified design live load factor of 1.6 for load combinations specified in South African Transport Services [1983]. The dominant load effects for assessment are shear at spans less than 5m and interior support moments at span length of 10m.

Different extrapolation techniques were used to obtain load effects from the same block maxima data. It was shown that the normal, GEV and Bayesian extrapolation methods give load effects within 1% of each other with the normal extrapolation being marginally on the lower end. This observation holds across beam types and span lengths from 5m to 50m. Although the GEV allows for all the three extreme type distributions, an analysis based on available weigh-in-motion data of axle weights show that the fitted distributions using Bayesian and Maximum Likelihood Estimate for all load effects for the span ranges are all Weibull type. On the other hand it is known that the domain of

attraction for the normal distribution is Gumbel type. The study also found that extrapolated loads effects are less sensitive to increase in return period beyond 50 years. This aspect is significant as return period is a measure of safety target when determining design values for loads.

The study investigated the impact of traffic volume increase and wagon axle load dependencies. The load effects on heavy-haul were shown to be more sensitive to the weak dependence than to traffic growth over the remaining service life of 50 years. The increase in return levels of load effects is less than 1% for traffic volume growth of 4% over a period of 50 years in contrast to the much higher values between 6% and 9% reported on highway bridges for 3% traffic volume growth over 40 year period. Assessment loads that account for some wagon axle dependence have lower return values of load effects than the assume that axle loads are independent which is consistent with theory.

9.3 Recommendations for further work

A number of areas that require further field study are frequency reductions on single span, 2 span and 4 span bridges on heavy haul in order check validity of approximate formulae and provide a point for comparison for analytical work. The influence of wagon suspension stiffness on frequency reductions should be verified through field measurements. Field measurements of amplification factors should be carried out on short to medium span bridges of various structural forms on heavy-haul line. The amplification factor study should identify the contribution of rail irregularity, wheel irregularity and a decomposition of dynamic amplification factors into local and global amplification factors.

In addition, the influence of train accelerations and decelerations should be investigated for other bridge types and span lengths. Finally a detailed reliability analysis of typical bridges on heavy haul should be undertaken that includes use of non-destructive tests and health monitoring data for model updating.

References

South African Transport Services, “Bridge code,” 1983.

Appendices

Appendix A

DYNAMIC AMPLIFICATION FACTORS

A.1 Bridge natural frequencies

Table A.1 gives the computed bridge natural frequencies for the first 4 frequency cluster.

Table A.1: Natural frequencies for 11 span continuous bridge

Mode	Non-dimensionalised Freq Frequency	Frequency (Hz)
1	3.141592654	4.085221062
2	3.178360862	4.181404915
3	3.281754623	4.457876457
4	3.435287632	4.884746479
5	3.620763095	5.426452891
6	3.822972747	6.04948245
7	4.030236185	6.723212108
8	4.232777837	7.41594954
9	4.420287227	8.087546631
10	4.579036115	8.678885419
11	4.689603683	9.103074589

Table A.1 —continued from previous page

Mode	Non-dimensionalised Freq Frequency	Frequency (Hz)
12	6.283185307	16.34088425
13	6.323045543	16.54887352
14	6.431848988	17.12330117
15	6.587573298	17.96249822
16	6.770772749	18.9754591
17	6.967900732	20.09646758
18	7.169264593	21.27477791
19	7.366379727	22.46073799
20	7.549498979	23.59131114
21	7.705010398	24.57323168
22	7.813507121	25.27015126
23	9.424777961	36.76698956
24	9.464500678	37.07756717
25	9.573074316	37.93312985
26	9.72871694	39.17661893
27	9.912021855	40.66682987
28	10.10936851	42.30228943
29	10.31098375	44.0064182
30	10.50833096	45.7070615
31	10.69163935	47.31560727
32	10.8472912	48.70330294
33	10.9558781	49.68327315

Table A.1 —continued from previous page

Mode	Non-dimensionalised Freq Frequency	Frequency (Hz)
34	12.56637061	65.363537
35	12.60609927	65.77748471
36	12.71468284	66.91552353
37	12.87032902	68.56383735
38	13.05362939	70.53072918
39	13.25096659	72.67933334
40	13.45257096	74.90768928
41	13.64990814	77.12146562
42	13.83320836	79.20665153
43	13.98885414	80.9990827
44	14.09743714	82.26141026

A.2 Dynamic amplification of bridge strains at midspan of span 20

The following figures show the dynamic response of bridge strain at mid span location obtained from meaurements covering the period from June 2016 to April 2017.

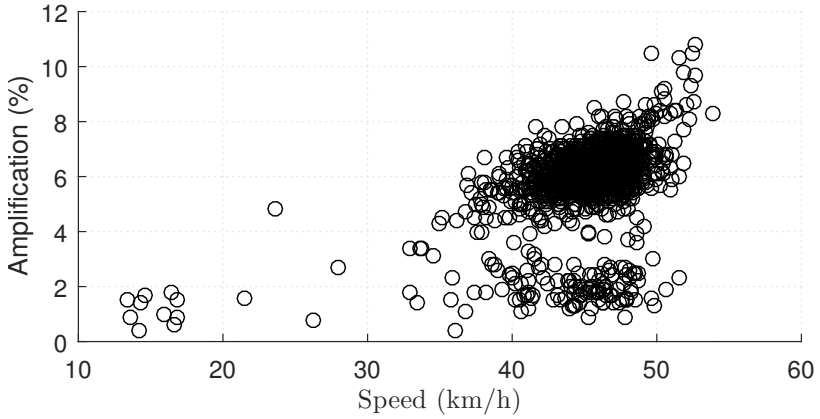

Figure A.1: Plot of DA against speed caused by loaded trains: June 2016 to April 2017

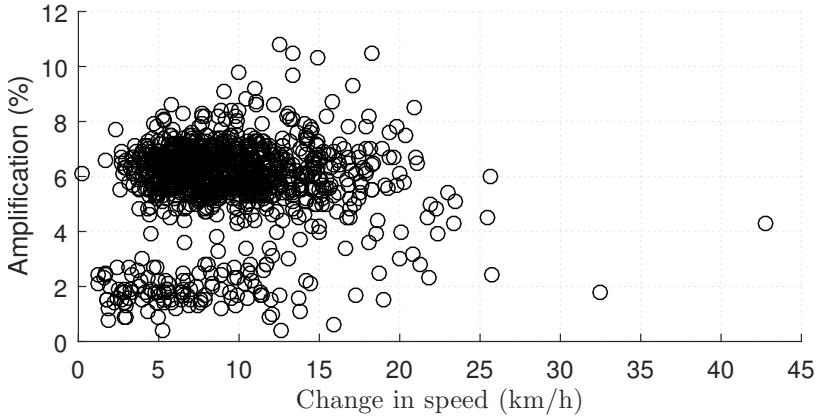

Figure A.2: Plot of DA against change in speed caused by loaded trains: June 2016 to April 2017

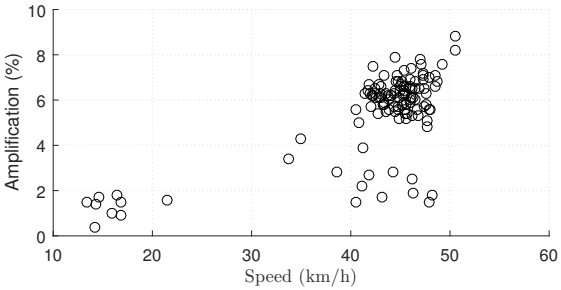

Figure A.3: June 2016 (Loaded)

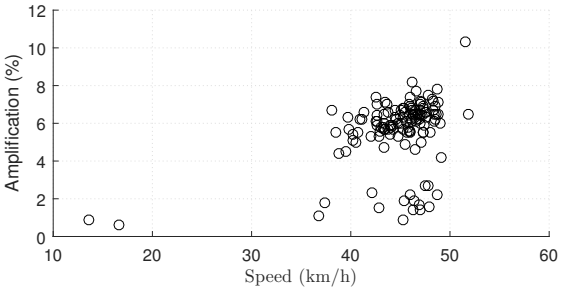

Figure A.4: July 2016 (Loaded)

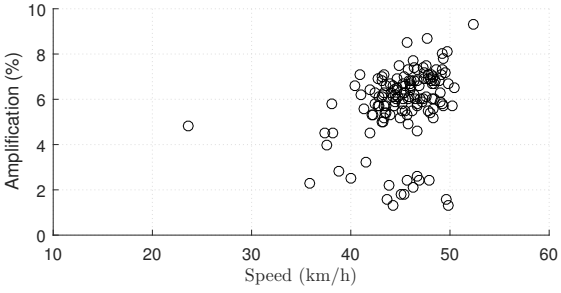

Figure A.5: August 2016 (Loaded)

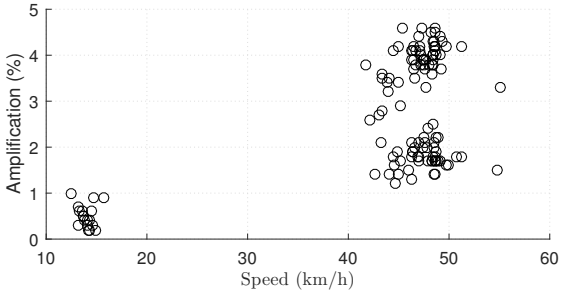

Figure A.6: June 2016 (Empty)

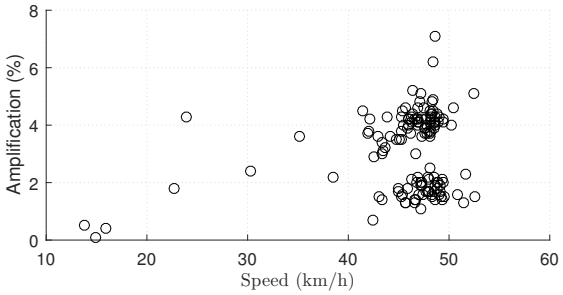

Figure A.7: July 2016 (Empty)

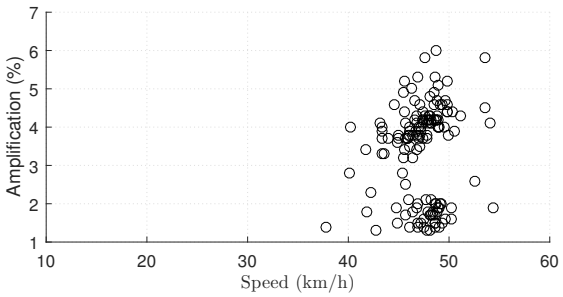

Figure A.8: August 2016 (Empty)

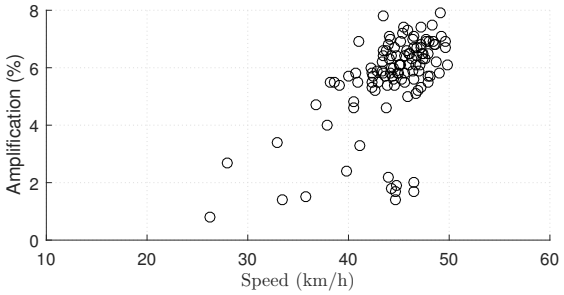

Figure A.9: September 2016 (Loaded)

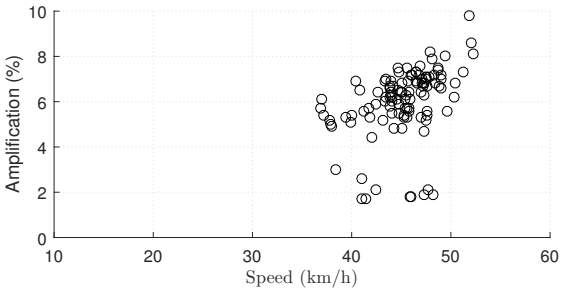

Figure A.10: October 2016 (Loaded)

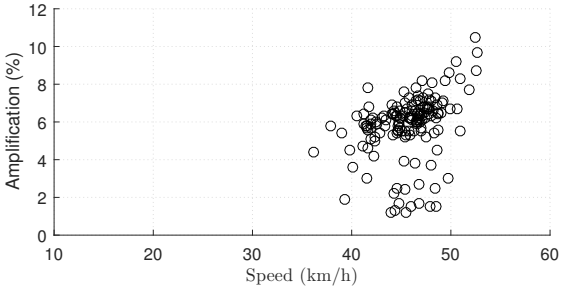

Figure A.11: November 2016 (Loaded)

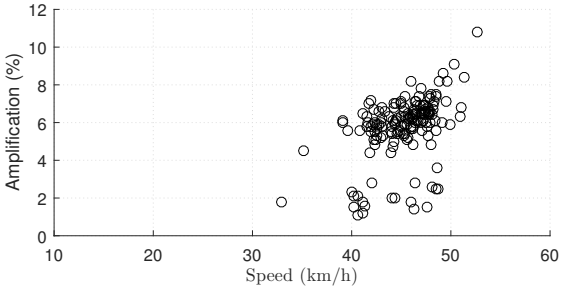

Figure A.12: December 2016 (Loaded)

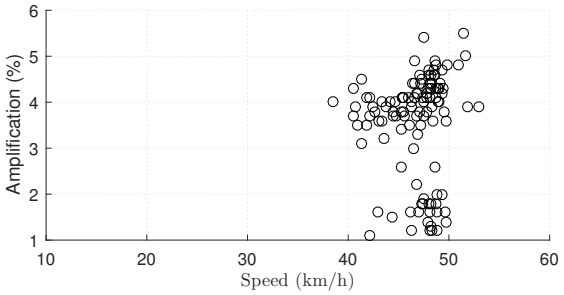

Figure A.13: September 2016 (Empty)

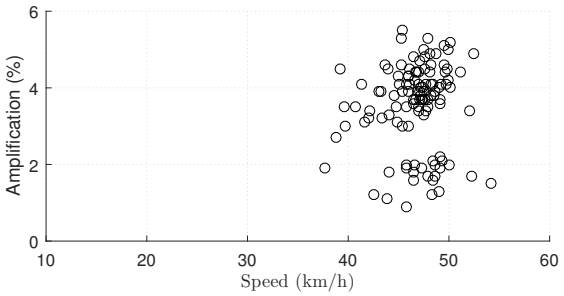

Figure A.14: October 2016 (Empty)

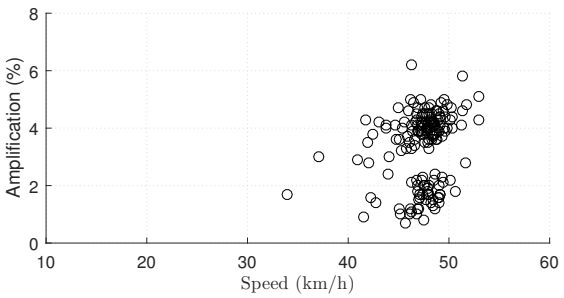

Figure A.15: November 2016 (Empty)

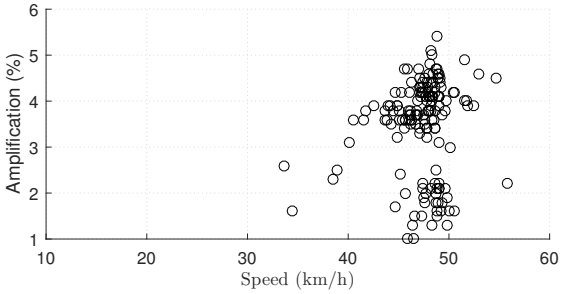

Figure A.16: December 2016 (Empty)

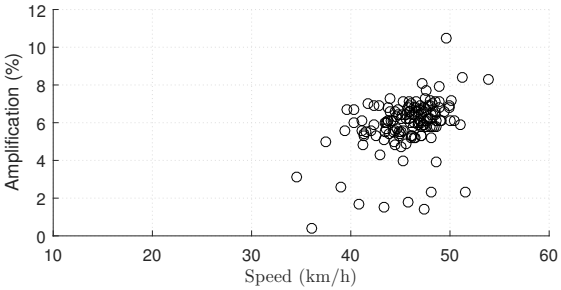

Figure A.17: January 2017 (Loaded)

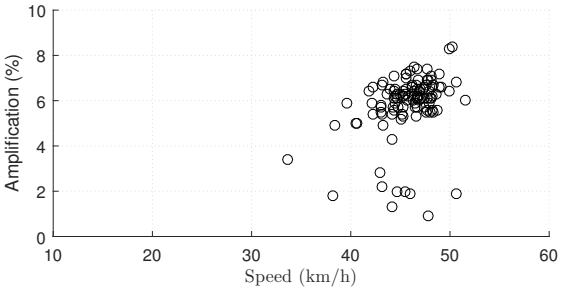

Figure A.18: February 2017 (Loaded)

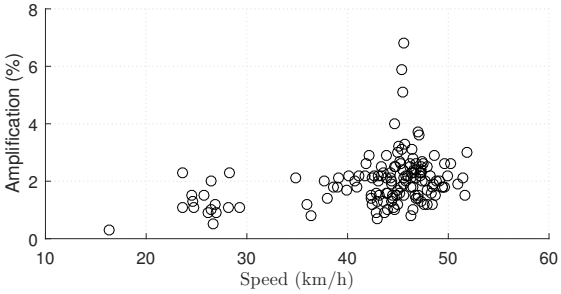

Figure A.19: March 2017 (Loaded)

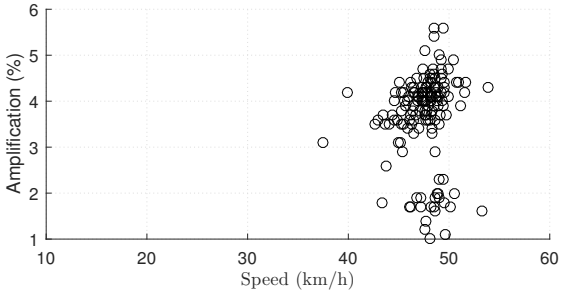

Figure A.20: January 2017 (Empty)

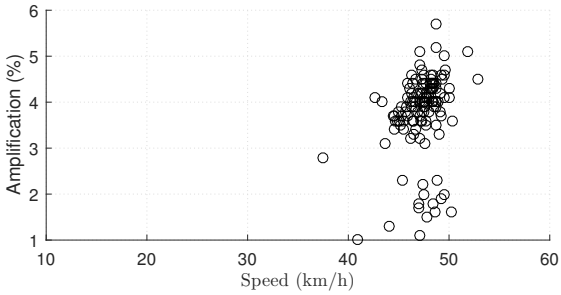

Figure A.21: February 2017 (Empty)

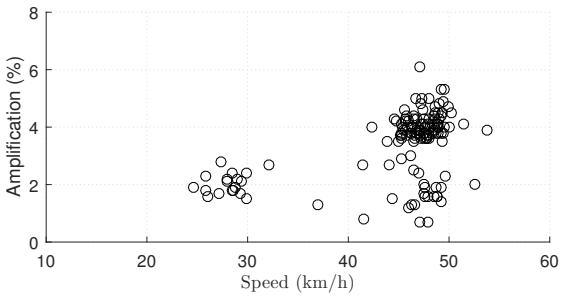

Figure A.22: March 2017 (Empty)

A.3 Dynamic amplification of bridge strains at support section of span 20

The following figures show the dynamic response of bridge strain at support location obtained from meaurements covering the period from June 2016 to April 2017.

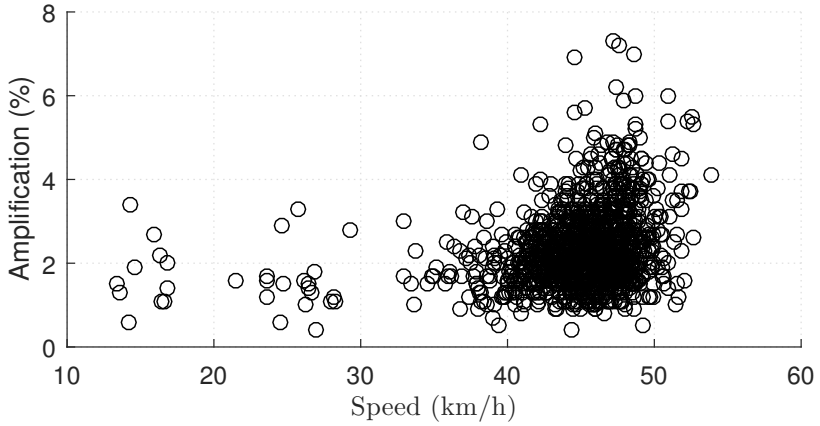

Figure A.23: Plot of DA against speed caused by loaded trains: June2016 to March 2017

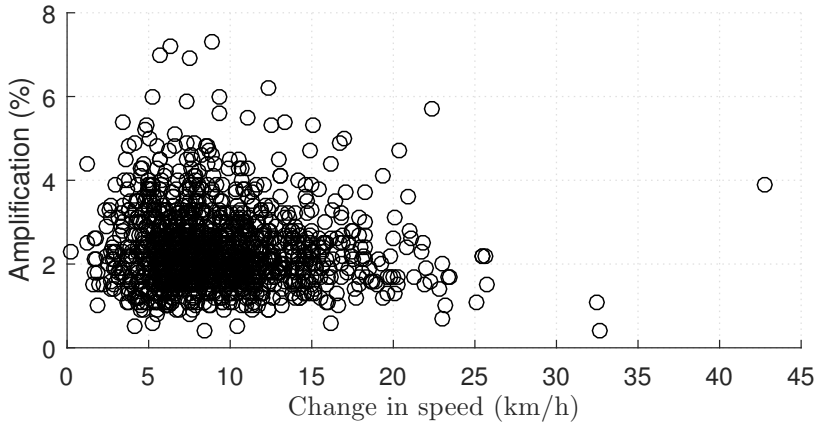

Figure A.24: Plot of DA against change in speed of loaded trains: June2016 to March 2017

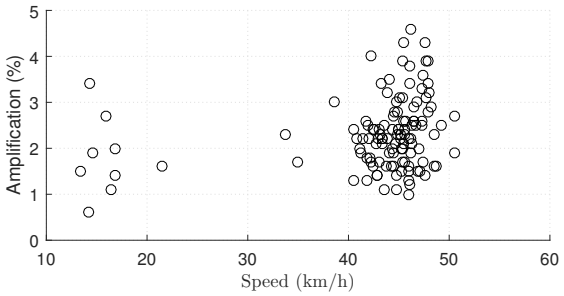

Figure A.25: June 2016 (Loaded)

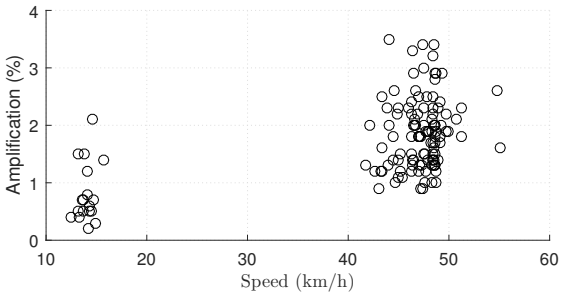

Figure A.26: June 2016 (Empty)

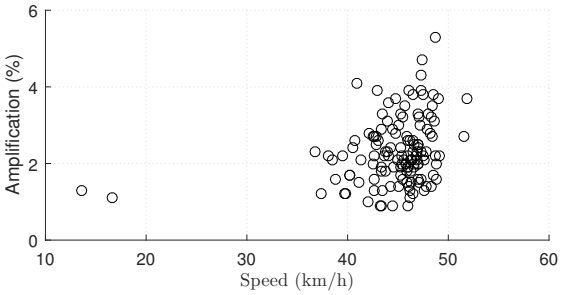

Figure A.27: July 2016 (Loaded)

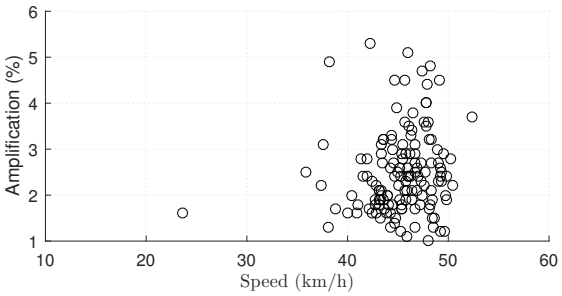

Figure A.28: August 2016 (Loaded)

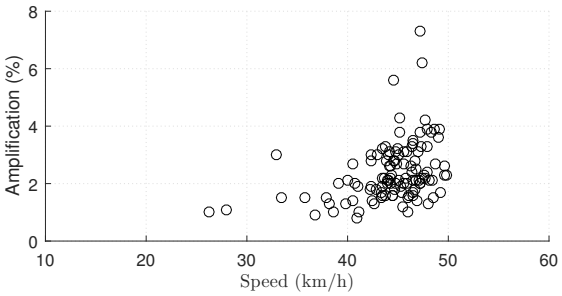

Figure A.29: September 2016 Loaded)

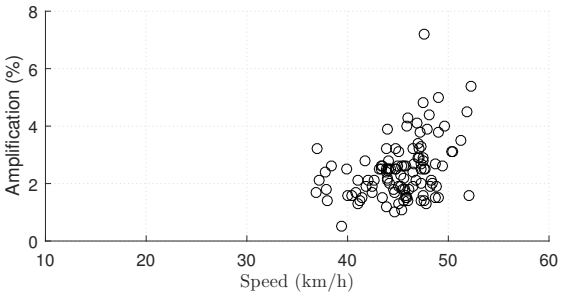

Figure A.30: October 2016 (Loaded)

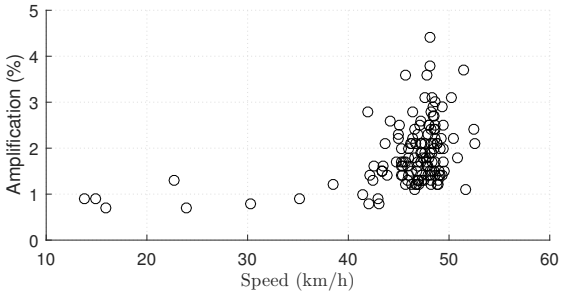

Figure A.31: July 2016 (Empty)

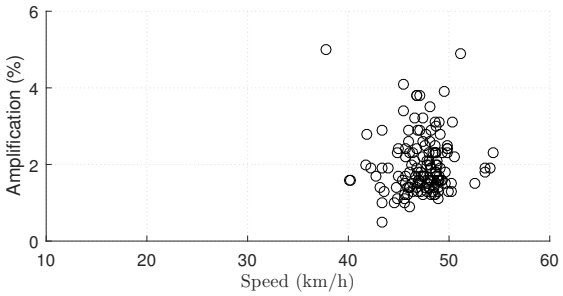

Figure A.32: August 2016 (Empty)

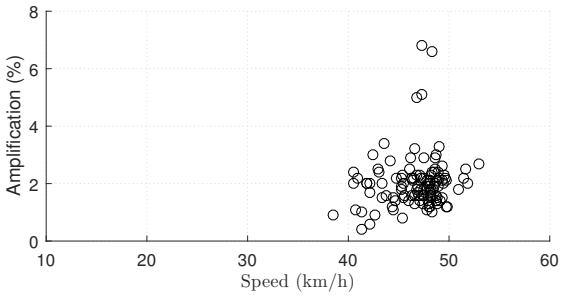

Figure A.33: September 2017 (Empty)

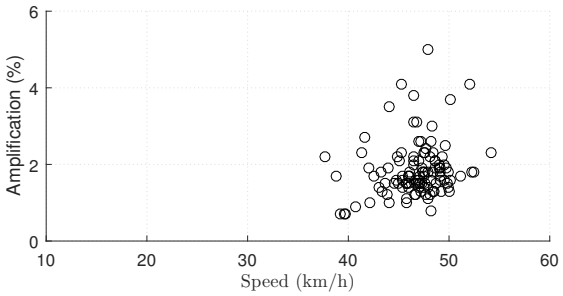

Figure A.34: October 2016 (Empty)

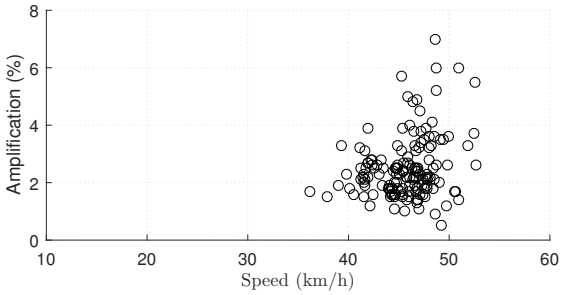

Figure A.35: November 2016 (Loaded)

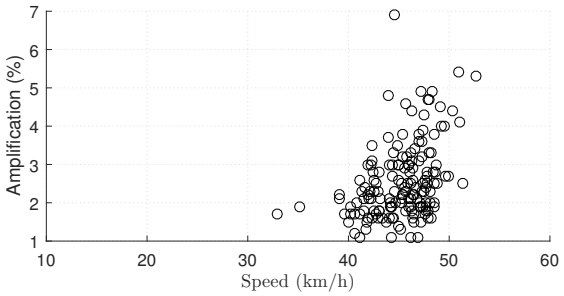

Figure A.36: December 2016 (Loaded)

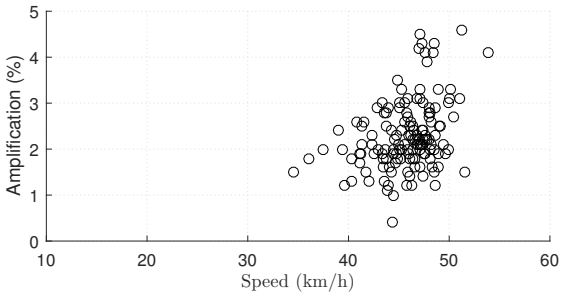

Figure A.37: January 2017 (Loaded)

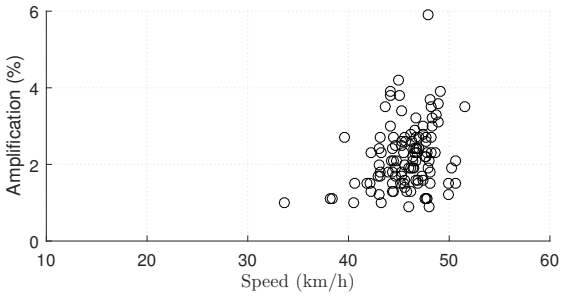

Figure A.38: February 2017 (Loaded)

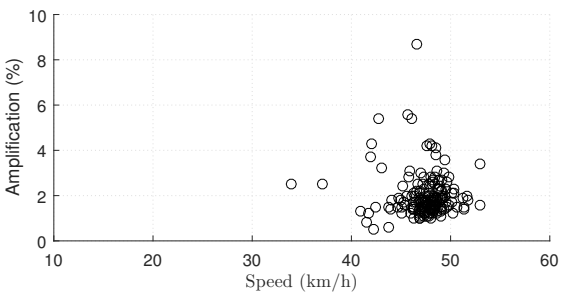

Figure A.39: November 2016 (Empty)

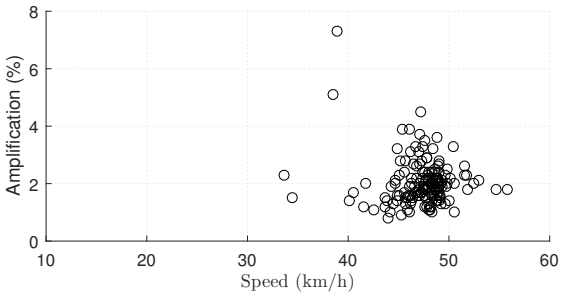

Figure A.40: December 2016 (Empty)

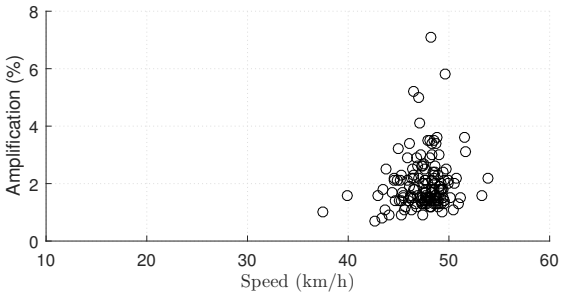

Figure A.41: January 2017 (Empty)

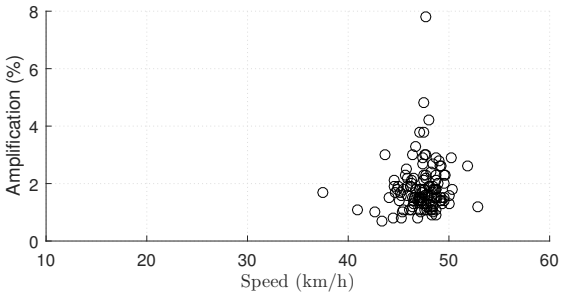

Figure A.42: February 2017 (Empty)

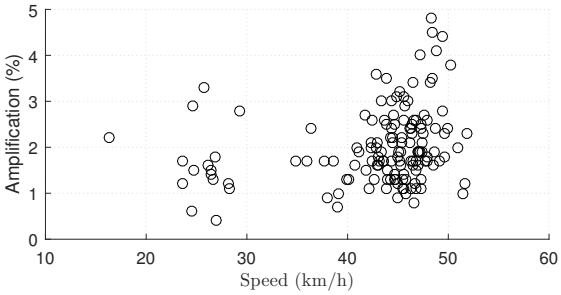

Figure A.43: March 2017 (Loaded)

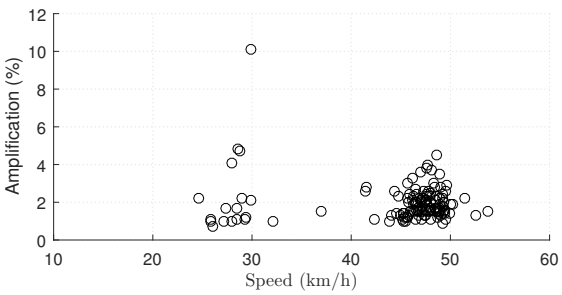

Figure A.44: March 2017 (Empty)

Appendix B

PROBABILISTIC LOAD EFFECTS

B.1 GEV parameter variation with span length

The following figures show an investigation of GEV parameter against span length. The GEV was fitted to load effects data simulated from iid axle loads.

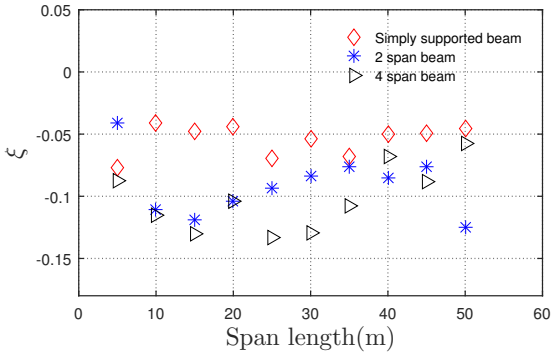

Figure B.1: Midspan moment

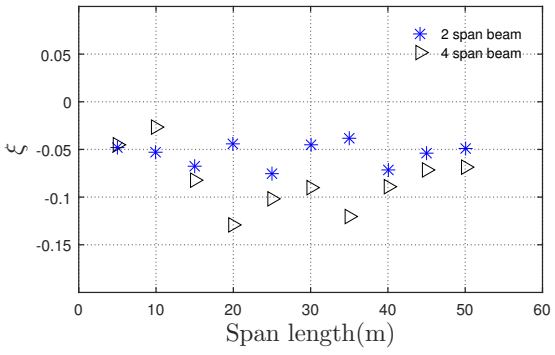

Figure B.2: Support moment

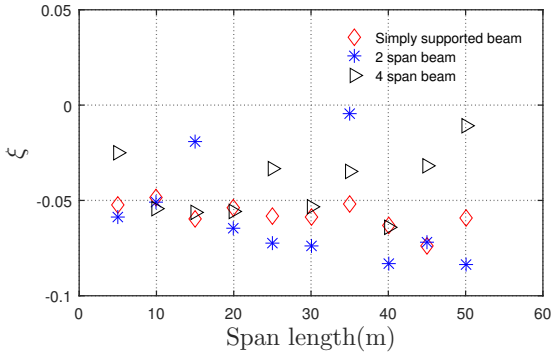

Figure B.3: Support shear

Figure B.4: Variation of shape factor with span length

B.2 Comparison of extrapolation methods

The following tables give a comparison of load effects obtained from different extrapolation techniques for 50 year return levels.

Table B.1: Mid-span moment of simply supported beam

Influence line 

Span length	Bending moment (kNm)				
(m)	Daily Traffic	Sats83	GEV	Normal	Bayesian
5	485.8	511.2	552.9	543.3	552.9
10	1746.8	1878.1	1932.1	1913.9	1931.9
15	3277.3	3882.9	3605.7	3571.2	3604.7
20	5504.9	6512.7	5986.4	5937.7	5986.5
25	8601.6	9767.5	9242.7	9186.5	9241.4
30	12557.4	13647.2	13388.4	13321.2	13393.9
35	16846.5	18152.0	17895.1	17803.1	17899.6
40	21727.9	23281.8	23047.2	22925.4	23061.9
45	27488.8	29036.6	29054.0	28910.1	29068.0
50	34178.6	35416.4	35949.4	35839.1	35973.6

Table B.2: Support shear of simply supported beam

Influence line 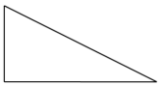

Span length	Support shear(kN)				
(m)	Daily Traffic	Sats83	GEV	Normal	Bayesian
5	467.6	462.3	510.1	503.1	509.4
10	773.0	814.8	822.9	816.0	823.8
15	1032.0	1102.7	1092.8	1086.4	1093.1
20	1298.2	1371.7	1387.1	1378.2	1387.4
25	1596.8	1633.1	1651.7	1642.4	1651.6
30	1892.9	1890.6	1946.8	1934.6	1946.9
35	2163.4	2146.1	2218.6	2204.1	2217.4
40	2433.7	2400.1	2502.1	2491.8	2503.2
45	2722.8	2653.3	2769.2	2760.8	2769.7
50	3011.5	2905.8	3058.4	3047.2	3058.1

Table B.3: Mid-span moment for 2 span continuous beam

Influence line	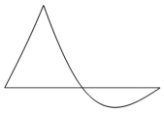				
Span length	Bending moment (kNm)				
(m)	Daily Traffic	Sats83	GEV	Normal	Bayesian
5	341.1	386.3	387.3	384.3	387.5
10	1101.1	1437.9	1218.3	1203.9	1218.8
15	2468.5	3007.8	2670.8	2637.8	2670.7
20	4181.7	5050.4	4482.6	4449.5	4482.2
25	6493.0	7563.6	6900.8	6837.4	6908.6
30	9200.0	10546.4	9735.4	9686.4	9742.4
35	12550.2	13998.5	13193.1	13154.3	13242.1
40	16319.6	17919.8	17120.5	17060.3	17133.7
45	20636.3	22310.0	21591.6	21497.3	21629.4
50	25445.8	27169.2	26491.5	26411.1	26519.9

Table B.4: Support moment for 2 span continuous beam

Influence line	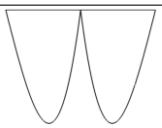				
Span length	Bending moment (kNm)				
(m)	Daily Traffic	Sats83	GEV	Normal	Bayesian
5	457.8	475.4	496.8	491.3	491.3
10	1590.0	1569.2	1813.1	1801.7	1801.7
15	3297.3	3345.7	3299.7	3380.4	3380.4
20	5767.9	5736.9	6042.9	6021.4	6021.4
25	8908.9	8748.8	9045.3	9014.9	9014.9
30	12767.7	12383.5	13023.8	12982.6	12982.6
35	17329.5	16641.9	17491.9	17441.0	17441.0
40	22556.1	21524.5	22779.1	22296.1	22296.1
45	28548.6	27031.6	28660.6	28556.6	28556.6
50	35143.0	33163.3	35246.3	35187.9	35187.9

Table B.5: Support shear for 2 span continuous beam

Influence line 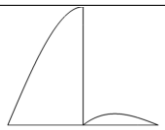

Span length	Support shear(kN)				
(m)	Daily Traffic	Sats83	GEV	Normal	Bayesian
5	567.4	613.6	624.7	618.4	624.5
10	967.8	1083.6	1049.2	1038.6	1049.2
15	1314.3	1467.4	1414.3	1402.0	1414.1
20	1712.9	1830.8	1813.0	1801.5	1813.2
25	2077.0	2188.1	2174.5	2166.8	2174.2
30	2483.2	2543.1	2579.4	2569.7	2579.8
35	2838.5	2897.1	2960.3	2940.7	2959.5
40	3229.6	3250.5	3337.1	3327.0	3338.4
45	3602.6	3603.6	3713.0	3694.3	3712.3
50	3997.9	3956.5	4099.4	4081.9	4100.8

Table B.6: Mid-span moment for 4 span continuous beam

Influence line 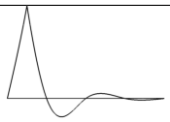

Span length	Bending moment (kNm)				
(m)	Daily Traffic	Sats83	GEV	Normal	Bayesian
5	346.2	394.1	408.3	402.4	406.6
10	1102.7	1472.0	1218.1	1210.0	1215.9
15	2418.5	3090.4	2611.7	2591.5	2610.1
20	4087.6	5204.1	4381.7	4340.9	4383.4
25	6343.9	7810.7	6722.1	6692.4	6724.5
30	8991.3	10909.5	9482.6	9437.0	9489.3
35	12259.1	14499.9	12894.0	12823.5	12901.2
40	15934.9	18581.8	16748.7	16668.5	16774.0
45	20148.8	23155.0	21077.8	21038.9	21106.1
50	24847.6	28219.4	25988.4	25841.6	26020.8

Table B.7: Support moment for 4 span continuous beam

Influence line	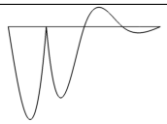				
Span length	Bending moment (kNm)				
(m)	Daily Traffic	Sats83	GEV	Normal	Bayesian
5	390.6	455.7	448.3	444.2	449.5
10	1450.6	1547.4	1564.1	1553.6	1569.0
15	2978.4	3283.3	3135.0	3119.7	3149.1
20	5170.5	5611.0	5403.4	5383.6	5396.9
25	8017.8	8536.7	8342.8	8328.0	8352.5
30	11478.5	12062.7	11877.0	11873.1	11920.3
35	15564.8	16190.0	16068.5	16056.9	16093.2
40	20283.3	20919.1	20933.4	20882.1	20968.2
45	25617.0	26250.4	26397.3	26350.5	26449.8
50	31589.6	32183.9	32506.0	32449.1	32572.9

Table B.8: Support shear for 4 span continuous beam

Influence line	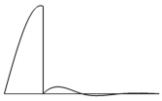				
Span length	Support shear(kN)				
(m)	Daily Traffic	Sats83	GEV	Normal	Bayesian
5	567.4	613.6	634.5	630.4	638.4
10	967.8	1083.6	1061.7	1058.6	1063.7
15	1314.3	1467.4	1422.9	1409.6	1419.8
20	1712.9	1830.8	1825.3	1819.9	1829.4
25	2077.0	2188.1	2195.9	2178.2	2194.7
30	2483.2	2543.1	2599.0	2595.8	2606.1
35	2838.5	2897.1	2964.7	2958.8	2977.9
40	3229.6	3250.5	3372.1	3359.4	3371.4
45	3602.6	3603.6	3736.2	3728.7	3752.7
50	3998.0	3956.5	4135.3	4131.8	4160.2

B.3 Load effects at 50 years and 1000 years return levels

The following figures show GEV fitting of load effects for single span, 2 span continuous beams and 4 span continuous beams.

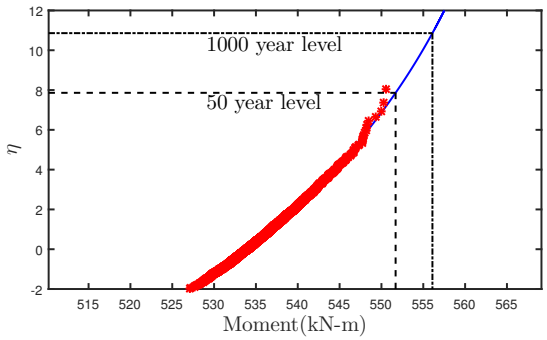

5m span bridge

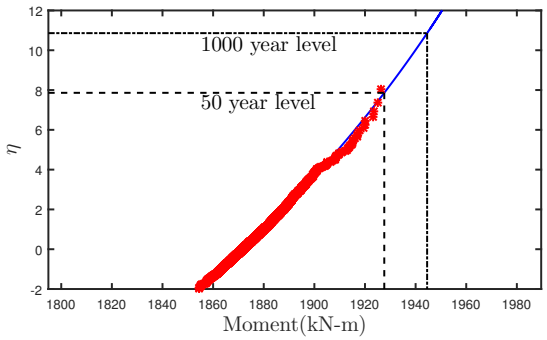

10m span bridge

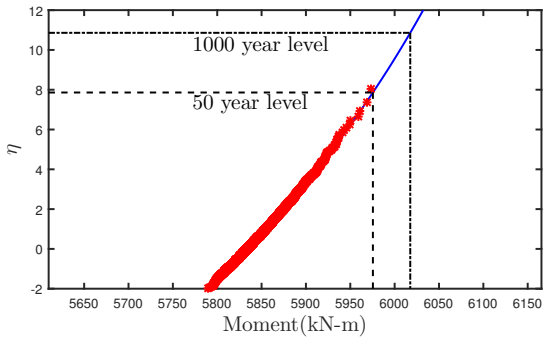

15m span bridge

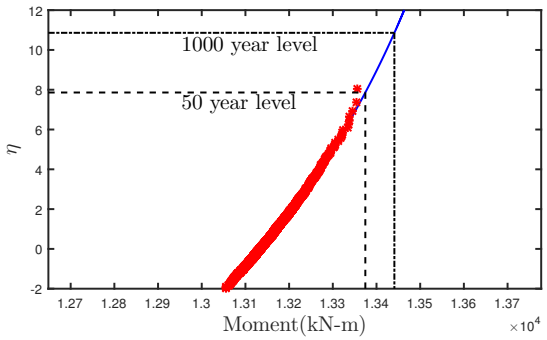

20m span bridge

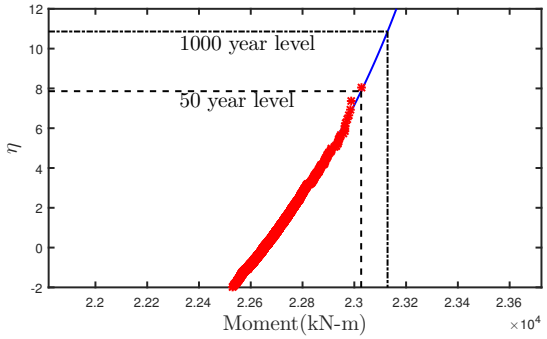

25m span bridge

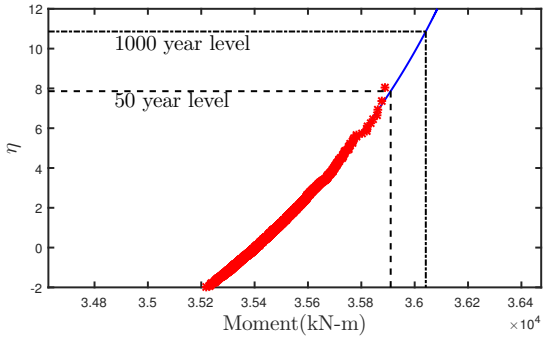

30m span bridge

Figure B.5: Midspan moment for single span bridges

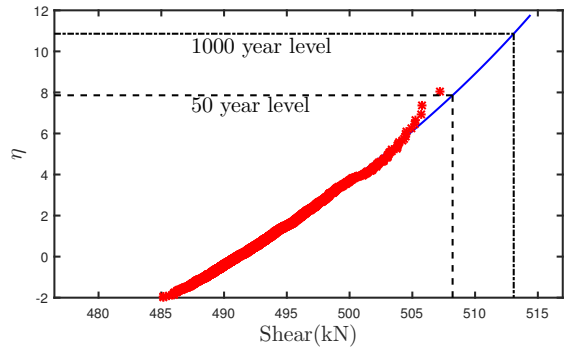

5m span bridge

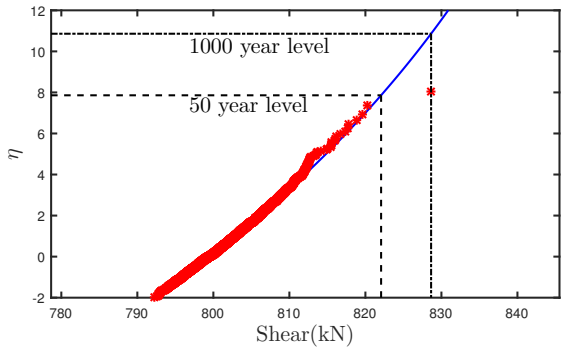

10m span bridge

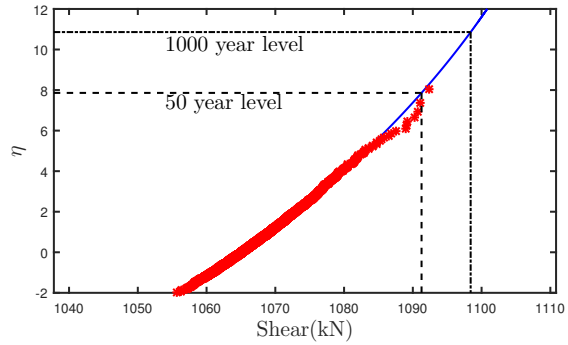

15m span bridge

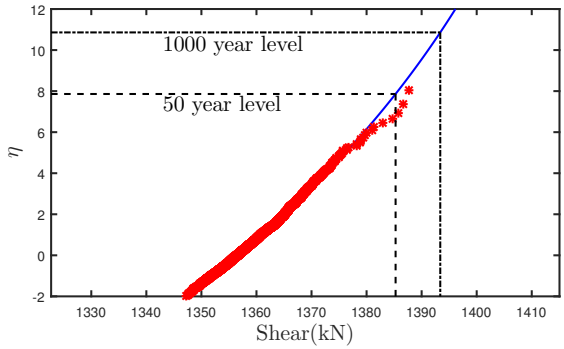

20m span bridge

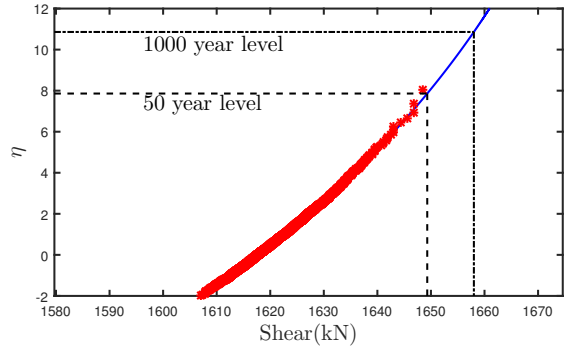

25m span bridge

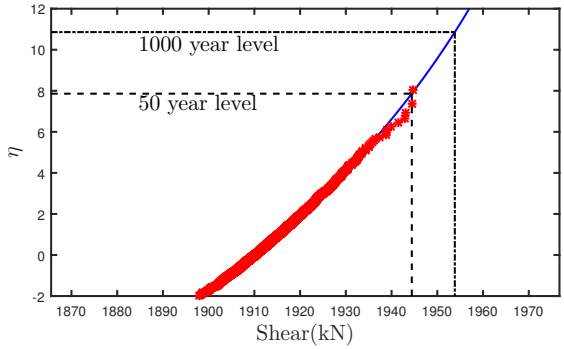

30m span bridge

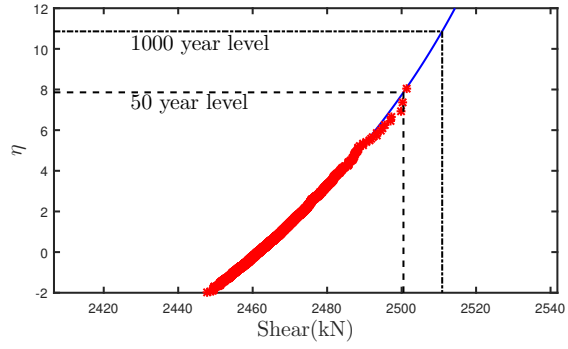

40m span bridge

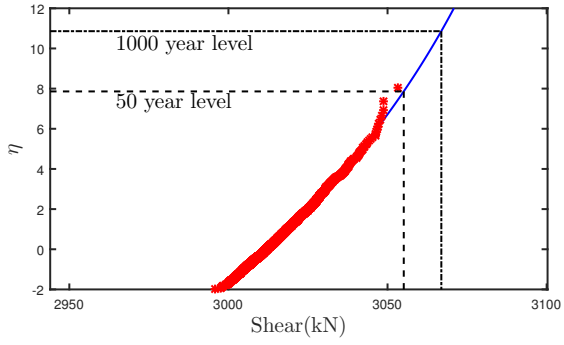

50m span bridge

Figure B.6: Support shear for single span bridges

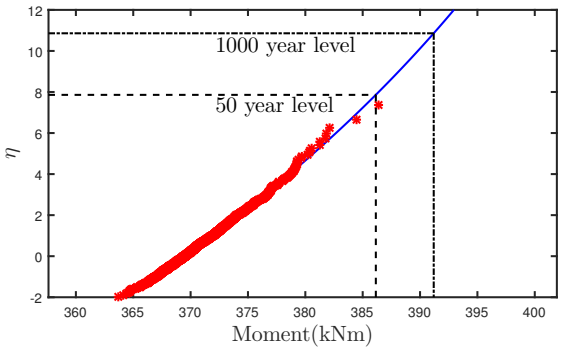

5m span bridge

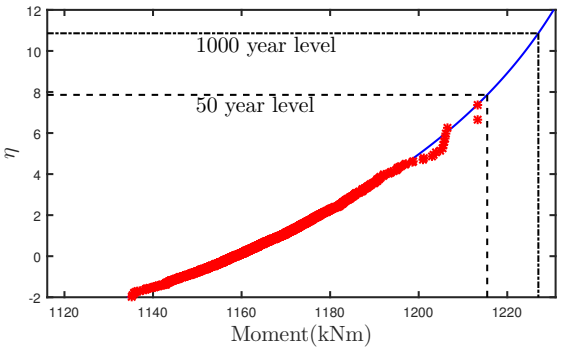

10m span bridge

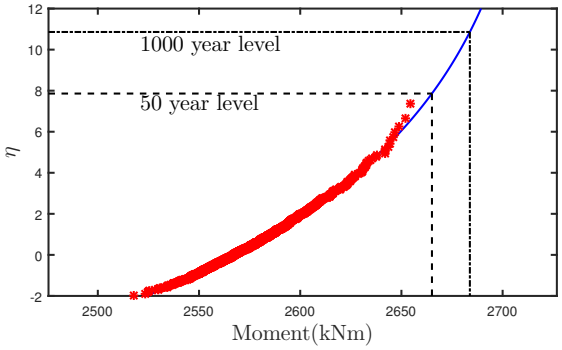

15m span bridge

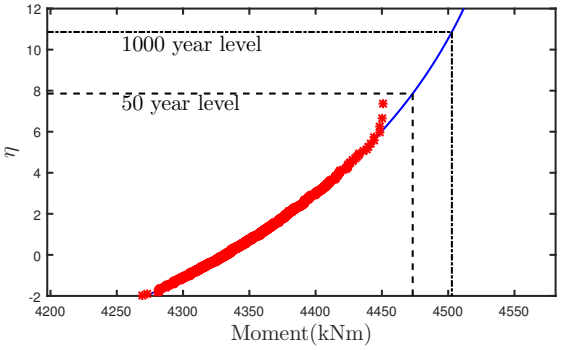

20m span bridge

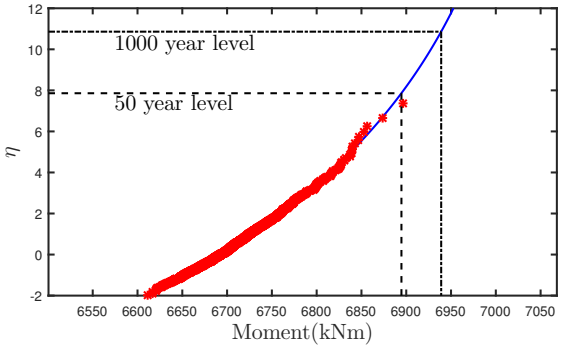

25m span bridge

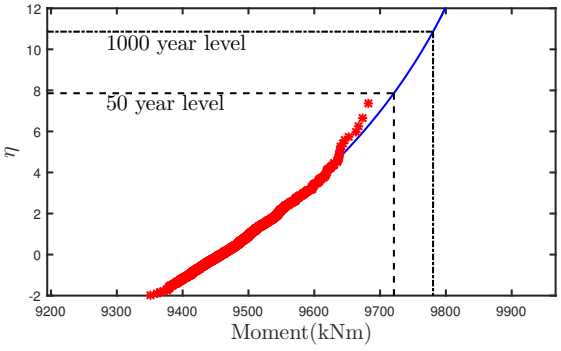

30m span bridge

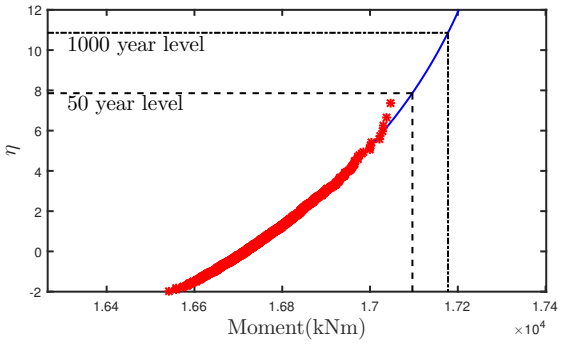

40m span bridge

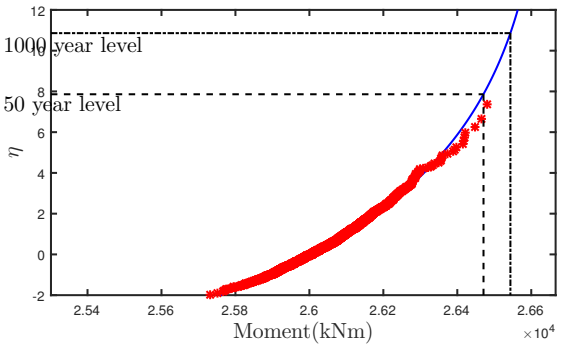

50m span bridge

Figure B.7: Midspan moment for 2 span continuous bridges

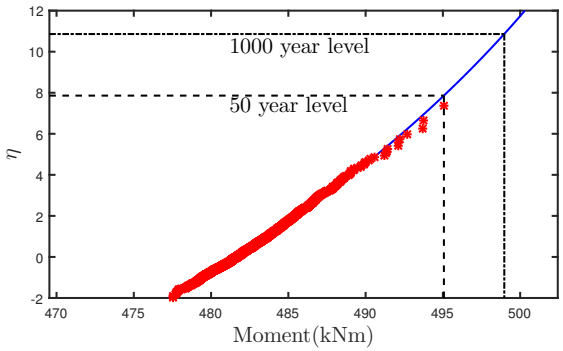

5m span bridge

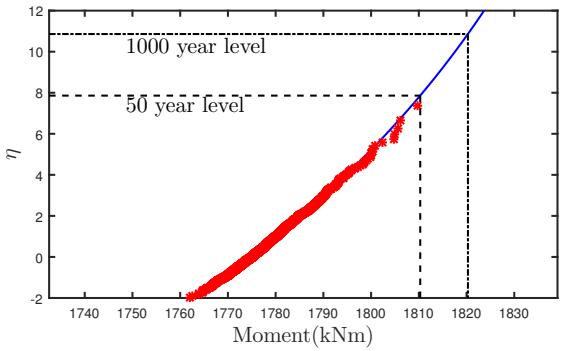

10m span bridge

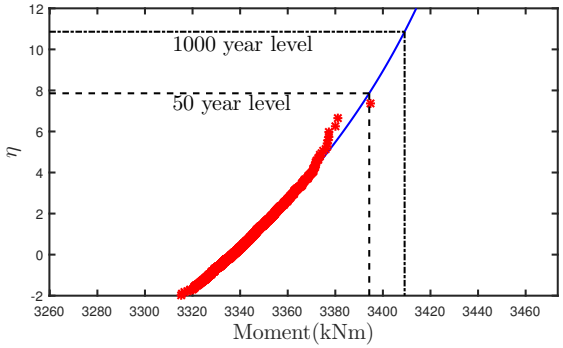

15m span bridge

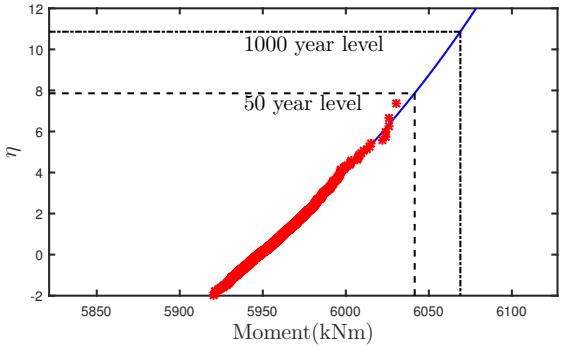

20m span bridge

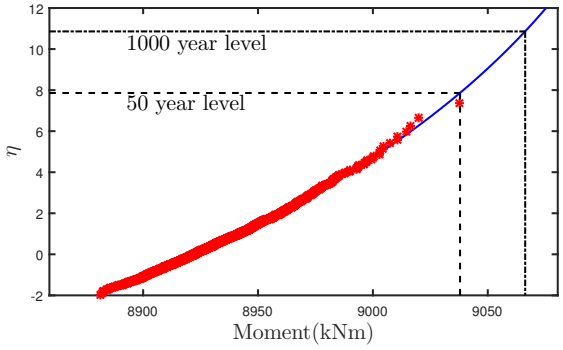

25m span bridge

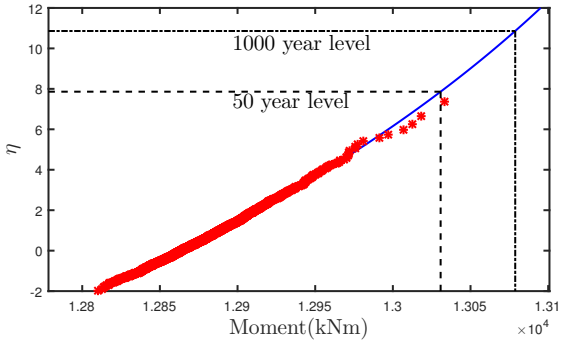

30m span bridge

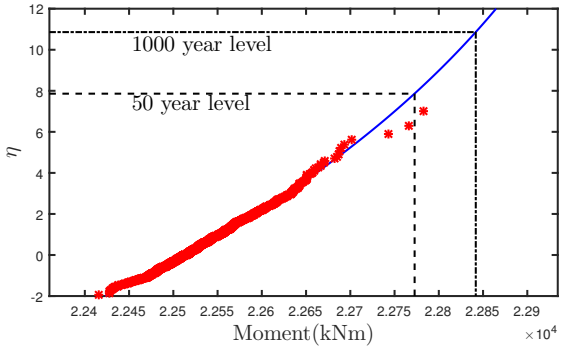

40m span bridge

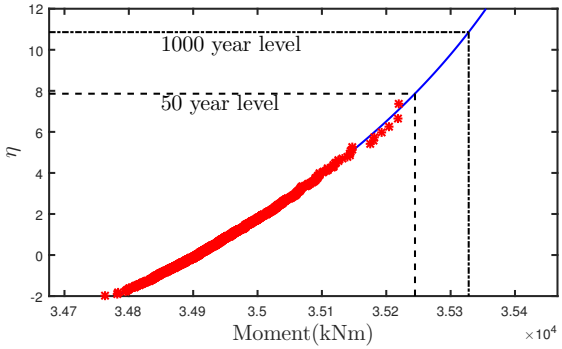

50m span bridge

Figure B.8: Interior support moment for 2 span continuous bridges

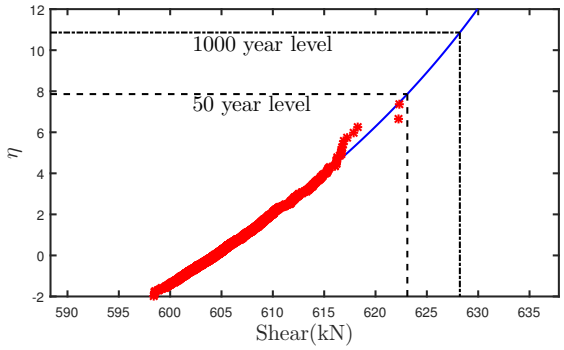

5m span bridge

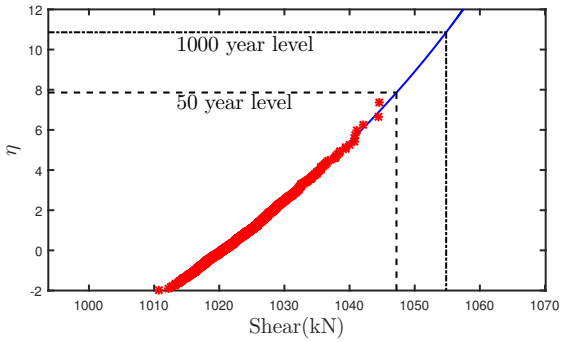

10m span bridge

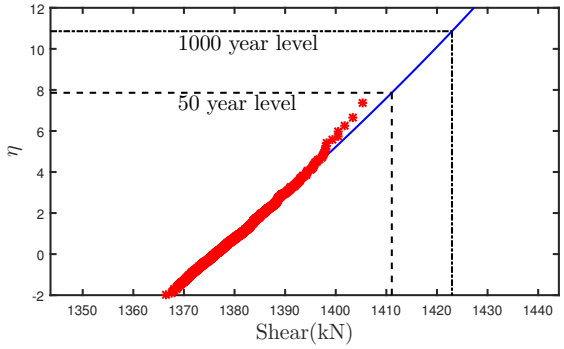

15m span bridge

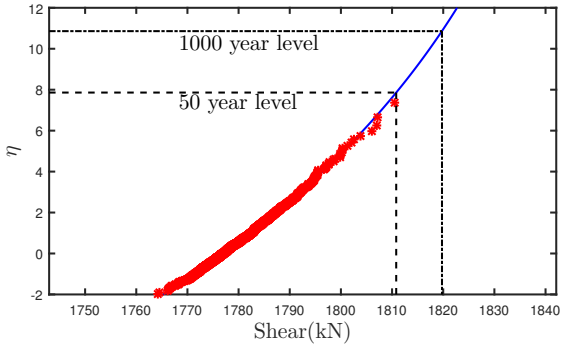

20m span bridge

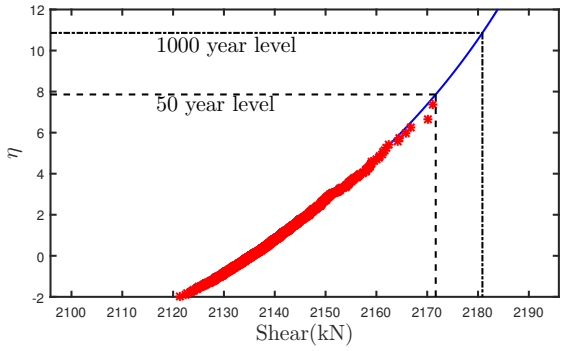

25m span bridge

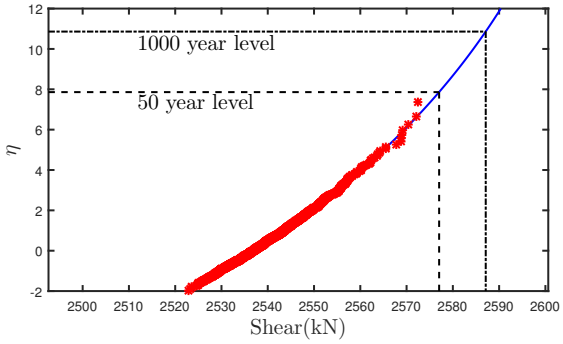

30m span bridge

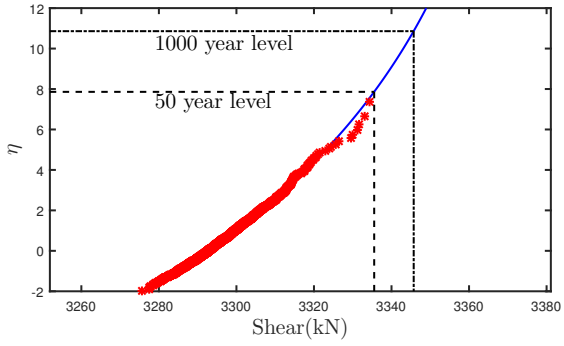

40m span bridge

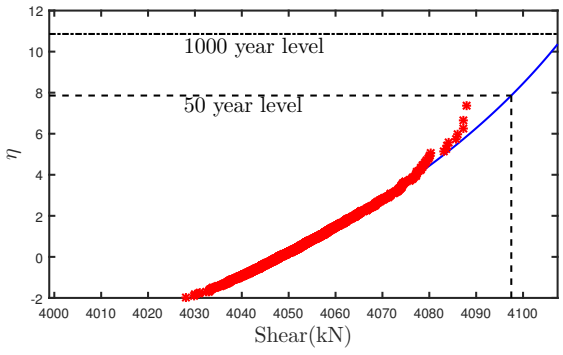

50m span bridge

Figure B.9: Interior support shear for 2 span continuous bridges

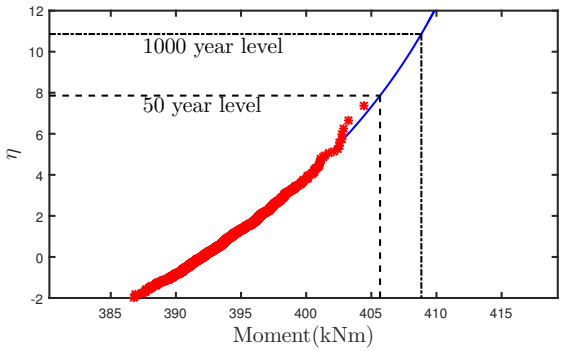

5m span bridge

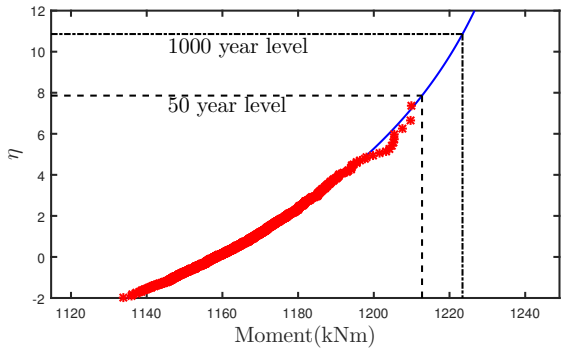

10m span bridge

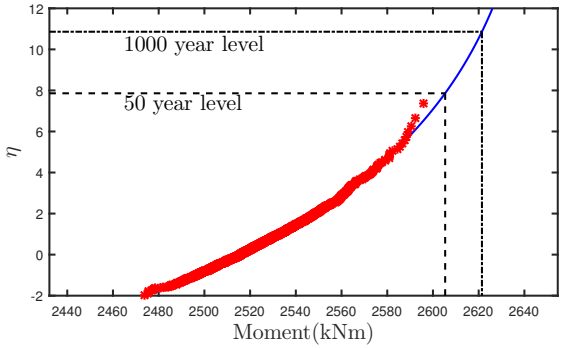

15m span bridge

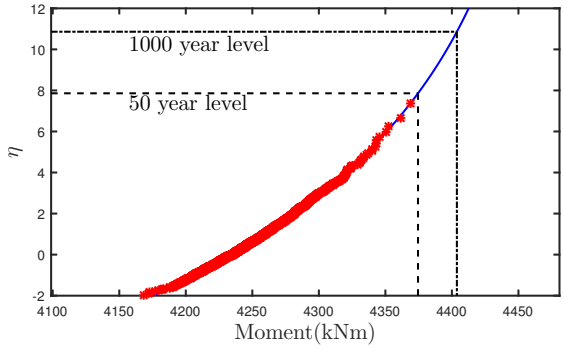

20m span bridge

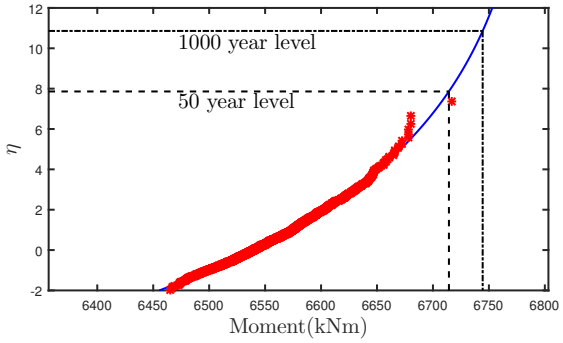

25m span bridge

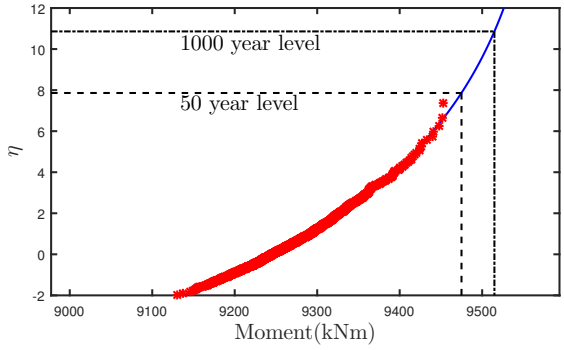

30m span bridge

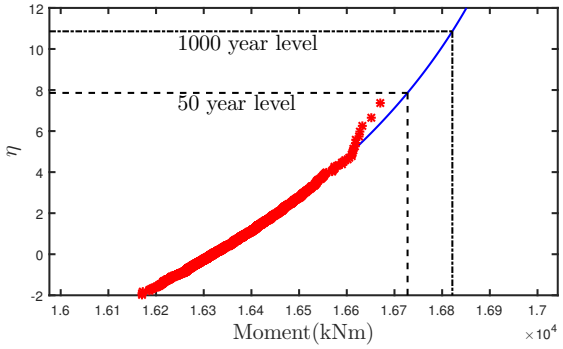

40m span bridge

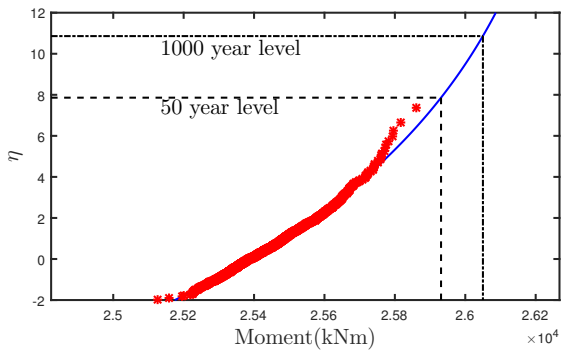

50m span bridge

Figure B.10: Midspan moment for 4 span continuous bridges

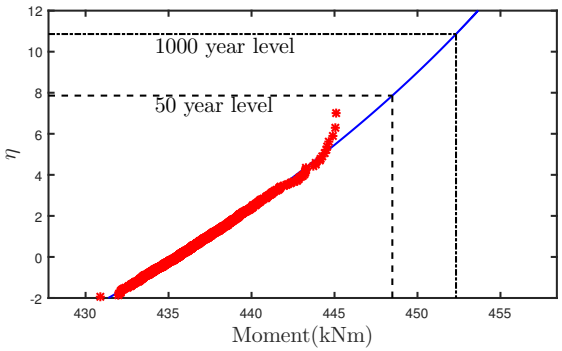

5m span bridge

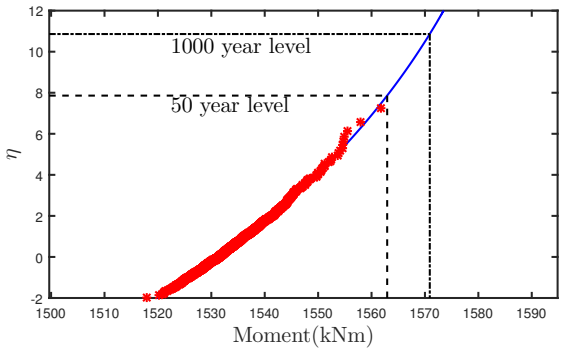

10m span bridge

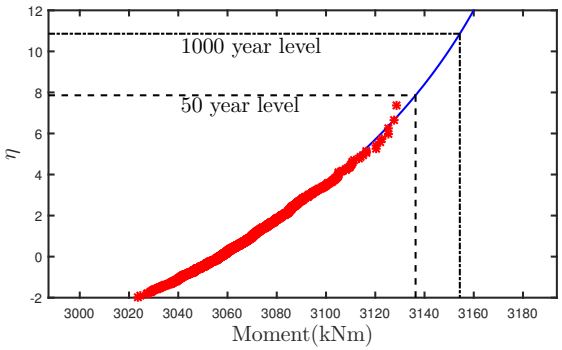

15m span bridge

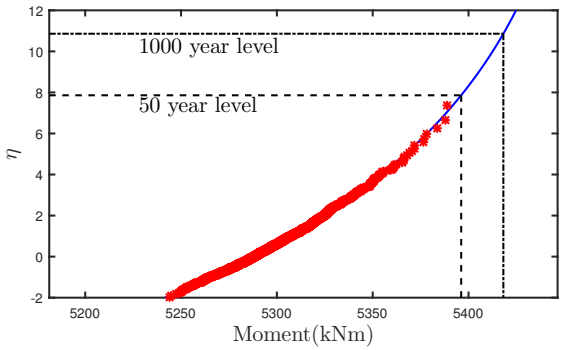

20m span bridge

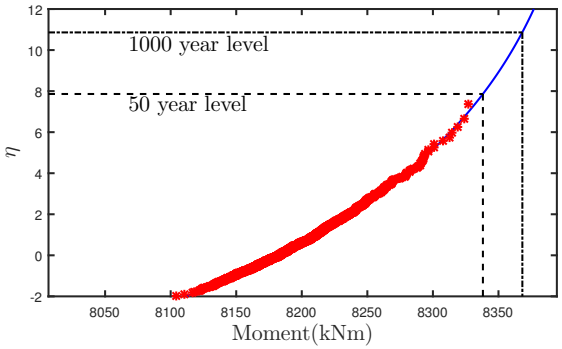

25m span bridge

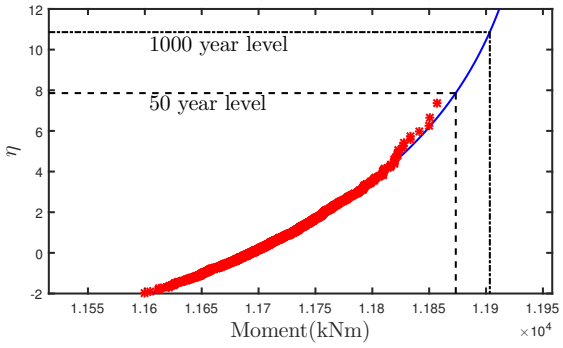

30m span bridge

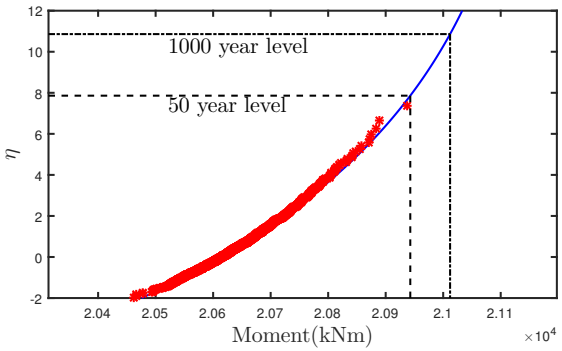

40m span bridge

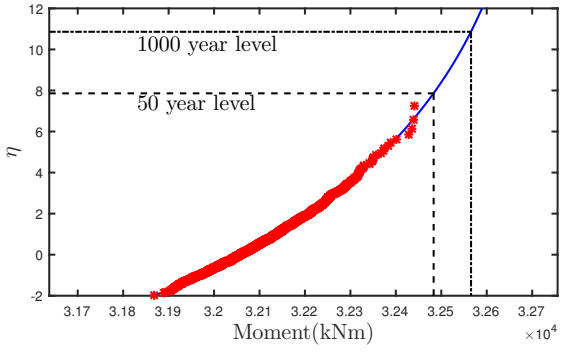

50m span bridge

Figure B.11: Interior support moment for 4 span continuous bridges

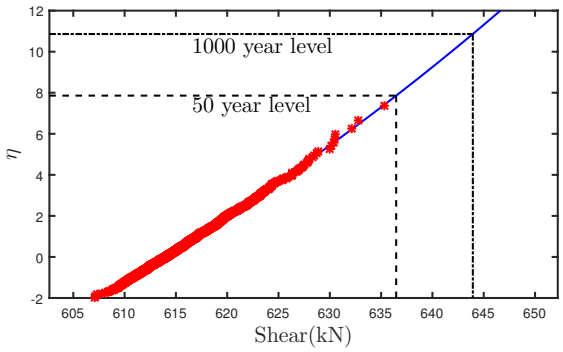

5m span bridge

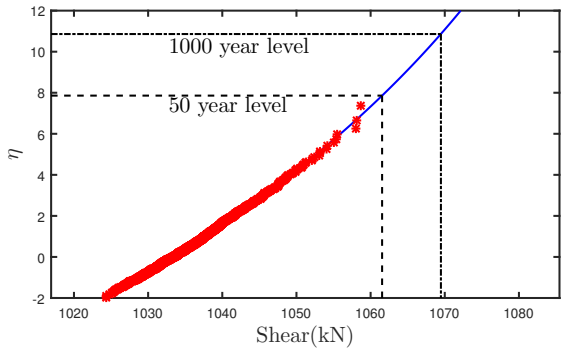

10m span bridge

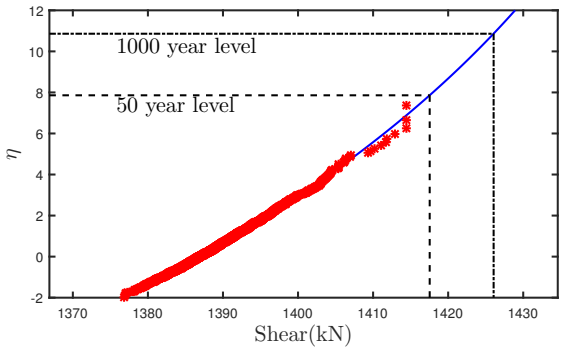

15m span bridge

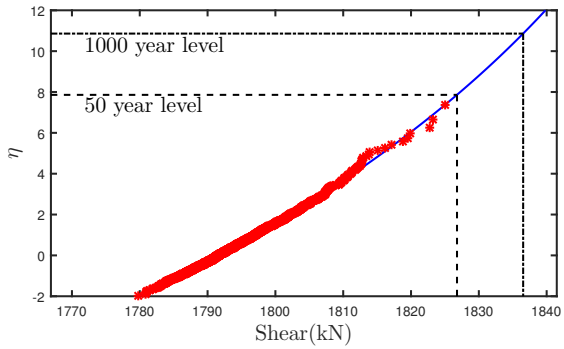

20m span bridge

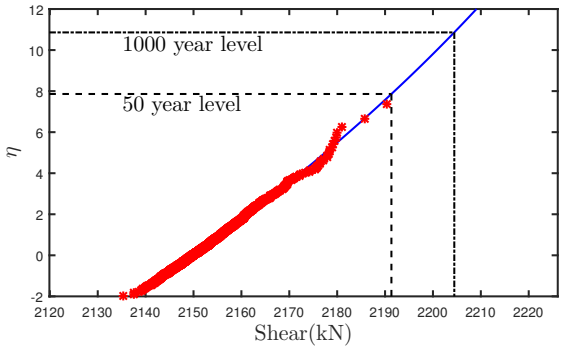

25m span bridge

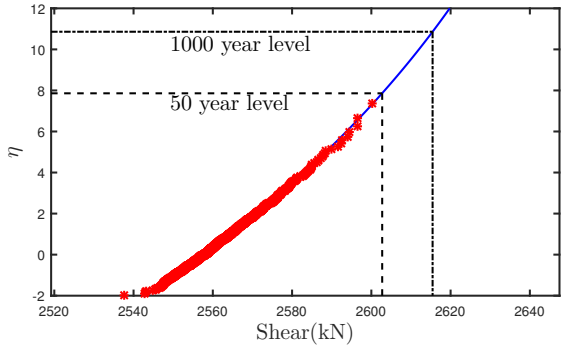

30m span bridge

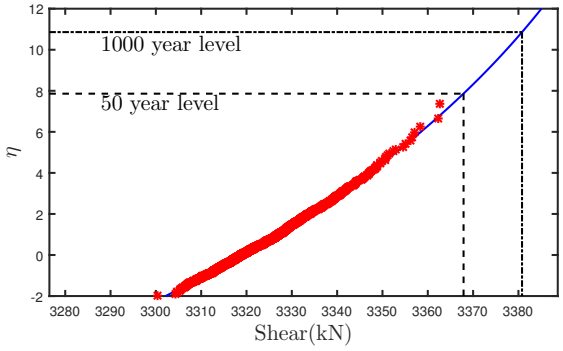

40m span bridge

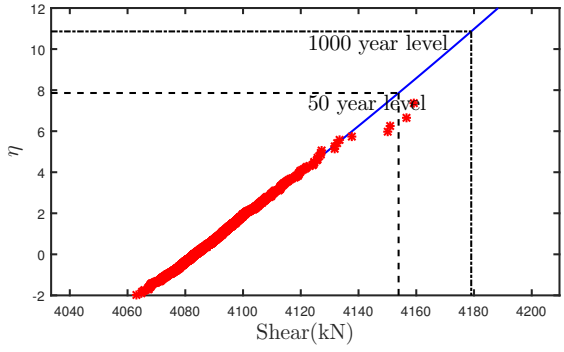

50m span bridge

Figure B.12: Interior support shear for 4 span continuous bridges

B.4 Comparison of GEV fitted to axle loads simulated based on iid and weak dependance

The following figures show a comparison GEV fitting of load effects for single span, 2 span continuous beams and 4 span continuous beams.

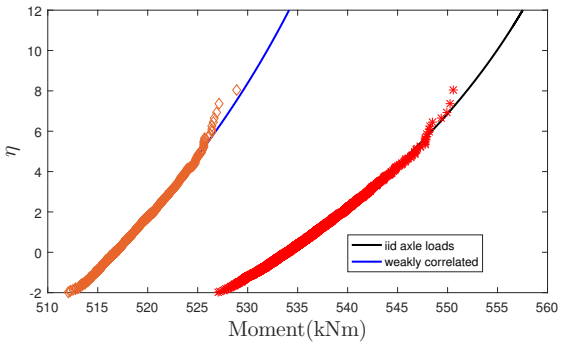

5m span bridge

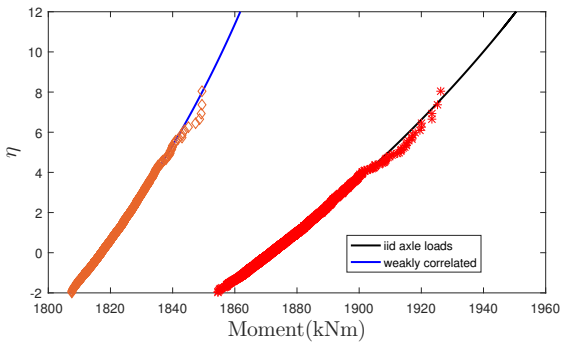

10m span bridge

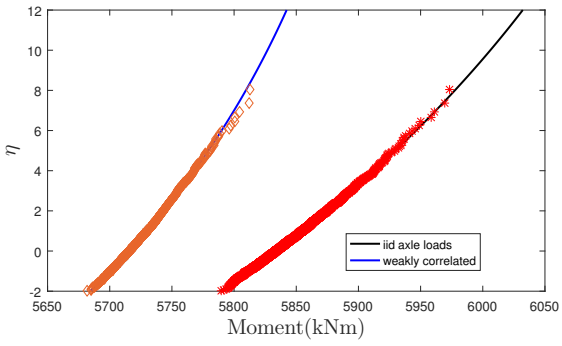

15m span bridge

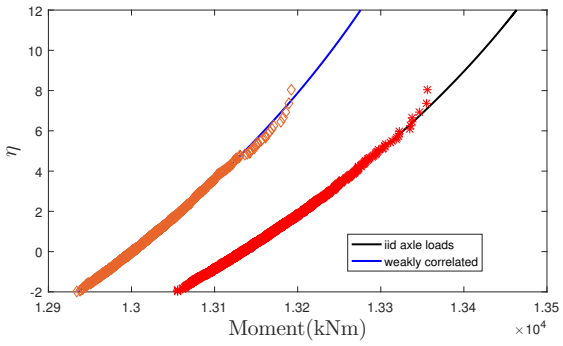

20m span bridge

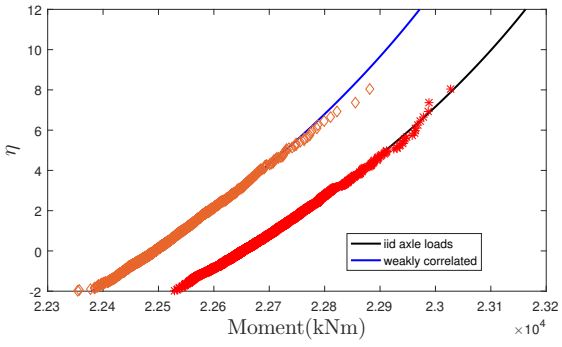

25m span bridge

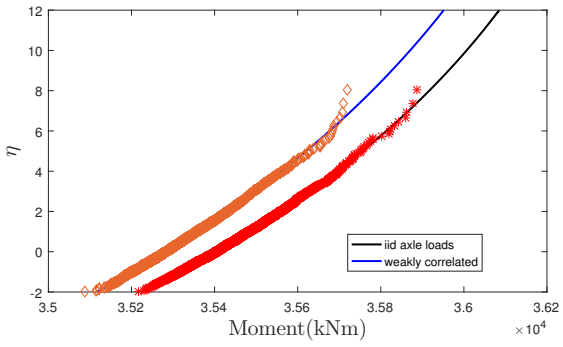

30m span bridge

Figure B.13: Midspan moment for single span bridges

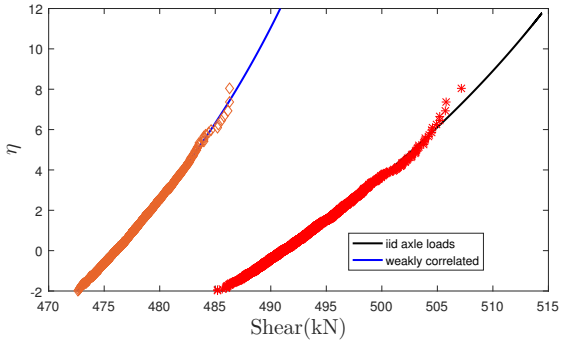

5m span bridge

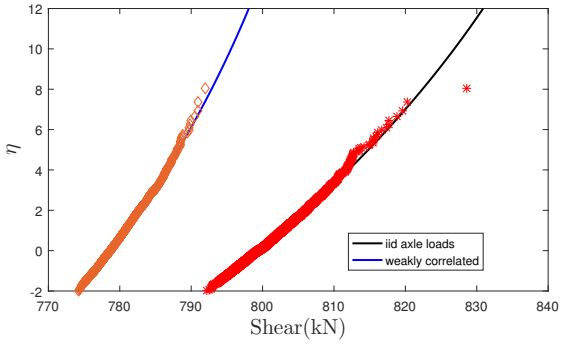

10m span bridge

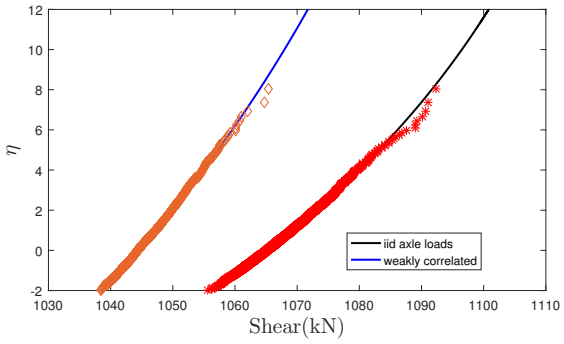

15m span bridge

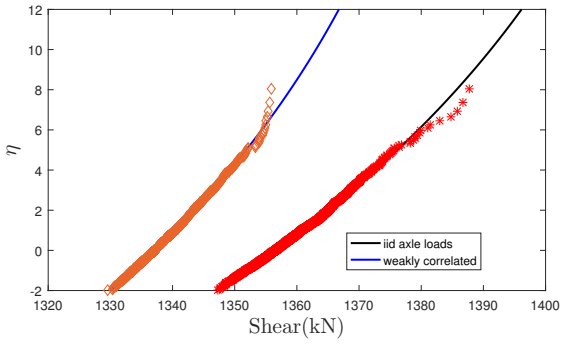

20m span bridge

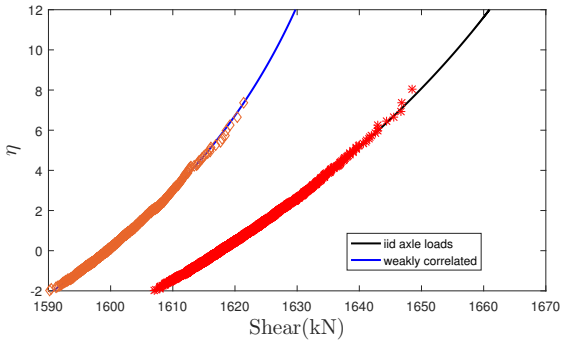

25m span bridge

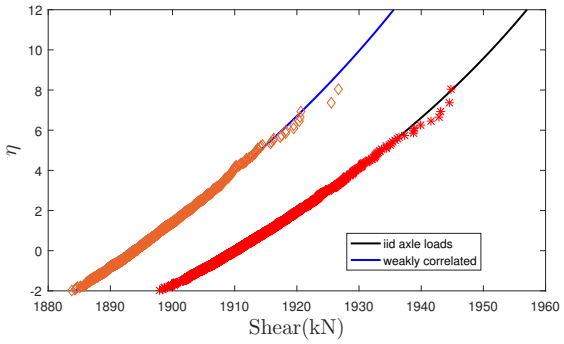

30m span bridge

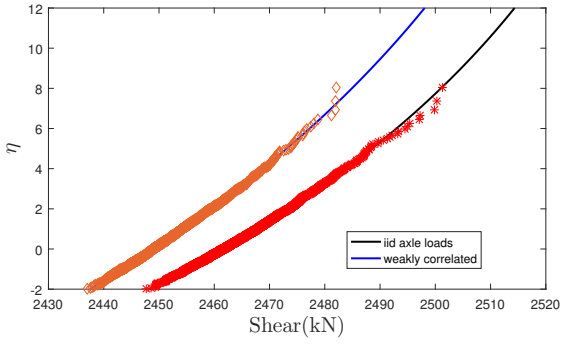

40m span bridge

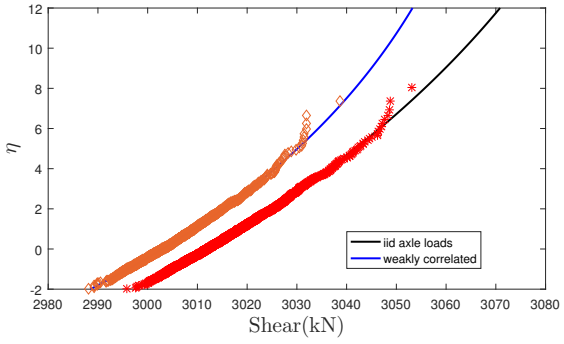

50m span bridge

Figure B.14: Support shear for single span bridges

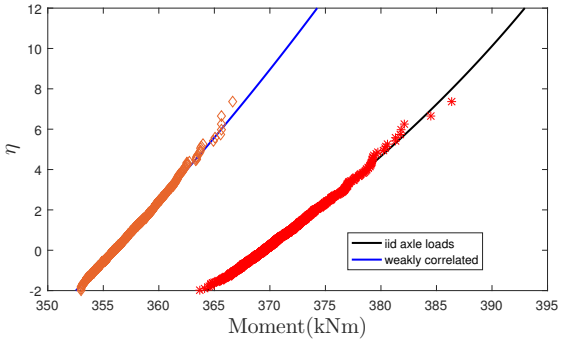

5m span bridge

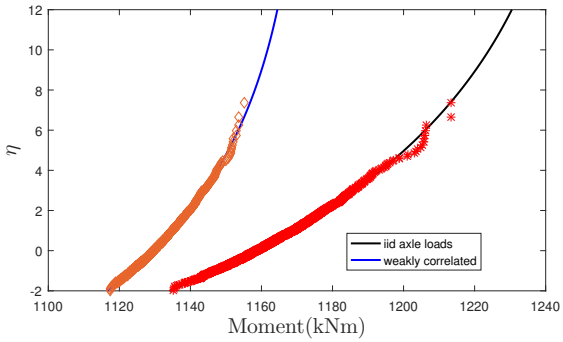

10m span bridge

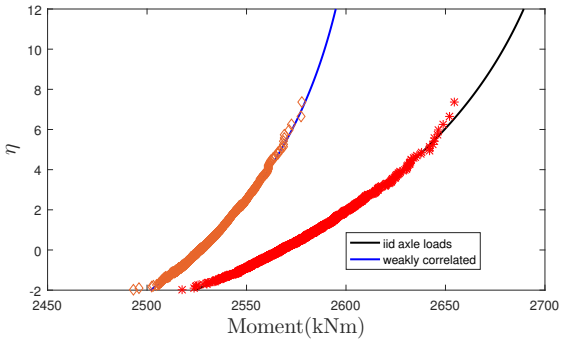

15m span bridge

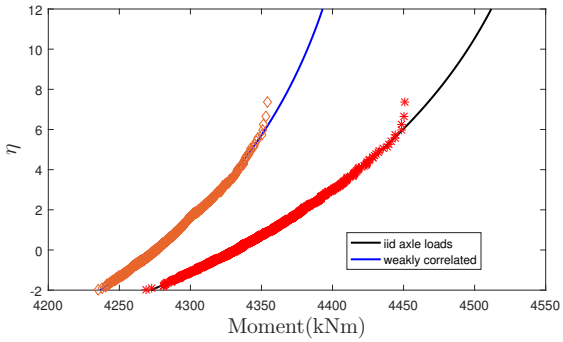

20m span bridge

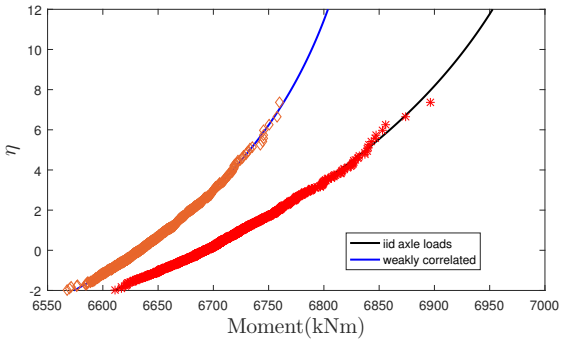

25m span bridge

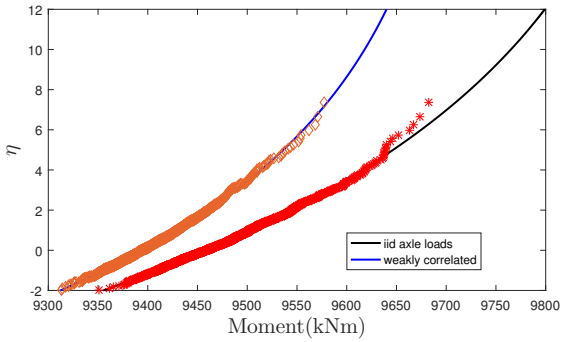

30m span bridge

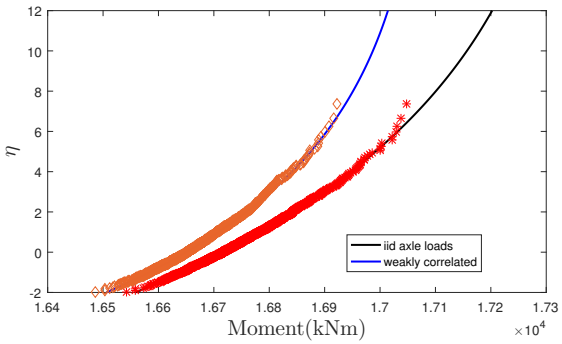

40m span bridge

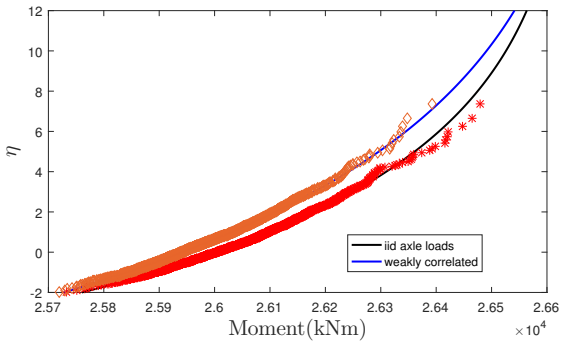

50m span bridge

Figure B.15: Midspan moment for 2 span continuous bridges

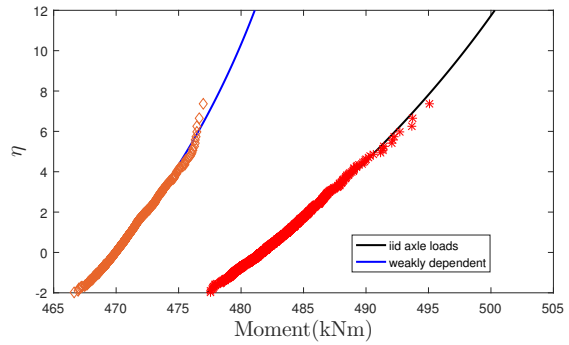

5m span bridge

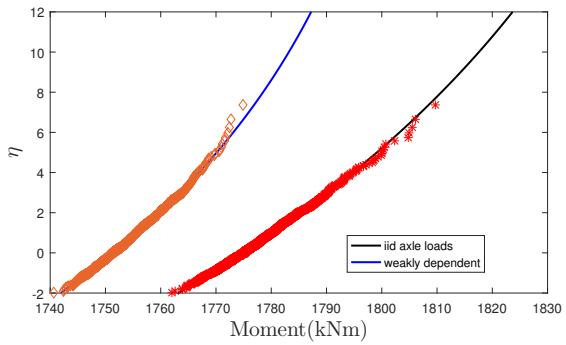

10m span bridge

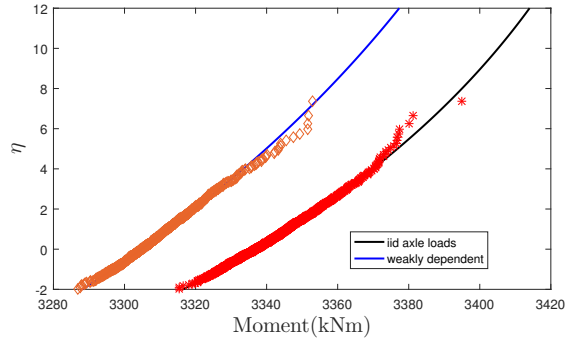

15m span bridge

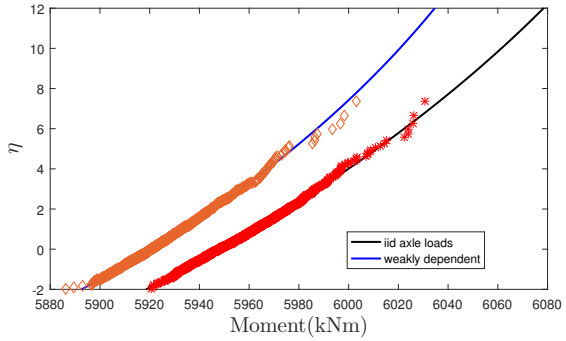

20m span bridge

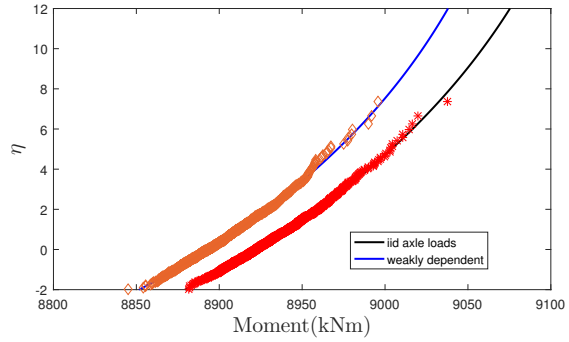

25m span bridge

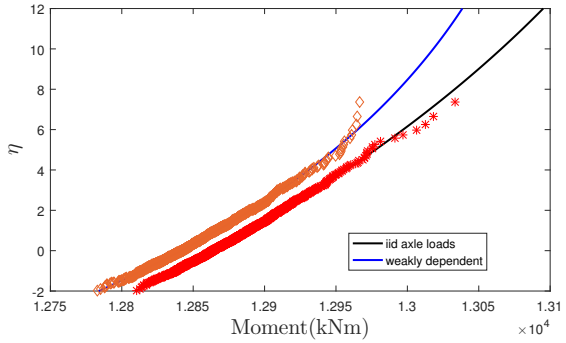

30m span bridge

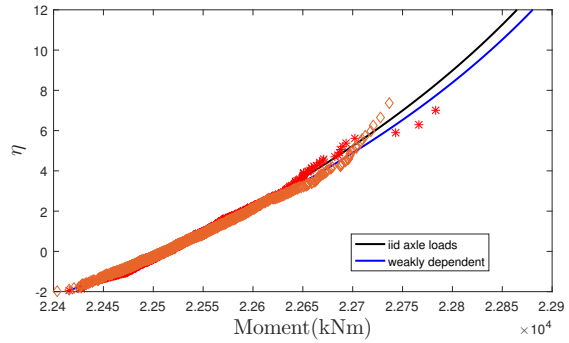

40m span bridge

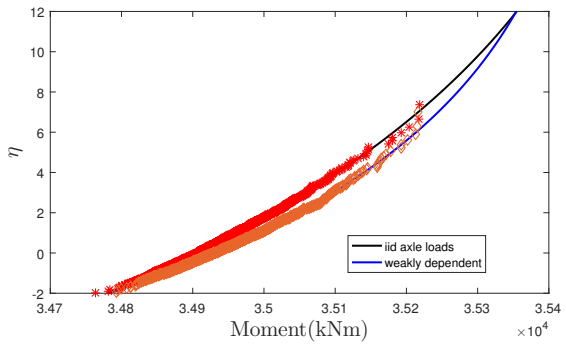

50m span bridge

Figure B.16: Interior support moment for 2 span continuous bridges

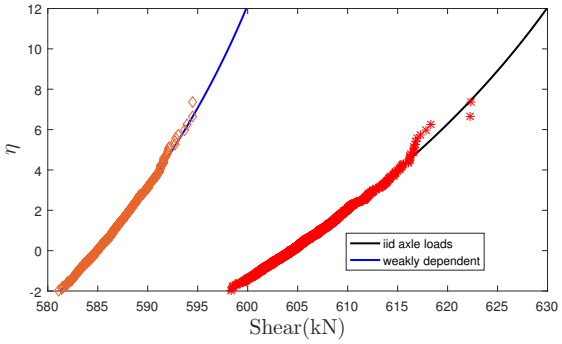

5m span bridge

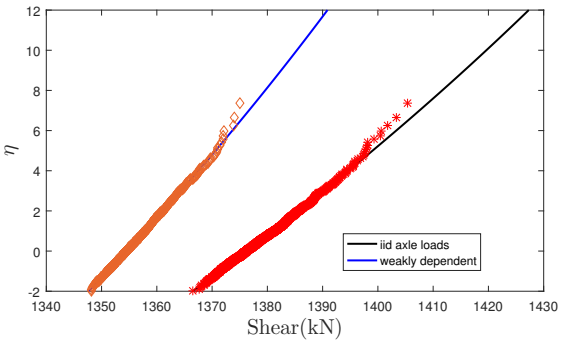

10m span bridge

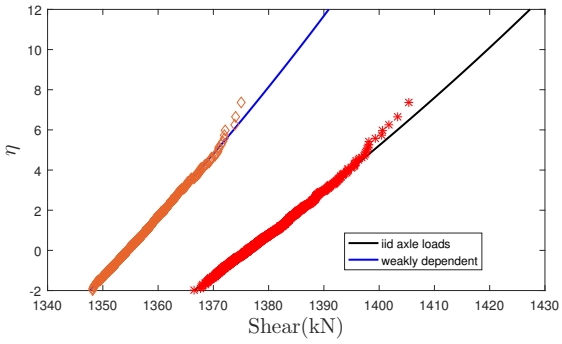

15m span bridge

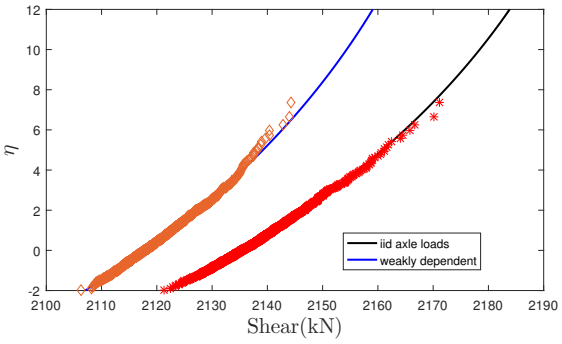

20m span bridge

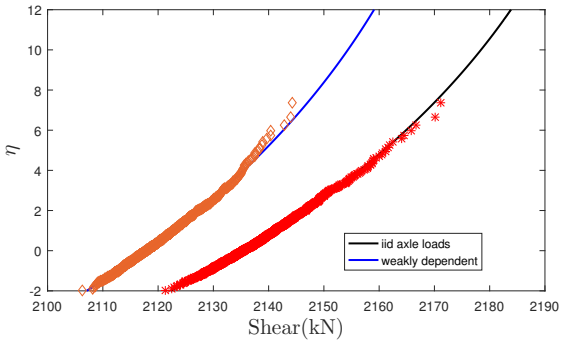

25m span bridge

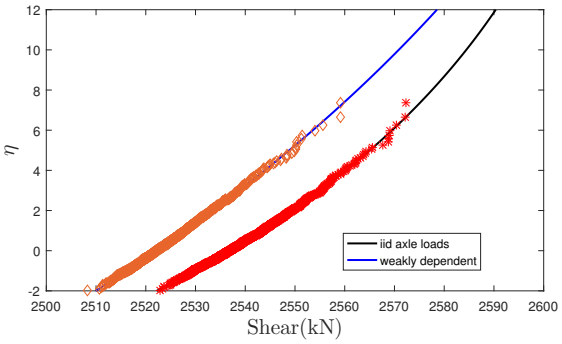

30m span bridge

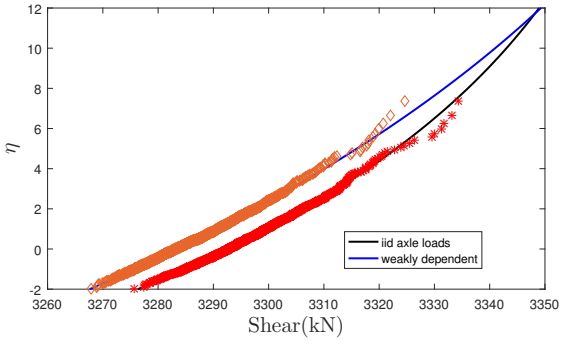

40m span bridge

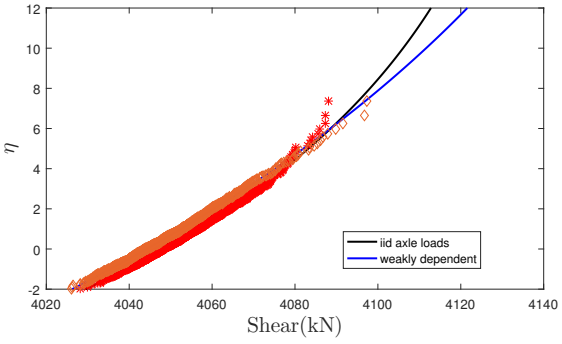

50m span bridge

Figure B.17: Interior support shear for 2 span continuous bridges

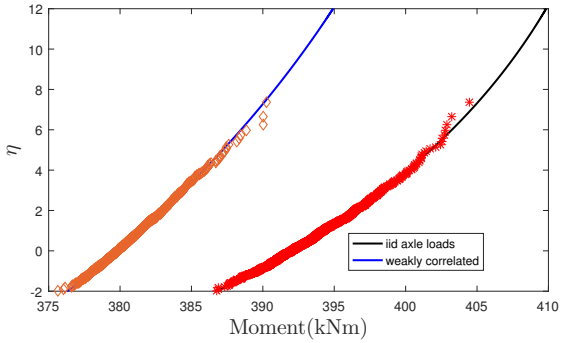

5m span bridge

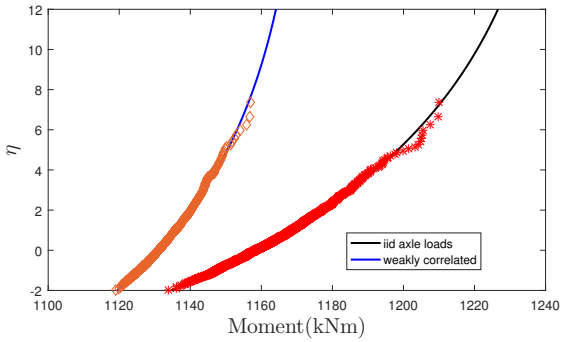

10m span bridge

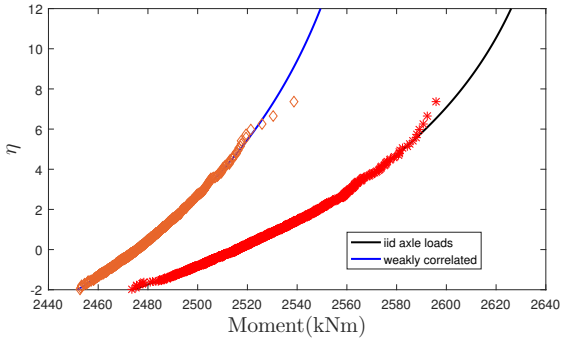

15m span bridge

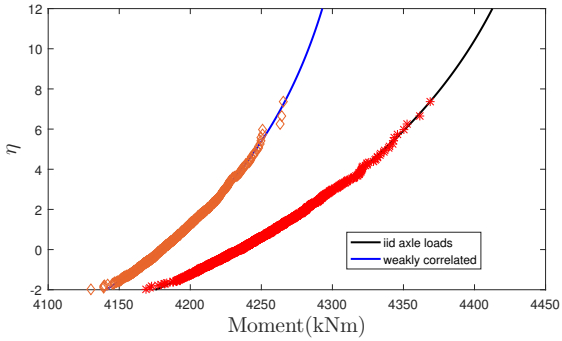

20m span bridge

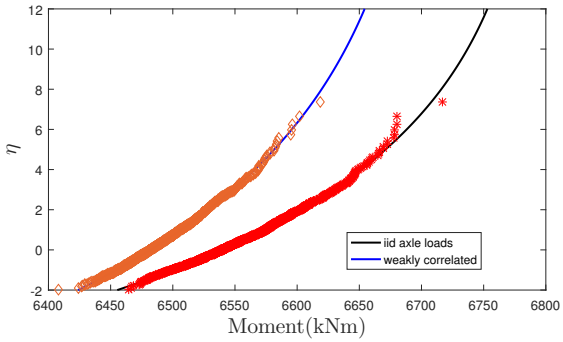

25m span bridge

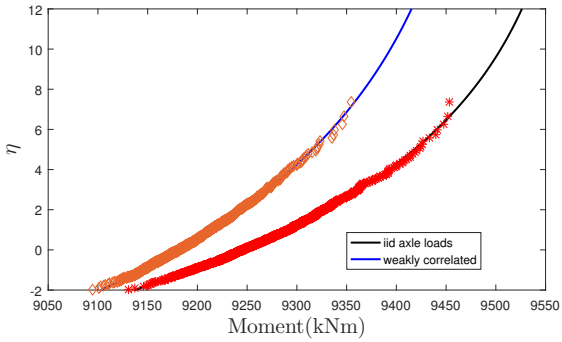

30m span bridge

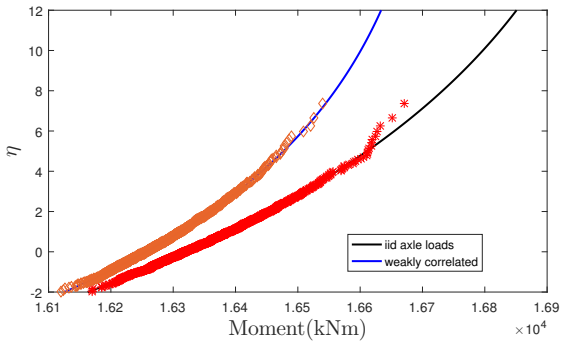

40m span bridge

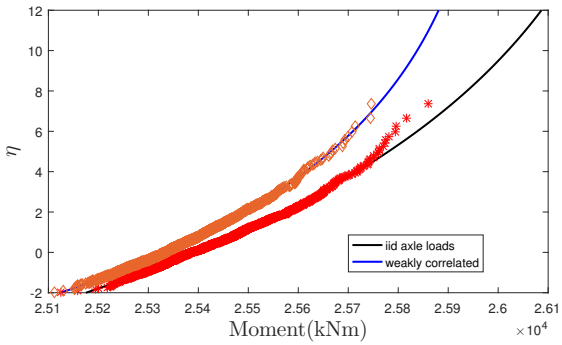

50m span bridge

Figure B.18: Midspan moment for 4 span continuous bridges

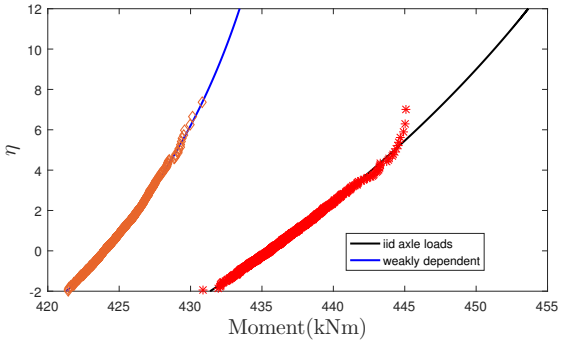

5m span bridge

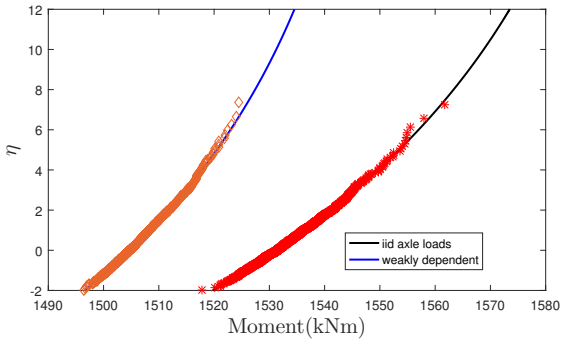

10m span bridge

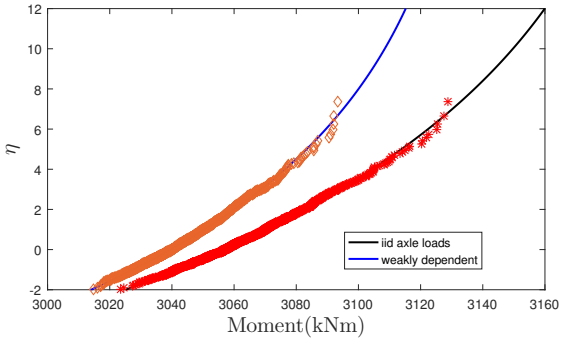

15m span bridge

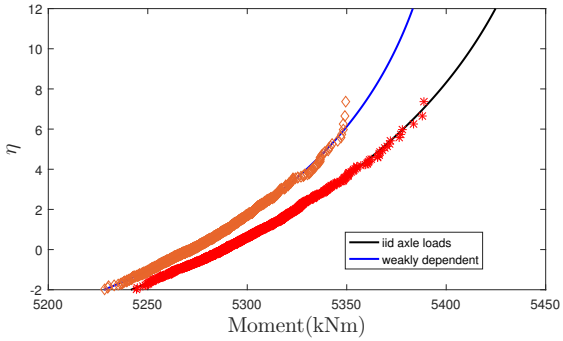

20m span bridge

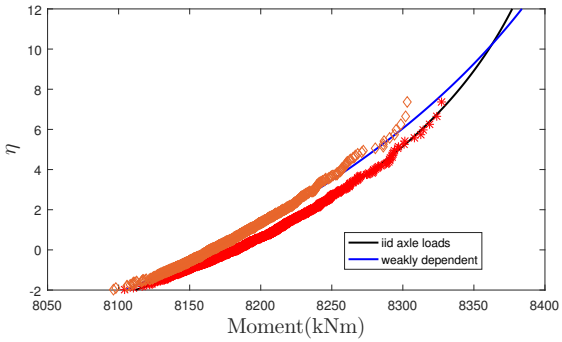

25m span bridge

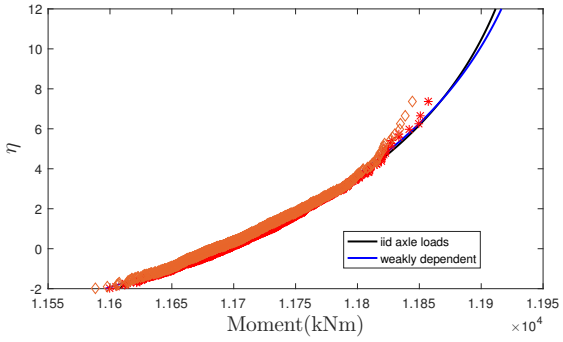

30m span bridge

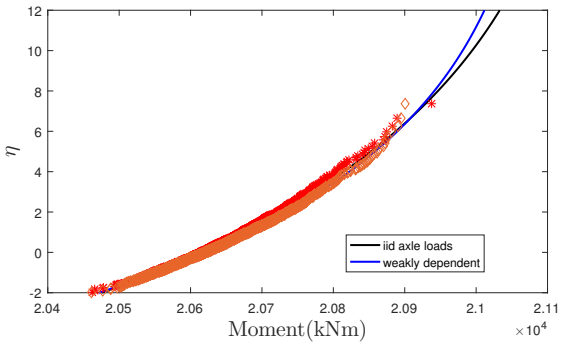

40m span bridge

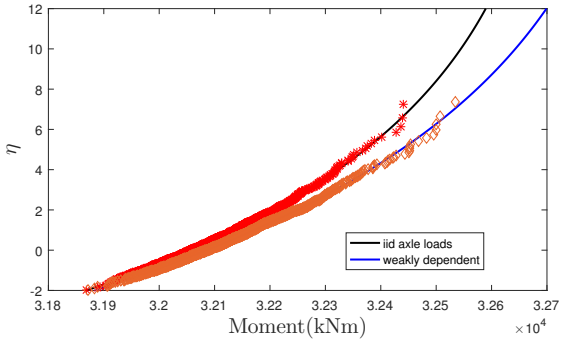

50m span bridge

Figure B.19: Interior support moment for 4 span continuous bridges

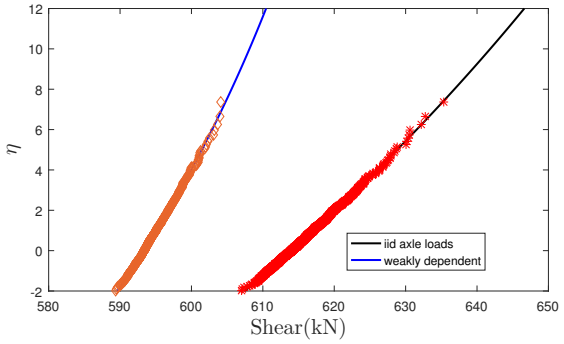

5m span bridge

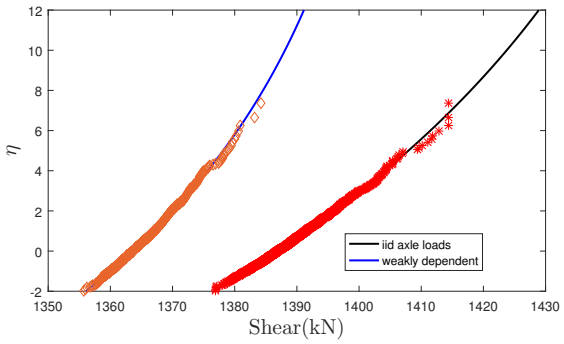

10m span bridge

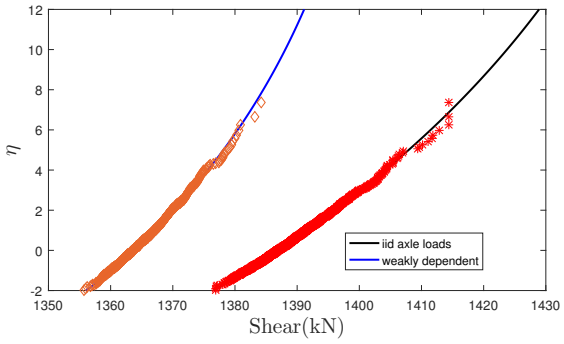

15m span bridge

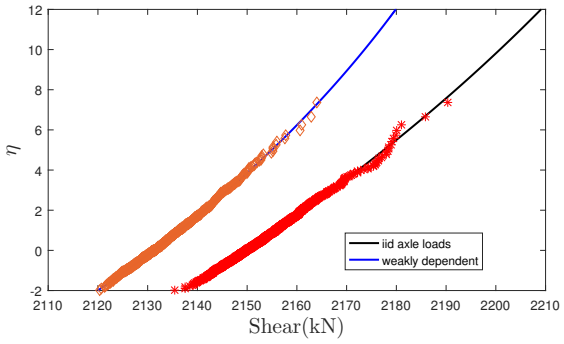

20m span bridge

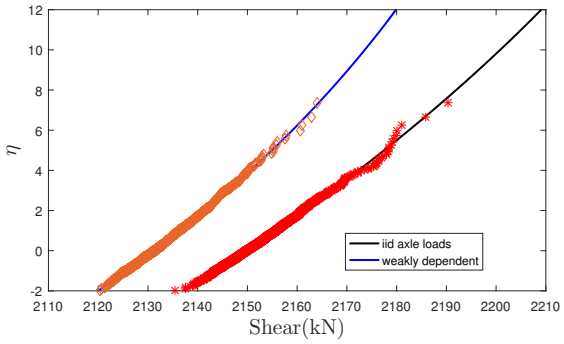

25m span bridge

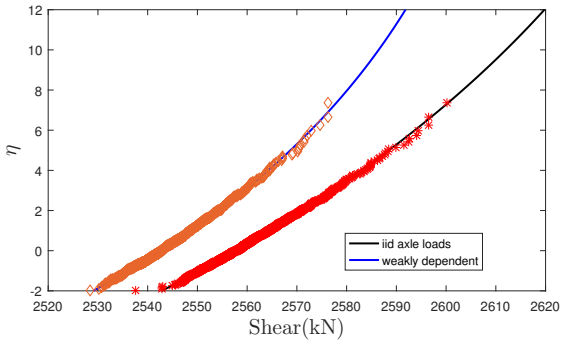

30m span bridge

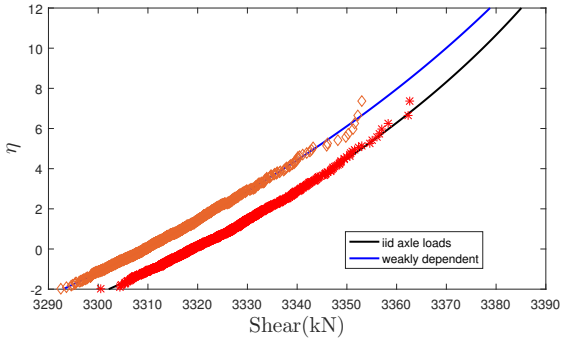

40m span bridge

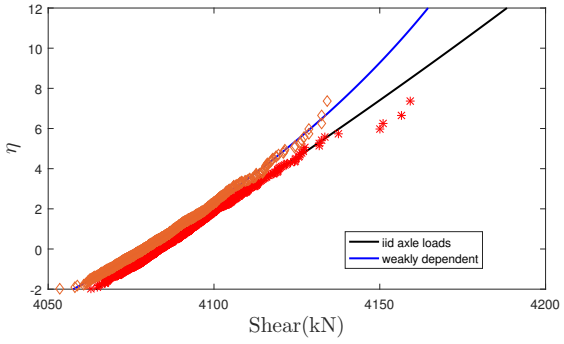

50m span bridge

Figure B.20: Interior support shear for 4 span continuous bridges

Appendix C

ASSESSMENT LOADS UNDER INCREASING TRAFFIC VOLUMES

C.1 Spatial dependence loading cases

The figures show the variation of computed GEV parameters as traffic volumes are increased at 4% per annum.

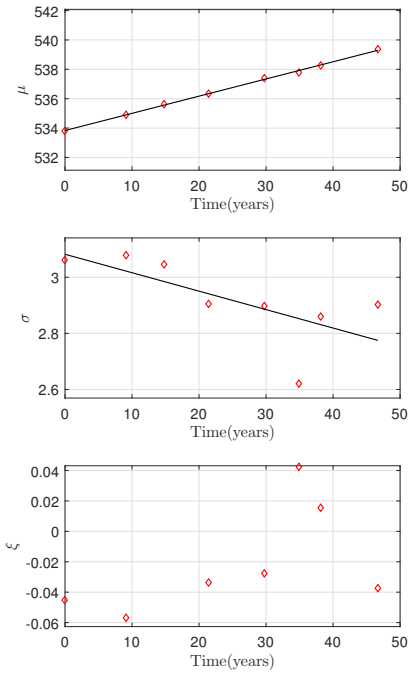

5m beam (Midspan moment)

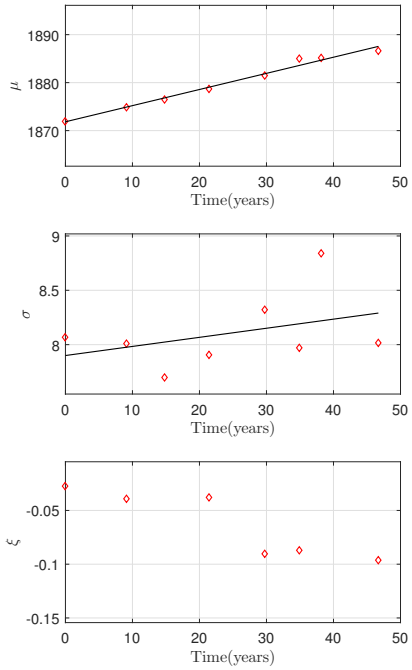

10m beam (Midspan moment)

Figure C.1: Parameter changes for 5m and 10m simply supported beam due to 4% annual traffic growth

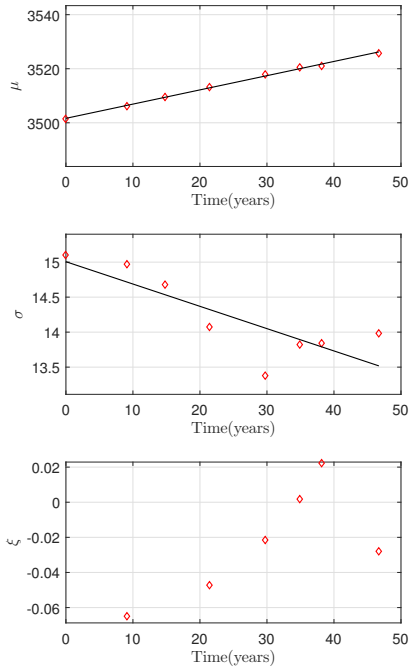

15m beam (Midspan moment)

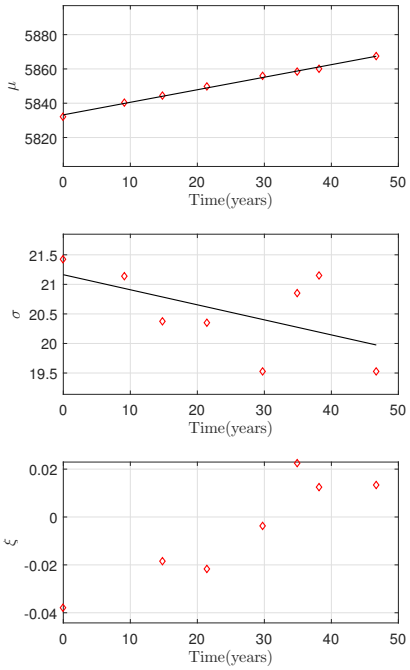

20m beam (Midspan moment)

Figure C.2: Parameter changes for 15m and 20m simply supported beam due to 4% annual traffic growth

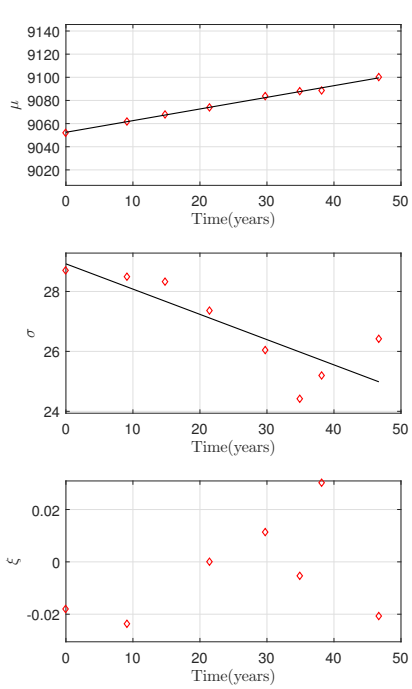

25m beam (Midspan moment)

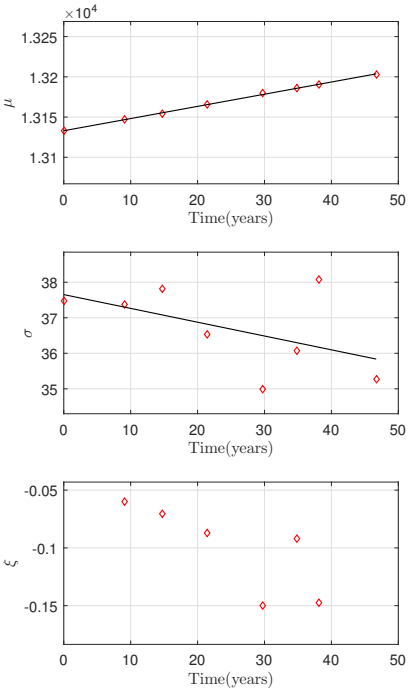

30m beam (Midspan moment)

Figure C.3: Parameter changes for 25m and 30m simply supported beam due to 4% annual traffic growth

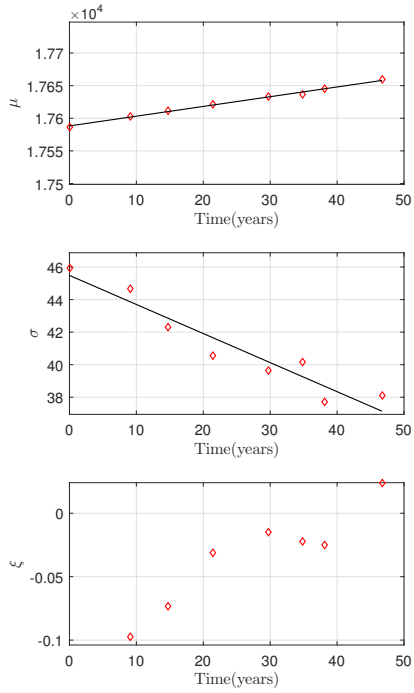

35m beam (Midspan moment)

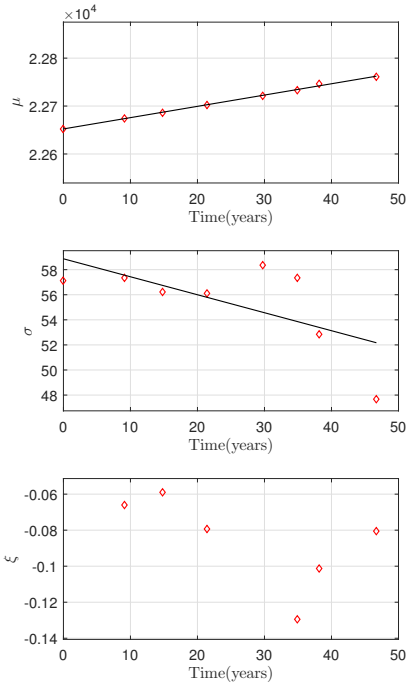

40m beam (Midspan moment)

Figure C.4: Parameter changes for 35m and 40m simply supported beam due to 4% annual traffic growth

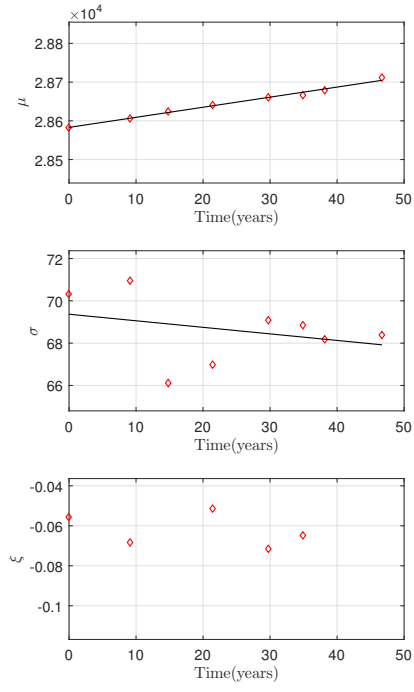

45m beam (Midspan moment)

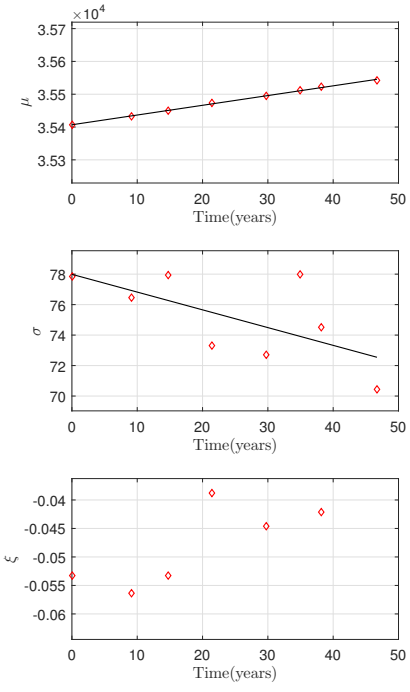

50m beam (Midspan moment)

Figure C.5: Parameter changes for 45m and 50m simply supported beam due to 4% annual traffic growth

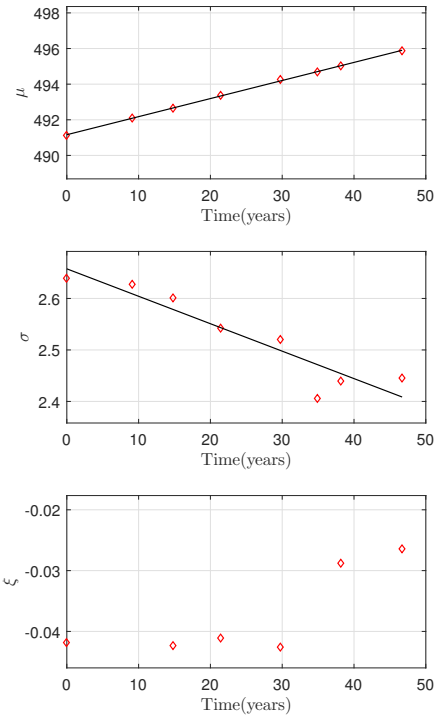

5m beam (Support shear)

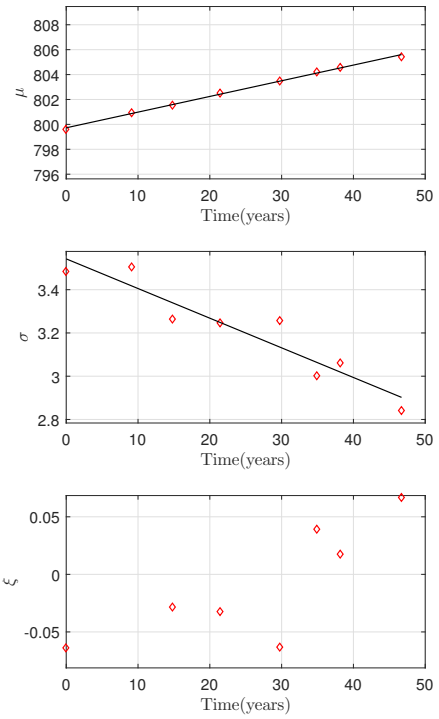

10m beam (Support shear)

Figure C.6: Parameter changes for 5m and 10m simply supported beam due to 4% annual traffic growth

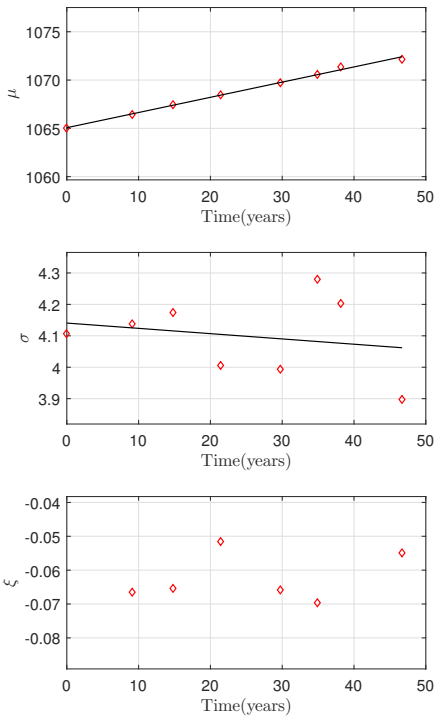

15m beam (Support shear)

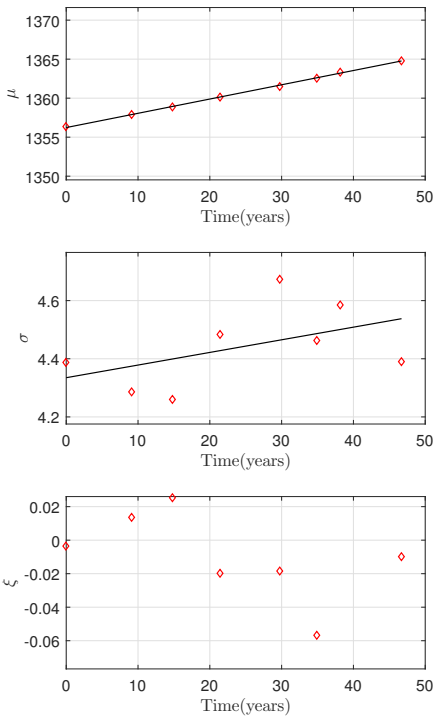

20m beam (Support shear)

Figure C.7: Parameter changes for 15m and 20m simply supported beam due to 4% annual traffic growth

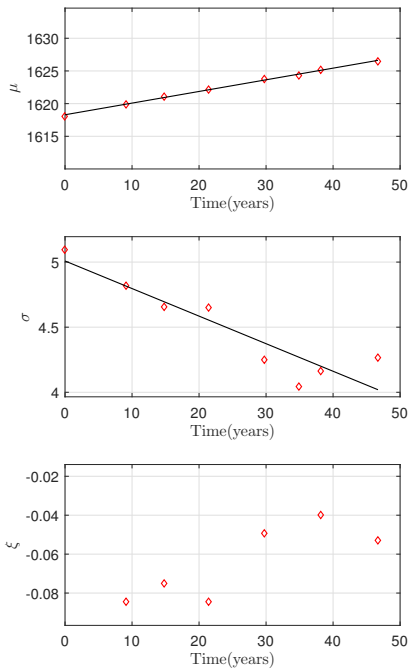

25m beam (Support shear)

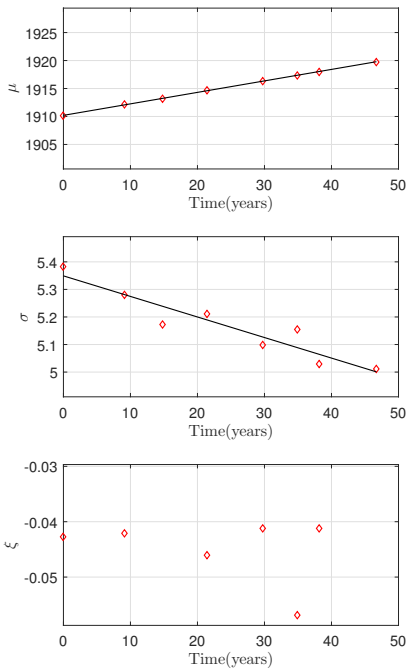

30m beam (Support shear)

Figure C.8: Parameter changes for 25m and 30m simply supported beam due to 4% annual traffic growth

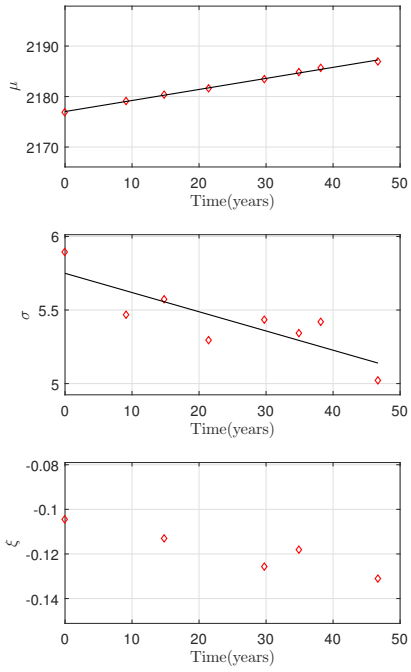

35m beam (Support shear)

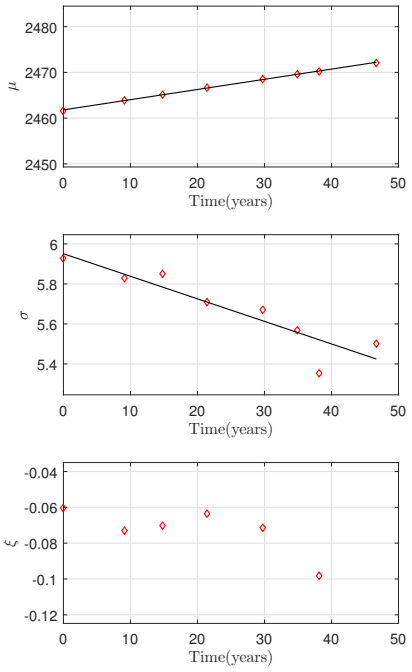

40m beam (Support shear)

Figure C.9: Parameter changes for 35m and 40m simply supported beam due to 4% annual traffic growth

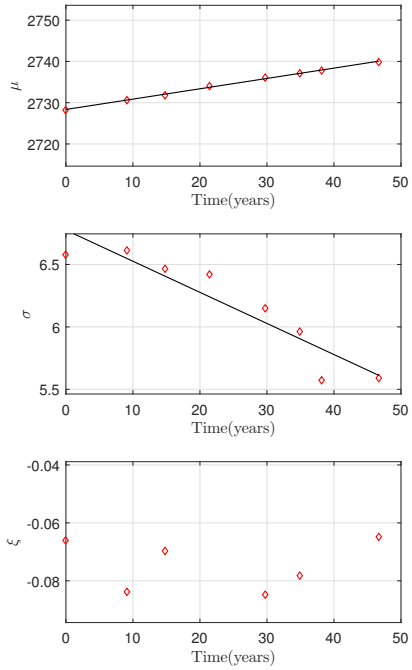

45m beam (Support shear)

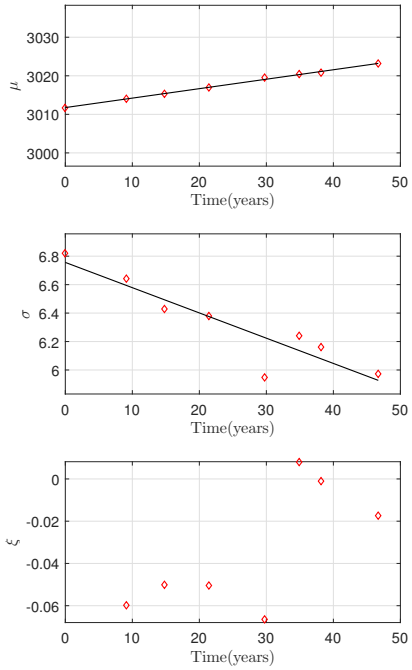

50m beam (Support shear)

Figure C.10: Parameter changes for 45m and 50m simply supported beam due to 4% annual traffic growth

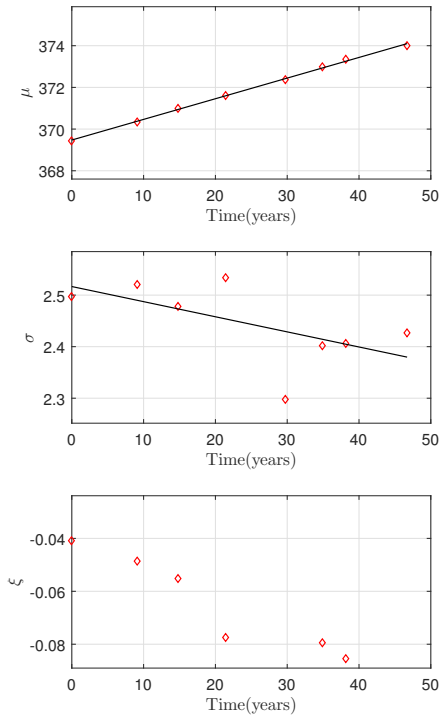

5m span (Midspan moment)

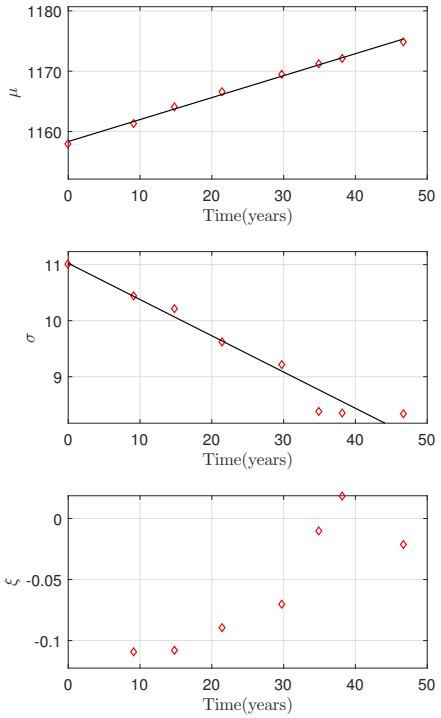

10m span (Midspan moment)

Figure C.11: Parameter changes for 2 span continuous beam due to 4% annual traffic growth

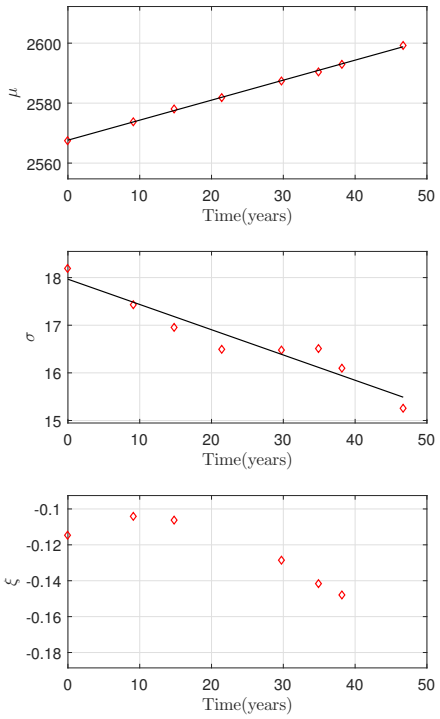

15m span (Midspan moment)

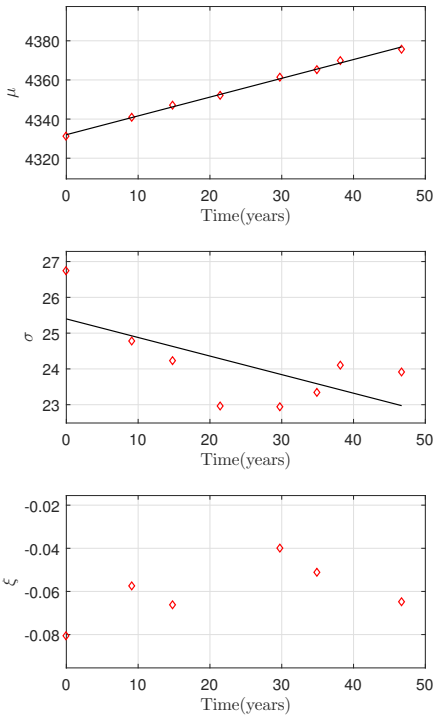

20m span (Midspan moment)

Figure C.12: Parameter changes for 2 span continuous beam due to 4% annual traffic growth

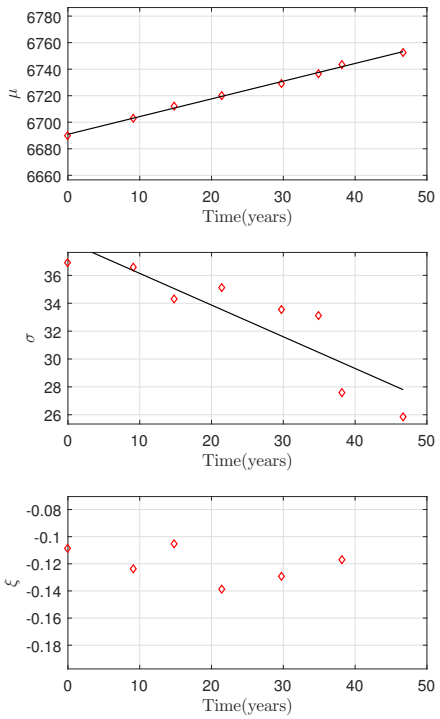

25m span (Midspan moment)

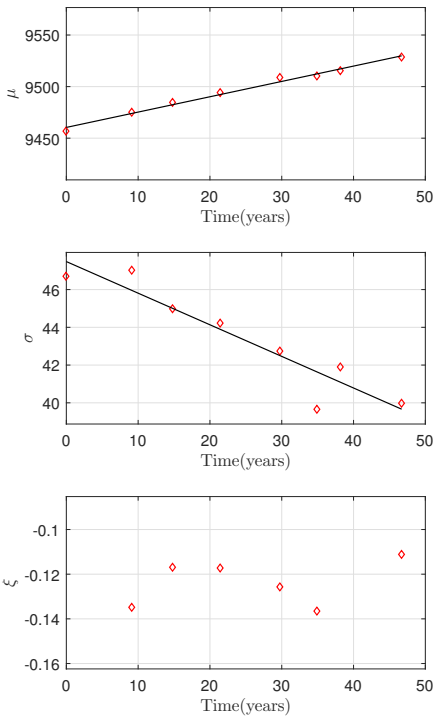

30m span (Midspan moment)

Figure C.13: Parameter changes for 2 span continuous beam due to 4% annual traffic growth

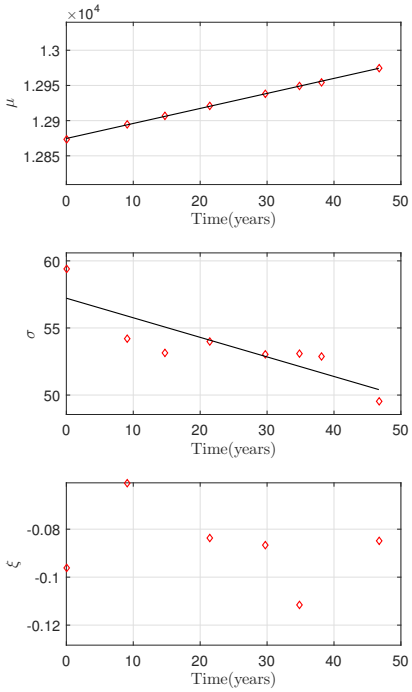

35m span (Midspan moment)

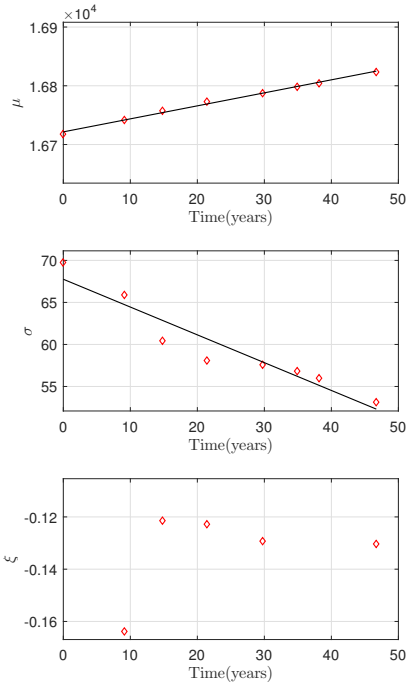

40m span (Midspan moment)

Figure C.14: Parameter changes for 2 span continuous beam due to 4% annual traffic growth

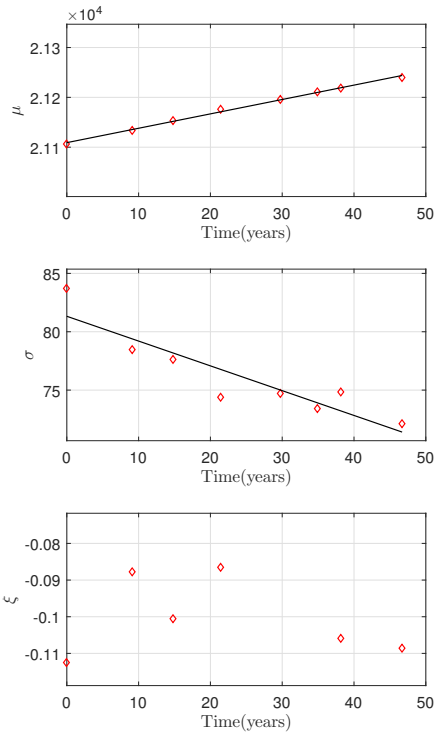

45m span (Midspan moment)

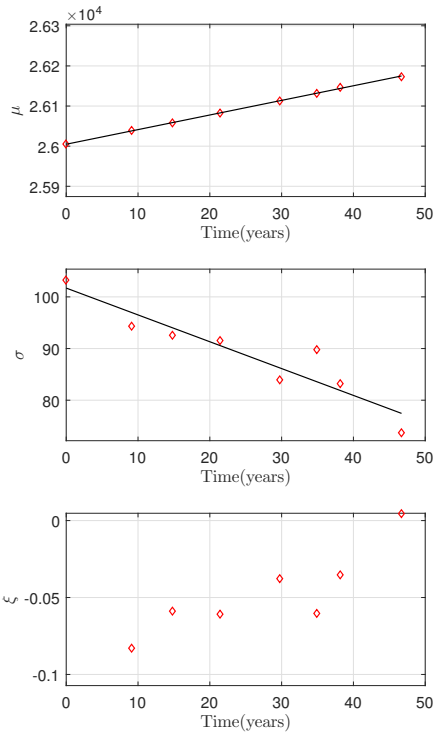

50m span (Midspan moment)

Figure C.15: Parameter changes for 2 span continuous beam due to 4% annual traffic growth

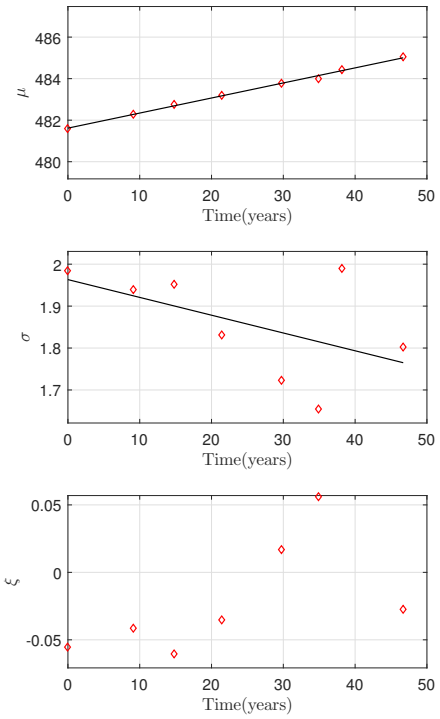

5m span (Support moment)

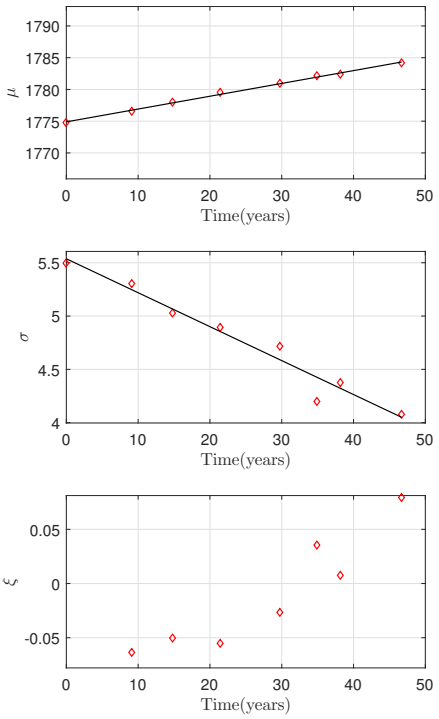

10m span (Support moment)

Figure C.16: Parameter changes for 2 span continuous beam due to 4% annual traffic growth

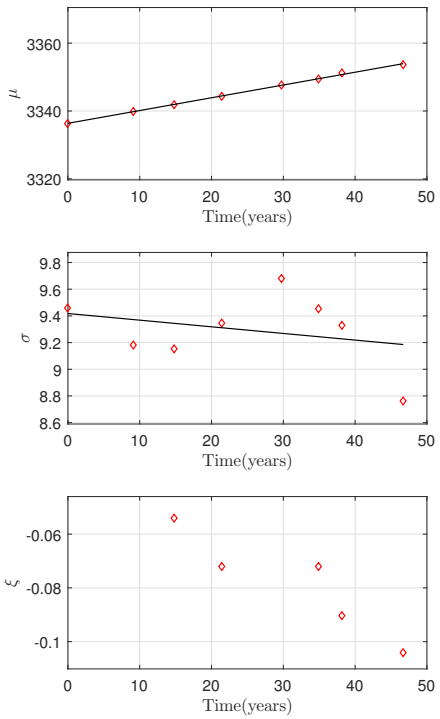

15m span (Support moment)

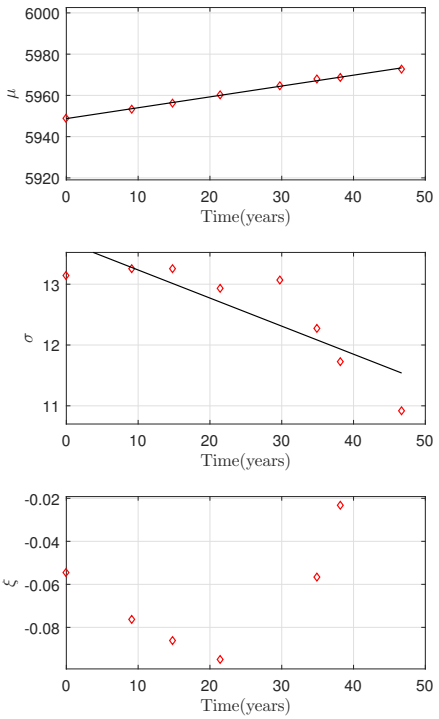

20m span (Support moment)

Figure C.17: Parameter changes for 2 span continuous beam due to 4% annual traffic growth

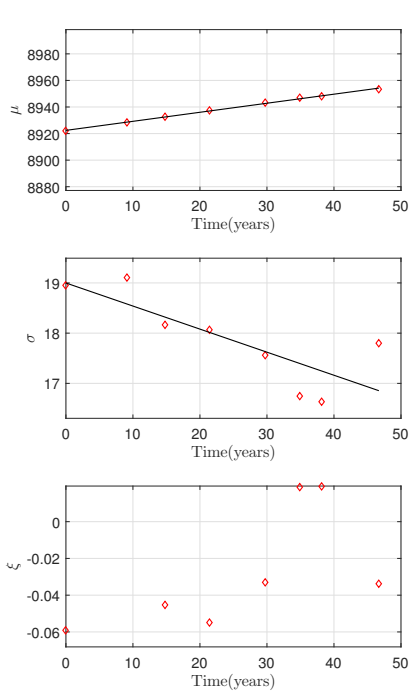

25m span (Support moment)

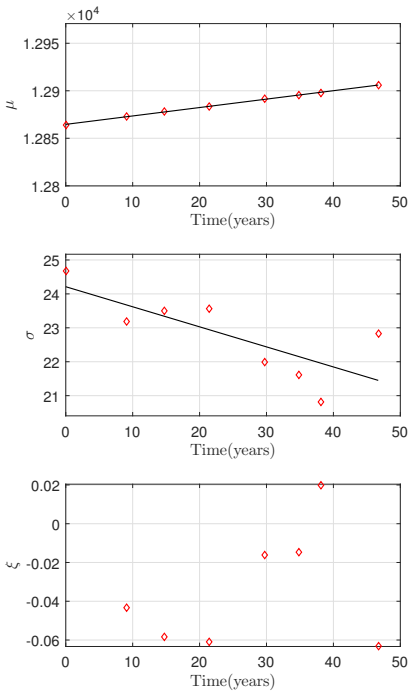

30m span (Support moment)

Figure C.18: Parameter changes for 2 span continuous beam due to 4% annual traffic growth

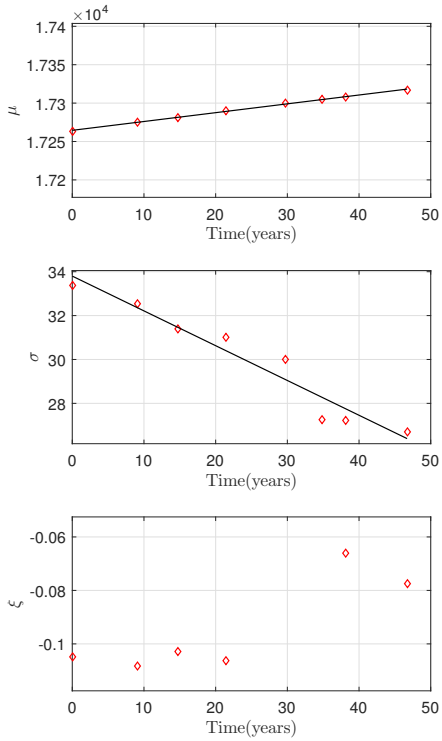

35m span (Support moment)

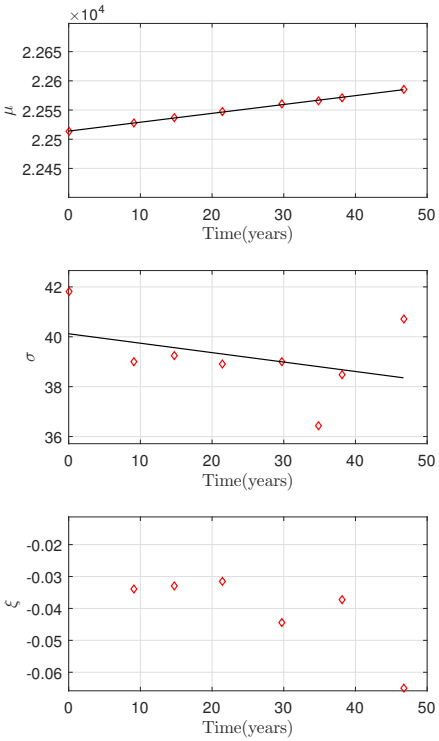

40m span (Support moment)

Figure C.19: Parameter changes for 2 span continuous beam due to 4% annual traffic growth

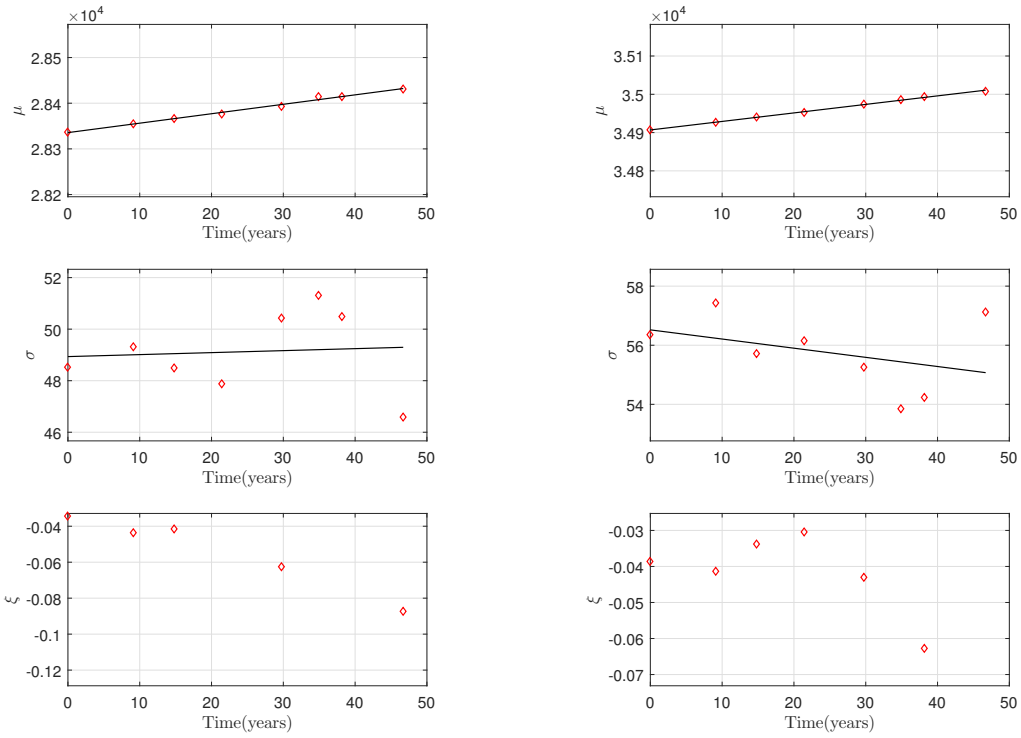

45m span (Support moment) 50m span (Support moment)

Figure C.20: Parameter changes for 2 span continuous beam due to 4% annual traffic growth

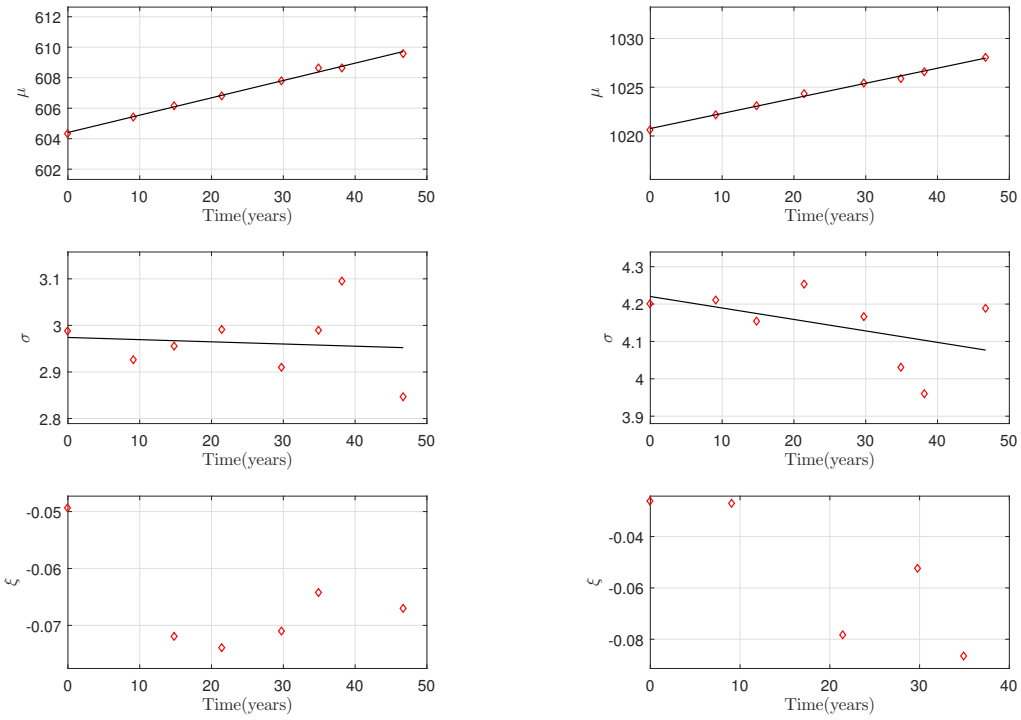

5m span (Support shear) 10m span (Support shear)

Figure C.21: Parameter changes for 2 span continuous beam

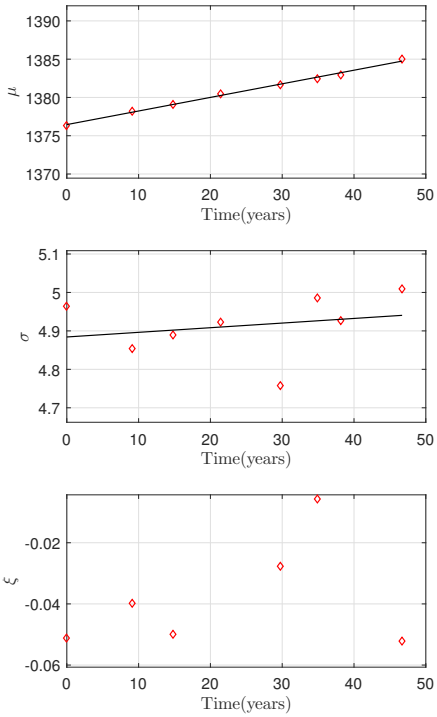

15m span (Support shear)

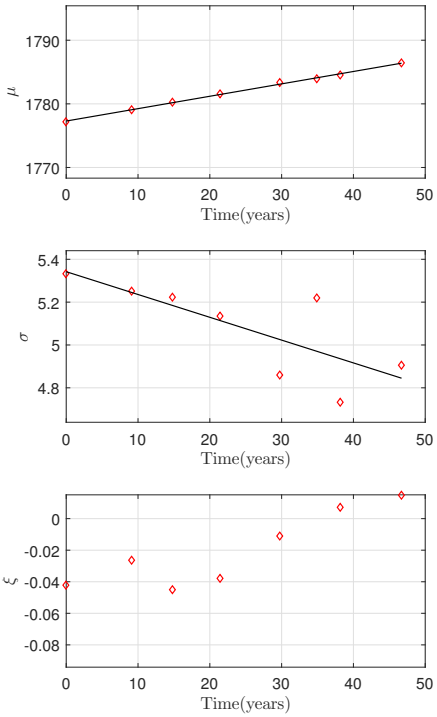

20m span (Support shear)

Figure C.22: GEV Parameter changes for 2 span continuous beam due to 4% annual traffic growth

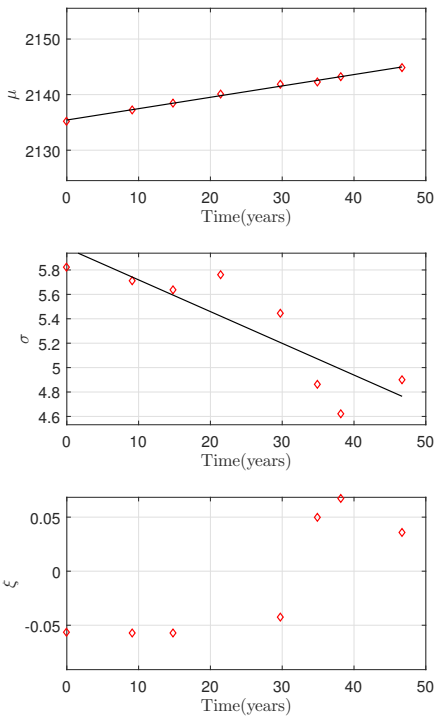

25m span (Support shear)

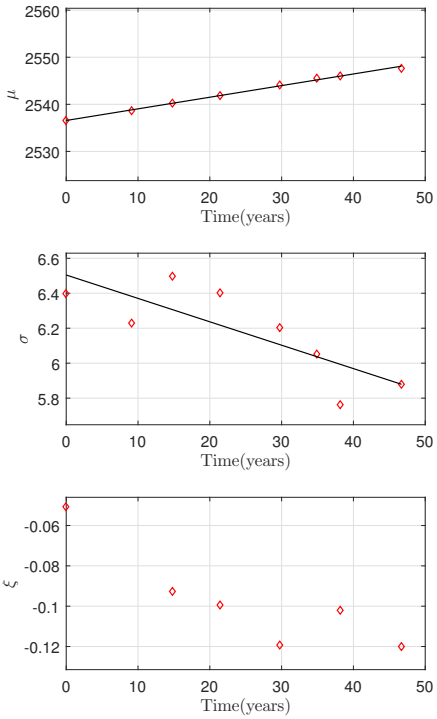

30m span (Support shear)

Figure C.23: GEV Parameter changes for 2 span continuous beam due to 4% annual traffic growth

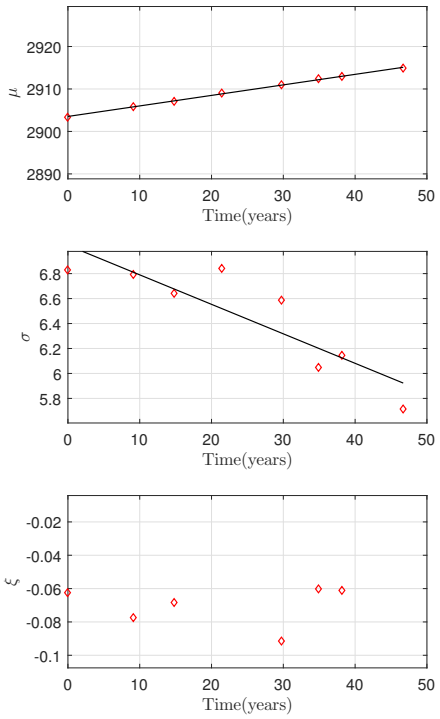

35m span (Support shear)

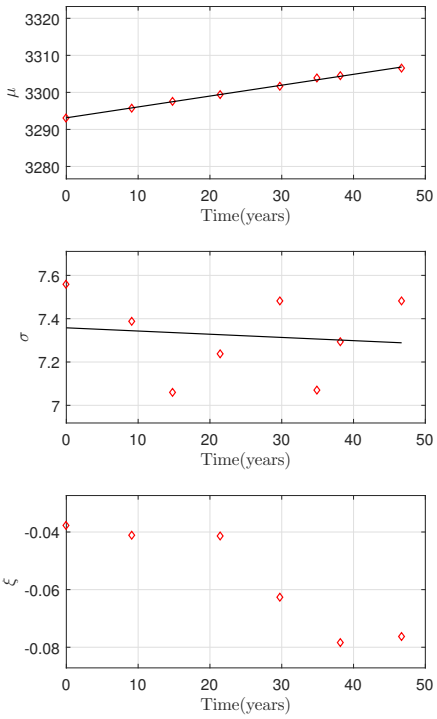

40m span (Support shear)

Figure C.24: GEV Parameter changes for 2 span continuous beam due to 4% annual traffic growth

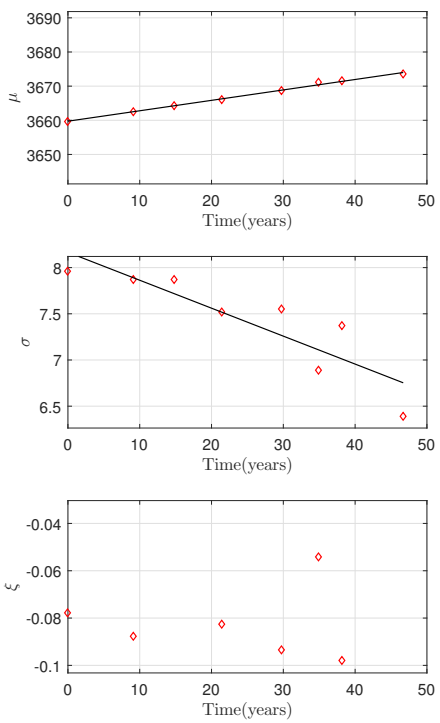

45m span (Support shear)

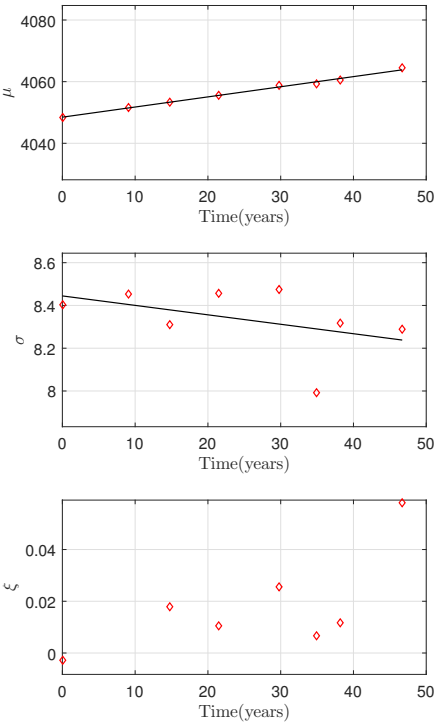

50m span (Support shear)

Figure C.25: GEV Parameter changes for 2 span continuous beam due to 4% annual traffic growth

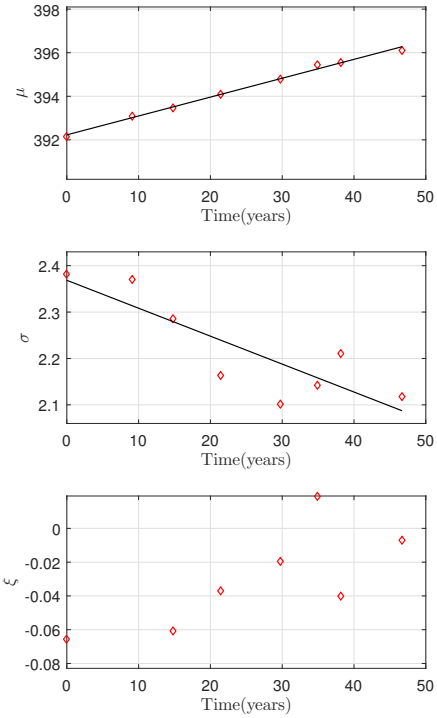

5m span (Midspan moment)

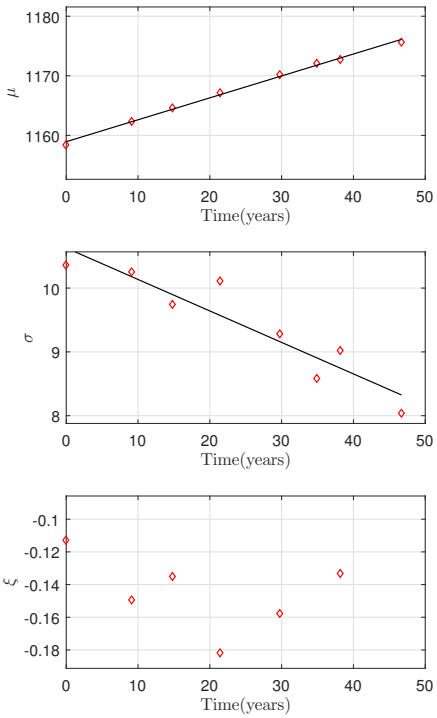

10m span (Midspan moment)

Figure C.26: GEV Parameter changes for 4 span continuous beam

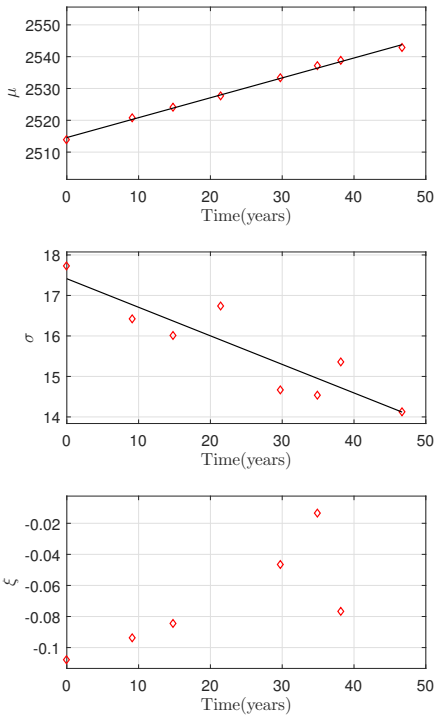

15m span (Midspan moment)

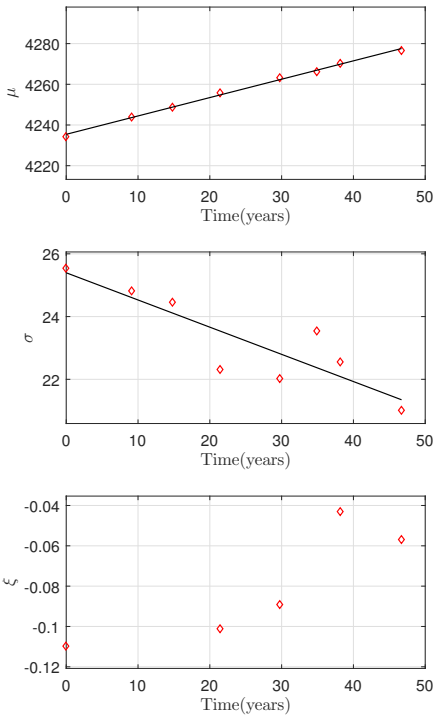

20m span (Midspan moment)

Figure C.27: GEV Parameter changes for 4 span continuous beam due to 4% annual traffic growth

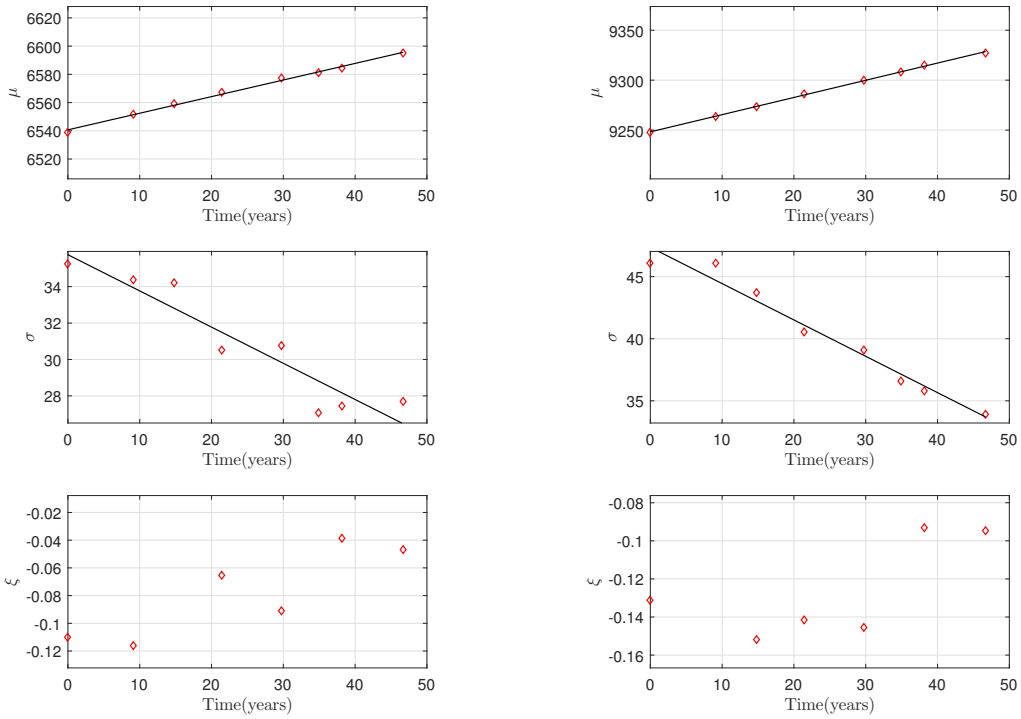

25m span (Midspan moment) 30m span (Midspan moment)

Figure C.28: GEV Parameter changes for 4 span continuous beam due to 4% annual traffic growth

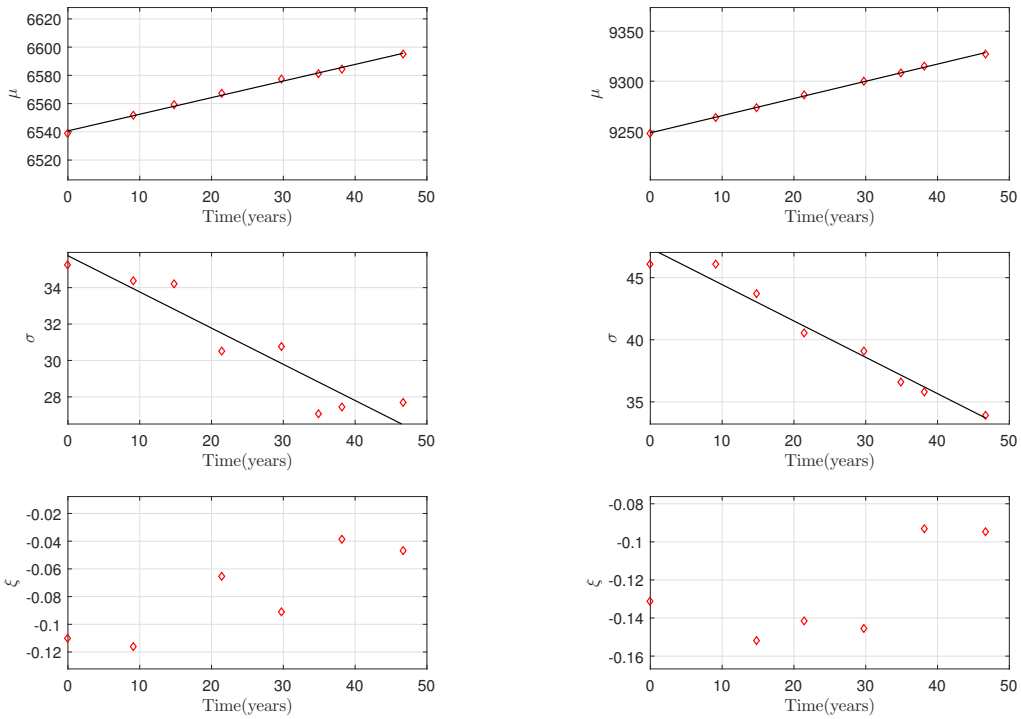

25m span (Midspan moment) 30m span (Midspan moment)

Figure C.29: GEV Parameter changes for 4 span continuous beam due to 4% annual traffic growth

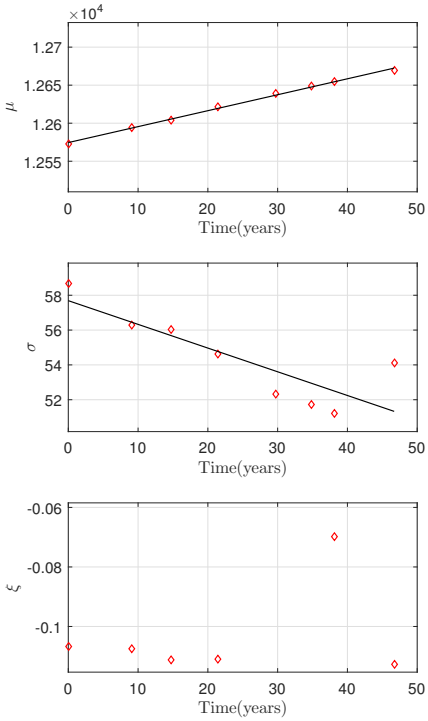

35m span (Midspan moment)

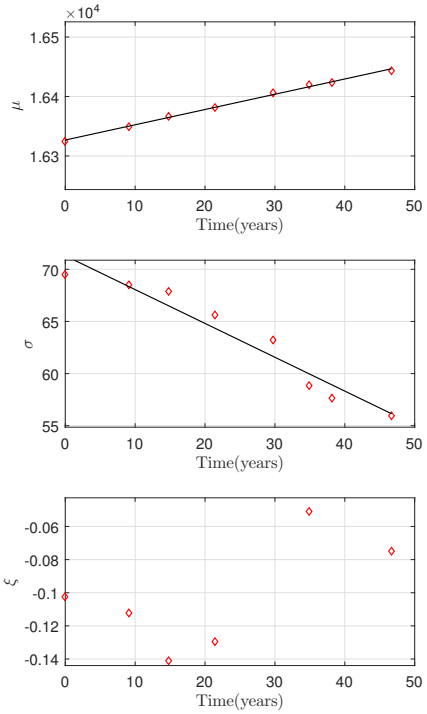

40m span (Midspan moment)

Figure C.30: GEV Parameter changes for 4 span continuous beam due to 4% annual traffic growth

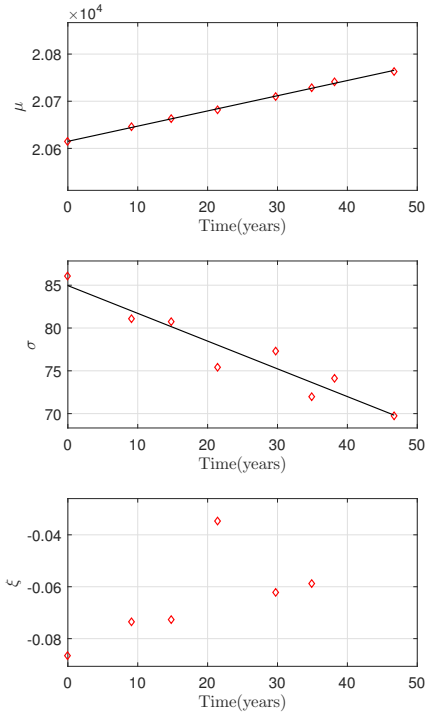

45m span (Midspan moment)

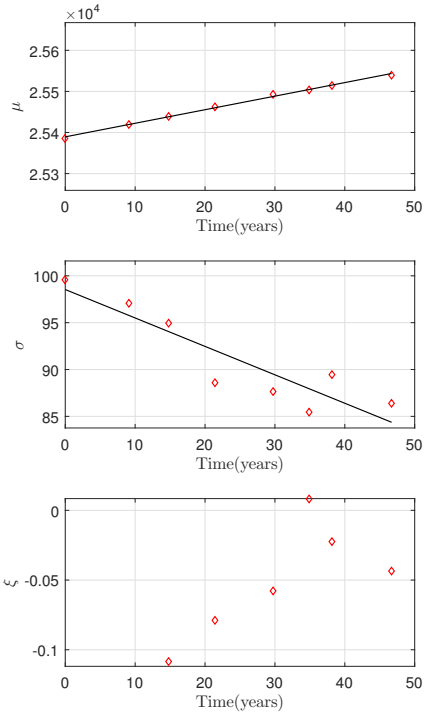

50m span (Midspan moment)

Figure C.31: GEV Parameter changes for 4 span continuous beam due to 4% annual traffic growth

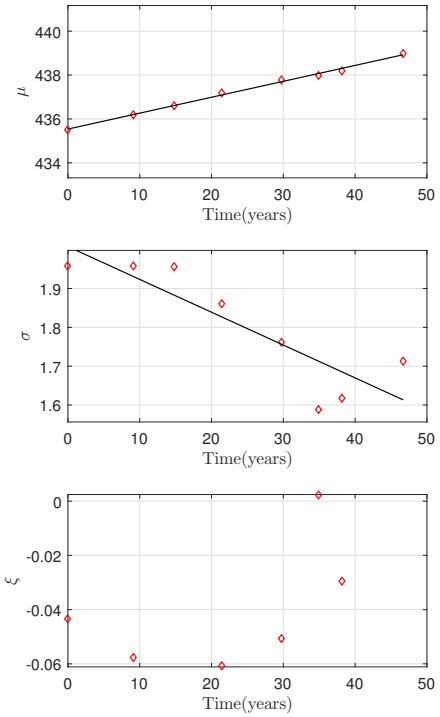

5m span (Support moment)

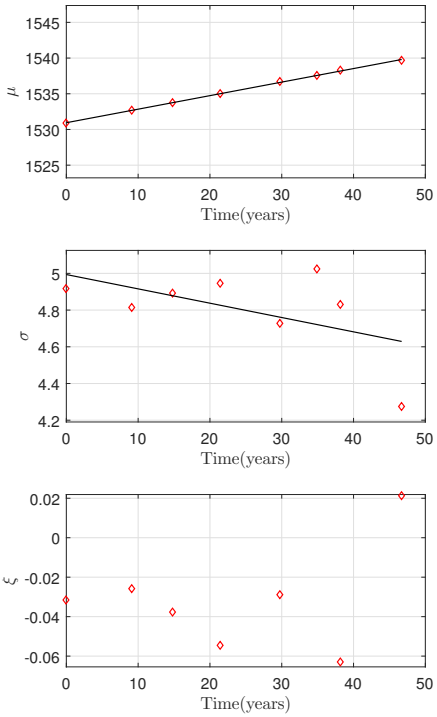

10m span (Support moment)

Figure C.32: GEV Parameter changes for 4 span continuous beam

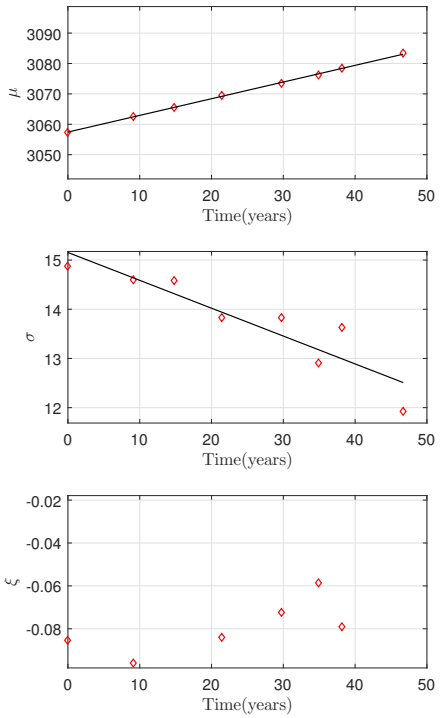

15m span (Support moment)

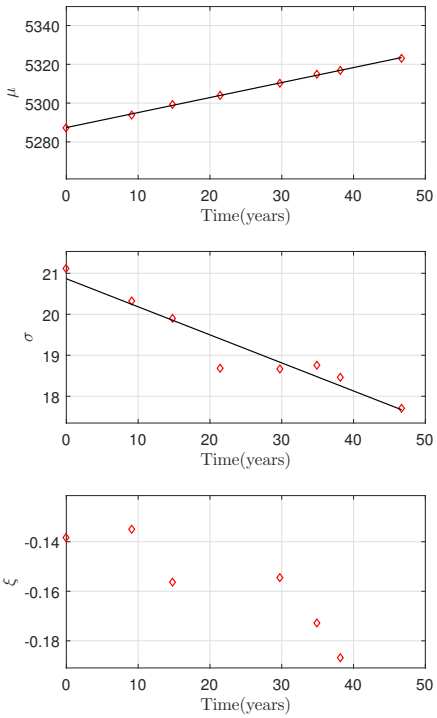

20m span (Support moment)

Figure C.33: GEV Parameter changes for 4 span continuous beam due to 4% annual traffic growth

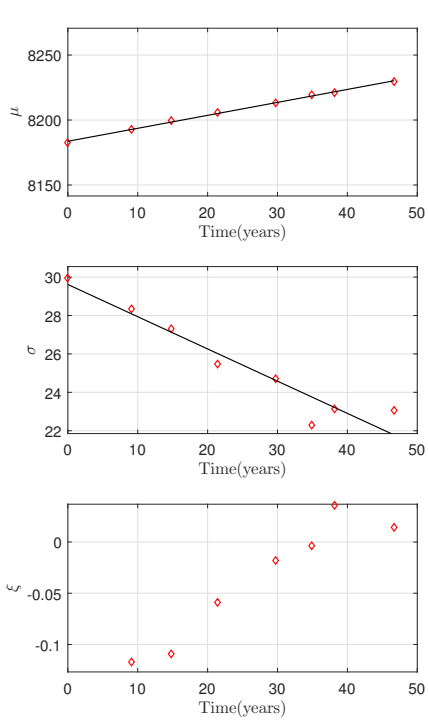

25m span (Support moment)

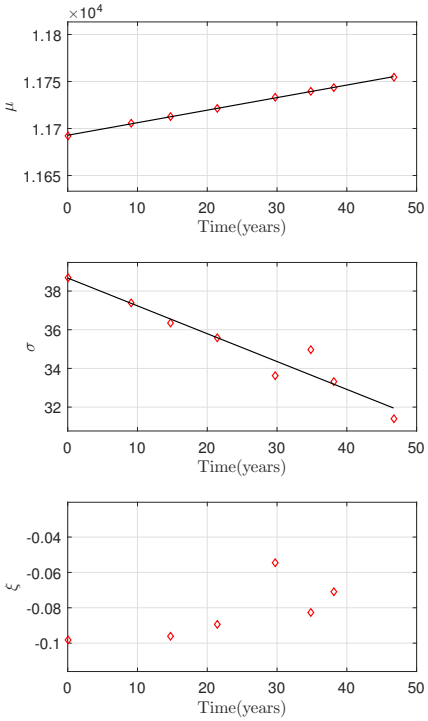

30m span (Support moment)

Figure C.34: GEV Parameter changes for 4 span continuous beam due to 4% annual traffic growth

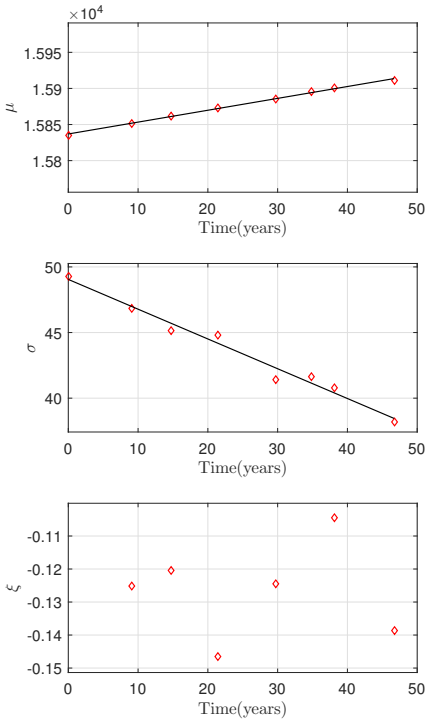

35m span (Support moment)

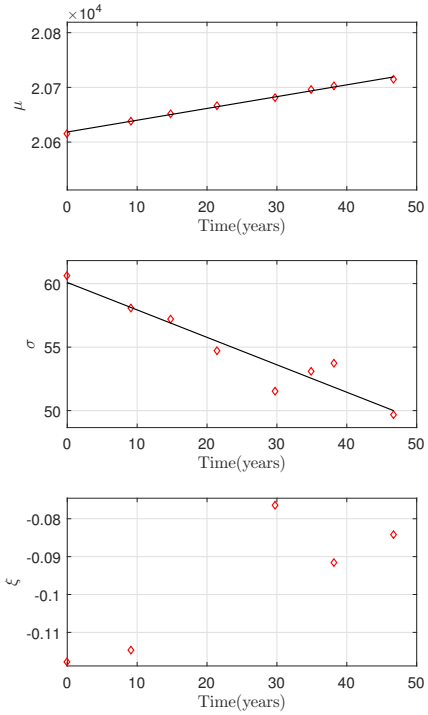

40m span (Support moment)

Figure C.35: GEV Parameter changes for 4 span continuous beam due to 4% annual traffic growth

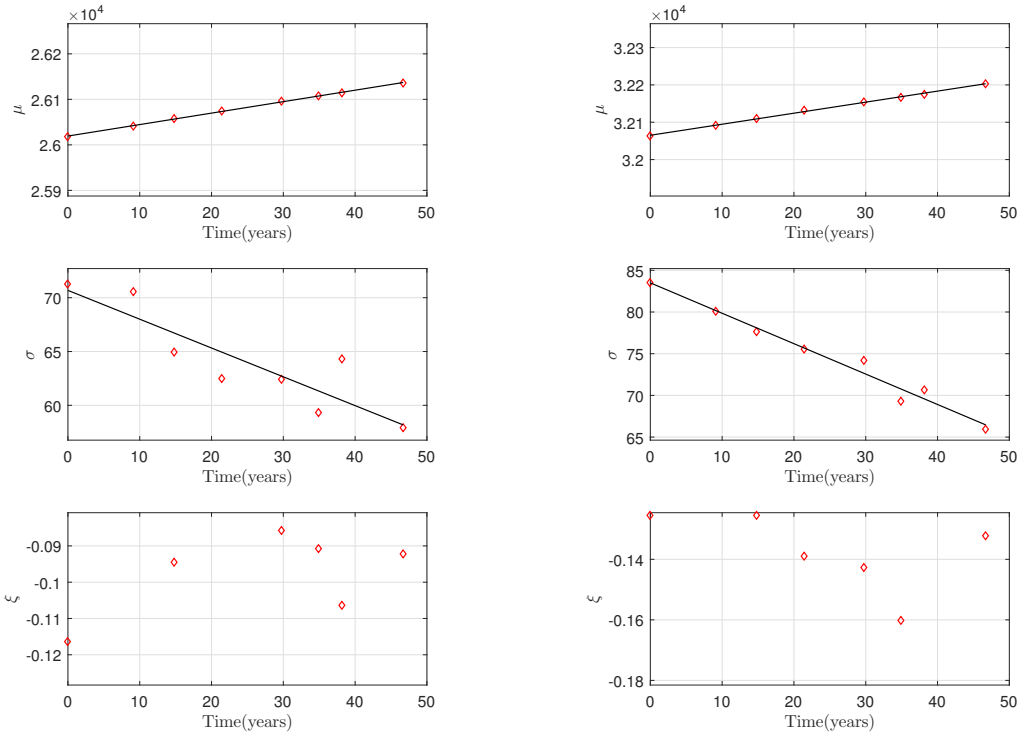

45m span (Support moment) 50m span (Support moment)

Figure C.36: GEV Parameter changes for 4 span continuous beam due to 4% annual traffic growth

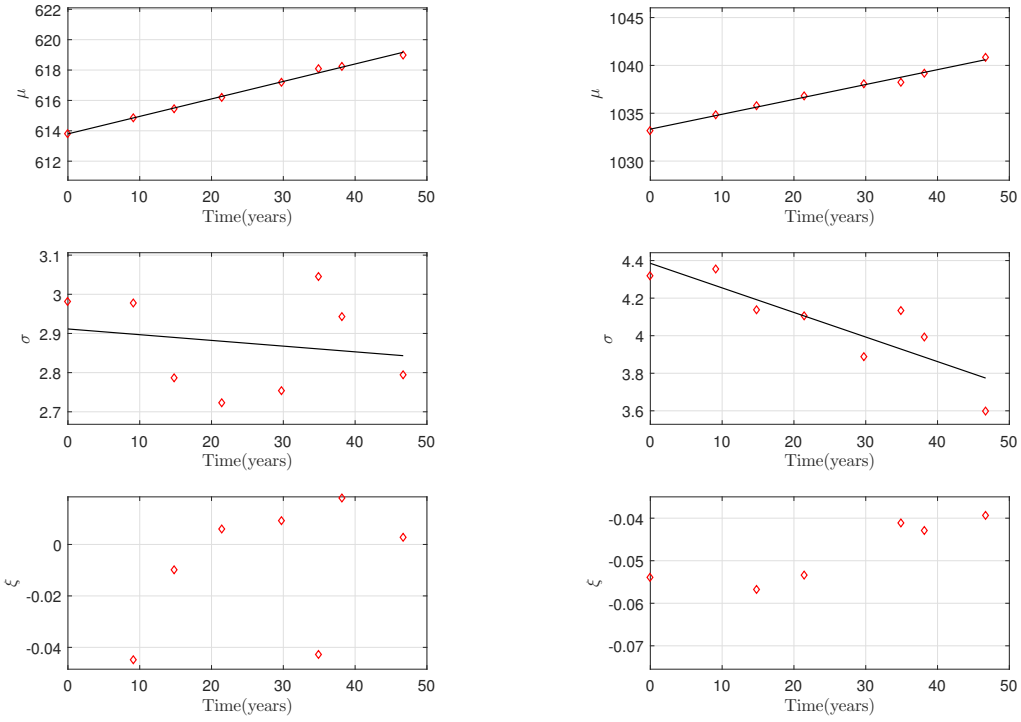

5m span (Support shear) 10m span (Support shear)

Figure C.37: GEV Parameter changes for 4 span continuous beam

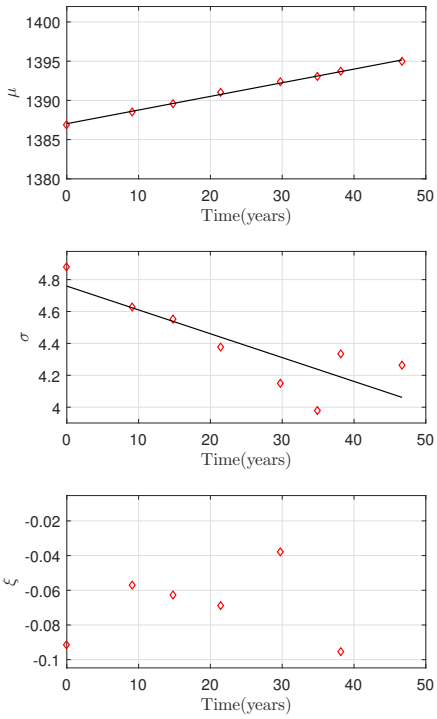

15m span (Support shear)

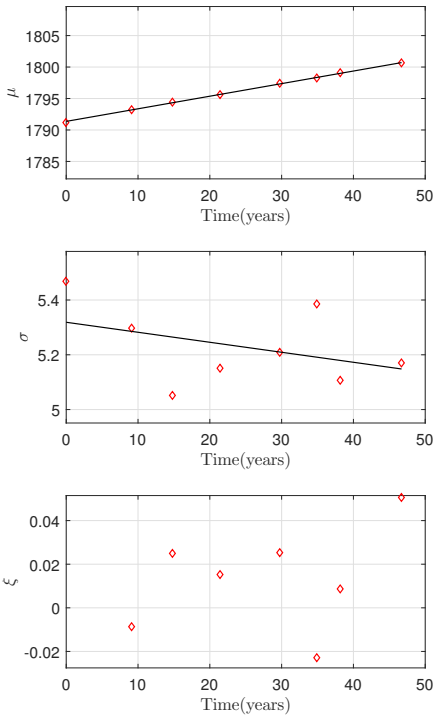

20m span (Support shear)

Figure C.38: GEV Parameter changes for 4 span continuous beam due to 4% annual traffic growth

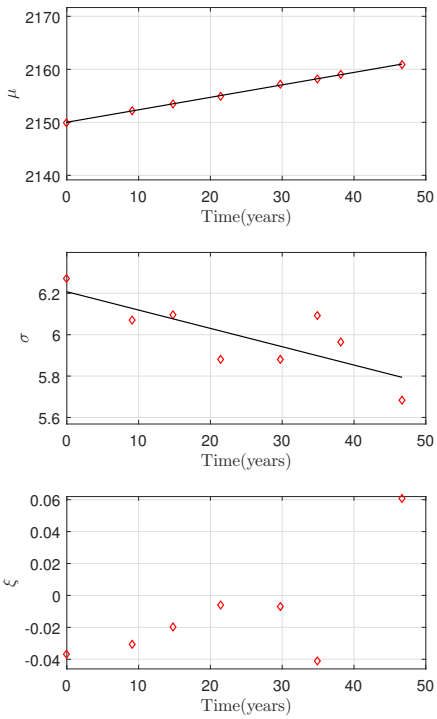

25m span (Support shear)

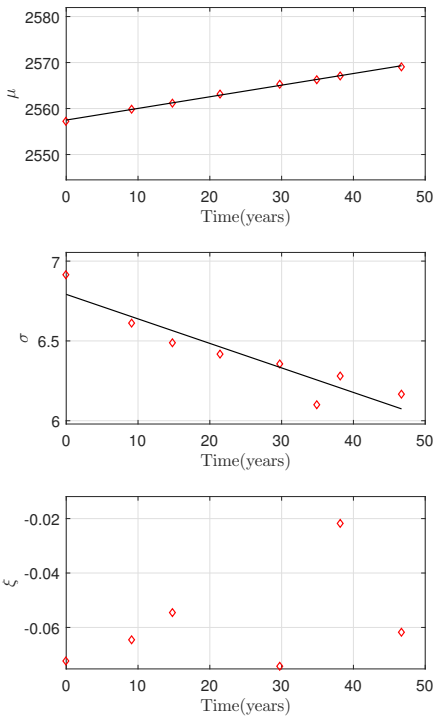

30m span (Support shear)

Figure C.39: GEV Parameter changes for 4 span continuous beam due to 4% annual traffic growth

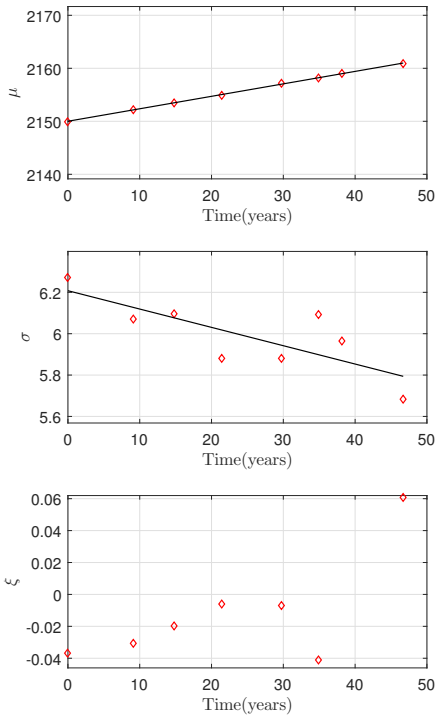

25m span (Support shear)

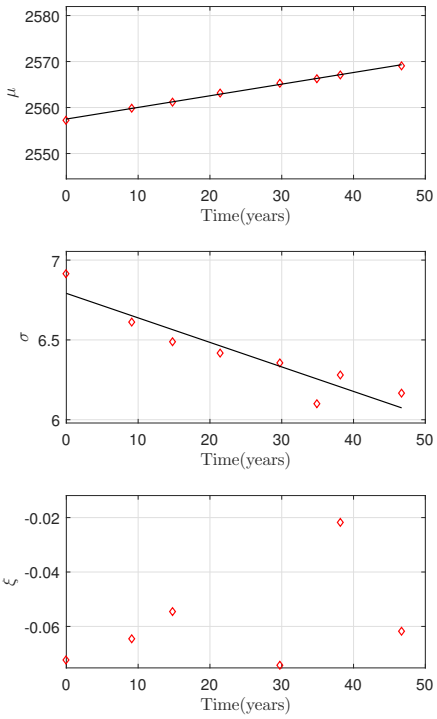

30m span (Support shear)

Figure C.40: GEV Parameter changes for 4 span continuous beam due to 4% annual traffic growth

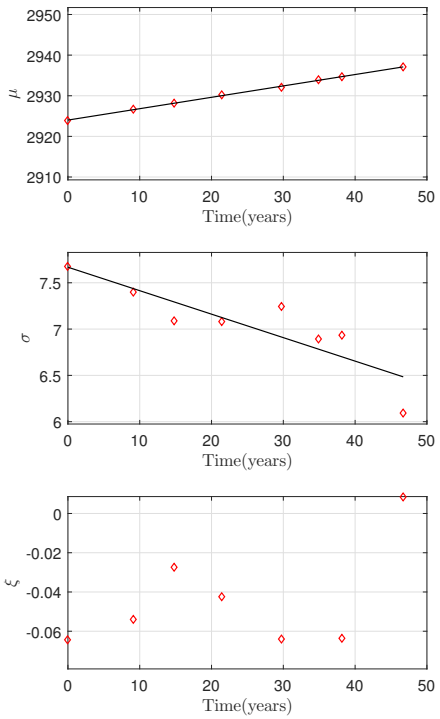

35m span (Support shear)

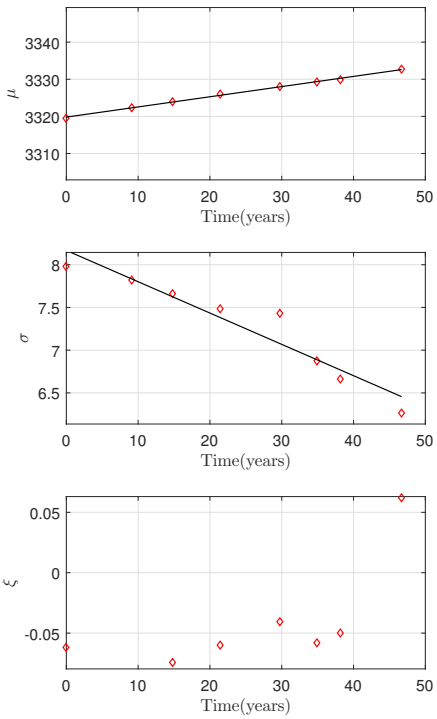

40m span (Support shear)

Figure C.41: GEV Parameter changes for 4 span continuous beam due to 4% annual traffic growth

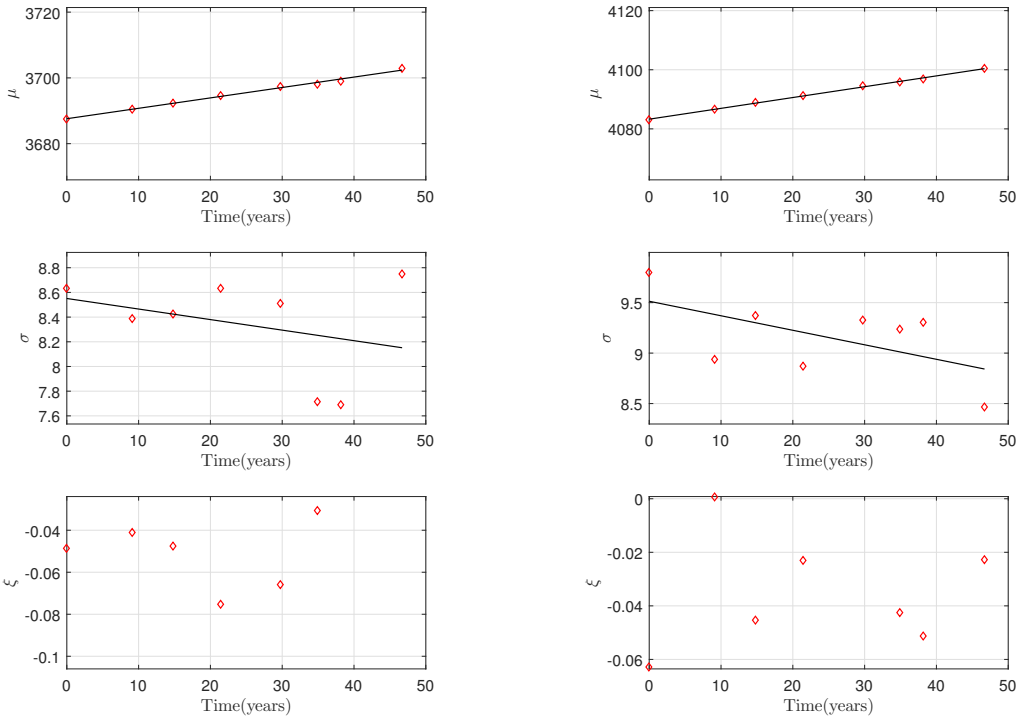

45m span (Support shear) 50m span (Support shear)

Figure C.42: GEV Parameter changes for 4 span continuous beam due to 4% annual traffic growth